



4-2014

Numerical and Experimental Investigation of Orthopaedic Fracture Fixation

Bipinchandra Patel

Western Michigan University, usabips@gmail.com

Follow this and additional works at: <https://scholarworks.wmich.edu/dissertations>



Part of the Biomechanical Engineering Commons, and the Orthopedics Commons

Recommended Citation

Patel, Bipinchandra, "Numerical and Experimental Investigation of Orthopaedic Fracture Fixation" (2014).
Dissertations. 258.

<https://scholarworks.wmich.edu/dissertations/258>

This Dissertation-Open Access is brought to you for free and open access by the Graduate College at ScholarWorks at WMU. It has been accepted for inclusion in Dissertations by an authorized administrator of ScholarWorks at WMU. For more information, please contact wmu-scholarworks@wmich.edu.



NUMERICAL AND EXPERIMENTAL INVESTIGATION OF ORTHOPAEDIC FRACTURE FIXATION

by

Bipinchandra Patel

A dissertation submitted to the Graduate College
in partial fulfillment of the requirements
for the degree of Doctor of Philosophy
Department of Mechanical and Aeronautical Engineering
Western Michigan University
April 2014

Doctoral Committee:

Dr. Peter A. Gustafson, Ph.D., Chair
Dr. Judah Ari-Gur, D.Sc.
Dr. Daniel Kujawski, Ph.D., D.Sc.
Dr. James R. Jastifer, M.D.

NUMERICAL AND EXPERIMENTAL INVESTIGATION OF ORTHOPAEDIC FRACTURE FIXATION

Bipinchandra Patel, Ph.D.

Western Michigan University, 2014

Poor bone fracture fixation leads to malunion, delayed union, non-union, or infection. These malunited fractures affect a bone's ability to carry loads. Patient outcomes regarding fixation quality can be affected by the healing environment and human factors such as bone quality and surgeons' perception. Furthermore, the stiffness and strength of the screw-plate construct affect the healing environment. Therefore, this dissertation investigates the stiffness and strength of the non-locking (conventional) and locking (fixed angle) type screw-plate constructs and the factors that contribute to them, such as screw-plate interface, screw design, bone density, cortical bone thickness and load orientation. Additionally, the surgeon's ability to perceive stripping of the bone while driving screws is evaluated. Finite element analyses and experiments are performed for these investigations.

The type of construct is found to have a minimal effect on the stiffness of the construct, whereas the plate thickness has a larger influence. Moreover, it is observed that the uniformity of force distribution at the bone-screw interface and the bone plastic strain distribution determine the construct strength behavior. The locking screw construct provides the greater strength under shear load and the conventional screw construct offers greater strength under pullout loads for the analyzed cortex thicknesses, cancellous bone densities and screw diameters. The load-displacement plot from the finite element analysis was compared to the experimental data. The correlation validates the finite element model.

In non-locking plates, construct stability relies on the friction between the plate and bone. This friction is controlled by the compressive force produced through applied screw torque. The finite element analysis demonstrates that an over-tightened (higher pre-tension) screw deteriorates the load carrying ability of the bone. In addition, the surgeons' perception was found to be unrelated to the likelihood of bone stripping. Furthermore, the maximum torque achieved before stripping is surgeon dependent and surgeons stripped bone more frequently than they perceived.

© Bipinchandra Patel 2014

Acknowledgments

First of all, I am extremely grateful to my PhD advisor, Dr. Peter A Gustafson, for his valuable guidance and all the useful discussions and brainstorming sessions. I also appreciate his understanding, efforts and support during difficult times. I learned a lot from his deep insights, thought process, views, and expertise on several computational tools. He is an inspiration.

I offer my sincerest gratitude to the dissertation committee members Dr. Judah Ari-Gur, Dr. Daniel Kujawski and Dr. James R. Jastifer for their valuable guidance and motivation during the PhD process and also during my graduate courses. I will always be thankful to them for investing their valuable time in reviewing my dissertation process.

Very special thanks to Dr. Michael Stoesz, and Dr. James R. Jastifer for their valuable guidance on orthopedic fundamentals, support during the lab experiments and publications. A big "Thank you!" also goes out to all the volunteer surgeons associated with Kalamazoo Center for Medical Studies (KCMS) and Bronson hospitals, who participated in the "Surgeon perception" study in spite of their extremely busy schedules.

I am also grateful to the countless contributors to the "Open Source" programming community for providing the numerous tools and systems I have used to produce both my results and this dissertation.

My deepest gratitude to my parents and my in-laws for their constant unconditional support. It is amazing to have such a family being far away from home.

Finally, my heartfelt appreciation goes to my wife Aalapee. She has been a constant source of strength and inspiration during tough times in past four years. Her determination, compromise and constant encouragement have played an important role to bring this project through to the end.

Bipinchandra Patel

Table of Contents

ACKNOWLEDGMENTS	ii
LIST OF TABLES	vi
LIST OF FIGURES	vii
1 INTRODUCTION	1
1.1 Significance of the research	1
1.2 Background	2
1.2.1 Conventional versus locking screw-plates	2
1.2.2 Stability and bone healing	4
1.3 Objective and structure of the dissertation	5
1.4 Publications related to this dissertation	7
2 LITERATURE REVIEW	9
2.1 Locking versus non-locking screw-plate system	9
2.1.1 Fixation performance	9
2.1.2 Stiffness influence on fracture healing	10
2.2 Screw pullout strength	11
2.2.1 Experimental evaluation	11
2.2.2 Finite element modeling	12
2.3 Screw torque studies	12
2.4 Shortcomings of existing literature	13
3 DEVICE INFLUENCE ON MECHANICAL HEALING ENVIRONMENT: STIFFNESS OF CON- VENTIONAL AND LOCKING SCREW-PLATE CONSTRUCTS	15
3.1 Finite element model	15
3.2 Results	23

Table of Contents—Continued

3.2.1	Comparison of displacement contours of the distal fibula	23
3.2.2	Comparison of construct stiffnesses about the fracture plane	25
3.3	Validation	28
3.4	Clinical relevance	30
3.5	Conclusions	30
4	DEVICE INFLUENCE ON HEALING ENVIRONMENT: STRENGTH OF CONVENTIONAL AND LOCKING SCREW-PLATE CONSTRUCTS	31
4.1	Experimental investigation of screw construct strength	31
4.1.1	Oblique load	32
4.1.2	Normal load	41
4.1.3	Shear load	44
4.1.4	Effect of cortex on load angle vs. construct type relationship	47
4.2	Finite element investigation of screw construct strength	50
4.2.1	Strength evaluation matrix	52
4.2.2	Normal load	58
4.2.3	Shear load	69
4.2.4	Oblique load	81
4.2.5	Conclusions	90
5	SURGEON PERCEPTION AND ITS INFLUENCE ON FRACTURE FIXATION QUALITY	91
5.1	Effect of applied torque (pre-tension) on construct strength	91
5.2	Evaluation of surgeon ability to perceive optimum torque in synthetic cancellous bones	94
6	SUMMARY	103
7	FUTURE RESEARCH	105
	REFERENCES	112
A	GLOSSARY OF ORTHOPAEDIC TERMS	114
B	COMPARISON OF DISPLACEMENT CONTOURS OF THE DISTAL FIBULA	116
B.1	Displacement contours for comminuted fracture	116
B.2	Displacement contours for danis-weber B fracture	118

Table of Contents—Continued

C	COMPARISON OF CONSTRUCT STIFFNESSES ABOUT THE FRACTURE PLANE	120
C.1	Stiffness for comminuted fracture	120
C.2	Stiffness for danis-weber B fracture	127
D	FORCE DISTRIBUTION AT SCREW BONE INTERFACE	133
D.1	Normal load	133
D.2	Shear load	145
D.3	Oblique load	156
E	TOTAL STRAIN COMPARISON PLOTS	167
E.1	Normal load	167
E.2	Shear load	180
F	PLASTIC ENERGY TO TOTAL WORK RATIO PLOTS	191
F.1	Normal load	191
F.2	Shear load	193
F.3	Oblique load	195
G	PLASTIC STRAIN AT THE FAILURE INITIATION	197
G.1	Normal load	197
G.2	Shear load	201
H	HSIRB APPROVAL FORMS	203

List of Tables

3.1	Material properties utilized in the model	16
3.2	Fracture-plate-combinations	17
3.3	Contact relationship between components	18
3.4	Load cases and associated displacements	19
4.1	Assumed bone material properties for elastic perfectly plastic analysis	50
5.1	Relationship of stripping with density	100
5.2	Relationship of stripping with rank of surgeon	100
5.3	Importance of individual surgeon to stripping	100
5.4	Importance of screw sequence	101
5.5	Mean max. torque +/- standard deviation	102

List of Figures

1.1	Internal and external fixation of fractured bone	2
1.2	Conventional (non-locking) and locking plate-screw mechanisms	3
1.3	Phases of bone fracture healing	4
1.4	Research approach	6
2.1	Load to failure as a function of bone density	11
3.1	Model overview and applied loads	20
3.2	Boundary condition and loading techniques	21
3.3	Plate types	21
3.4	Plate-screw relationship in conventional and locked screw constructs	22
3.5	Displacement ($ \Delta\vec{u} $) due to fibulotalar reaction load and external moment with comminuted fracture	24
3.6	Displacement ($ \Delta\vec{u} $) due to fibulotalar reaction load and external moment with danis-weber B fracture	24
3.7	Definition of relative motion at fracture surfaces	25
3.8	Relative motion of the comminuted fracture surfaces due to the applied fibulotalar load and external moment	27
3.9	Relative motion of the Danis-weber B fracture surfaces due to the applied fibulotalar load and external moment	29
4.1	Load patterns on plate-bone constructs	32
4.2	Experimental setup for oblique load pullout	33
4.3	Fixture for surrogate bone and plate dimensions	34
4.4	Experimental results for oblique load (without cortex)	36
4.5	Box and whisker plot for peak (failure) oblique load (without cortex)	37
4.6	Interaction effect between construct type and bone density for oblique load (without cortex)	38

List of Figures—Continued

4.7	Experimental setup for oblique load pullout with cortical bone layer	39
4.8	Box and whisker plot for normal and oblique peak (failure) load (with cortex)	39
4.9	Experimental results for oblique pull (with cortex)	40
4.10	Experimental setup for normal load pullout with 1mm thick cortical layer	41
4.11	Box and whisker plot for peak (failure) normal load (without cortex)	42
4.12	Interaction effect between construct type and bone density for normal load (without cortex)	42
4.13	Experimental results for normal pull (with cortex)	43
4.14	Experimental setup for shear load	44
4.15	Box and whisker plot for peak (failure) shear load (without cortex)	45
4.16	Locking and conventional constructs under shear load (with cortex)	46
4.17	Box and whisker plot for peak (failure) shear load (with cortex)	47
4.18	Interaction effect between construct type and load type (without cortex, density=0.08gpcc)	48
4.19	Interaction effect between construct type and load type (with cortex)	48
4.20	Finite element model boundary conditions	51
4.21	Finite element vs experiment under normal load (Density=0.16 g cm ⁻³)	52
4.22	Pullout force (Fy) distribution over the threads	54
4.23	Plastic strain under normal load (Cortex thickness=1mm)	55
4.24	Total strain under normal load (Cortex thickness=0mm)	56
4.25	Plastic energy dissipation comparison under normal load	57
4.26	The force extraction process using python script	58
4.27	Pullout force (Fy) distribution over the threads (cortex thickness = 0mm)	60
4.28	Pullout force (Fy) distribution over the threads (cortex thickness = 1mm)	61
4.29	Pullout force (Fy) distribution over the threads (cortex thickness = 2mm)	62
4.30	Total strain under normal load (Bone density = 0.24 g cm ⁻³ , Cortex thickness=0mm)	63
4.31	Total strain under normal load (Bone density = 0.32 g cm ⁻³ , Cortex thickness=1mm)	64
4.32	Total strain under normal load (Bone density = 0.32 g cm ⁻³ , Cortex thickness=2mm)	65
4.33	Plastic strain under normal load (Bone density = 0.32 g cm ⁻³ , Cortex thickness=1mm)	66
4.34	Plastic energy dissipation comparison under normal load	67
4.35	Plastic strain for the failure initiation under normal load (Cancellous density = 0.16 gpcc, cortex thickness=1mm)	68
4.36	Plastic strain for the failure initiation under normal load (Cancellous density = 0.16 gpcc, cortex thickness=2mm)	69

List of Figures—Continued

4.37 Shear force (Fx) distribution over the threads (cortex thickness = 0mm)	70
4.38 Shear force (Fx) distribution over the threads (cortex thickness = 1mm)	71
4.39 Shear force (Fx) distribution over the threads (cortex thickness = 2mm)	72
4.40 Moment (Mz) distribution over the threads (cortex thickness = 0mm)	73
4.41 Moment (Mz) distribution over the threads (cortex thickness = 1mm)	74
4.42 Total strain under shear load (Bone density = 0.24 g cm ⁻³ , Cortex thickness=0mm)	75
4.43 Total strain under shear load (Bone density = 0.24 g cm ⁻³ , Cortex thickness=1mm)	76
4.44 Total strain under shear load (Bone density = 0.24 g cm ⁻³ , Cortex thickness=2mm)	77
4.45 Plastic strain under shear load (Bone density = 0.32 g cm ⁻³ , Cortex thickness=1mm)	78
4.46 Plastic energy dissipation comparison under shear load	79
4.47 Plastic strain for the failure initiation under shear load (Cancellous density = 0.08 gpcc, cortex thickness=1mm)	80
4.48 Plastic strain for the failure initiation under shear load (Cancellous density = 0.08 gpcc, cortex thickness=2mm)	81
4.49 Force (Fy) distribution over the threads under oblique load (cortex thickness = 0mm)	82
4.50 Force (Fy) distribution over the threads under oblique load (cortex thickness = 1mm)	83
4.51 Force (Fy) distribution over the threads under oblique load (cortex thickness = 2mm)	84
4.52 Total strain under oblique load (Bone density = 0.24 g cm ⁻³ , Cortex thickness=0mm)	85
4.53 Total strain under oblique load (Bone density = 0.32 g cm ⁻³ , Cortex thickness=1mm)	86
4.54 Total strain under oblique load (Bone density = 0.24 g cm ⁻³ , Cortex thickness=2mm)	87
4.55 Plastic strain under oblique load (Bone density = 0.32 g cm ⁻³ , Cortex thickness=1mm)	88
4.56 Plastic energy dissipation comparison under oblique load	89
4.57 Plastic strain for the failure initiation under oblique load (Cancellous density = 0.08 gpcc, cortex thickness=1mm)	90
5.1 Effect of pre-tension on force at screw-bone interface (Cancellous density = 0.24 gpcc, cortex thickness=0mm)	92
5.2 Effect of pre-tension on force at screw-bone interface (Cancellous density = 0.24 gpcc, cortex thickness=1mm)	93
5.3 Surgeon evaluation test setup	94
5.4 Bone stripped by surgeon (TS<TI)	95
5.5 Bone not stripped by surgeon (TS>TI)	96

List of Figures—Continued

5.6	Effects of applied axial force and bone density ($0.08\text{g}/\text{cm}^{-3}$)	96
5.7	Effects of applied axial force and bone density ($0.16\text{g}/\text{cm}^{-3}$)	97
5.8	Effects of applied axial force and bone density ($0.32\text{g}/\text{cm}^{-3}$)	97
5.9	Max torque and standard deviation ($0.08\text{g}/\text{cm}^{-3}$)	98
5.10	Max torque and standard deviation ($0.16\text{g}/\text{cm}^{-3}$)	98
5.11	Max torque and standard deviation ($0.32\text{g}/\text{cm}^{-3}$)	99
7.1	A combination of conventional plate with anti-pullout nut	105

Chapter 1

Introduction

The most basic requirements for fracture healing include mechanical stability, an adequate blood supply (i.e., bone vascularity), and bone-to-bone contact. The absence of one or more of these factors can cause fracture non-union or malunion [1]. Bone has unique ability of self-repair. However, healing and weight bearing ability of a fractured bone is greatly influenced by the fixation device performance and human factors. The stiffness and strength of the screw-plate construct can influence the healing environment for timely bone healing and weight bearing. Moreover, human factors such as bone quality and surgeons' ability to achieve stable construct are also important factors and contribute to fixation quality.

There are two ways that a displaced fracture can be reduced: 1. Open reduction and internal fixation (operative treatment) and 2. Closed reduction (non-operative treatment). Open reduction of a fracture involves making an incision in the skin, putting the fractured bones together, stabilizing the fracture with screws or plates or rods. Closed reduction means no incision is made; the fracture is manipulated under radiographic grid and bone is immobilized. Operative treatment usually leads to the faster mobilization. A fractured bone must be carefully fixed in position and stabilized until healing causes it to be strong enough to bear weight.

Open reduction with internal fixation is commonly used in cases of multi-trauma when the bone cannot be reliably healed using external methods such as casting [2]. The internal screw-plate fixation is a commonly used operative treatment for fractures.

1.1 Significance of the research

According to the National Ambulatory Medical Care Survey & American Academy of Orthopaedic, approximately 6.3 million bone fractures occur each year in the United States. Worldwide, an osteoporotic (age-related) fracture is estimated to occur every 3 seconds [3]. The selection of a fracture fixation device can have the significant impact in controlling postoperative complications and pain [4, 5, 6, 7]. The selection of a proper fixation

device in fixation of osteoporotic bone (lower bone mass density) fracture is even more difficult and sensitive due to decreased mechanical properties. Therefore, the outcomes of this dissertation will help understand the screw-bone interface mechanism and help improve an appropriate device selection based on the physiological load at the fracture site. In addition, an experimental investigation performed to evaluate the surgeons' ability to perceive stripping of the bone with varying cancellous bone densities will evaluate the influence of the human factors on fixation quality. This research will help enhance engineers' and surgeons' knowledge of the mechanics of fracture fixation.

1.2 Background

1.2.1 Conventional versus locking screw-plates

Until the last century, physicians relied on external fixation (Fig. 1.1a) [8] to aid healing of fractured bone. The development of sterile surgery reduced the risk of infection so that doctors could work directly with the bone and could implant materials in the body. Classically, methods of internal fracture fixation have used pins, wires screws, and plates to rigidly stabilize the fracture site. Plates and screws are the most commonly used internal fixators (Fig. 1.1b) to support the bone directly. In 1958, AO formulated four basic principles: Anatomic reduction, stable fixation, preservation of blood supply and early mobilization. These principles are the guidelines for internal fixation. The internal fracture fixation typically provides mechanical stability to the fractured bone, allowing some weight bearing, faster mobilization and return to function. Fracture plating can be generally classified into locking and conventional plates.

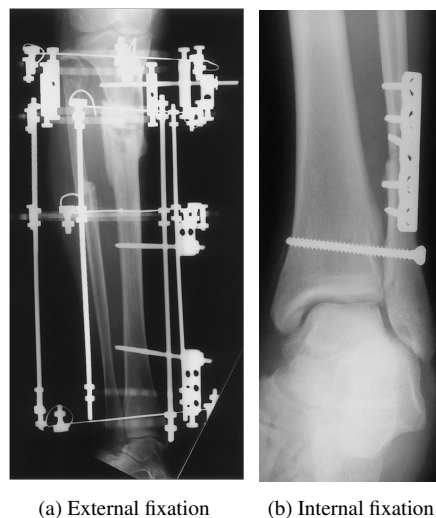


Figure 1.1: Internal and external fixation of fractured bone [9]

In conventional plating, fixation relies on compression and friction between the plate and bone (Fig. 1.2b).

The screws for conventional plating pass through chamfered clearance holes (Fig. 1.2a). The screw-plate angle is restrained by contact forces and friction, which are primarily the result of screw pre-tension (the quality of the “bite” a screw obtains on insertion). These forces prevent plate lift off, screw toggling (change of the screw-plate angle), and pull out [10]. Conversely, in locked plate constructs, the screw is fixed to the plate by thread engagement (Fig. 1.2c). This functionally “locks” the angle between the screw and the plate, eliminating the ability of the screw to toggle and pull straight out. This simple difference has important biomechanical implications.

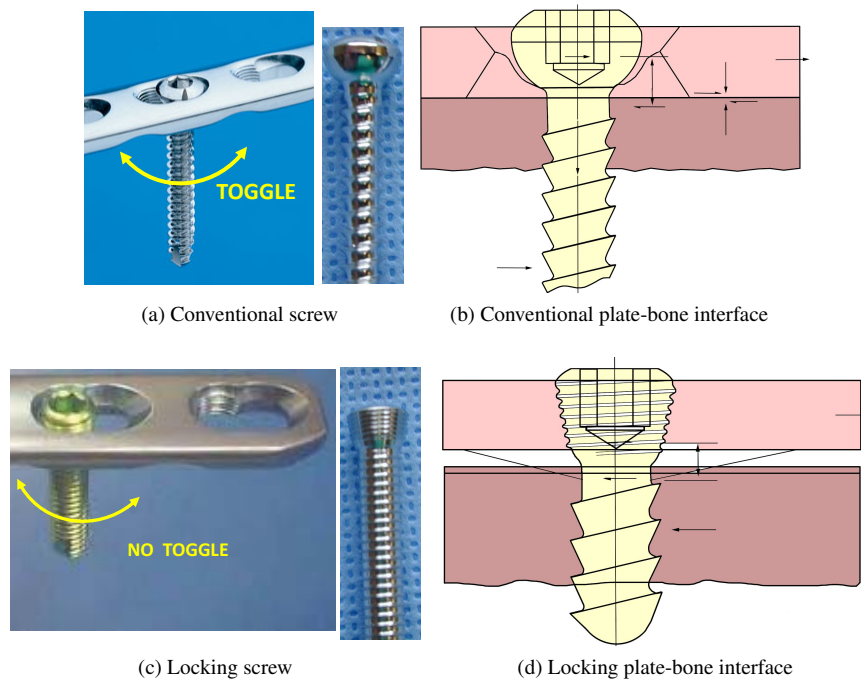


Figure 1.2: Conventional (non-locking) and locking plate-screw mechanisms [11]

There are some advantages and disadvantages of locking plates over conventional plates [12, 9, 13]

Advantages

The bone thread can no longer be stripped during insertion due to locking of the screw head to the plate. The compression between the plate and bone is unnecessary with a locking screw head; therefore, periosteal blood supply is preserved, which improves bone vascularity. Moreover, the plates do not need to be anatomically contoured and do not need to sit flush against the surface of the bone.

Disadvantages

On the other hand there are several disadvantages of using locked screw fixation such as, lack of ability to introduce lag screws through the plate in intra-articular fractures and simple oblique fractures, loss of tactile feel when inserting a screw in the bone, the fixed orientation of locking head screw, and a loss of ability to use the plate as a reduction tool. Moreover, over-tightening of the locking head makes removal difficult due to the cold-welding of the screw head to the plate. In addition, the locking plates are more expensive as compared to conventional plates.

1.2.2 Stability and bone healing

The stability at the fracture surfaces is an important precondition for successful healing [2]. In orthopaedics, a fracture or joint is considered stable when small changes in applied loads lead to small changes in motion. The compressed fracture interfaces may have no clinically perceivable displacement, indicating absolute stability of the fixation. Fractures that are splinted by implants without application of compression undergo small relative displacements. The displacement is controlled by the applied load and the stiffness of the construct [14].

Depending upon the stability at the fracture site, the bone experiences either direct (primary) or indirect (secondary) healing [15]. The healing of unstable fractures (2% to 10% strain) is characterized by an intermediate callus formation prior to healing (Fig. 1.3). This type of healing is referred to as indirect or secondary healing, which is divided into three phases: (1) inflammation, (2) repair, and (3) remodeling (Fig. 1.3). The amount of the callus formation depends on the stability of the fracture: greater instability increases the callus produced. The inflammatory phase begins just after the initial damage to bone and surrounding tissues, and at the end of this phase patients experience a decrease in pain and swelling. This phase, therefore, lasts for 3-4 days or longer, depending on the amount of force that caused the fracture. During the repair phase, the hematoma (clotted blood tissue) transforms into granulation tissues, which mature into the tissues and end with woven bone formation. Finally, in the remodeling phase, the woven bone is replaced by cortical bone. This pattern of healing occurs without stabilization or flexible internal fixation [15].

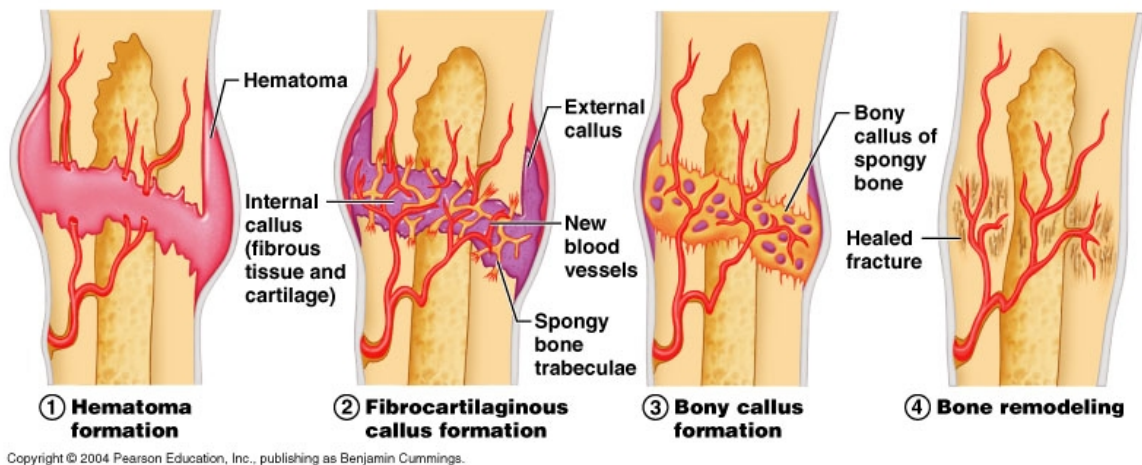


Figure 1.3: Phases of bone fracture healing

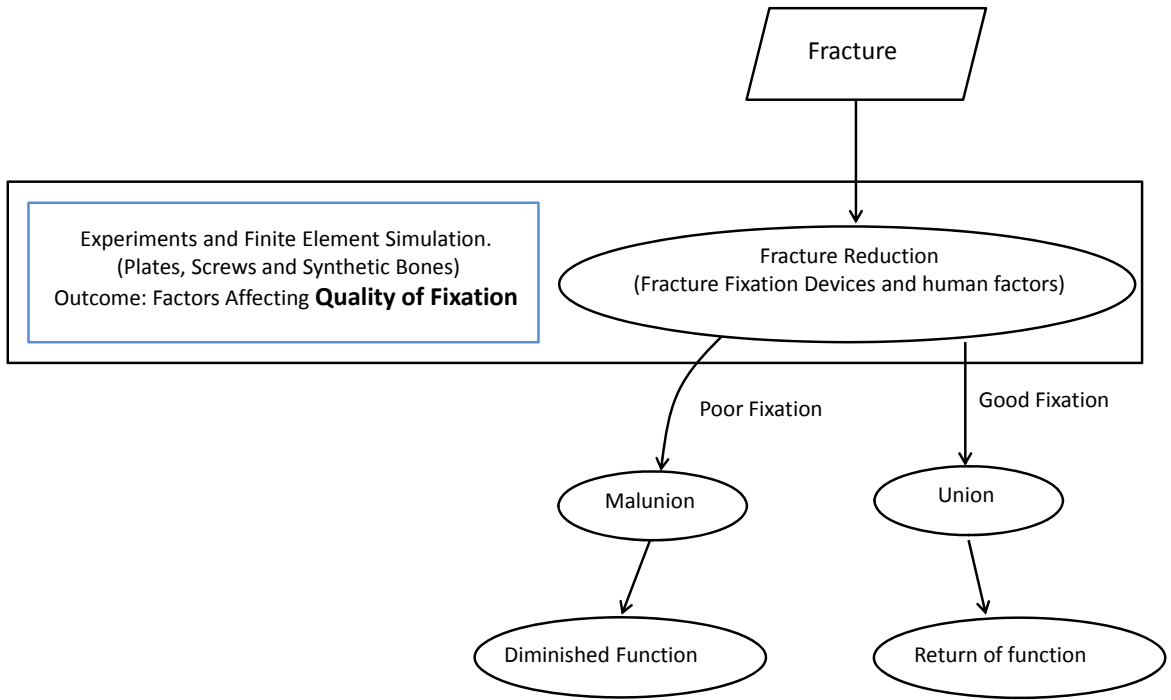
Stable fracture fixation (less than 2% strain) causes direct or primary healing without a callus formation and is characterized by gradual disappearance of the fracture line [16]. This process requires an adequate blood supply and absolute rigidity at the fracture site. The direct healing occurs in two forms, depending on the proximity of the fracture ends: 1. Contact healing and 2. Gap healing. In contact healing, bone union and remodeling occurs simultaneously, while in gap healing they are sequential steps. However, the bone formation by contact healing

only occurs when the gap between the ends is less than 0.01 mm and the strain¹ at fracture surfaces is less than 2 % ([17, 18, 19, 20]). Thus, the healing rate can be affected by the screw-plate fixation stability. The greater stiffness and strength of the fixation can create an appropriate healing environment for the faster return of function.

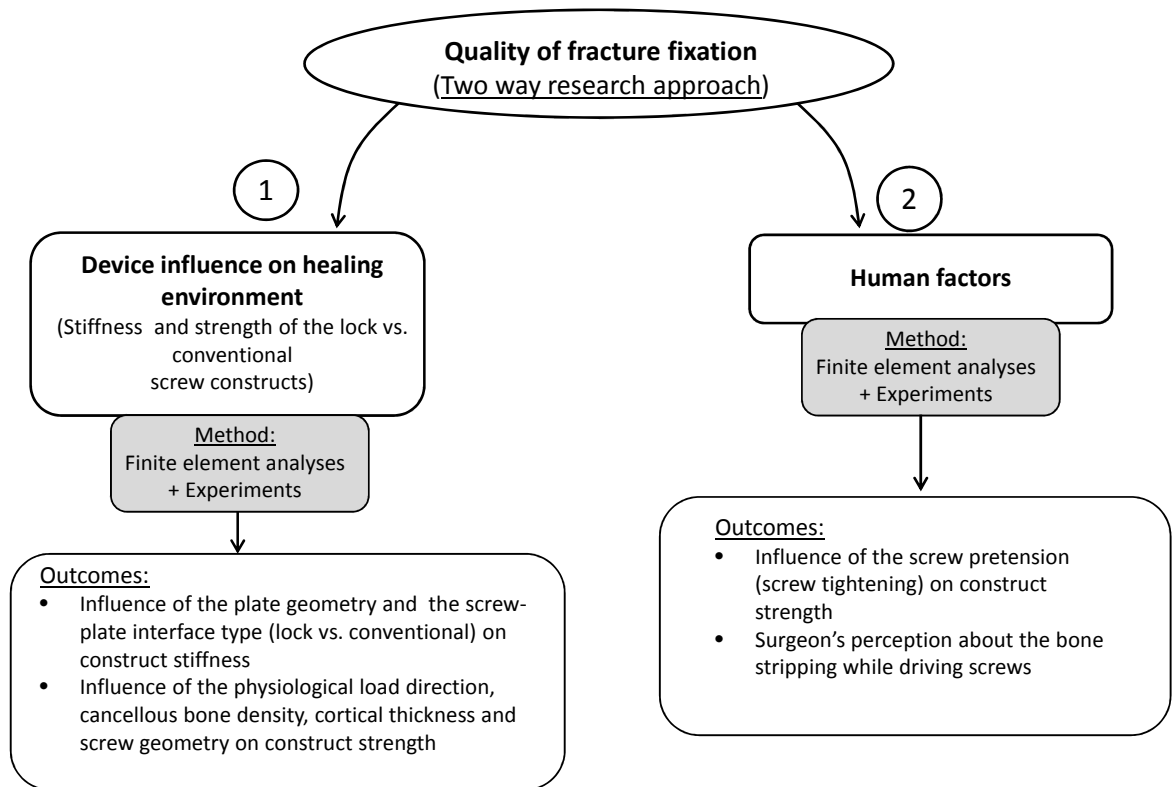
1.3 Objective and structure of the dissertation

Patient outcomes regarding fixation quality can be affected by the healing environment and human factors such as bone quality and surgeons' perception about fixation quality. Furthermore, the stiffness and strength of the screw-plate construct affect the healing environment. Therefore, this dissertation investigates the stiffness and strength of the non-locking (conventional) and locking (fixed angle) type screw-plate constructs and the factors that contribute to them, such as screw-plate interface, screw design, bone density, cortical bone thickness and load orientation. Additionally, the surgeon's ability to perceive stripping of the bone while driving screws is evaluated. Finite element analyses and experiments are performed for these investigations. Fig. 1.4 shows the graphical representation of the research approach.

¹Relative movement at the fracture surfaces



(a) Proposed research objectives



(b) Two way approach to the research objectives

Figure 1.4: Research approach

Locking and non-locking fracture plates are commonly used implants in orthopaedic fracture fixation. In chapters 3 and 4, finite element analyses and lab experiments are used to discern the behavior of locking and non-locking screw-plate constructs and their effects on fracture stiffness and strength. Chapter 3 includes the finite element analysis of the construct stiffness with locking and non-locking plating. Two plate types are examined with two different distal fibula fracture patterns. The stiffnesses of the locking and non-locking constructs are computed in terms of: (1) displacements at the distal end of fibula, and (2) the relative motion between fracture surfaces under several load cases. The pullout strength and shear strength of constructs under physiological loads is a deciding parameter of long term stability of fixation [21, 10]. Therefore, chapter 4 includes experimental and finite element studies performed to investigate the variability in strengths of locking and non-locking screw constructs subjected to normal, oblique and shear loads. In assessing performance, surrogate bones (i.e. polyurethane foam) of three different densities are used to represent cancellous bones of different age groups.

In non-locking plates, fracture fixation stability is related to the ability of a construct to resist motion between the plate and bone [21, 10, 22]. Sufficient friction between the plate and bone is required to resist this motion is dictated by generating adequate compressive force at the plate-bone interface (Fig. 1.2a). This compression is directly proportional to the applied torque [21]. Thus, chapter 5 includes the finite element analysis to evaluate the effects of the screw pre-tension (screw tightening) on construct strength followed by the evaluation of surgeon's ability to perceive stripping of the bone while driving screws.

1.4 Publications related to this dissertation

1. Bipinchandra Patel, Peter A. Gustafson, and James Jastifer, "The stiffness of locking and conventional plates in the fixation of distal fibula fractures; a finite element study", *ASME 2010 International Mechanical Engineering Congress and Exposition, Nov 12-18, Vancouver, BC, 2010. Also presented at 28th Annual Kalamazoo Community Medical and Health Sciences Research Day, April 14, 2010. Received Best Orthopaedic Presentation Award.*
2. Jastifer, Joseph Chess, Bipinchandra Patel, and Peter A. Gustafson, "Strength of locking plate constructs versus conventional plate constructs in osteoporotic bone: An experimental study", *ASME Applied Mechanics and Materials Conference, Chicago IL, May 31-June 2, 2011. McMat2011-4469.*
3. Michael Stoesz, James Jastifer, Bipinchandra Patel, and Peter A. Gustafson, "Characterization of torque curves of orthopaedic screws in surrogate bone", *In 29th Annual Kalamazoo Community Medical and Health Sciences Research Day, April 13 2011.*
4. James Jastifer, Peter A. Gustafson, Bipinchandra Patel, and Joseph Chess, "Strength of locking plate constructs versus conventional plate constructs in osteoporotic bone: An experimental study", *29th Annual*

Kalamazoo Community Medical and Health Sciences Research Day, April 13 2011.

5. Michael Stoesz, Peter A Gustafson, Bipinchandra Patel, James R Jastifer, and Joseph L Chess, “Surgeon Perception of Cancellous Screw Fixation”, *Journal of Orthopaedic Trauma* (2013).
6. Bipinchandra Patel, Peter A Gustafson, and James R Jastifer, “The effect of clavicle malunion on shoulder biomechanics”, *Clinical Biomechanics* 27.5 (2012), pp. 436 to 442.

Chapter 2

Literature Review

2.1 Locking versus non-locking screw-plate system

2.1.1 Fixation performance

Locked plate systems have been associated with improved stability in several biomechanical studies and have demonstrated advantages in several areas of fracture fixation. Sikes et al [23] investigated adult bovine ribs plated using the Synthes locking-head plate with either two or four bicortical locking-head (4.0-mm) or conventional (2.7-mm) screws per segment. The fixed ribs were loaded to 150 N, and the displacement was recorded. Locking-head screws provided significantly increased resistance to displacement when only two screws per segment were used in the reconstruction model. When four screws per segment were used, there was no significant difference between locking-head and conventional screw types in either model. Spivac et al [24] evaluated the effect of locking fixation screws on the stability of anterior cervical plating and found that locking screws significantly increased the rigidity of the tested screw-plate systems initially and after cyclic loading compared to the non-locking. In a clinical studies [25, 26] several distal femoral fractures treated with Less Invasive Stabilization System (plates with locking screws) and observed that it maintained the soft tissue envelope around fractures with improved efficacy in increasing osseous healing and decreasing infection. Thus, they have increased in popularity in recent years [27].

Several recent studies, however, have failed to consistently support the biomechanical superiority of locking plate and screw constructs compared to conventional plate and screw constructs in osteoporotic bone and bone surrogate. Egol et al [10] conducted study to review the biomechanical principles that guide fracture fixation with plates and screws; specifically to compare and contrast the function and roles of conventional unlocked plates to locked plates in fracture fixation. Authors have concluded that locked plates and conventional plates rely on completely different mechanical principles to provide fracture fixation and in so doing they provide different

biological environments for healing. Locked plates may increasingly be indicated for indirect fracture reduction, diaphyseal/metaphyseal fractures in osteoporotic bone, bridging severely comminuted fractures, and the plating of fractures where anatomical constraints prevent plating on the tension side of the bone. Conventional plates may continue to be the fixation method of choice for periarticular fractures which demand perfect anatomical reduction and to certain types of nonunions which require increased stability for union [10]. Gardner et al [28] investigated that locked screw construct provided better stability and timely bone healing for comminuted diaphyseal and metaphyseal fractures and fractures in osteoporotic bone. But, they claimed that locking plates have not completely replaced conventional plates as the fixed angle screw construct restrict bone compression and angle variability. These can be necessary depending on the situation and the anatomy. Simple diaphyseal, metaphyseal and articular fractures are still best treated with anatomical reduction and conventional compression plating [28]. Minihane et al [29] have compared the lateral locking plate and antiglide non-locking plate for fixation of distal fibular fractures in osteoporotic bone, and observed that the antiglide constructs with non-locking screws were stiffer and withstood greater torque to failure.

Based on experimental investigation of the biomechanical stiffness on cadaveric osteoporotic bone, Kim et al [30] concluded that the torque to failure of the conventional plate was dependent on bone mass density ($r^2 = .67$), while the failure load of the locked-plate construct was independent of bone mass density. Unfortunately, the conclusions of the study would be different if one specimen (1 of 8) at the extreme end of the bone density range were removed from the data set. It is unclear whether this sample is an outlier since there were no repetitions at that bone density (Fig. 2.1). Since the conclusions of the paper are in doubt, further investigation is warranted.

In addition, Trease et al [31] performed a biomechanical study to examine the behavior of locking versus non-locking T-plates and concluded that the locking plates failed to increase the stiffness or strength of dorsally comminuted distal radius fractures compared with the non-locking plates. A similar experimental study was performed on fresh frozen osteoporotic cadaver feet with calcaneal fractures [32] investigated whether a locking calcaneal plate provides more stiffness in osteoporotic bone compared to non locking (conventional) plate. There were no statistically significant differences between the non-locking and locking plate constructs with respect to number of cycles to failure or displacement of the posterior facet. The locked screw-plates stabilize the fracture site and allow early weight bearing by carrying more load compared to the conventional screw-plate construct. This, however, can weaken the bone by stress shielding and cause re-fracture [33, 34]. Thus, experimental outcomes have failed to prove absolute superiority of locking plates. Also the conventional plates are relatively less expensive and offer versatility in variable angle fixation.

2.1.2 Stiffness influence on fracture healing

Clinical and radiological assessments can lead to removal of fixation devices, however, both metric are subjective. In the clinical study by Joslin et al [35] weight bearing is considered as a metric of healing after tibial

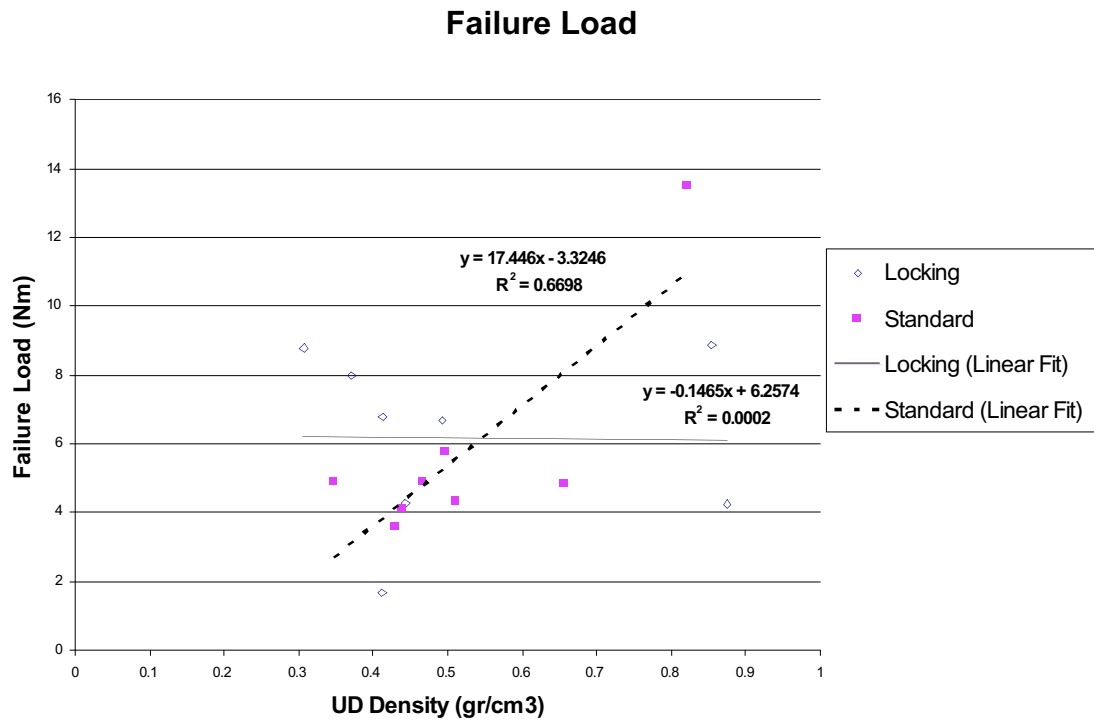


Figure 2.1: Load to failure as a function of bone density [30]

fracture and it was found that the weight bearing correlates well with the fracture stiffness. In the clinical study by Moorecroft et al [36], the fracture stiffness is considered a reliable measure of clinical union and visco elastic properties of callus. Shah et al [37] considered the fracture stiffness as a non-invasive method of fracture healing. This non-invasive method of measuring the fracture stiffness supported the clinical impression of union and healing. In a numerical study of patient specific fracture healing processes, Wehner et al [38] studied the influence of the fixation stability on the healing time. The healing time showed good agreement of the interfracture movement compared with in vivo measurements. Experimental studies have shown that the bone healing is influenced by the relative movement of the bone fragments [39, 40, 41]. These clinical studies demonstrate the importance of stability at the fracture site. Hence, in the current finite element study, stiffness was observed as relative motion between the fracture surfaces.

2.2 Screw pullout strength

2.2.1 Experimental evaluation

Asnis et al [42] performed pull-out tests on synthetic cancellous bone surrogate to isolate the parameters of host density, outer diameter (OD), root diameter (RD), and pitch in cancellous bone screw design and their effect on maximum pull-out force. The effect on this force of the different parameters of the custom screws in order

of importance was (a) host material density, (b) OD (c) pitch, and (d) RD. Chapman et al [43] observed that experimental pullout force was highly correlated to the predicted shear failure force (slope = 1.05, $R^2 = 0.947$) demonstrating that it is controlled by the major diameter of the screw, the length of engagement of the thread, the shear strength of the material into which the screw is embedded. According to Brown et al [44] the screws with the largest major thread diameter and longest thread length had the greatest pull-out force, compressive strength, and stripping torque.

Zedro et al [45] had extracted screws at pullout rates of 1 mm/min, 2.5 mm/min, 5 mm/min, 7.5 mm/min, 10 mm/min, 20 mm/min, 30 mm/min, 40 mm/min, 50 mm/min, and 60 mm/min from synthetic cancellous bone surrogate. They found that failure force, failure stress, and resistance force increased and were highly linearly correlated with pullout rate ($R^2=0.78, 0.76, \text{ and } 0.74$, respectively). In proposed research, pullout rate of 5 mm/min is used. It is more convenient to observe the failure mode with slower pullout rate. Moreover, the slower pullout rate avoids the influence of dynamic force on bone failure.

The study by Singh et al [46] evaluated the efficacy of a 2.0-mm locking plate/screw system compared with a 2.0-mm non-locking plate/screw system in mandibular fractures. The statistical showed no statistically significant difference between the locking and non-locking plates ($p > 0.05$). In conclusion, mandible fractures treated with 2.0-mm locking plates and 2.0-mm non-locking plates present similar short-term complication rates.

2.2.2 Finite element modeling

Hou et al [47] investigated axial push out strength with six types of different locking screws using finite element model. The outcomes showed that descending order of the contribution of design factors was: screw outer diameter, pitch, inner diameter, root radius and thread width. However, in this study the load was purely axial (along the screw length) and evaluation was made using the finite element model of a screw with only four thread counts which does not represent the real physiological scenario.

2.3 Screw torque studies

Cordey et al [22] performed experiments in vivo and in vitro with conventional plates, and found that motion as prevented by friction and depends upon the axial force of the screw, pressing the plate into the bone. Thus, the torque applied to the screws is crucial.

Cleek et al [48] investigated effect of screw torque level on cortical bone pullout strength of ten pairs of ovine (sheep) tibia. Torque to failure tests indicated tightening to 86% T_{max} (T_{max} is max torque achieved before bone stripping) occurs after yield and leads to an average 51% loss in stiffness. These findings do not provide the bone density effects. So, the effects of bone densities may have on yield torque should be evaluated.

Collinge et al [49] performed tests on bone substitute model and observed that drilling bigger pilot hole and

"stripping" the screw by over-tightening resulted in 76% and 82% less pullout strength, respectively, than when the proper technique was used. Hence, surgeons' ability to control applied torque has an important biomechanical implication.

Ricci et al [21] analyzed the effect of screw thread pitch on generation of maximum insertion torque (MIT) and pullout strength (POS) and the relationship between MIT and POS in an osteoporotic cancellous bone model of density 0.16 g cm^{-3} . There was a significant difference in mean MIT based on screw pitch, whereas POS did not show statistically significant differences among the different screw pitches ($P = 0.052$).

The knowledge from these outcomes was utilized in this research to address the omissions and unexplored concepts. The next section (section 2.4) includes the shortcomings, omissions and unexplored concepts of reviewed literatures.

2.4 Shortcomings of existing literature

It is observed from the literature review that several biomechanical studies indicate that the locked plate systems offer improved stability and specific advantages in various fracture fixations [23, 24, 25, 26, 50, 51, 52]. Thus, locked plate systems have increased in popularity in recent years [27]. Several recent studies, however, have failed to consistently support the biomechanical superiority of locking plate and screw constructs compared to conventional plate and screw constructs in osteoporotic bone and bone surrogate [10, 28, 29, 53]. Thus, the superiority of one construct (locking plate or non-locking plate) over another is in doubt.

Although previous studies have attempted to compare the locking and non-locking plates, they have considered the roles of screw design and plate types one at a time. Commercially available locking and non-locking screw-plate combinations used in these studies have geometrical differences in terms of screw pitch, outer diameter, length and plate geometry. In fact, the effects of locking and non-locking screw-plate interfaces on fracture fixation stability and strength can only be differentiated if other geometrical parameters such as screw and plate geometry are identical in both cases.

Bone is anisotropic material, which means the performance of the bone varies with loading direction. In addition, in cadaveric (or in-vivo) bones, properties may vary within the bone and between the bones of an individual. Thus, to better compare the performances of locking and non-locking fracture plates, investigations should be done on specimens with consistent properties.

Existing pullout studies are valuable because they reveal information about general comparisons of the behaviors of both locking and non-locking screws. However, the existing studies compare the plate constructs based on loading mechanisms, which are laboratory-centric, i.e. the loads are non-physiological. Instead, the applied loads are based on laboratory and analytical convenience (axial loads).

Prior torque studies with non-locking plates either performed on the cadaveric bone or surrogate bone model

representing one density group [21]. Moreover, the surgeon's perception about achieving optimum torque for a stable construct with varying bone density has not been evaluated.

None of the previous research studies have investigated the details of load transfer mechanisms (force distribution) at screw-bone interface to differentiate the strength of conventional and locked screw mechanisms.

Chapter 3

Device influence on mechanical healing environment: Stiffness of conventional and locking screw-plate constructs

The healing environment at the fracture site is affected by the stiffness at the fracture site. Thus, this chapter includes the finite element study to investigate the fixation stiffness with locking and non-locking screw-plate constructs. This finite element investigation is a step towards understanding the behavior of locking and conventional plating in fracture fixation stiffness. In this investigation, distal fibular fractures are modeled and analyzed for stability dependence on plate-screw construct type. The objective is to establish and differentiate the stiffness of conventional and fixed angle (locking) screw constructs for the treatment of distal fibula fractures. Two plate types are examined; a fibular neutralization plate and a lateral periarticular distal fibular plate with fixed angle (locked) screws. The neutralization plate is considered with two construct types; conventional and locked screws. Several comparisons were made to differentiate the stiffness of the plate constructs. First, the neutralization plate is examined with conventional and locked screws when used for fixation of Danis-Weber B and comminuted fractures. Second, neutralization and periarticular plates are compared with locked screws for the same fracture patterns. The stiffnesses of the constructs are computed with the finite element method based on several load cases.

3.1 Finite element model

Two plates types constituting three constructs are investigated; a fibular neutralization plate with conventional screws, a fibular neutralization plate with locked screws, and a lateral periarticular distal fibular plate with locked screws.

A finite element model of fibular anatomy was constructed in Abaqus (Simulia Corp, Version 6.8) [54] from a rough surface model of CT data. The cross section of the bone is composed of two sets of solid hexahedral elements (Fig. 3.4) representing cortical and cancellous bone. Cortical bone surrounds the cancellous bone and is assumed to have a nominal thickness of 2 mm. Small variations of cortical bone thickness (≈ 0.2 to 0.45 mm) were introduced due to the manual meshing procedure. Distinct material properties were assigned to each set; the material properties are drawn from several references [55, 56, 57, 58, 30]. The interosseous membrane was modeled using shell elements and was assumed to have a uniform thickness of 2 mm. All structures were assumed to be isotropic; their properties are listed in Tab. 3.1. The interosseous membrane connects to the tibia (not modeled) at nodes that are assumed to be fixed. In essence, the tibia is assumed to be rigid to simplify the interaction between the two bones.

Table 3.1: Material properties utilized in the model

Component	Elastic modulus (MPa)	Poisson's ratio
Cortical bone	20,000	0.4
Cancellous bone	1,000	0.3
Screw/Plate	210,000	0.3
IO membrane	450	0.4

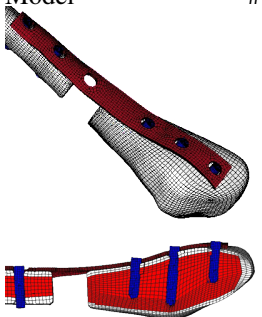
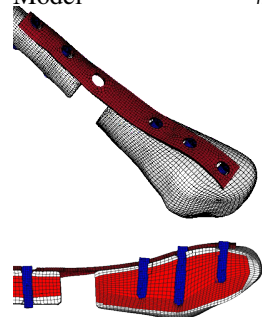
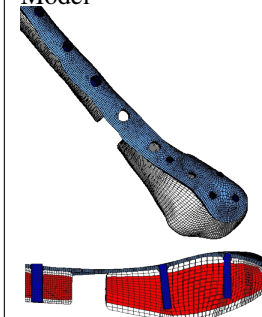
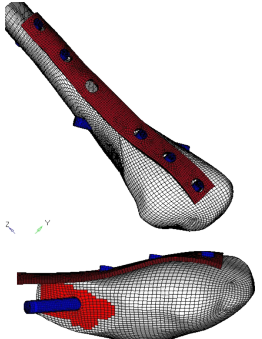
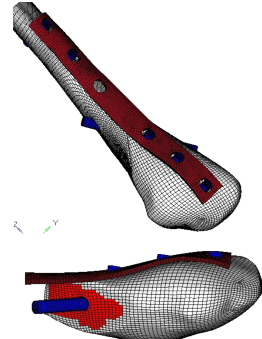
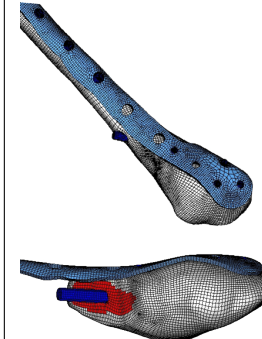
Two biomechanical cadaver studies have been published on locked plates in distal fibula fractures [30, 29]. Both investigated short oblique (Danis-Weber B) fractures of the distal fibula at the level of the syndesmosis as the fracture pattern. Thus, this paper studies the Danis-Weber B fracture as one of two fracture patterns. Each construct (of three) was also modeled for fixation of a comminuted fracture. Therefore, six models were created in total (see Tab. 3.2).

To simulate a Danis-Weber B fracture, a fracture surface was modeled at approximately 45° angle (shown in Tab. 3.2) to the longitudinal axis of the fibula at the level of the syndesmosis. The bone segments distal and proximal to the fracture site were modeled as distinct volumes. To simulate a comminuted fracture, a segment of ≈ 10 mm was removed from the distal fibula.

The neutralization plate construct model includes a stainless steel plate, two bi-cortical screws proximally, and three cancellous screws distally. The plate is modeled as a one third tubular plate (i.e. the plate form of $1/3$ of the circumference of a cylinder)¹ with six holes. The plate is 76 mm long, 9 mm wide and 1 mm thick and was generated with hex elements. The 3.5 mm cortical and cancellous screws were modeled without threads in holes modeled in the fractured fibula. A 3.5 mm lag screw was modeled across the fracture surface. In its clinical application, the purpose of the lag screw is to impart a sufficient screw tension to cause full surface compression (ie no separation) on the fracture surface. Each screw/plate and screw/bone interface as well as the fractured surfaces required an interaction assumption in the finite element model. Tab. 3.3 describes the assumed relationships at

¹Narang Medical Limited (<http://www.ortho.in/small-fragment-implants-instruments/plates/one-third-tubular-plates-ss.php>)

Table 3.2: Fracture-plate-combinations

Fracture type	Construct Neutralization plate (Conventional construct)	Construct Neutralization plate (Fixed angle construct)	Construct Lateral periarticular distal fibular plate (Fixed angle screw construct)
Comminuted fracture	Model #1 	Model #3 	Model #5 
Danis-Weber B fracture	Model #2 	Model #4 	Model #6 

these interfaces. Similarly, a 105 mm long by 10 mm wide by 1 mm thick lateral periarticular distal fibular plate with locked screws was modeled with four 2.7 mm distal screws and four 3.5 mm proximal screws.

The screw heads and their bearing surfaces were not modeled. Instead, a control node was used to represent the head. The control node was centered on the screw shank and located in the plane of the bearing surface. The shank nodes in the plane of the bearing surface were rigidly constrained to translate and rotate with the control node. To represent the neutralization plate conventional screw construct that may allow toggling of the screw head, the controlled shank nodes were allowed to swivel within the plate hole. This connection was modeled in Abaqus as a universal joint (UJOINT element [54]) having rotational degrees of freedom connecting the control node to nodes on the bearing surface of the plate. Conversely, the fixed angle construct was modeled in Abaqus using rigid BEAM connector elements [54] at the identical nodes in the locked plate model. The rigid beam elements fixed all controlled degrees of freedom between plate and screw. The control node and controlled shank nodes can be visualized in Fig. 3.4. The conventional screw model also included pre-tension surfaces in the shanks of the screws using Abaqus' standard methods for this purpose [54]. Other than these differences in the screw assumptions, the neutralization plate models with conventional and fixed angle screws were identical.

Plate performance was evaluated as representative nominal loads were applied at nodes at the distal end of

Table 3.3: Contact relationship between components

Components	Relationship	Comments
Screw-Bone (i.e. screw threads)	Rigid (tied contact)	Fixed all DOF
Plate-Bone	Contact pair	Friction sliding ($\mu = 0.3$)
Fracture surfaces	Contact pair	Friction sliding ($\mu = 1.0$)
Plate-Screw (Conventional)	Universal joint	Provide a universal connection between the screw control node and nodes on the bearing surface of the plate.
Plate-Screw (Locked)	Rigid	Provide a rigid connection between the screw control node and nodes on the bearing surface of the plate.

fibula (see Fig. 3.1). The loads include 140 N resultant force (the resultant of the contact forces at the fibulotalar joint) [59], a 100 N lateral force (simulating the cotton test applied during the surgical procedure) [60] and a 7.5 Nm moment (representing external rotation) [60]. To react against the applied loads, the fibula was fixed at the proximal end and restrained along the interosseous membrane at its attachment to the tibia (see Fig. 3.1). These representative forces were applied individually and in combinations as shown in Tab. 3.4a. In the neutralization plate model with conventional screws, a pre-tension of 1000 N was applied to the screws going through the plate and a pre-tension of 500 N was applied to the lag screw across the fracture surface.

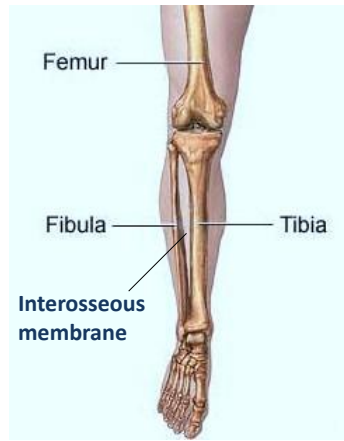
Table 3.4: Load cases and associated displacements

(a) Load combinations

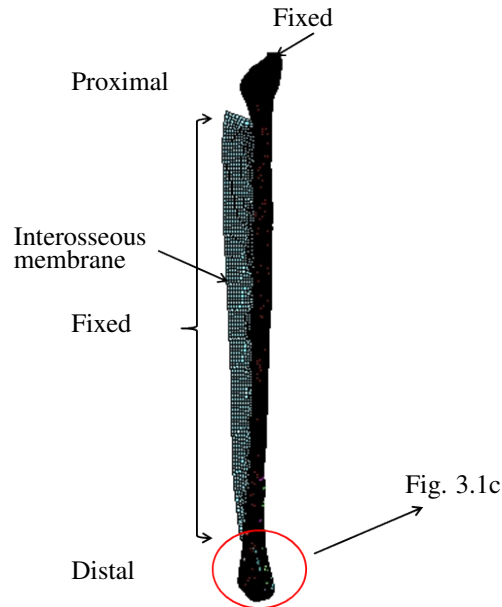
	Load Case 1	Load Case 2	Load Case 3	Load Case 4
Fibulotalar reaction 140 N	X			X
Cotton Test 100 N		X		
External Moment 7.5 Nm			X	X

(b) Comparison of maximum displacement at distal end

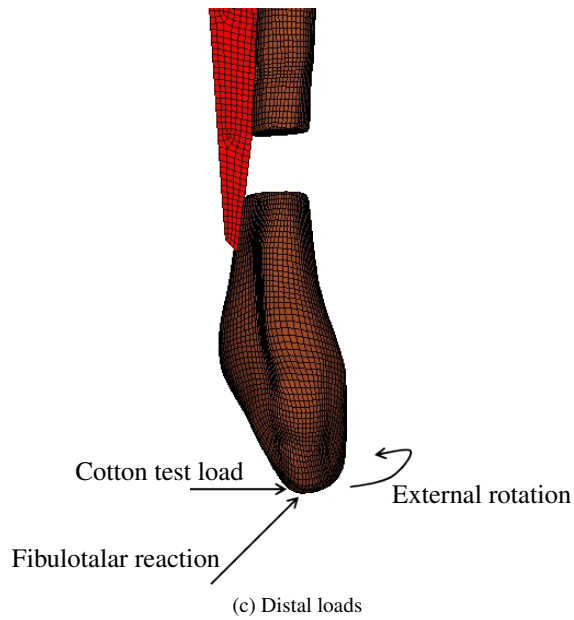
Fracture type	Load Case	Neutralization Plate		Periarticular Plate
		Conventional max. $ \Delta \vec{u} $ (mm)	Locked max. $ \Delta \vec{u} $ (mm)	Locked max. $ \Delta \vec{u} $ (mm)
Comminuted	Case 1	2.02 (Fig. B.1a)	2.07 (Fig. B.1b)	1.26 (Fig. B.1c)
	Case 2	1.67 (Fig. B.2a)	1.68 (Fig. B.2b)	1.20 (Fig. B.2c)
	Case 3	14.27 (Fig. B.3a)	13.99 (Fig. B.3b)	14.55 (Fig. B.3c)
	Case 4	10.66 (Fig. 3.5a)	11.77 (Fig. 3.5b)	12.25 (Fig. 3.5c)
Danis-Weber B	Case 1	1.50 (Fig. B.4a)	1.29 (Fig. B.4b)	1.65 (Fig. B.4c)
	Case 2	1.34 (Fig. B.5a)	1.21 (Fig. B.5b)	1.73 (Fig. B.5c)
	Case 3	7.66 (Fig. B.6a)	8.09 (Fig. B.6b)	6.20 (Fig. B.6c)
	Case 4	6.77 (Fig. 3.6a)	7.13 (Fig. 3.6b)	5.64 (Fig. 3.6c)



(a) Anatomy of fibula



(b) Overview



(c) Distal loads

Figure 3.1: Model overview and applied loads

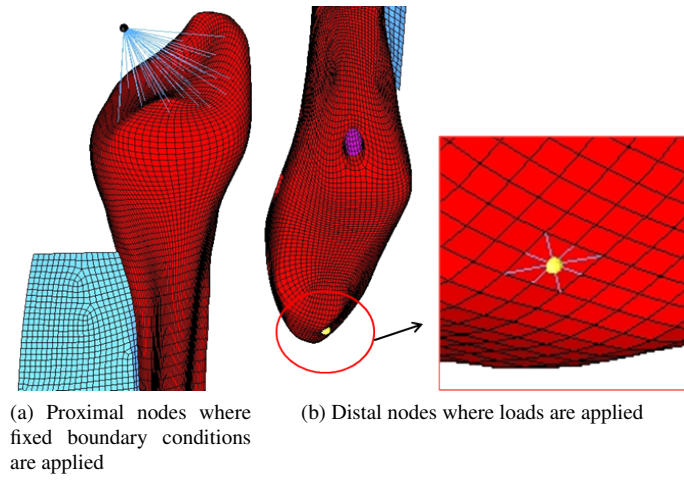


Figure 3.2: Boundary condition and loading techniques

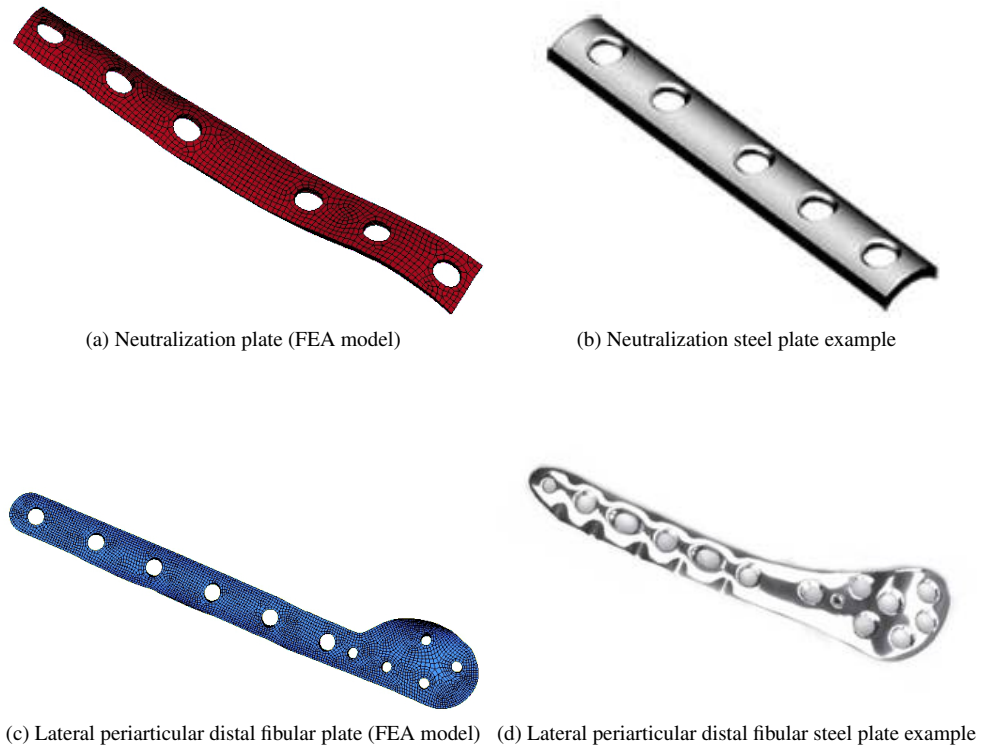


Figure 3.3: Plate types

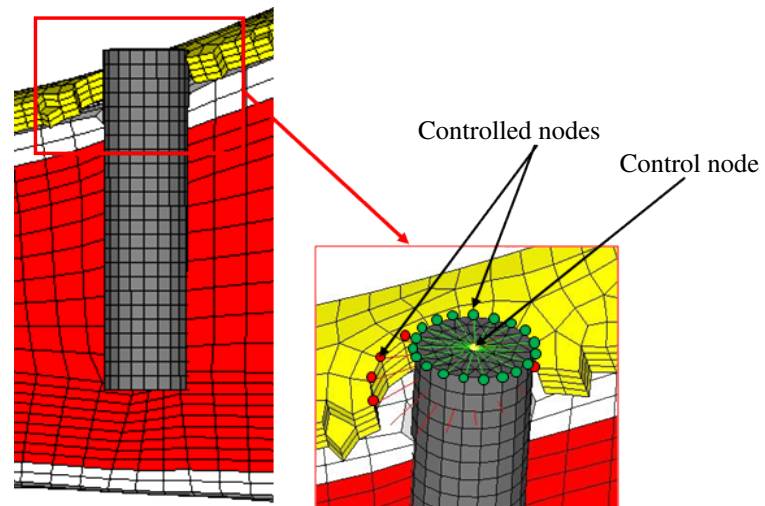


Figure 3.4: Plate-screw relationship in conventional and locked screw constructs

3.2 Results

Two types of comparisons are made to differentiate the stiffness of the plate-screw constructs. First, comparison is made between identical neutralization plates with conventional and locked screw constructs. Thus, the effect of the screw-plate interface is isolated. Then, locked screw constructs are compared for neutralization and lateral periarticular distal fibular plate with locked screws. Therefore, the effects of plate type are isolated. The stiffnesses are compared by contours of surface relative displacement.

3.2.1 Comparison of displacement contours of the distal fibula

Stiffness can be described as the relationship between load and displacement. Thus, the displacement contours in this section are a measure of stiffness for the applied loads. Tab. 3.4 shows predicted displacements for the comminuted and Danis-Weber B fracture for the fibulotalar reaction load, cotton test load, external moment, and combined fibulotalar reaction and external moment loads. In models with screw pre-tension (ie. the neutralization plate with conventional screws), the displacement associated with the pre-tension load has been subtracted from the final displacement. Thus, the reported displacements are associated only with the applied external loads.

The first comparison of displacement is between the neutralization plate with conventional and locked screws (sub-figures (a) and (b) in Figs. 3.5 and 3.6) (*please see appendix section B.1 for rest of the displacement contour plots with comminuted fracture*). The $|\Delta\vec{u}|$ (in mm) is the relative displacement magnitude due to the external loads. When subjected to the same boundary conditions and loads, there is a small difference in displacement at the distal end in the construct (≤ 0.21 mm for applied force loads, ≤ 1.11 mm for load cases with applied external rotation moments). This clinically negligible difference was predicted in both fracture types. Since the plate geometry is identical, the comparison suggests a negligible effect of locked screws on the stiffness of the construct. Since locked screws are commonly assumed to be biomechanically superior to screws that can toggle and because no superiority is found in construct stiffness, the strength of the construct must be assessed and will be modeled in future work.

The second comparison is between the neutralization plate and lateral periarticular distal fibular plate with locked screws (sub-figures (b) and (c) in Figs. 3.5 and 3.6) (*please see appendix section B.2 for rest of the displacement contour plots with weber-B fracture*). Again, the same boundary conditions and loads are modeled for each fracture. The neutralization plate allows more (≤ 0.83 mm) displacement for applied force loads. The displacement due to external rotation moment is higher in the neutralization plate in some cases and lower in others. The maximum difference is 1.89 mm which may be clinically significant if it originates from differences in the local “strains” across the fracture surface. These local strains are examined in the next section. Since the screw heads are locked in these constructs, the stiffness differences must be attributed to plate geometry. The

lateral periarticular distal fibular plate with locked screws is longer, has a wider cross section over a portion of the geometry, and has more screws than the neutralization plate.

Distal fibula displacement comparisons provide a gross measure of the stiffness of the constructs, however, the local relative displacements at the fracture surfaces are more important. Fracture healing is dependent on strain across the fracture surface [61, 62]. Thus, the following section is a comparison of relative fracture surface motion due to external loads.

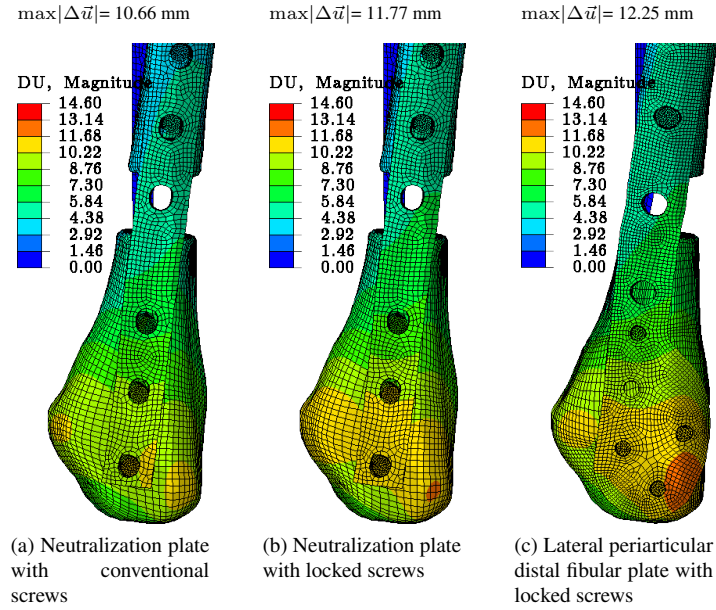


Figure 3.5: Displacement ($|\Delta\vec{u}|$) due to fibulotalar reaction load and external moment with comminuted fracture

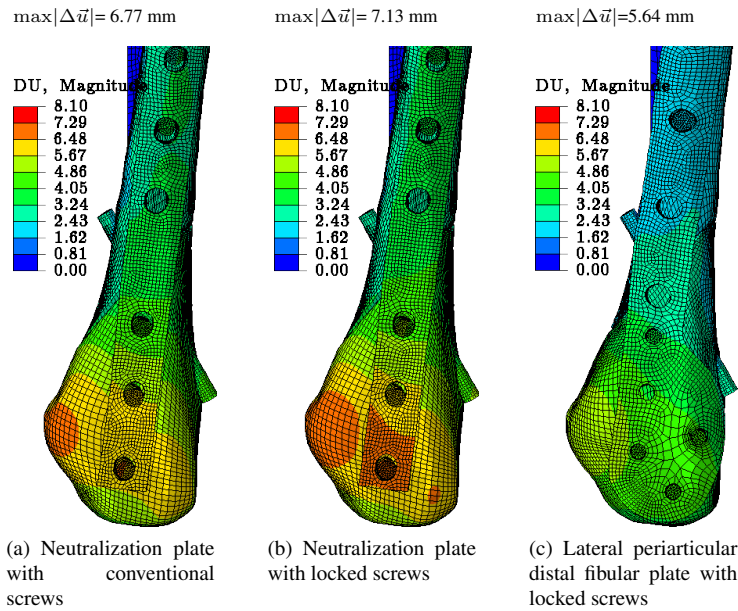


Figure 3.6: Displacement ($|\Delta\vec{u}|$) due to fibulotalar reaction load and external moment with danis-weber B fracture

3.2.2 Comparison of construct stiffnesses about the fracture plane

To investigate the motion of the fracture surfaces, the movements of eight reference nodes on the fracture surfaces (approximately located at the anterior, posterior, lateral and medial apices on each side of the fracture) were observed when subjected to the applied loading conditions. The nodal motion was used to compute the representative motion (i.e. strain) of the fracture surfaces across the fracture surface). These movements are defined in terms of anterior-posterior (A-P) sliding, lateral-medial (L-M) sliding, normal separation and relative rotation of fracture surfaces about the normal to the fracture (see Fig. 3.7). Vector algebra was used to recognize the in-plane and out-of-plane magnitudes and directions of the nodal motion.

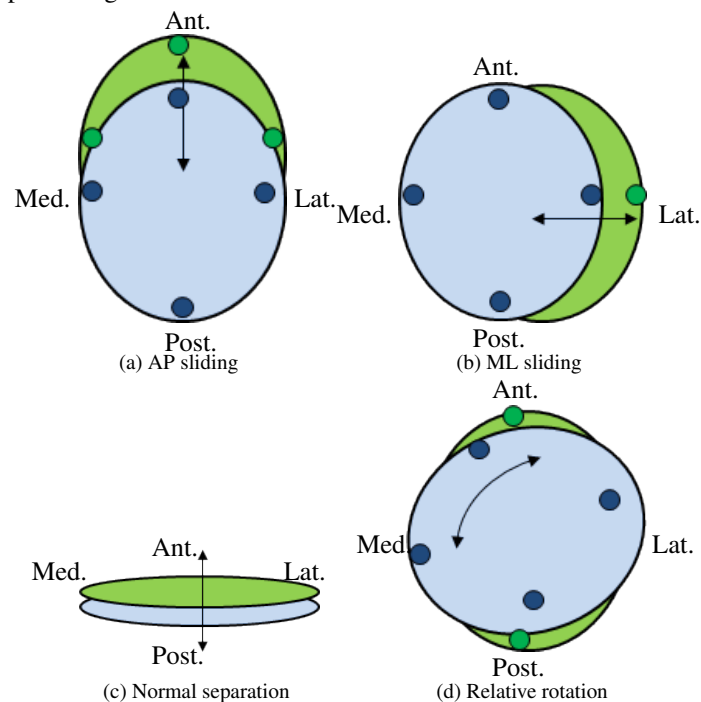


Figure 3.7: Definition of relative motion at fracture surfaces

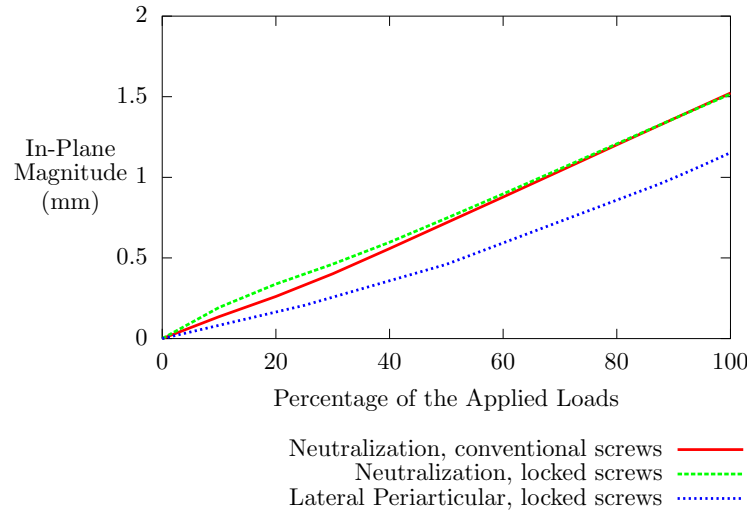
Comminuted fracture

Fig. 3.8 report the constructs' stiffnesses for a comminuted fracture in terms of relative motion across the fracture surfaces due to a combined fibulotalar-moment load. Plots for fibulotalar reaction load, a cotton test load, and an external rotation moment were consistent with Fig. 3.8 (*please see appendix section C.1 for rest of the stiffness comparison plots of comminuted fracture*).

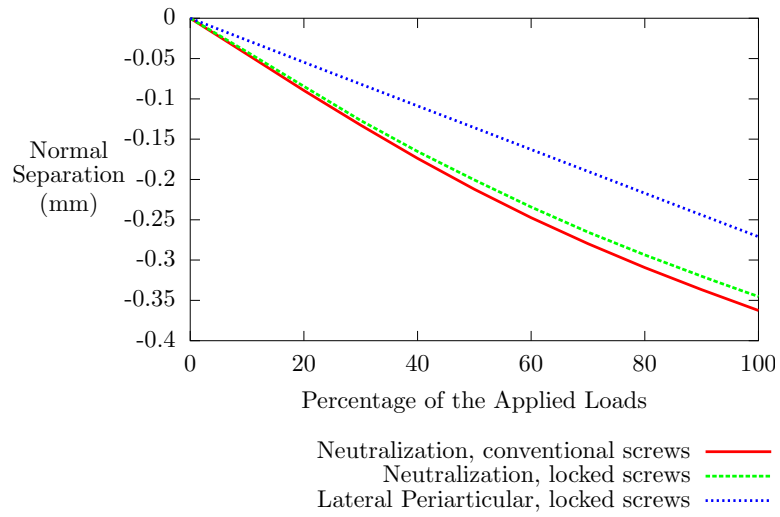
Fig. 3.8 illustrates a key finding: the fracture surface motion is very similar for neutralization plates regardless of the screw-plate interface. The stiffness difference, based on fracture surface motion, is negligible in most cases. This comparison is relevant because it isolates the effects of the screw-plate interface in plates that are otherwise identical. Where the stiffness difference appears to be large (ie Fig. 3.9), the magnitude of the surface motion is clinically insignificant. Differences in in-plane translation are less than 0.01 mm; in-plane rotations differ by less than 1°. Based on the predictions, there is likely no clinical difference in stiffness between locked and conventional

screws for neutralization plates when the assumptions in these models are appropriate.

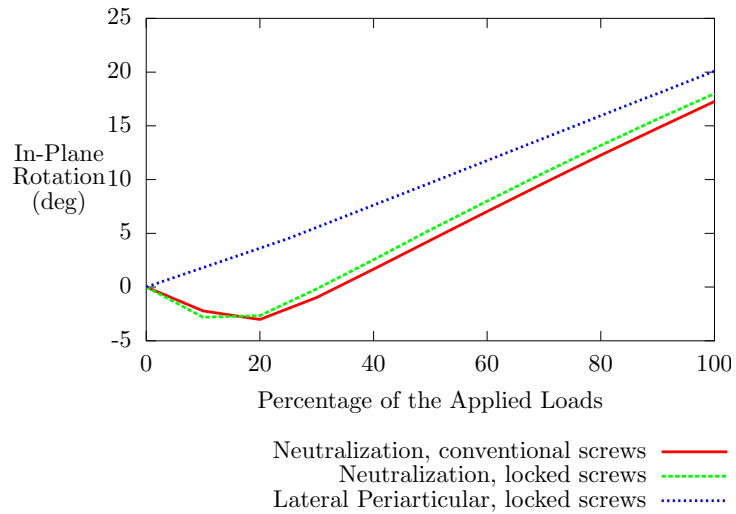
A second observation is also apparent in Fig. 3.8 for the fibulotalar reaction force and external rotation moment: the periarticular plate is as stiff or stiffer than the neutralization plate when subjected to the same loads. This isolates an important difference between the plates since the screw-plate interface is constant in the comparison. Nevertheless, the amplitudes of the fracture surfaces translations and rotations are small. This trend appears to be true for all investigated load cases. Thus, based on stiffness predictions, it appears that either plate construct would be clinically effective at maintaining stability of the fracture reduction. Although clinically relevant, strength predictions have not been completed for these constructs.



(a) Magnitude of the in-plane translation vector



(b) Normal separation



(c) In-plane rotation

Figure 3.8: Relative motion of the comminuted fracture surfaces due to the applied fibulotalar load and external moment

Danis-Weber B fracture

Fig. 3.9 illustrates the constructs stiffnesses for a Danis-Weber B fracture in terms of relative motion across the fracture surfaces due to a combined fibulotalar-moment load. Plots for fibulotalar reaction load, a cotton test load, and isolated external rotation moment are consistent with Fig. 3.9 (*Please see appendix section C.2 for rest of the stiffness comparison plots of danis-weber B fracture*). The trends in fracture surface motion are similar to those of the comminuted fracture, thus they are included for completeness and not described in detail. Predicted values of fracture surface motion do not exceed values that would allow healing (amplitude: $\approx 0.2 - 1$ mm of normal separation [63]).

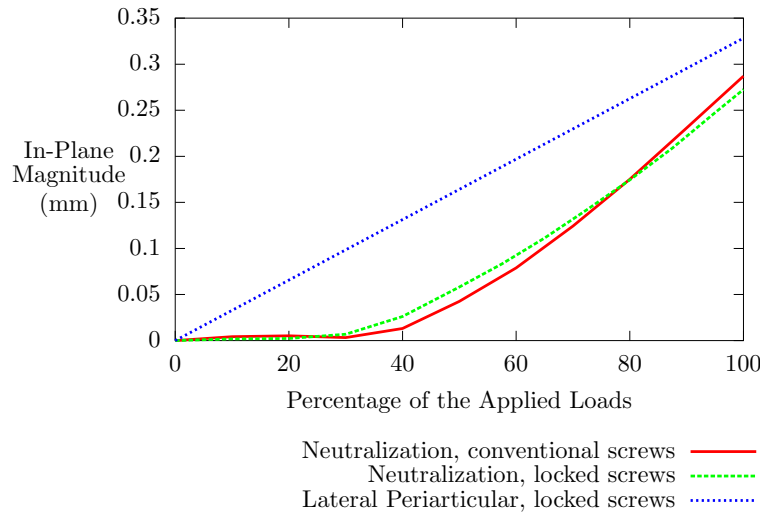
3.3 Validation

An important consideration when clinically interpreting the results of a finite element method biomechanical study is to analyze the reliability and validity of the results. This process includes ensuring that the data is internally consistent as well as consistent with existing literature[64]. Ideally, the results would be prospectively validated by clinical trials.

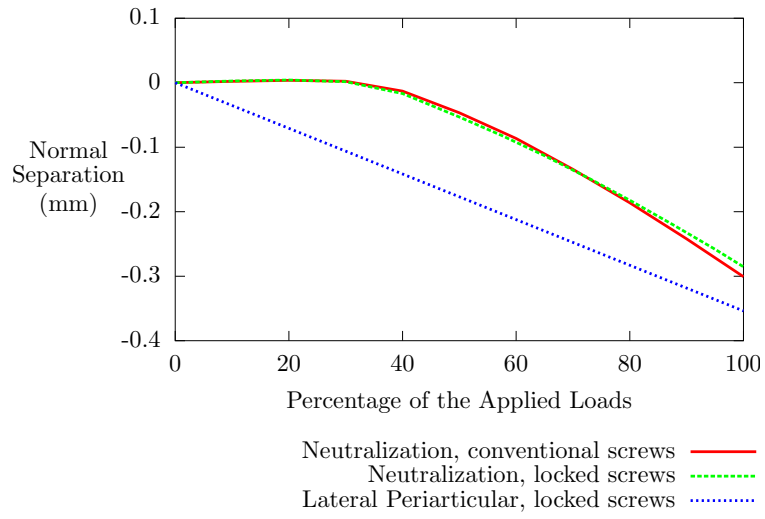
The geometric differences between the neutralization plate and the lateral periarticular distal fibular plate with locked screws are expected to produce different stiffnesses (based on simple structural mechanics principals). Since the periarticular locking plate is longer, wider (in places), made of the same material, and has more screws to achieve purchase with bone, it is expected to be as stiff or stiffer than the neutralization plate. Therefore, the finite element models are self-consistent in that the periarticular plate is predicted to be as stiff or stiffer. This behavior is noted on all simulated load cases and provides level 1 evidence² as described by Brown [64]. In addition, the clinical studies have demonstrated that the elastic motion at the fracture site and bending stiffness are influenced by length and cross-sectional area of the plate, diameter of the screws and unicortical versus bicortical screws ([10, 11, 65]), which provides additional level 3 evidence.

It is intuitive that an external rotation moment would cause a rotational displacement about the normal direction as was found in the current study. In Fig. 3.9c, a physiologic external moment (7.5 Nm) is predicted to cause a 2-4° in-plane rotation in a Danis-Weber B fracture. This value is consistent with the existing literature. Schaffer et al[66] used cadaveric bone and found that a 40 Nm Torque (5.3x the value used in this paper) produced a 20° (5-10x the value predicted in this paper) in-plane rotation. The comparison is not ideal since cadaveric bone was used (presumed to have different structural properties), some soft tissues were included, and inter-fragmentary lag screws were not used in all load cases. Although it is not appropriate to apply precise quantitative comparison of the results of the current study with those of Schaffer, qualitative comparison shows consistent results when the differences in study methods are considered. Thus, the comparison provides additional level 3 evidence.

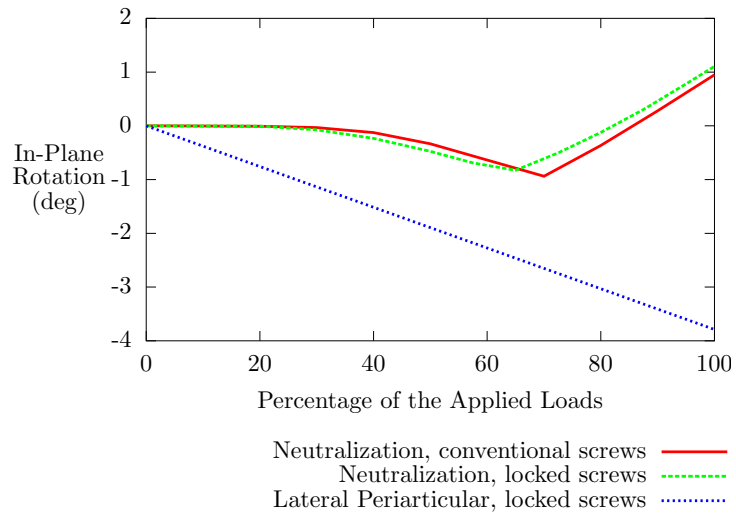
²Brown [64] described five levels of evidence 1-5 with 5 being the highest quality evidence.



(a) Magnitude of the in-plane translation vector



(b) Normal separation



(c) In-plane rotation

Figure 3.9: Relative motion of the Danis-weber B fracture surfaces due to the applied fibulotalar load and external moment

3.4 Clinical relevance

The results in this study provide displacement and stiffness comparisons between locked and conventional screw constructs for neutralization plates and lateral periarticular distal fibular plates with locked screws. The stiffness and the strength of a construct are clinically relevant to both the surgeon and the patient. During a surgical procedure after the construct is placed, the surgeon may apply a force to the distal fibula and “feel” the resulting displacement (ie the cotton test) to judge whether adequate fixation has been achieved and the need for further fixation. Thus, the stiffness influences surgical decision making and may cause or prevent the application of more invasive implants. Each additional implant adds time and cost to the procedure, thus, the stiffness affects health care costs in addition to patient outcomes.

During the recovery phase after surgery, both stiffness and strength are relevant to the patient and surgeon. In the fracture healing process, some displacement at the fracture site is beneficial in order to stimulate the body to heal the fracture [67]. This process whereby the bone forming units of the body sense strain and produce a physiologic response that produces bone, requires something less than 10% strain [68]. Thus, the fracture gap and the amplitude of movement should generally be kept small (amplitude: \approx 0.2-1 mm and fracture gap $<$ 2 mm) [63]. This movement is directly related to the stiffness of the construct. The fracture stiffness measurement is considered a non invasive method of fracture healing and union [37] as the healing time showed good agreement of the interfrangmentry movement compared with in vivo measurements [38, 39, 40, 41]. Strength is also necessary to avoid implant or construct failure prior to fracture healing.

3.5 Conclusions

It has been demonstrated that there is a negligible difference in construct stiffness between conventional and fixed angle screw constructs for a five screw neutralization plate when the plate geometry is identical. Thus, locked screw heads do not offer superiority in the biomechanical stiffness of the plate. This result is significant to clinical practice as the stiffness is used to judge stability and quality of fixation.

A locked fibular neutralization plate allowed more displacement of the distal fibula than was allowed by the lateral periarticular distal fibular plate with locked screws. Thus, the stiffness of the construct was found to be dependent on plate geometry and/or the number of screws used to hold the fracture. Although the difference in stiffness between these plates is expected, this result is self-consistent and provides a level of validation of the method used in the study. It also indicates that the lateral periarticular distal fibular plate may have advantages over the neutralization plate when greater stiffness is required.

Chapter 4

Device influence on healing environment: Strength of conventional and locking screw-plate constructs

Plate-screw constructs, used to stabilize a fractured bone, undergo various physiological loads. Therefore, in this chapter, the strength of the *screw* constructs are evaluated under pure normal, combined shear and normal (oblique), and pure shear loads applied at the plate end (Fig. 4.1). Finite element analysis and experiments were performed to evaluate the non-locking and locking plate-screw constructs strengths.

Pullout and shear strength are among the failure metrics used to evaluate the plate-screw fixation strength. This is consistent with the previous published studies as well as ASTM standards [69, 70]. Failure of the construct can be dependent on the factors such as, physiological load, screw geometry, screw-plate interface, bone density and thickness of the cortical bone layer. Thus, finite element analysis and experiments were performed on commercially available polyurethane foam with 0mm, 1mm and 2mm cortical thicknesses. The absence of a cortical bone (0mm) represents the extreme case of osteoporosis where a very thin cortical shell has a negligible contribution to the bone strength.

4.1 Experimental investigation of screw construct strength

This section includes the experimental investigations performed on commercially available polyurethane foam. The strength of locking and non-locking screw constructs were evaluated under applied oblique, normal and shear loads. The foam specimen with 0mm and 1mm cortical thicknesses were evaluated.

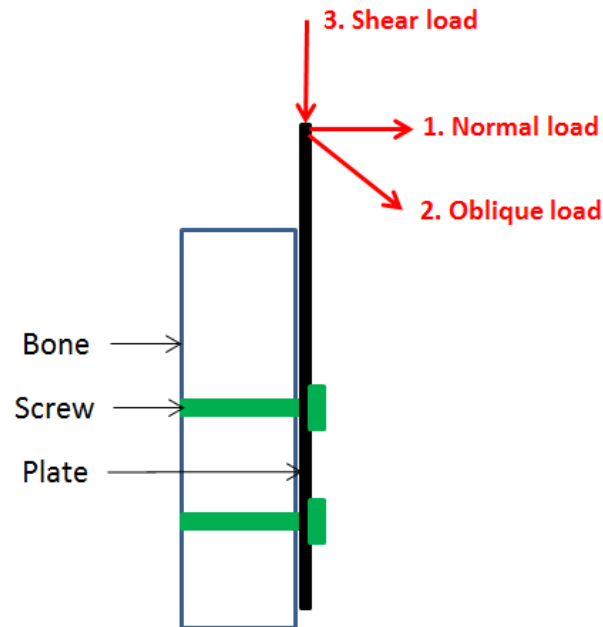


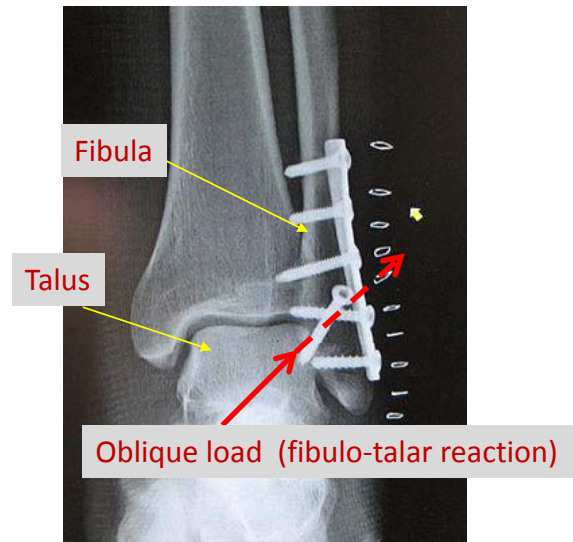
Figure 4.1: Load patterns on plate-bone constructs

4.1.1 Oblique load

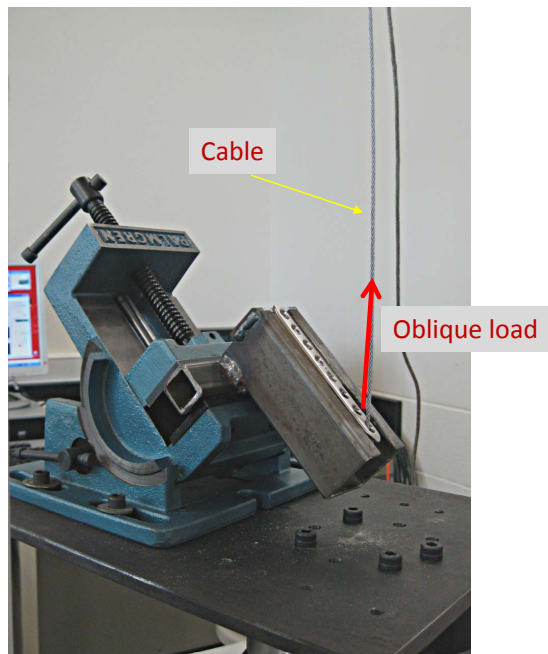
Construct strength without cortical layer

The oblique loading pattern was used because typical physiologic reaction force and load at the joints and bones (Fig. 4.2a) are rarely parallel or normal to the screw axis [58].

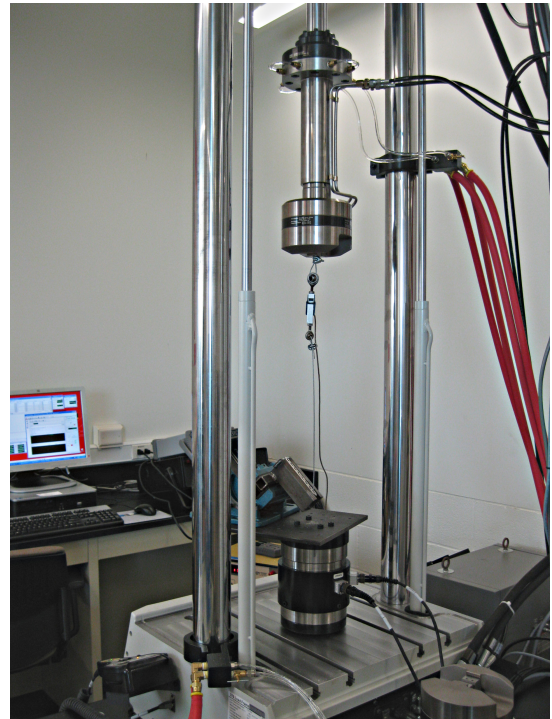
The bone surrogate used in this study consisted of commercially available polyurethane based foam (Sawbones, Pacific Research Laboratories, Vashon Island, WA, USA). Three densities of closed cell foam were used representing differing levels of osteoporotic cancellous bone (0.08 g cm^{-3} , 0.16 g cm^{-3} , and 0.32 g cm^{-3}). The foam sheets were processed into 40 mm by 40 mm by 60 mm specimens for experimental use. The sample size was selected based on ASTM standards and published papers [53, 70]. Bone surrogate was used to represent cancellous bone because of its uniform and consistent material properties compared to the variability and difficulty in handling fresh or cadaveric bone [71, 72]. The use of synthetic foam as a cancellous bone surrogate is well established for experimental characterization of bone and screw failure [43, 42, 73, 74, 45, 75].



(a) Oblique reaction load in fibular fracture fixation

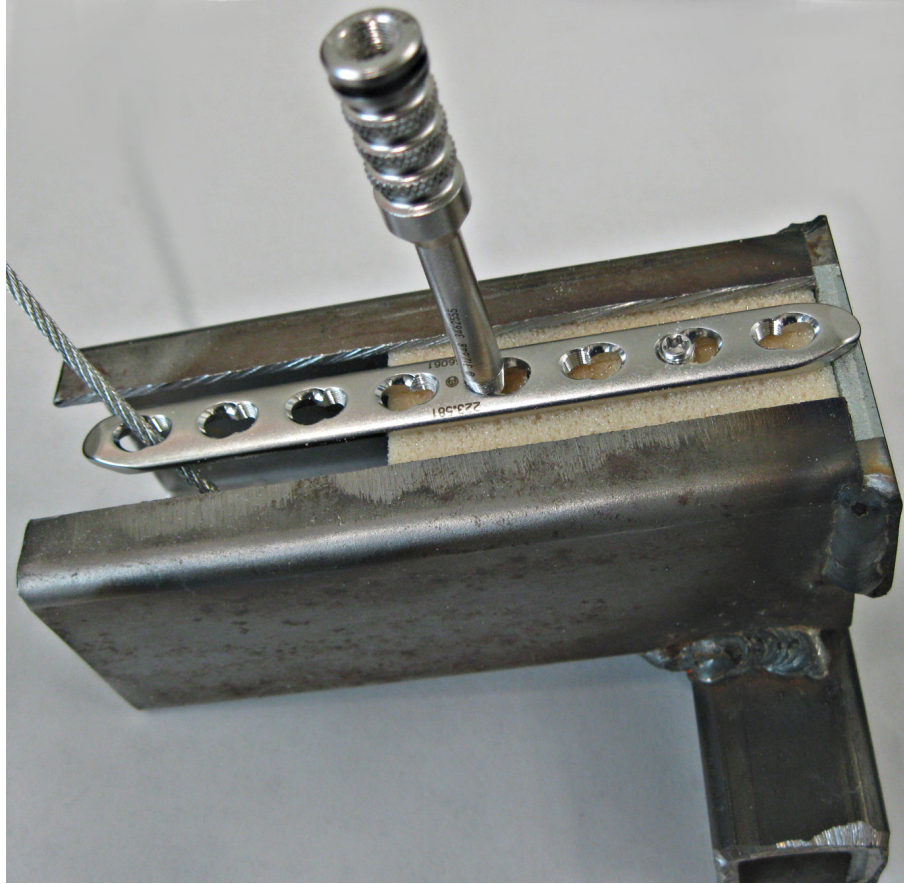


(b) Fixture

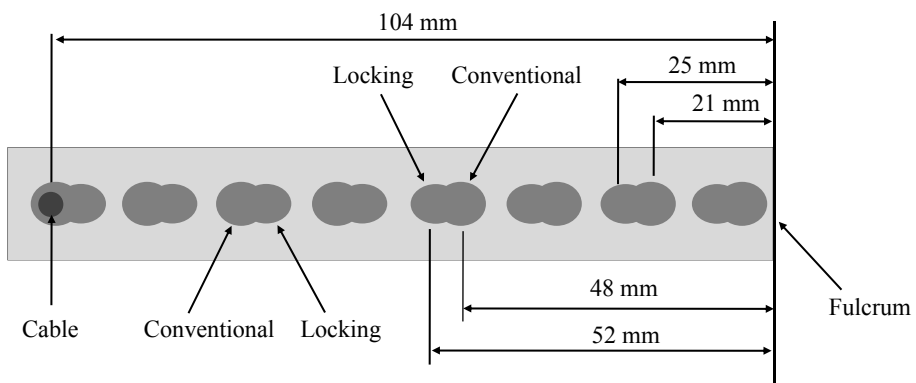


(c) Overview of experimental setup

Figure 4.2: Experimental setup for oblique load pullout



(a) Fixture including bone surrogate, plate, locking screw and locking drill guide



(b) Screw locations relative to the fulcrum (in mm)

Figure 4.3: Fixture for surrogate bone and plate dimensions

The experimental setup for strength under oblique loads consisted of a hybrid bone fixation plate (having locking and conventional screw holes), screw mounted on bone surrogate specimens and a fixture (Fig. 4.3a). The fixture was mounted to a Bionix servo-hydraulic testing frame (MTS Systems Corp, Eden Prairie, MN, USA). A force was applied to the plate with a 2.4 mm diameter steel cable through the eighth hole in the plate. The pullout load was measured with a 500N load cell placed in-line with the steel cable. The load was applied with traverse rate of 5mm/min [45]. This pull-out rate was selected from a previous study by Zedro et al [45], who studied the effects of pull-out rate on failure load. The data was acquired at a rate of 128 Hz.

For the locking screw and plate construct, two locking screws were inserted in the second and fourth locking hole positions of the plate (Fig. 4.2 and Fig. 4.3a). 2.8 mm pilot holes were drilled through a drill guide into the bone. A 32 mm 3.5 mm diameter, self-tapping locking screw was used in each hole. For the conventional screw and plate construct, two conventional cancellous bone screws were assembled in the second and fourth hole positions of the plate. A 32 mm, 4.0 mm diameter, fully threaded cancellous bone screw was used in each 2.5 mm pilot hole.

Statistical calculations were made using R, a statistical software package (<http://www.r-project.org/>). The two way anova analysis was performed to evaluate the main and interaction effect of bone density and a screw construct type on failure load.

Results

It was observed that in both the conventional and locking constructs the construct strength increased with increasing bone density. The experimental load-displacement curves for both constructs in the 0.08 g cm^{-3} and 0.16 g cm^{-3} specimens are shown in Fig. 4.4. The mean strength of each of these is given in anova box and whisker plot (Fig. 4.5). For both densities (0.08 g cm^{-3} and 0.16 g cm^{-3}), the conventional plate and screw construct had a greater strength than the locking plate and screw construct ($61.8 \pm 9.8 \text{ N}$ vs $46 \pm 5.3 \text{ N}$, $p=0.014$) and $161 \pm 26 \text{ N}$ vs $127 \pm 14 \text{ N}$, $p=0.011$). The plate experienced plastic deformation for 0.32 g cm^{-3} density specimen, so tests for this density were not repeated due to limited supply of plates.

For both the 0.08 g cm^{-3} and 0.16 g cm^{-3} specimens, there was a statistically significance difference (p values of 0.014 and 0.011 respectively) between the two constructs which demonstrated that the conventional plate and screw construct had a greater strength than the locking plate and screw construct. Moreover, the parallel (non-intersecting) lines in the interaction plot (Fig. 4.6) shows that there is no interaction between the construct type and bone density i.e, irrespective of the density the conventional screw construct was stronger than locked screw construct.

Video observation of the experiments demonstrated that the conventional screw-plate constructs failed by pullout and the locking screw-plate constructs failed by a combination of initial pullout followed by cut out. This is reflected on the load-displacement curves as a sharp drop in the load (pullout failure) followed by a second, usually lower, sustained peak strength follow by a slow failure (cut out failure). The observed cancellous pullout failure as

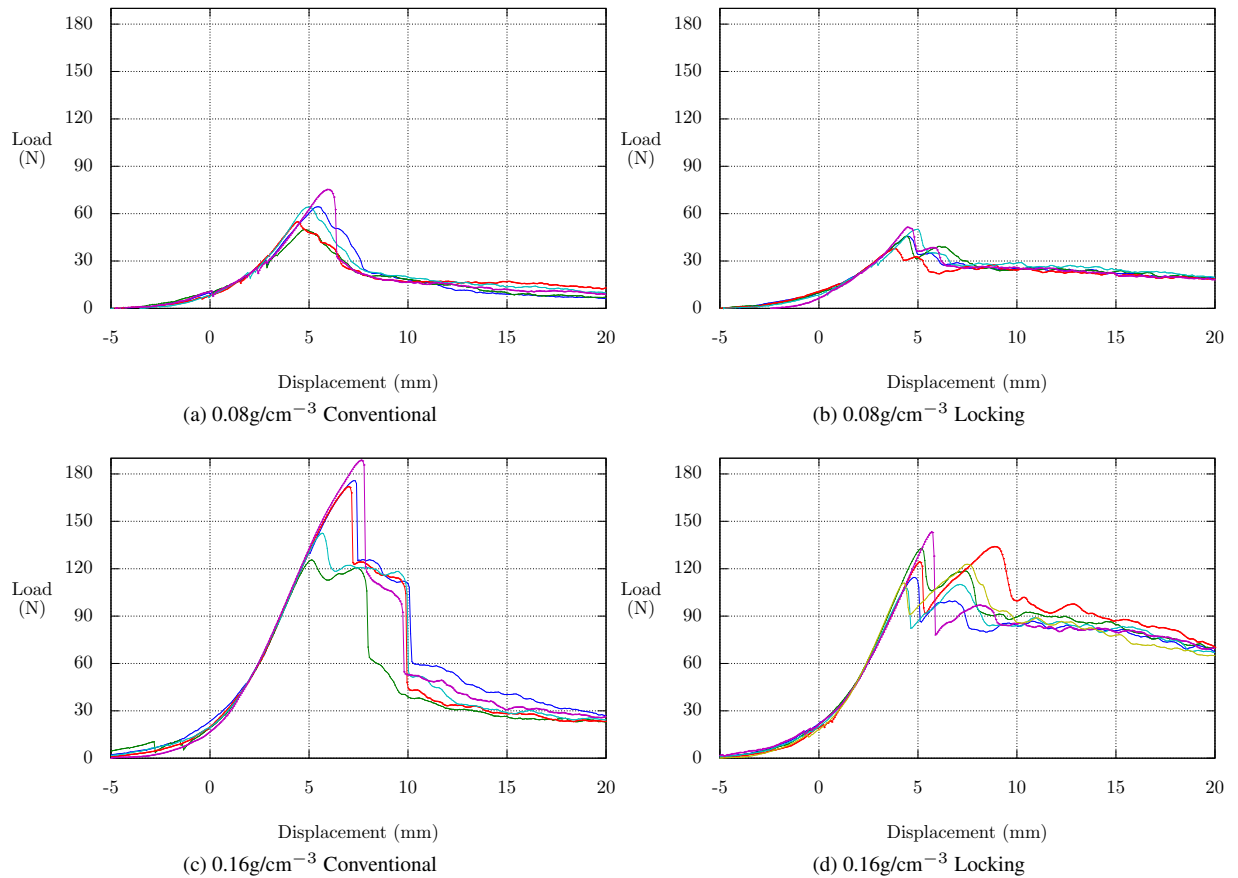


Figure 4.4: Experimental results for oblique load (without cortex)

well as analysis of extracted material between the threads is consistent with that observed by Chatzistergos [76].

This study finds a difference in the strength between conventional and locking plate constructs in synthetic osteoporotic bone. The conventional plate and screw constructs showed a greater strength than locking plate and screw constructs. The difference was statistically significant in both osteoporotic densities that had sufficient test data. This finding is contrary to the common assumption that locking plate constructs will provide greater strength in osteoporotic bone. However, it is consistent with the literature when other factors are considered including the major diameter and screw pitch of the screw.

Screw design is an important contributor to the results of this study. The screw designs in this study were selected because they are common combinations used clinically. This study demonstrates and confirms the importance of screw design on construct strength. While much attention has been paid to developing locking plate technology, screw design continues to prove itself worthy of future research. The implants available to surgeons should therefore include several screw designs for each clinical scenario and for each type of plate-screw construct.

In addition, the failure mechanism depends on the loading scenario in addition to the construct. A common orthopaedic mantra, “locking screws fail by cut out and conventional screws fail by pullout”, is not wholly accurate. This may hold for plates attached to cylindrical bones and loaded axially (i.e. load perfectly parallel to screw axis)

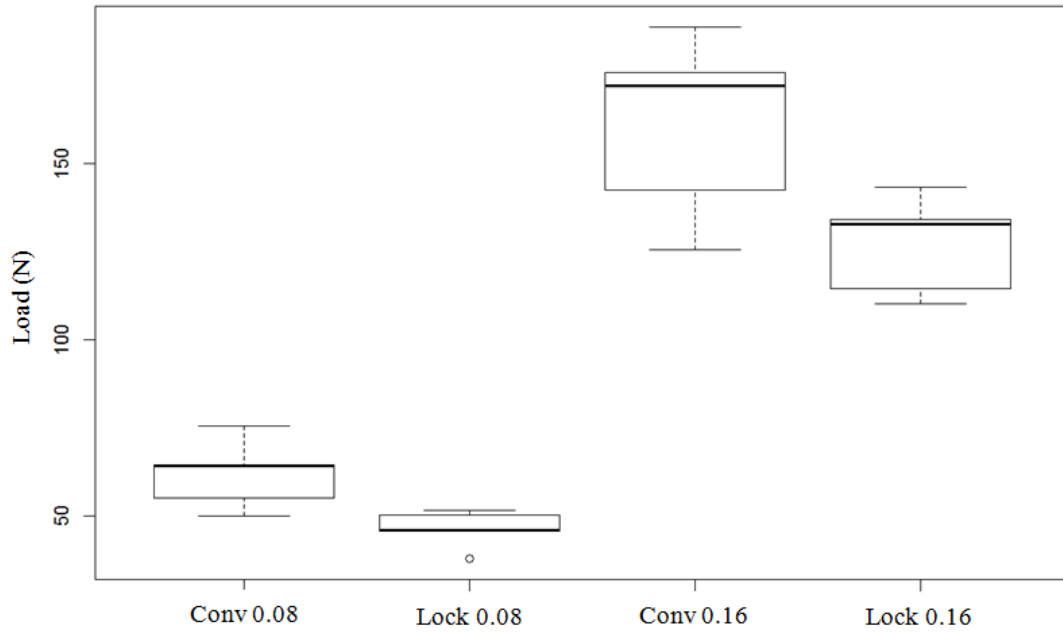


Figure 4.5: Box and whisker plot for peak (failure) oblique load (without cortex)

[22]. However, failure of the constructs is dependent on physiological load combinations and construct design. The shear load causes the locking screws to cut out of the bone where the conventional screws may pull out. However, under axial load both will fail by pure pullout. Thus, screw design is likely more important than the screw-plate interface. The load- deformation curves for this oblique loading pattern, disagree with the argument that locking plate biomechanics are better independent of bone density. Moreover, the parallel lines in the interaction plot (Fig. 4.6) of anova outcomes demonstrates that there is no interaction effect between the bone density and the screw-plate interface type. Thus, irrespective of the bone density always the conventional screw construct had the greater strength.

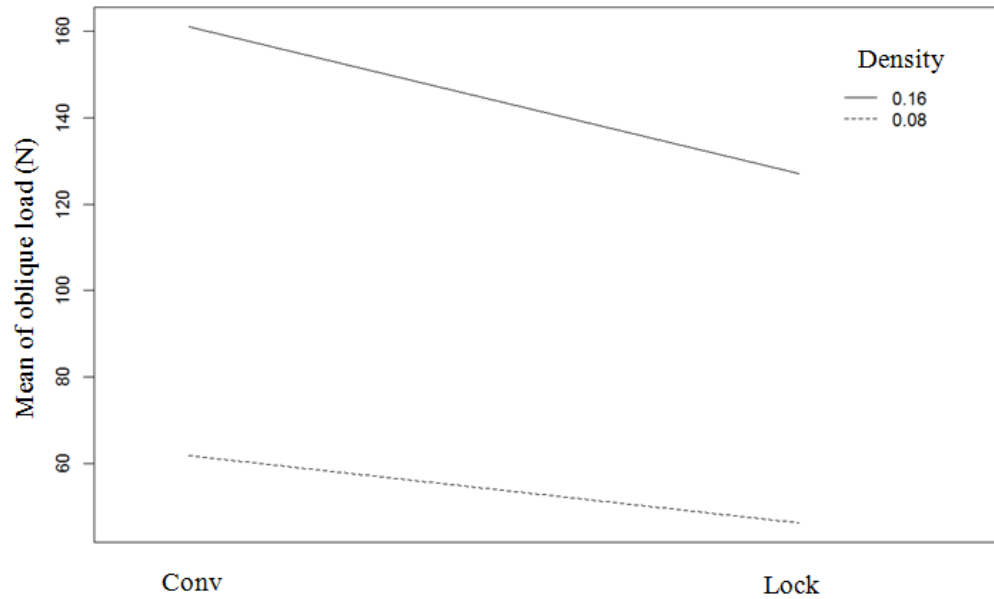


Figure 4.6: Interaction effect between construct type and bone density for oblique load (without cortex)

Construct strength with 1mm thick cortical layer

The oblique load experiment was repeated for a synthetic osteoporotic bone with 1mm cortical thickness (Fig. 4.7). The cortical layer consisted of short-fiber-filled epoxy sheets of 1.64 g cm^{-3} density. The cancellous bone was of 0.08 g cm^{-3} density. It was observed that with a cortical bone layer, the locked screw construct has a marginally higher mean strength ($167 \pm 14.7 \text{ N}$ vs $154 \pm 9.4 \text{ N}$, $p=0.053$) (Fig. 4.8). Moreover, the added cortical bone significantly increased the failure load for both conventional and locked constructs ($61.8 \pm 9.8 \text{ N}$ vs $167 \pm 14.7 \text{ N}$ and $46 \pm 5.3 \text{ N}$ vs $154 \pm 9.4 \text{ N}$). It was also observed that the conventional screw-plate constructs failed by pull out and the locking screw-plate constructs failed by a combination of initial pull out followed by the cutout (Fig. 4.9). The cortical bone caused the cutout force to be higher compared to the pullout force.



Figure 4.7: Experimental setup for oblique load pullout with cortical bone layer

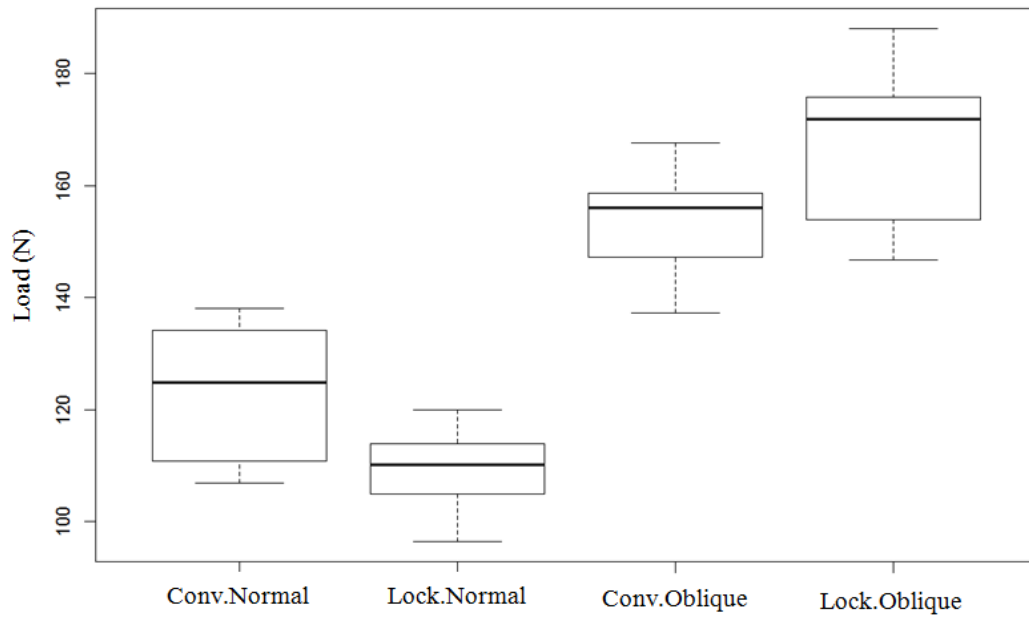


Figure 4.8: Box and whisker plot for normal and oblique peak (failure) load (with cortex)

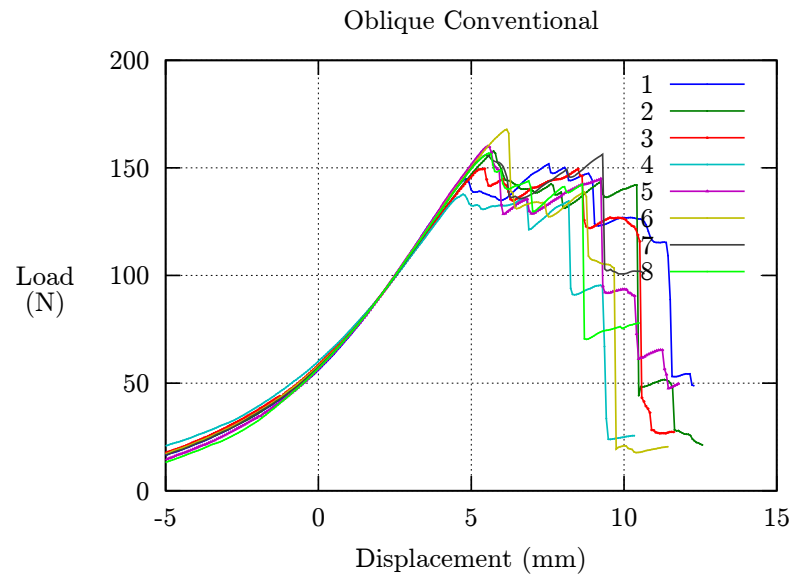
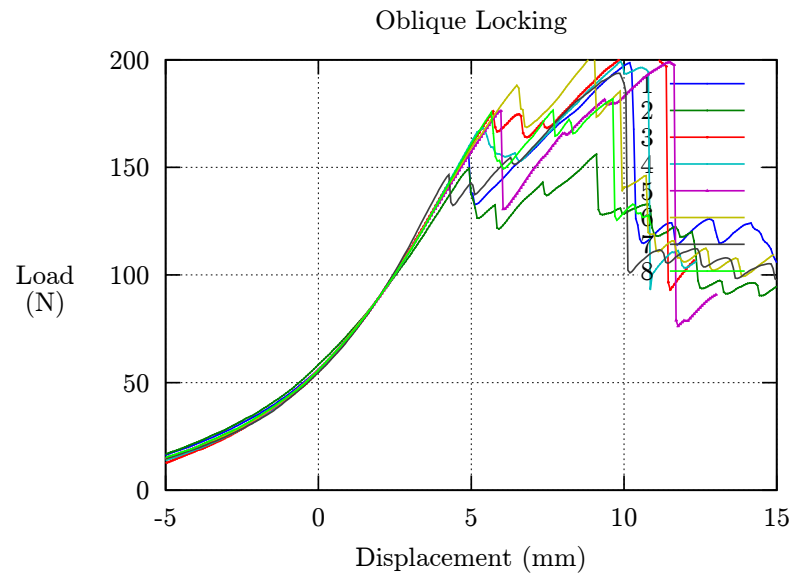
(a) 0.08g/cm^{-3} Conventional(b) 0.08g/cm^{-3} Locking

Figure 4.9: Experimental results for oblique pull (with cortex)

4.1.2 Normal load

Construct strength without cortical layer

The experiment under normal load was performed with the similar experimental setup as the oblique pullout. The normal load was applied at 90 ° to the plate (Fig. 4.10). For both densities (0.08 g cm^{-3} and 0.16 g cm^{-3}), the conventional plate and screw construct had a greater strength than the locking plate and screw construct ($47.8 \pm 2.9 \text{ N}$ vs $32.6 \pm 6.7 \text{ N}$, $p=0.0017$ and $128 \pm 10.6 \text{ N}$ vs $104.8 \pm 8.1 \text{ N}$, $p=0.011$) (Fig. 4.11). There was a statistically significance difference (p values of 0.0017 and 0.011 respectively) between the two constructs which demonstrated that the conventional plate and screw construct had a greater strength than the locking plate and screw construct. Moreover, the parallel (non-intersecting) lines in the interaction plot (Fig. 4.12) shows that there is no interaction between the construct type and bone density i.e. irrespective of the density the conventional screw construct was stronger than locked screw construct.



Figure 4.10: Experimental setup for normal load pullout with 1mm thick cortical layer

Construct strength with 1mm thick cortical layer

The normal load experiment was repeated for a synthetic osteoporotic bone with 1mm cortical thickness. It was observed that with a cortical bone, the conventional construct was statistically stronger ($123 \pm 13.1 \text{ N}$ vs $108 \pm 7.6 \text{ N}$, $p=0.021$) (Fig. 4.8). Similar to what was observed in case of the oblique load, an addition of the cortical bone significantly increased the pullout strength for both conventional and locking constructs ($47.8 \pm 2.9 \text{ N}$ vs $123 \pm 13.1 \text{ N}$ and $32.6 \pm 6.7 \text{ N}$ vs $108 \pm 7.6 \text{ N}$)

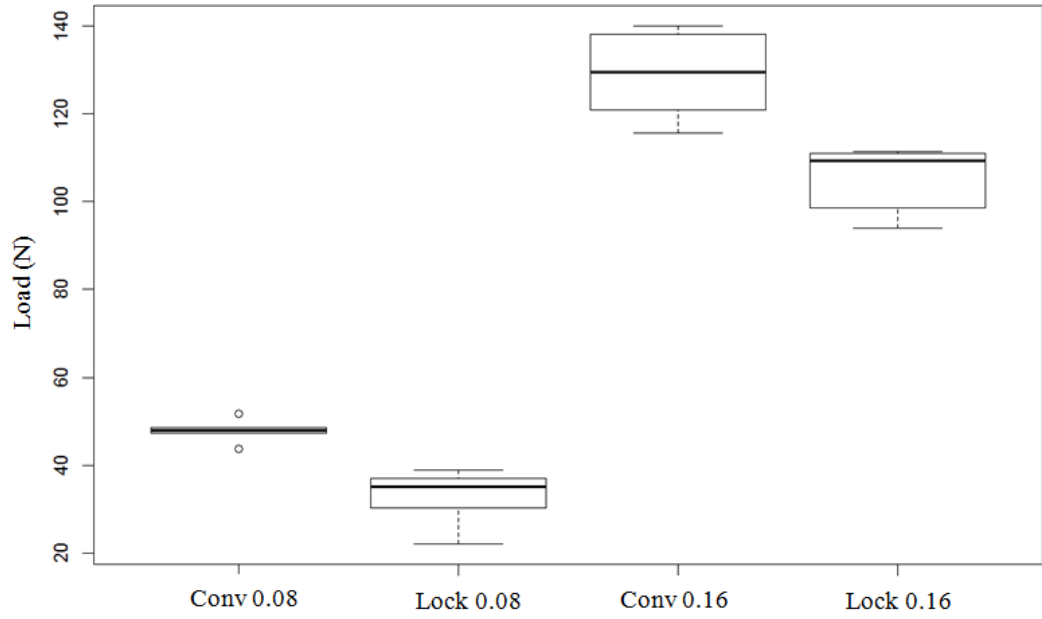


Figure 4.11: Box and whisker plot for peak (failure) normal load (without cortex)

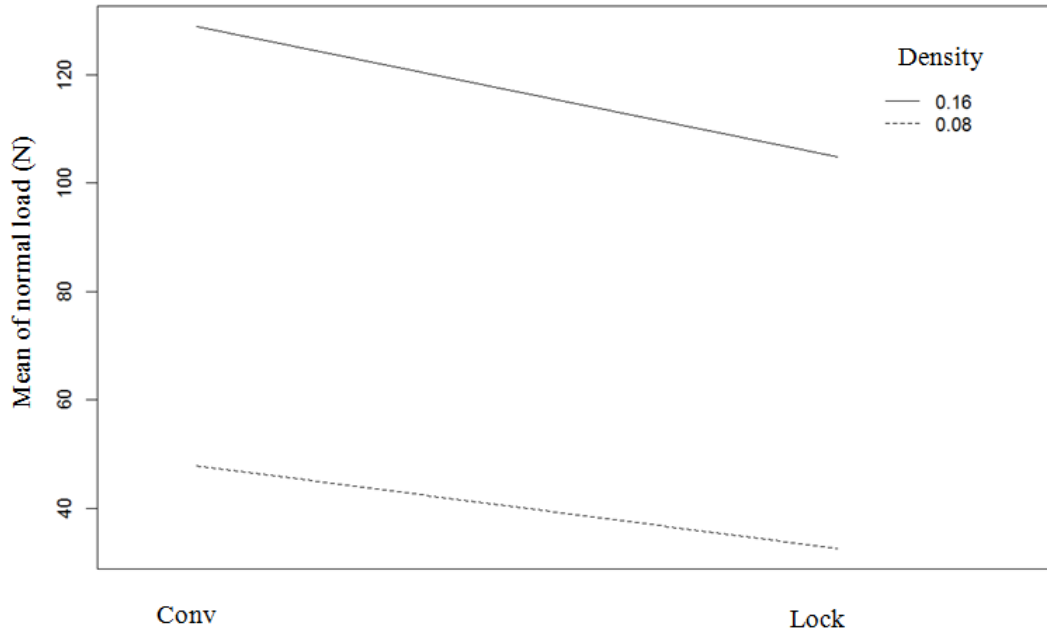
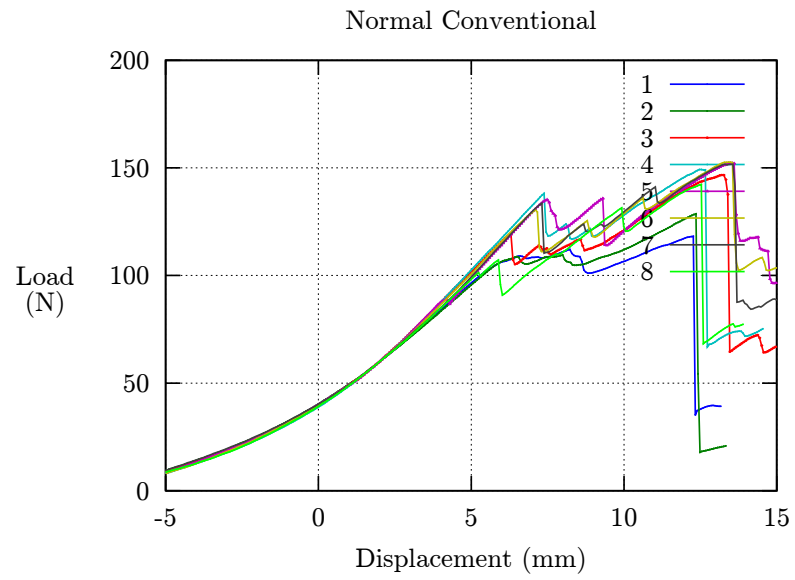
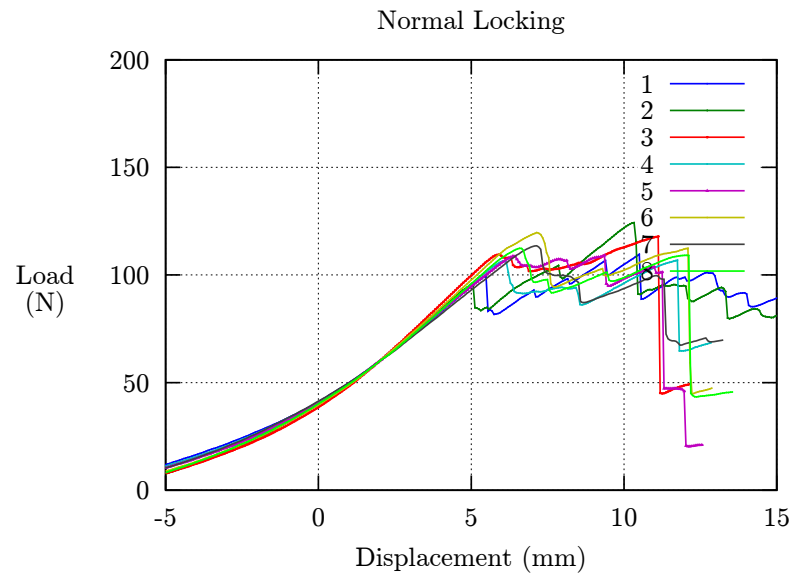


Figure 4.12: Interaction effect between construct type and bone density for normal load (without cortex)



(a) 0.08g/cm^{-3} Conventional



(b) 0.08g/cm^{-3} Locking

Figure 4.13: Experimental results for normal pull (with cortex)

4.1.3 Shear load

Construct strength without cortical layer

The shear load was applied along the plate length (Fig. 4.14). The load frame crosshead was advanced at 5 mm/min to a displacement of 50 mm. The strength of the construct under shear load was investigated only with 0.08 g cm^{-3} cancellous bone density due to the observed screw plastic deformation with the greater cancellous bone densities and limited supply of the screw and plates. The shear strength of the locking screw construct was significantly higher compared to the conventional screw construct ($262 \pm 35 \text{ N}$ vs $145 \pm 27 \text{ N}$, $p=0.001$) (Fig. 4.15) which is opposite to what was observed under normal and oblique loading, where the conventional screw construct had the greater strength. Under pure shear loads the screw plate interface type greatly affects the strength of the construct. The screw diameter and pitch may not have a significant effect on the construct strength under pure shear loads as screw pitch or thread surface area has a relatively lower contribution against bone shear perpendicular to the screw axis.



Figure 4.14: Experimental setup for shear load

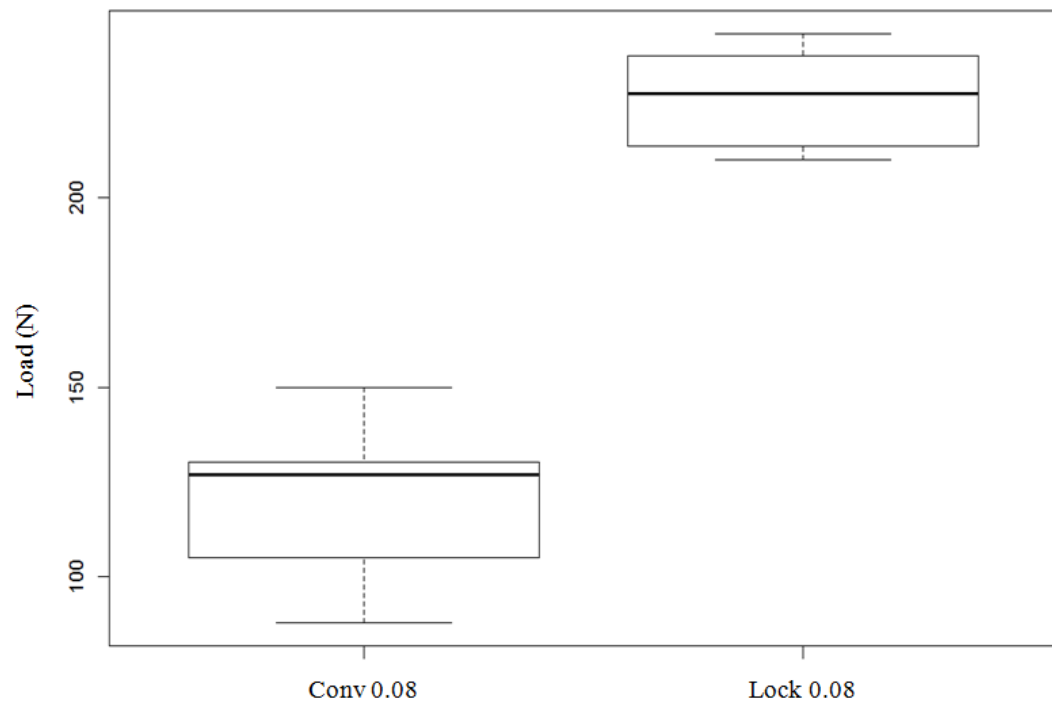


Figure 4.15: Box and whisker plot for peak (failure) shear load (without cortex)

Construct strength with 1mm thick cortical layer

The shear load experiment was repeated for a synthetic osteoporotic bone with 1mm cortical thickness. It was observed that with a cortical bone, the locking screw construct was statistically much stronger (1450 ± 257 N vs 910 ± 236 N, $p=0.001$) (Fig. 4.17). Similar to what observed in case of the oblique and normal loads, the addition of the cortical bone significantly increased the shear strength for both conventional and locking constructs. (1450 ± 257 N vs 262 ± 35 N and 910 ± 236 N vs 145 ± 27 N). Thus, the cortical bone had a significant contribution to construct strength under shear load.

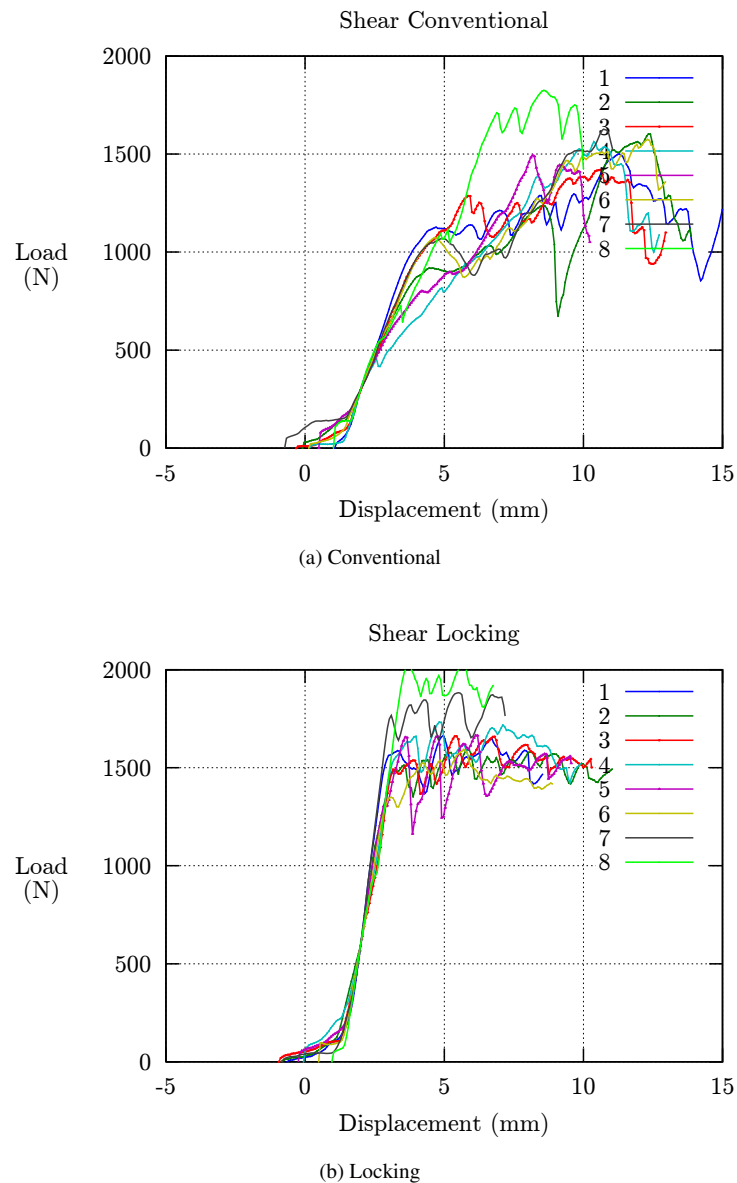


Figure 4.16: Locking and conventional constructs under shear load (with cortex)

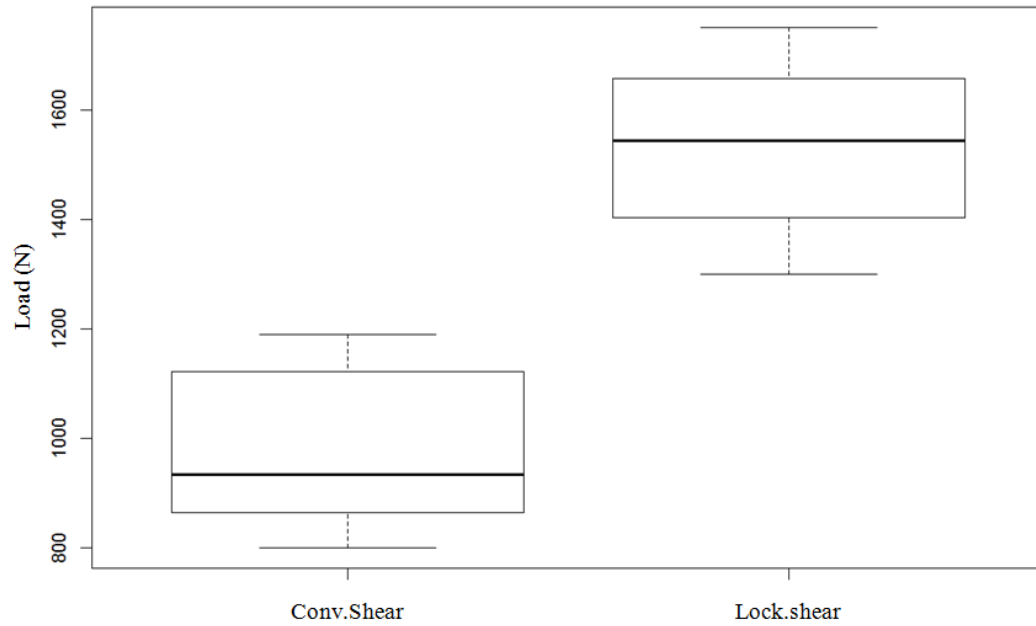


Figure 4.17: Box and whisker plot for peak (failure) shear load (with cortex)

4.1.4 Effect of cortex on load angle vs. construct type relationship

The interaction plots for the specimen with and without cortex show the interaction effect between the load type (normal vs oblique) and construct type (conventional vs locked). Parallel lines in Fig. 4.18 indicated that the load type did not have any interaction with construct type when there was no cortex. Thus, for both normal and oblique loads the conventional screw construct was stronger. However, the diverging (but not intersecting) lines in Fig. 4.19 showed weak interaction effect when cortex was present. Thus, the conventional screw construct was stronger under normal load and the locked screw construct had a greater strength under oblique load.

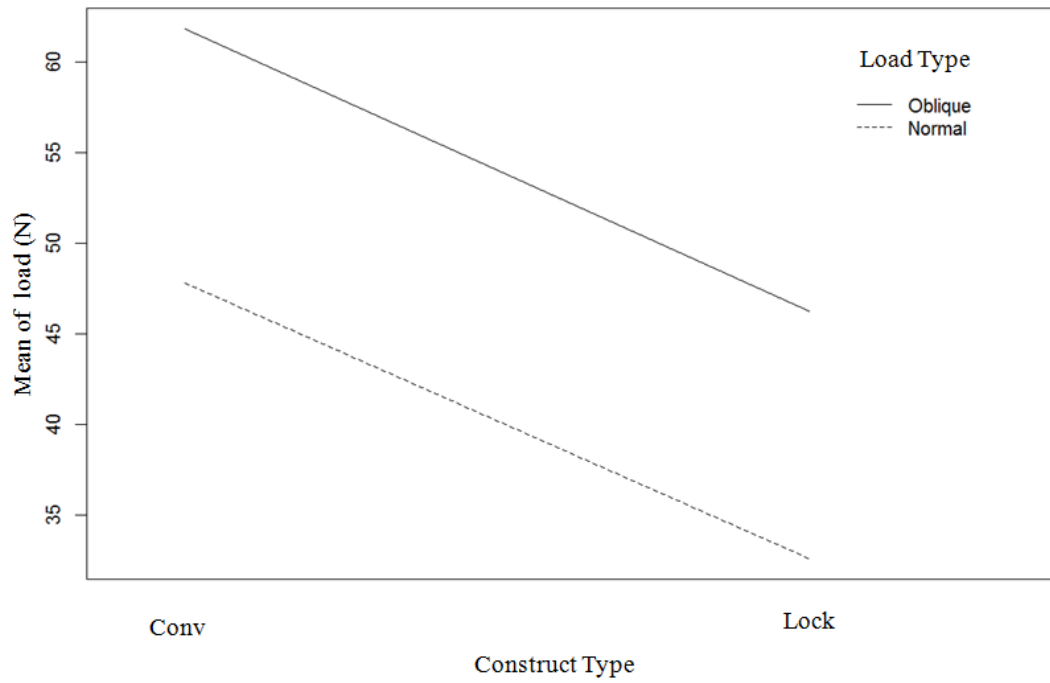


Figure 4.18: Interaction effect between construct type and load type (without cortex, density=0.08gpcc)

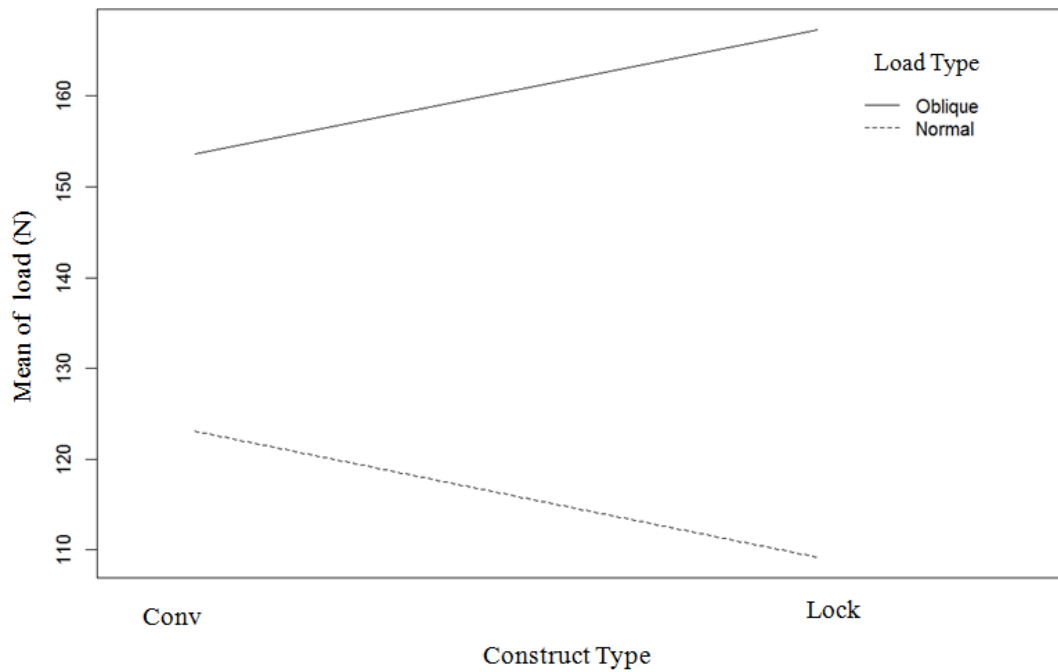


Figure 4.19: Interaction effect between construct type and load type (with cortex)

In summary, the conventional screw construct had the greater normal and oblique pullout strength. The locked screw constructs were stronger against shear loads. A locking-screw has much finer (lower) thread pitch compared to the conventional screw. However, increased shear area due to the lower pitch with locking screw did not offer advantage under pullout loads (parallel to screw axis) due to relatively lower screw diameter, thread depth and screw length compared to the conventional screw. Conversely, under the shear load (perpendicular to screw axis) the screw geometry (ie, diameter, pitch and thread depth) do not offer a significant advantage, rather the screw-plate interface (locking vs conventional) has an important contribution towards the cutout strength. Thus, the locked screw construct is stronger due to the greater amount of effective material available against shear out with fixed screw angle. An addition of the cortical bone significantly increased the strength for both conventional and locking constructs. Moreover, the strength of all the constructs were increased with bone density as expected. Hence, with a similar fixation device, fracture fixation performance is expected to be better with younger patients than with older patients because bone mass density and cortical bone thickness decreases at older age.

4.2 Finite element investigation of screw construct strength

The experimental outcomes provided the strength comparison between the locked and conventional screw constructs. However, the details of load transfer mechanism at screw-bone interface can accurately be observed through the finite element models. Thus, finite element analyses were performed on locking and conventional screw constructs with cancellous screw geometry to complement the experimental investigations. The objective of the finite element analysis was to isolate the influence of the screw-plate interface type on the constructs' strength with an identical screw design. Normal, oblique and shear loads were applied at the plate end to replicate the experiments. The boundary conditions of the experimental setup were incorporated to restrain the movement of the bone block against the applied load (Fig. 4.20). A half symmetry model was considered due to very high computational time with full model. Moreover, the half symmetry was appropriate for the symmetric loading. The bone block construct was meshed with first order hexahedral elements. The geometrical parameters of modeled cancellous screw were identical to the screws utilized for experimental setup. Furthermore, the locking and conventional screw-plate interfaces were modeled with abaqus BEAM and UJOINT connector elements as explained in chapter 3 (Fig. 3.4). Finite element analysis was performed with the synthetic cancellous bone of densities 0.08 g cm^{-3} , 0.16 g cm^{-3} , 0.24 g cm^{-3} and 0.32 g cm^{-3} and 0mm (no cortex), 1mm and 2mm thick cortical bone layers. Isotropic material properties were assumed for the synthetic bone (Tab. 4.1). The screw and plate were also modeled with isotropic elastic steel properties ($E=200,000\text{Mpa}$). Abaqus surface to surface contacts were defined at the screw-bone and plate-bone interfaces. The construct's strength was evaluated based on the force distribution into the bone at screw-bone interface. The uniform force distribution along the screw length represents the efficient load bearing through the bone.

Table 4.1: Assumed bone material properties for elastic perfectly plastic analysis

Cancellous: Density	Elastic modulus (Mpa)	Yield strength (Mpa)
0.08 g cm^{-3}	24.0	1.0
0.16 g cm^{-3}	74.0	2.2
0.24 g cm^{-3}	160.0	4.9
0.32 g cm^{-3}	247.0	8.4
Cortical: Density	Elastic modulus (Mpa)	Yield strength (Mpa)
1.70 g cm^{-3}	16700.0	157.0

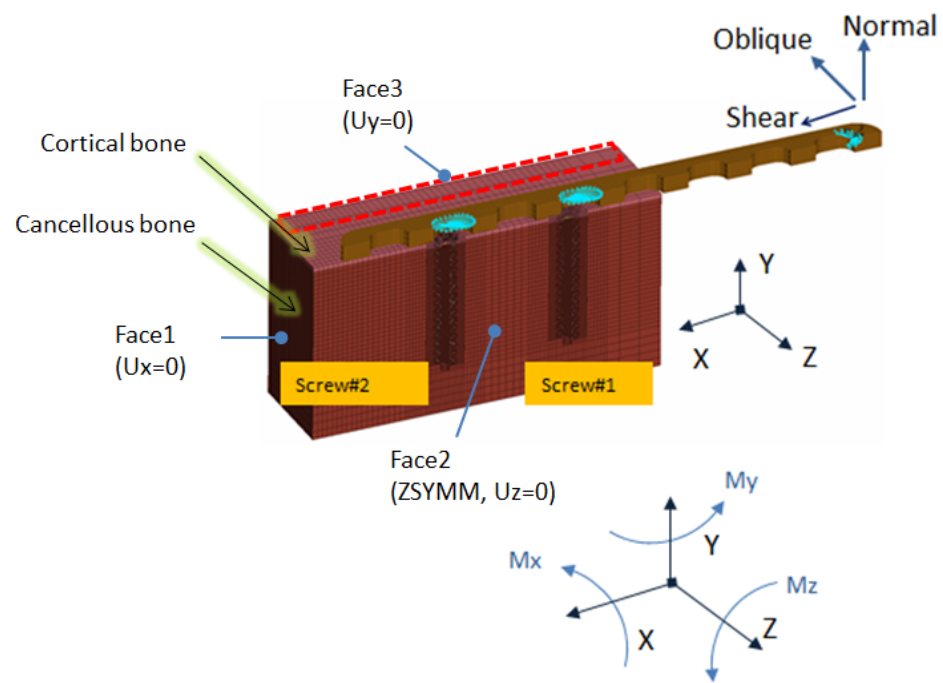


Figure 4.20: Finite element model boundary conditions

The load-displacement plot from the finite element analysis was compared to the experimental data (Fig. 4.21). The correlation validates the finite element model. The static finite element analysis failed to converge after the load increased beyond failure limit due to the sudden drop in load with the greater strain.

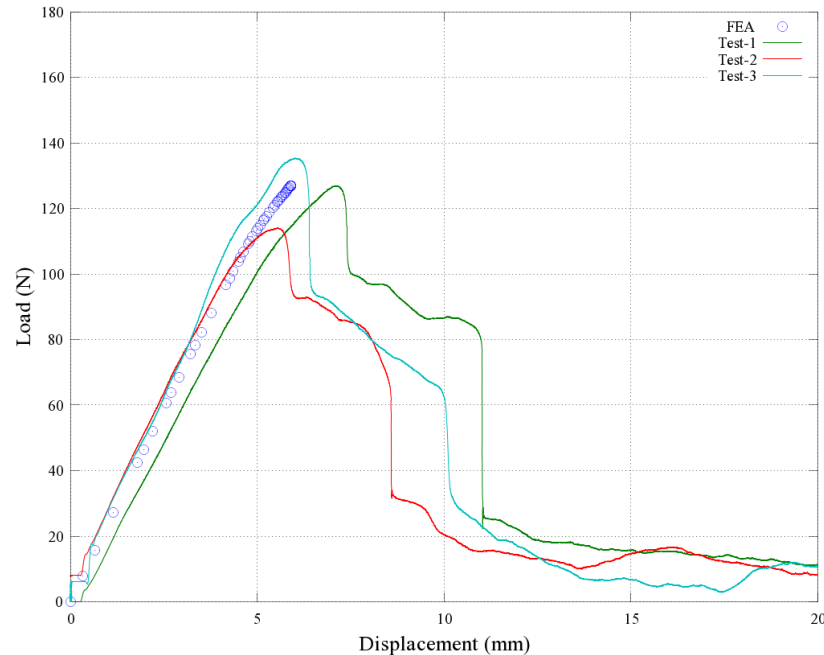


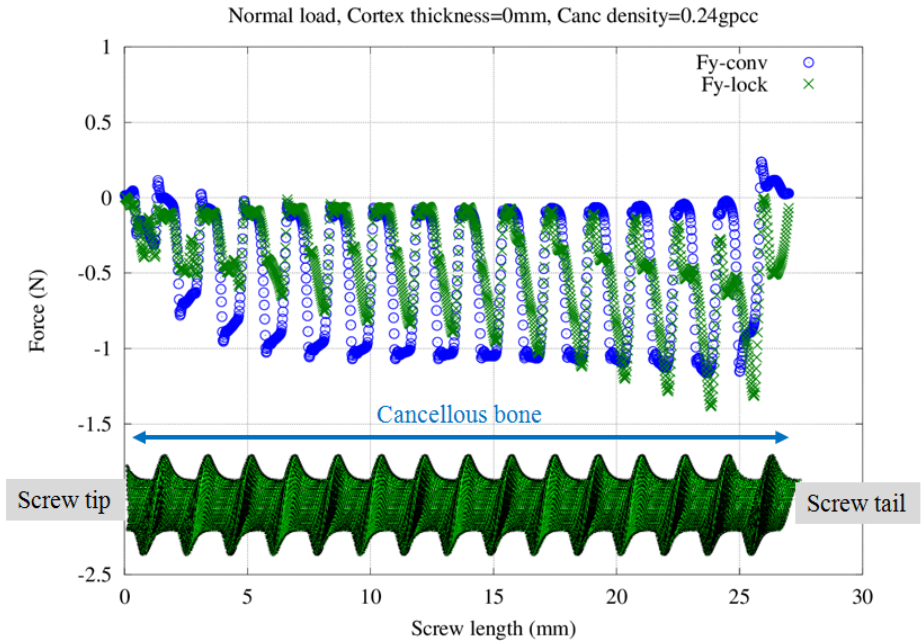
Figure 4.21: Finite element vs experiment under normal load (Density=0.16 g cm⁻³)

4.2.1 Strength evaluation matrix

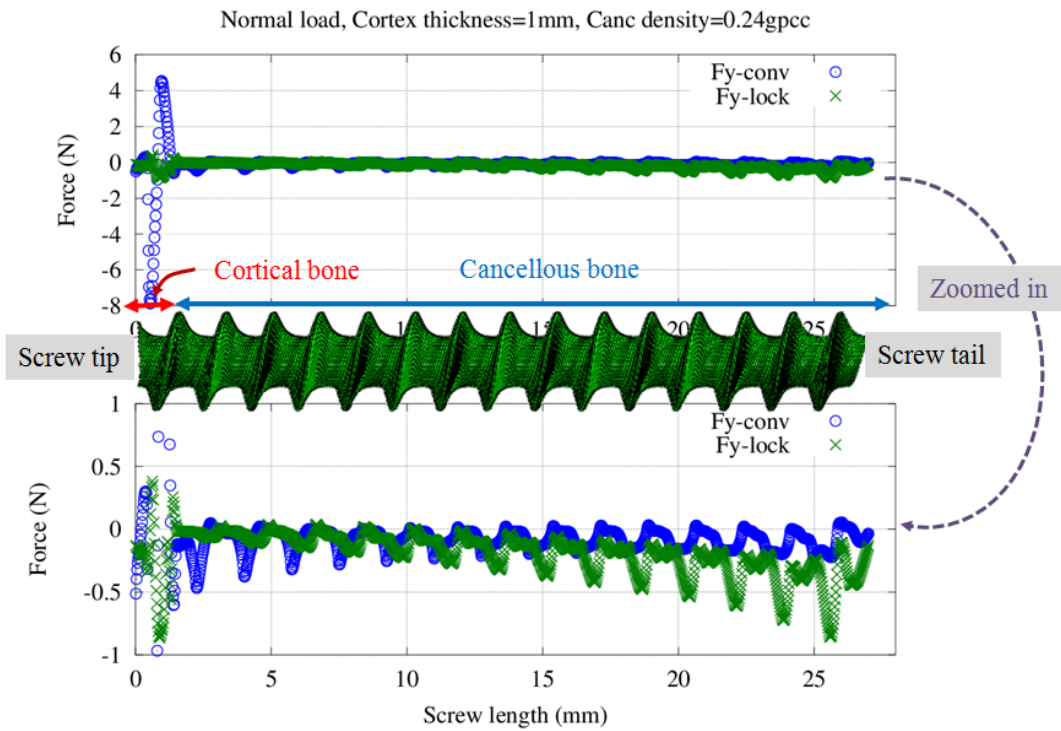
The uniformity of force distribution into the bone at screw-bone interface was evaluated as the construct strength criteria. A uniform force distribution along the screw length demonstrates an efficient load bearing through the bone-screw contact. Efficient load bearing leads to the lower bone plastic strain (i.e., permanent material deformation) and lower plastic energy dissipation. For example, Fig. 4.22 shows the force distribution at screw-bone interface under the normal load. The conventional screw experienced relatively more uniform force distribution compared to the locking screw irrespective of the cortical bone presence. However, presence of the cortical bone affected the load transfer mechanism (Fig. 4.22a vs Fig. 4.22b). Moreover, the conventional screw carried a greater load within the "near cortical" region around the screw tip (Fig. 4.22b). Thus, the conventional screw construct may sustain the greater external normal load before failure. The conventional screw caused less bone plastic strain (Fig. 4.23) due to the uniform force distribution at the screw-bone interface. The total strain plot shows the overall weight bearing mechanism comparison at the same applied external load (Fig. 4.24). The conventional screw construct experienced relatively more uniform material strain than did the locked screw construct. In addition, the plastic energy is the mechanical work consumed by plastic strain. At the assumed plastic

energy dissipation of 0.5%, the conventional screw construct sustained the greater normal load compared to the locking screw construct (220 N vs 150 N) (Fig. 4.25). Therefore, the conventional screw construct is stronger compared to the lock screw construct under normal load.

Similarly, in rest of the chapter 4, construct strength were evaluated under normal, shear and oblique loads based on these strength evaluation criteria.

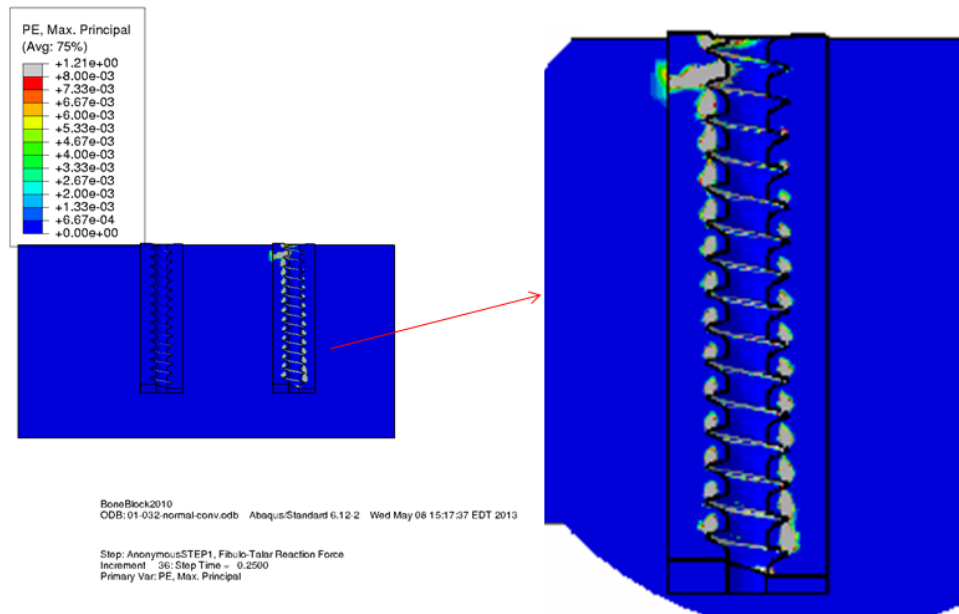


(a) Cortical thickness = 0mm

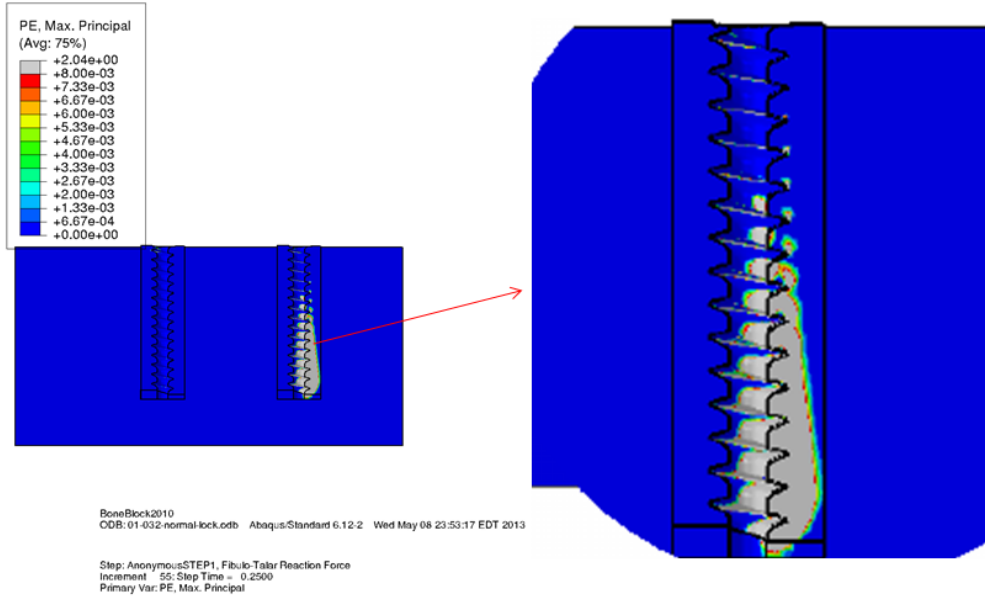


(b) Cortical thickness = 1mm

Figure 4.22: Pullout force (F_y) distribution over the threads (*The conventional screw experienced relatively more uniform force distribution compared to the locking screw irrespective of the cortical bone presence and carried a greater load within the "near cortical" region around the screw tip*)

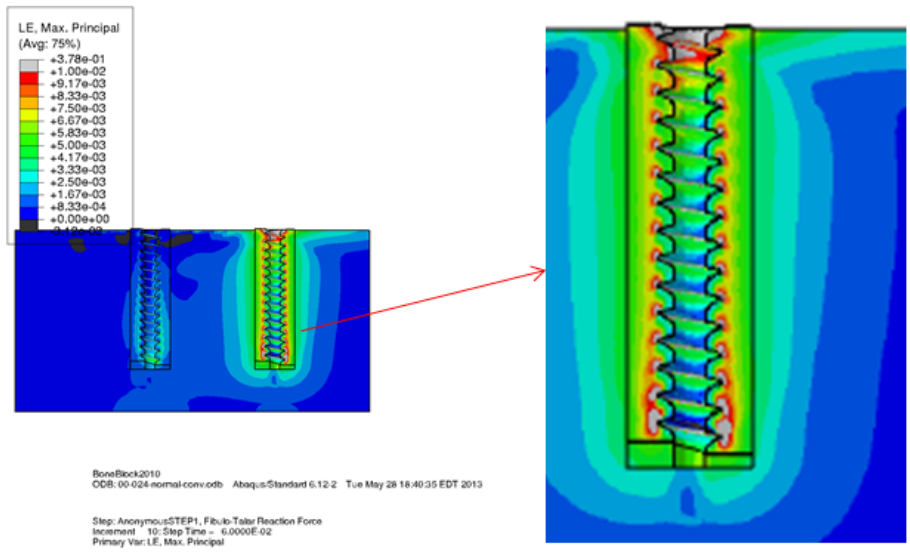


(a) Conventional screw construct

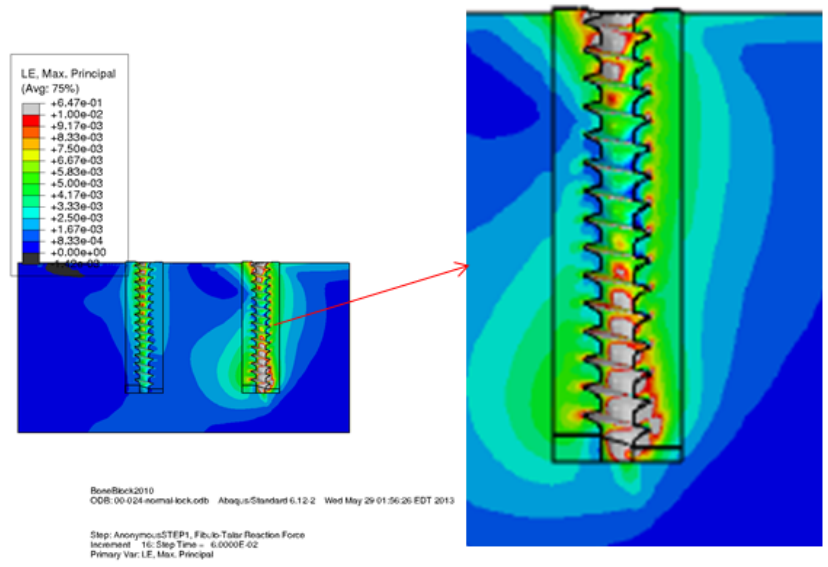


(b) Locking screw construct

Figure 4.23: Plastic strain under normal load (Cortex thickness=1mm) (*The conventional screw caused less bone plastic strain due to the uniform force distribution at the screw-bone interface*)



(a) Conventional screw construct



(b) Locking screw construct

Figure 4.24: Total strain under normal load (Cortex thickness=0mm) *(The conventional screw caused more uniform strain at screw-bone interface compared to the locked screw)*

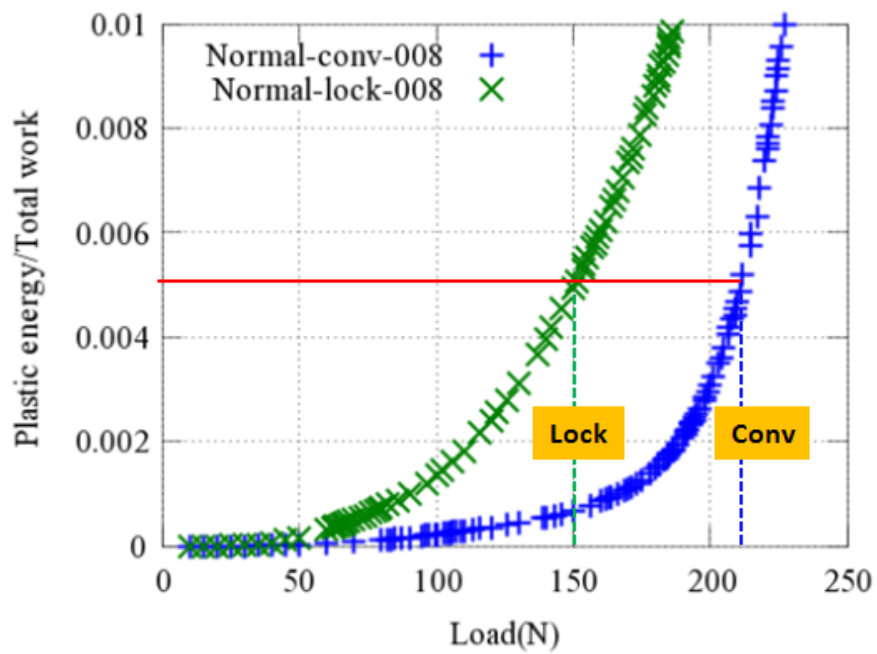


Figure 4.25: Plastic energy dissipation comparison under normal load (*The conventional screw construct sustained the greater normal load compared to the locking screw construct at 0.5% plastic energy dissipation*)

The process of calculating a force distribution at screw-bone interface was automated using an abaqus python script. The calculation process with a python script is shown in Fig. 4.26. A script reads the abaqus output file (.odb) and extracts a thin bone layer (approx. 0.033mm thick) at the screw thread contact. Several free body cuts (20 cuts per 1mm length) were then created along the axis of the extracted bone thread elements. At each of these sections' cuts the force components were calculated and recorded in text format (.rpt file). These text files were processed by an octave script to create the "force vs screw length" plots.

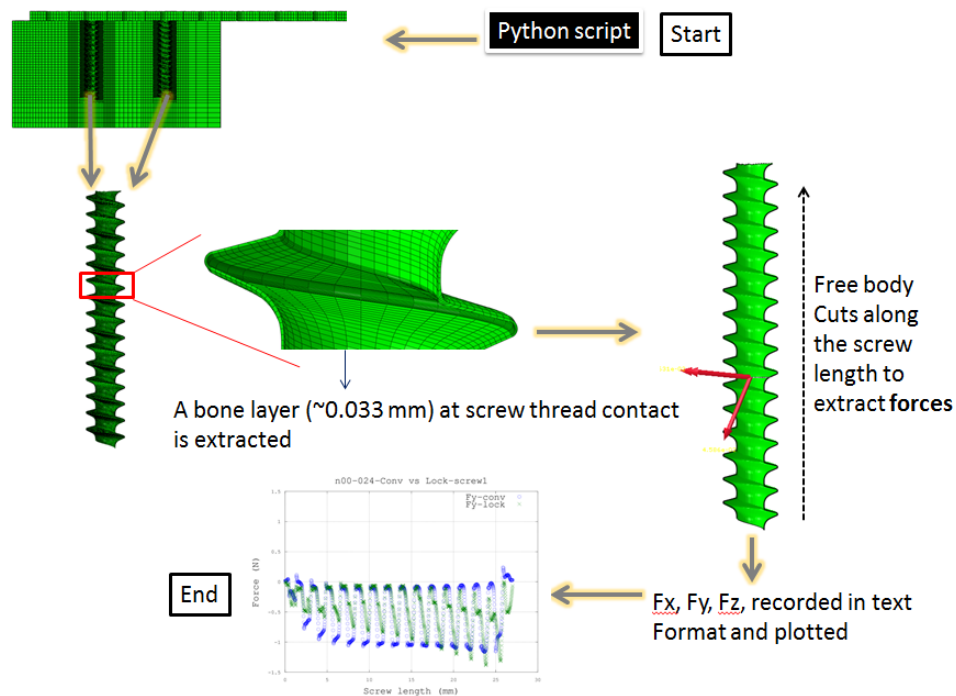
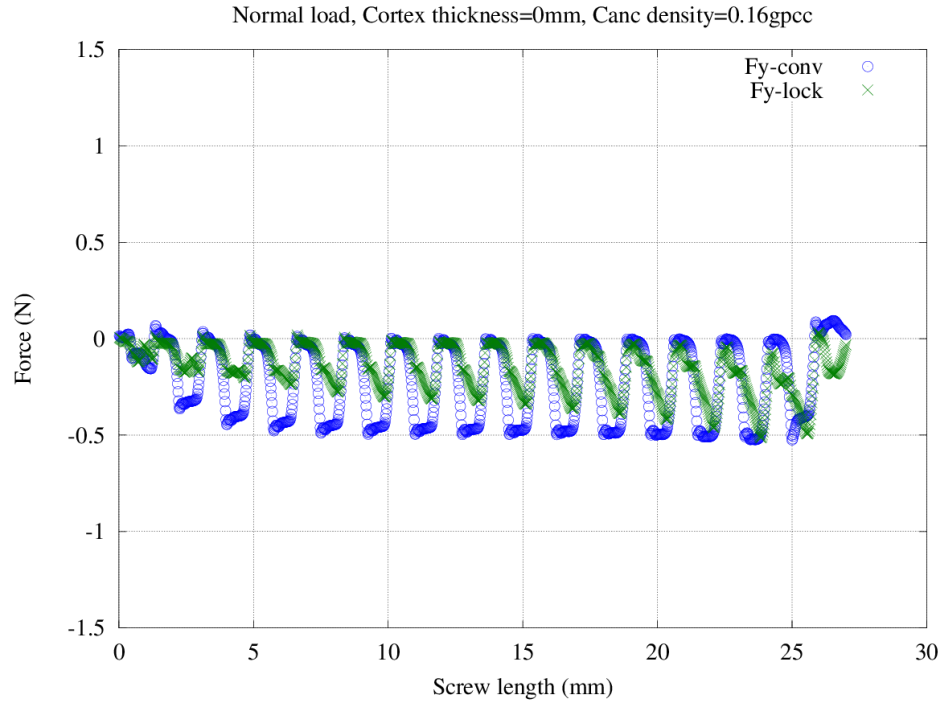


Figure 4.26: The force extraction process using python script

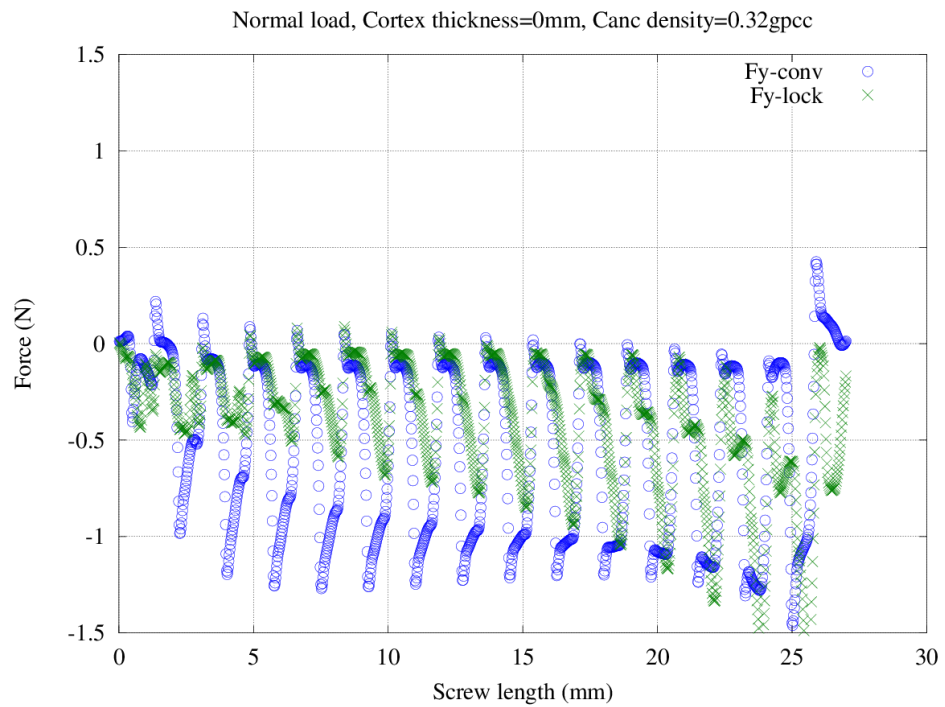
4.2.2 Normal load

The normal pullout load was applied at the plate end (Fig. 4.20). In order to evaluate the load transfer mechanism, the pullout force component (F_y) was plotted along the screw length. It was observed that the force transfer mechanism at threads was not affected by the cancellous bone density (Fig. 4.27). Moreover, the conventional screw caused a relatively more uniform force distribution along the screw length for the constructs with 0mm, 1mm and 2mm cortex thicknesses (Fig. 4.27 to Fig. 4.29). Conversely, the locked screw experienced a non-uniform load transfer i.e. the greater force concentration towards the tail of the screw. The uniform force distribution with conventional screws leads to the lower bone strain (Fig. 4.30 to Fig. 4.32) and hence the lower plastic dissipation (Fig. 4.34). The plastic strain plots (Fig. 4.33) compare the material damage for both construct types under the same external load. The bone at conventional screw interface experienced a lesser and uniform damage. However, the locked screw caused a greater and non-uniform damage. Thus, a conventional screw construct offer a greater

strength compared to the lock screw construct under normal load. In addition, the uniformity of force distribution and load transfer mechanism were affected by the cortex thickness. The percentage of load transfer through the cortical bone increased with the cortex thickness (Fig. 4.28 vs Fig. 4.29). This provides a partial explanation for why a healthy bone with a greater cortex thickness may form a stronger construct. *(please see appendix sections D.1, E.1 and F.1 for remaining of the force distribution, strain and plastic energy plots with normal load)*

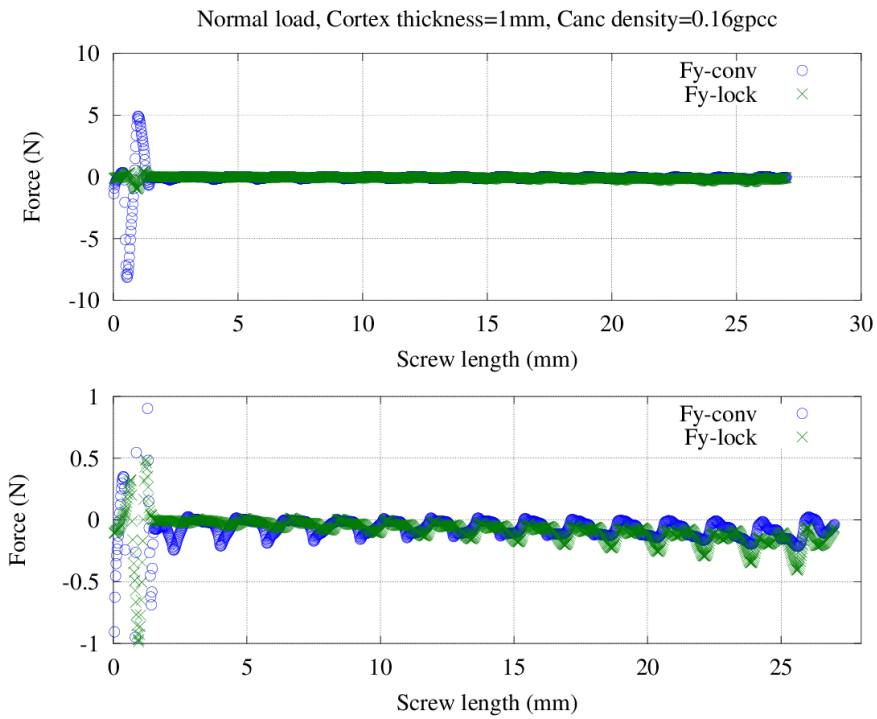


(a) Cancellous density = 0.16gpcc

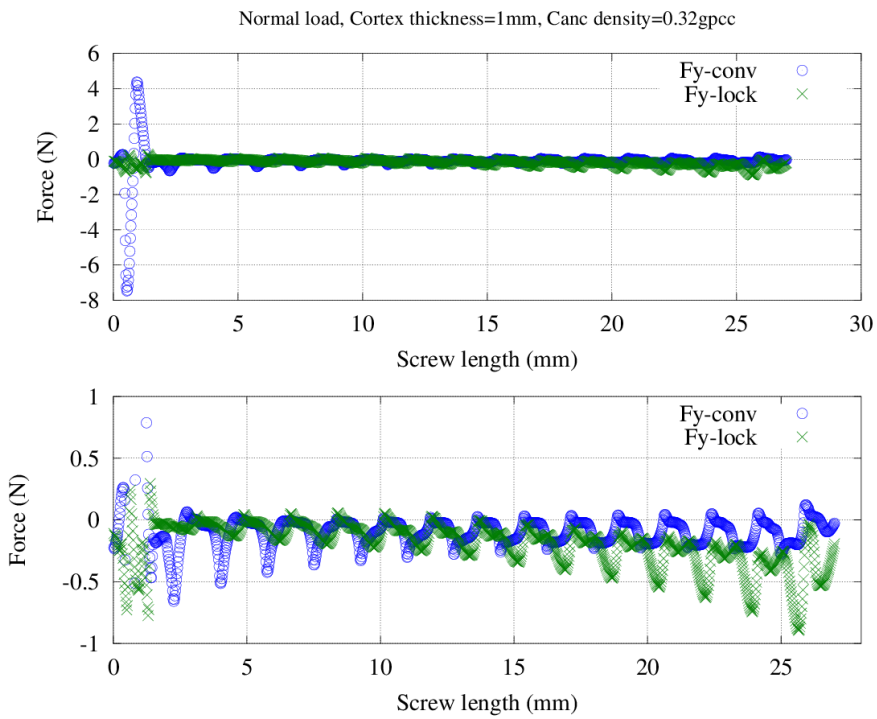


(b) Cancellous density = 0.32gpcc

Figure 4.27: Pullout force (F_y) distribution over the threads (cortex thickness = 0mm) (*The conventional screw caused a relatively more uniform force distribution along the screw length*)



(a) Cancellous density = 0.16gpcc



(b) Cancellous density = 0.32gpcc

Figure 4.28: Pullout force (F_y) distribution over the threads (cortex thickness = 1mm) (*The conventional screw caused a relatively more uniform force distribution along the screw length and carried a greater load within the cortical bone region*)

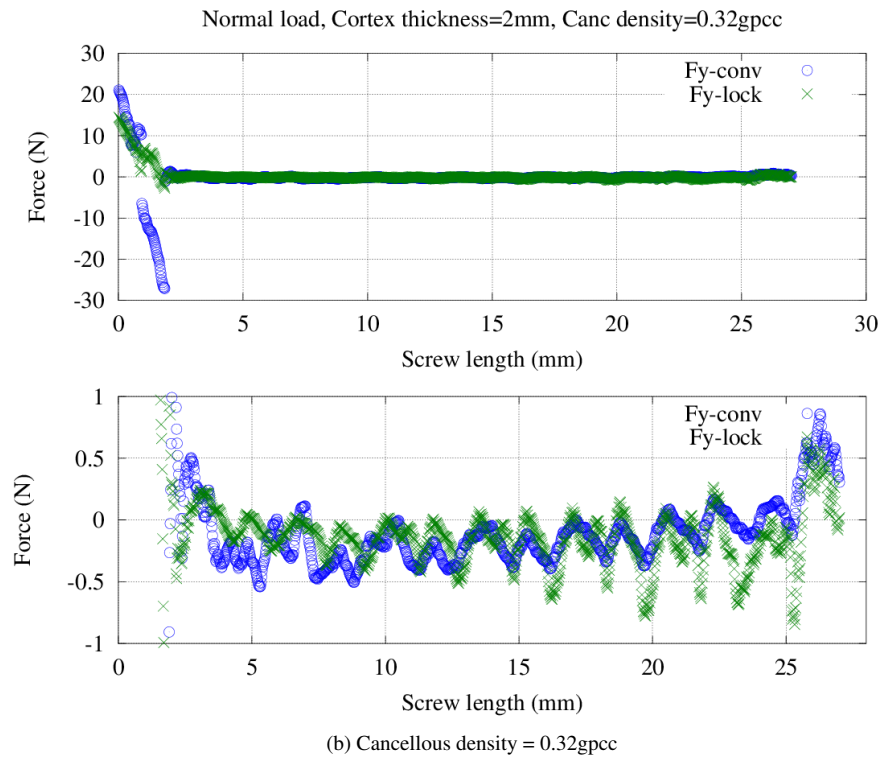
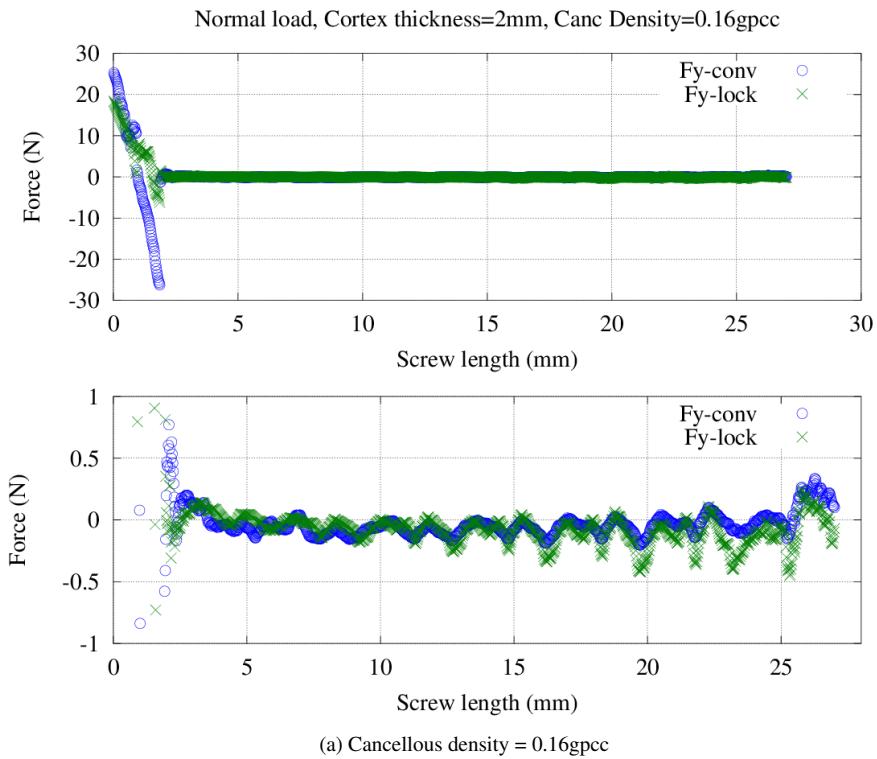
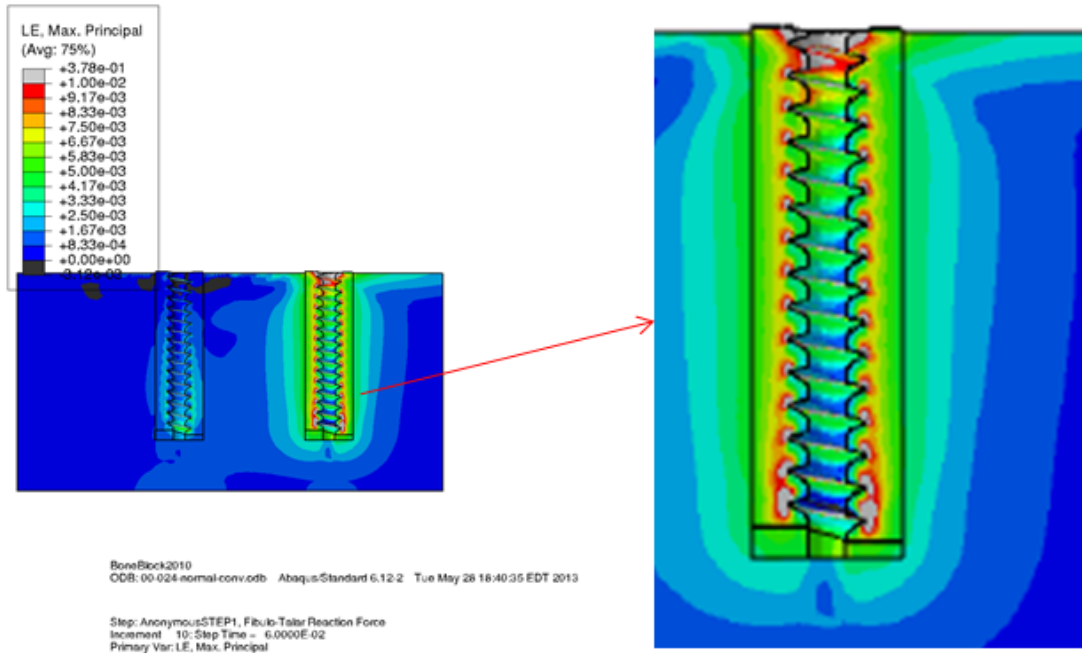
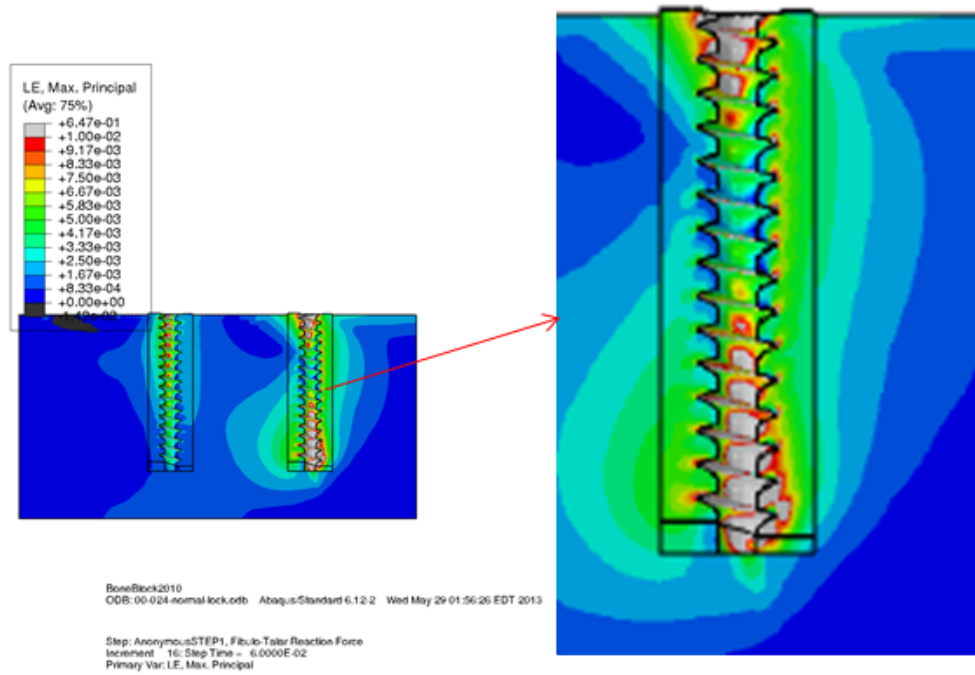


Figure 4.29: Pullout force (F_y) distribution over the threads (cortex thickness = 2mm) (*The conventional screw caused a relatively more uniform force distribution along the screw length and carried a greater load within the cortical bone region*)

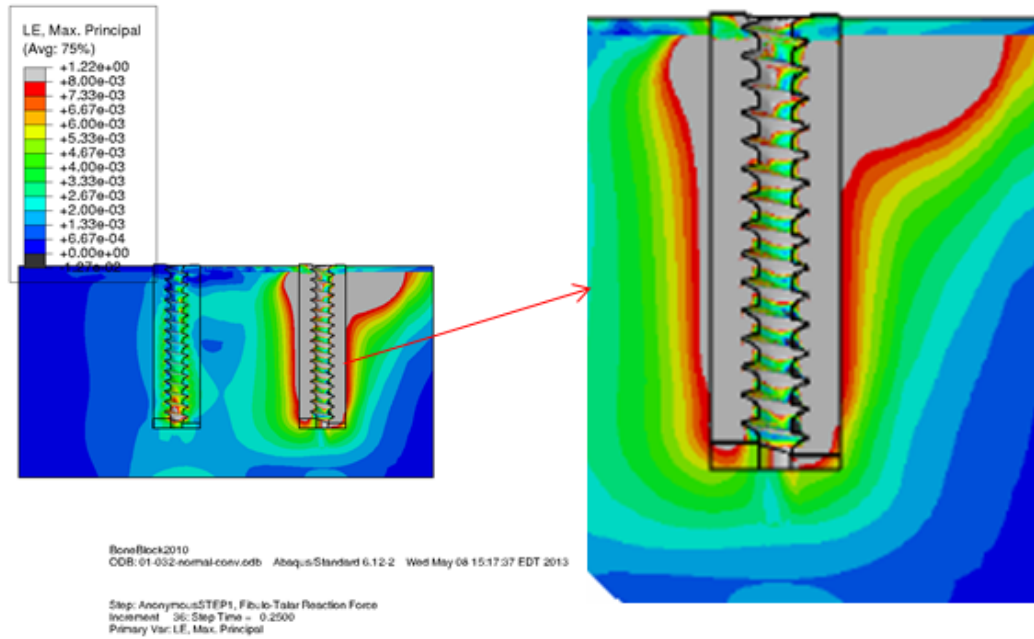


(a) Conventional screw construct

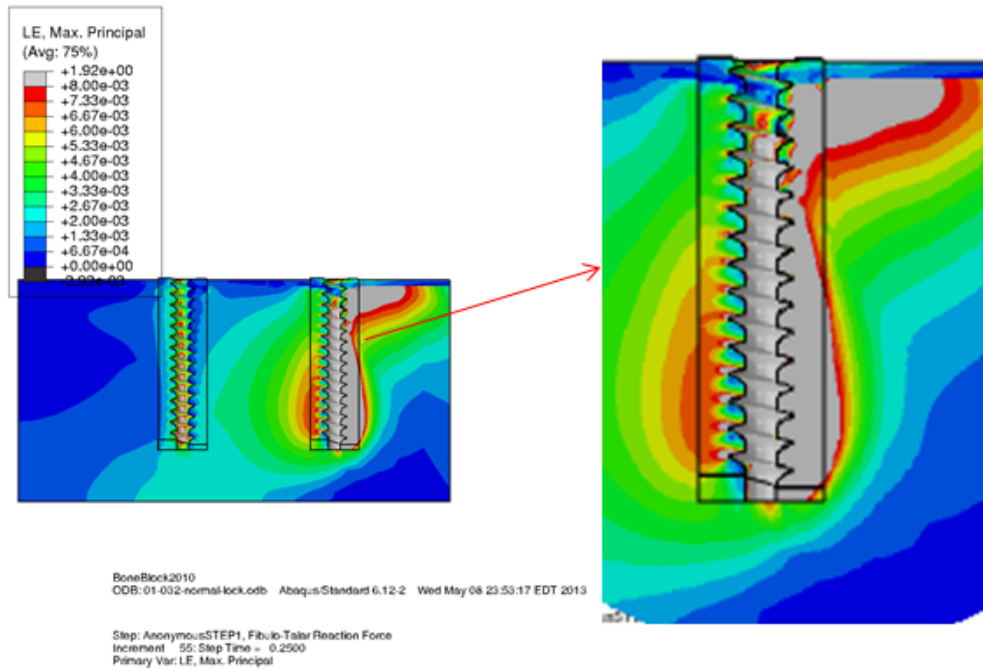


(b) Locking screw construct

Figure 4.30: Total strain under normal load (Bone density = 0.24 g cm^{-3} , Cortex thickness=0mm) (The conventional screw caused more uniform strain at screw-bone interface compared to the locked screw)

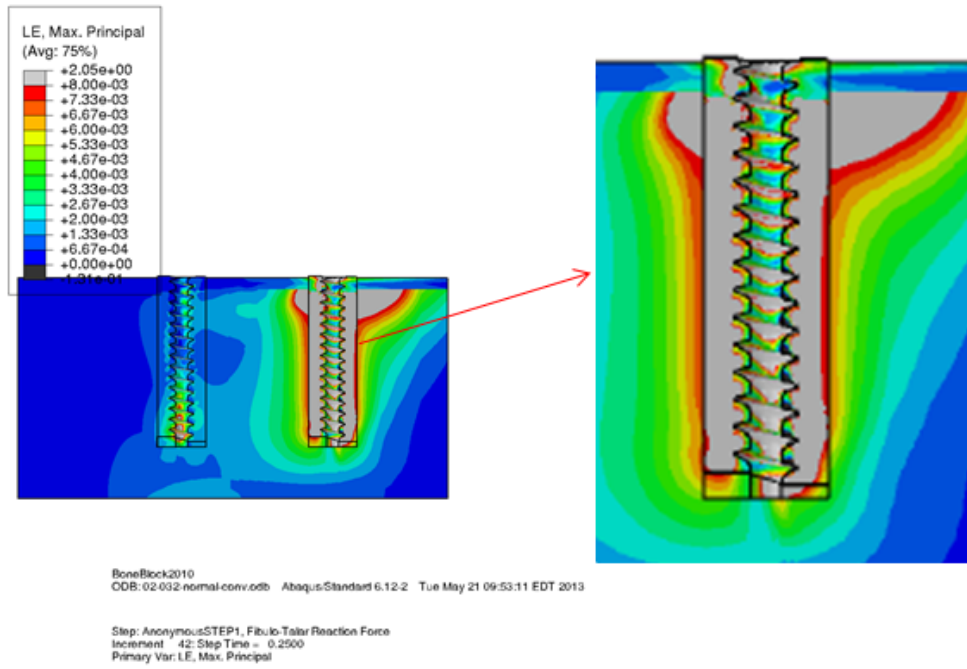


(a) Conventional screw construct

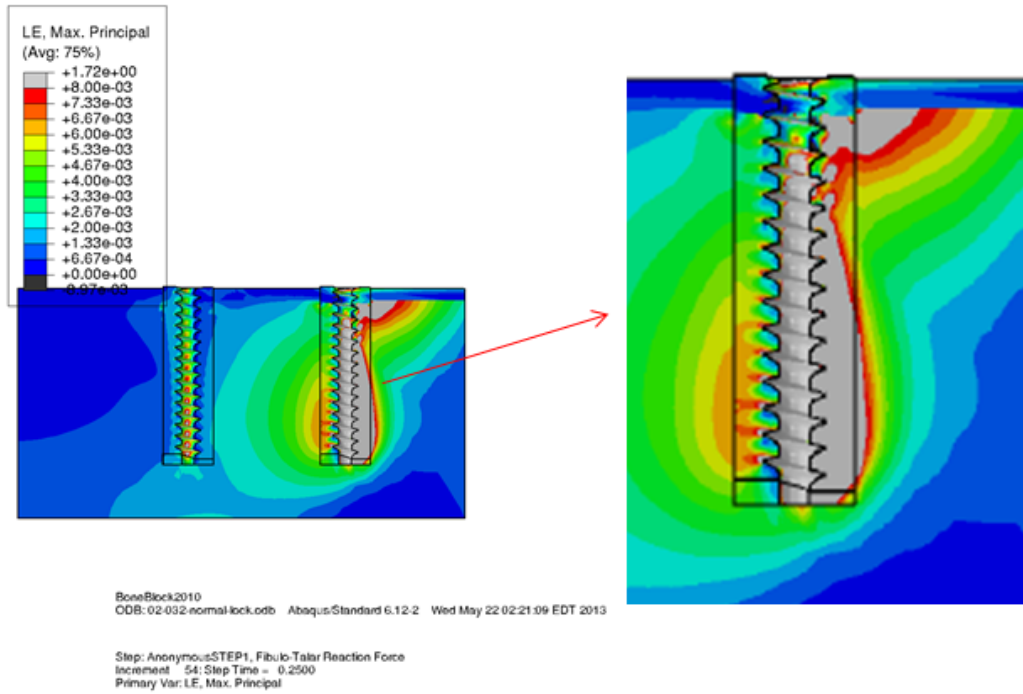


(b) Locking screw construct

Figure 4.31: Total strain under normal load (Bone density = 0.32 g cm^{-3} , Cortex thickness=1mm) (The conventional screw caused more uniform strain at screw-bone interface compared to the locked screw)

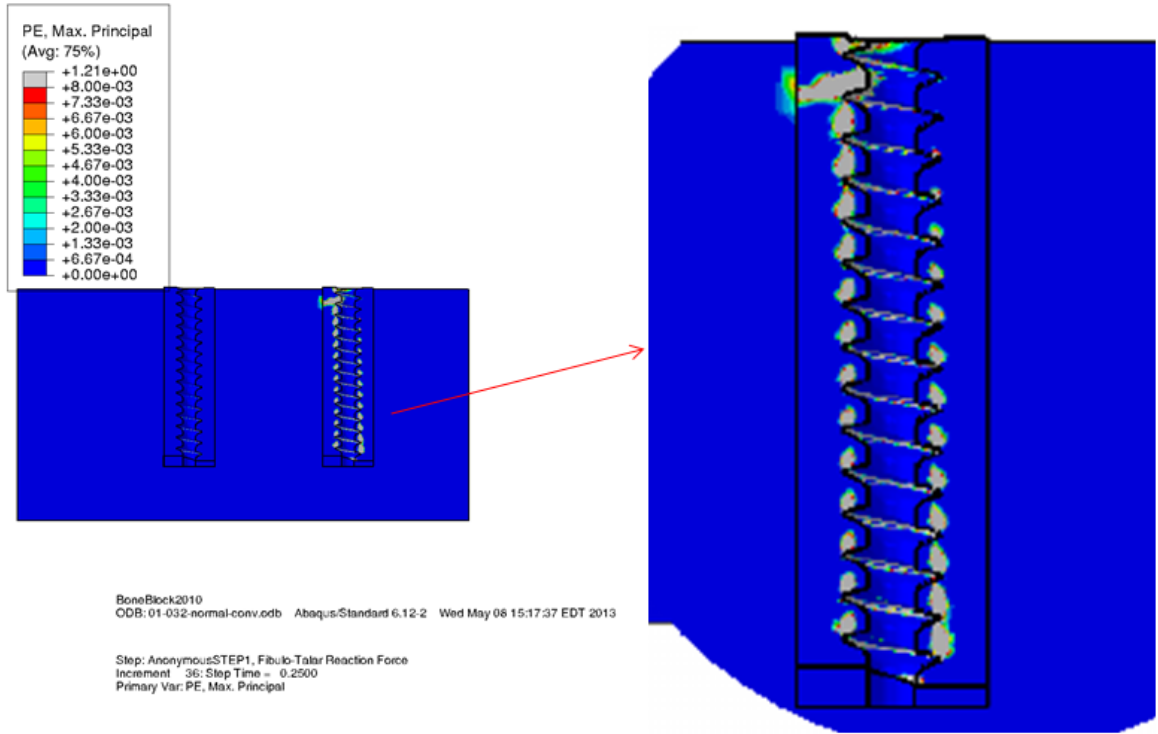


(a) Conventional screw construct

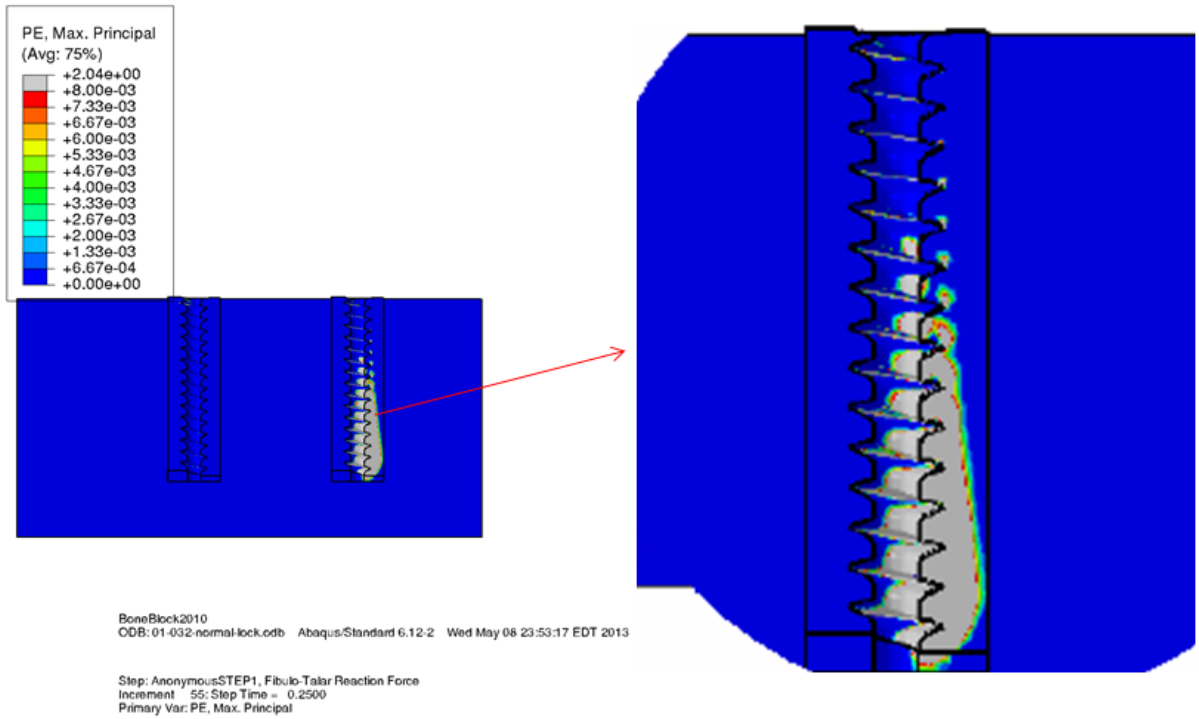


(b) Locking screw construct

Figure 4.32: Total strain under normal load (Bone density = 0.32 g cm^{-3} , Cortex thickness=2mm) (The conventional screw caused more uniform strain at screw-bone interface compared to the locked screw)



(a) Conventional screw construct



(b) Locking screw construct

Figure 4.33: Plastic strain under normal load (Bone density = 0.32 g cm^{-3} , Cortex thickness=1mm) (The conventional screw caused less bone plastic strain due to the uniform force distribution at the screw-bone interface)

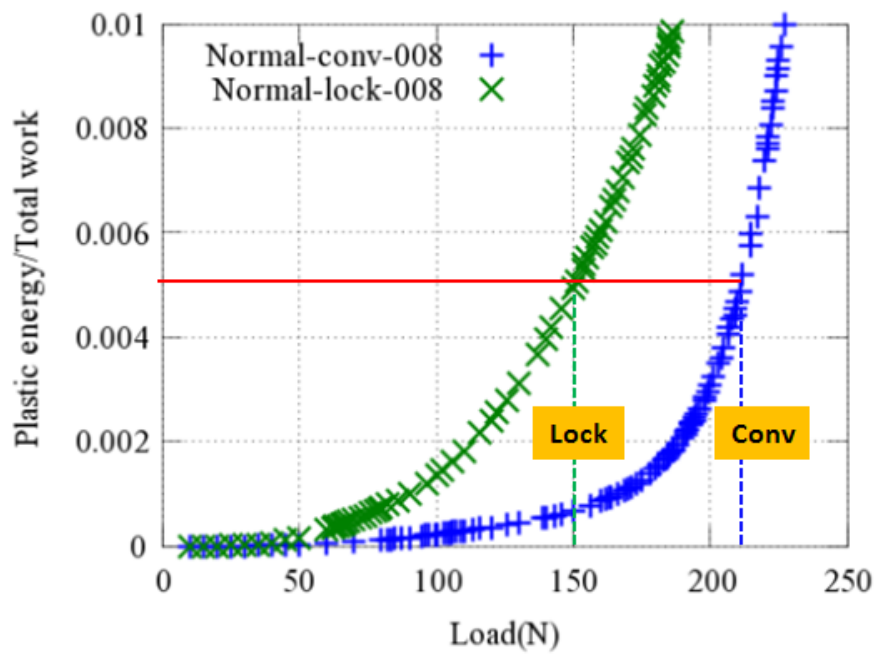


Figure 4.34: Plastic energy dissipation comparison under normal load (*The conventional screw construct sustained the greater normal load compared to the locking screw construct at 0.5% plastic energy dissipation*)

The 'plastic failure initiation' plots (Fig. 4.35) show the load transfer sequence through the cortical and cancellous portion of the bone. Plastic strain limits of 0.8% for a cortical bone and 1% for a cancellous bone were assumed failure initiation criteria [58]. It was observed that under the applied normal load a failure initiated at the cancellous portion of the bone followed by the cortical bone failure. The cancellous bone failure initiated at the lesser load with the locked screw compared to the conventional screw construct (17 N vs 32 N). Moreover, the failure initiation from a cancellous bone region indicates that initially the construct strength rely more on the cancellous bone followed by the load bearing through the cortical bone layer. The delayed failure initiation of cortical bone with the locked screw construct compared to the conventional screw construct (97 N vs 61 N) shows an inactivity of the cortical bone during an initial load bearing. Therefore, an overall strength of the locked screw construct was compromised through the greater cancellous bone damage (plastic strain). Moreover, this failure sequence within the cortical and cancellous bone regions showed a similar trend for all analyzed cancellous bone densities and cortex thicknesses (Fig. 4.35 vs Fig. 4.36). Thus, irrespective of the bone quality (i.e. cancellous densities and cortex thicknesses) the conventional screw construct offered the greater strength under the applied normal load. (Please see appendix section G.1 for rest of the plastic strain plots with normal load).

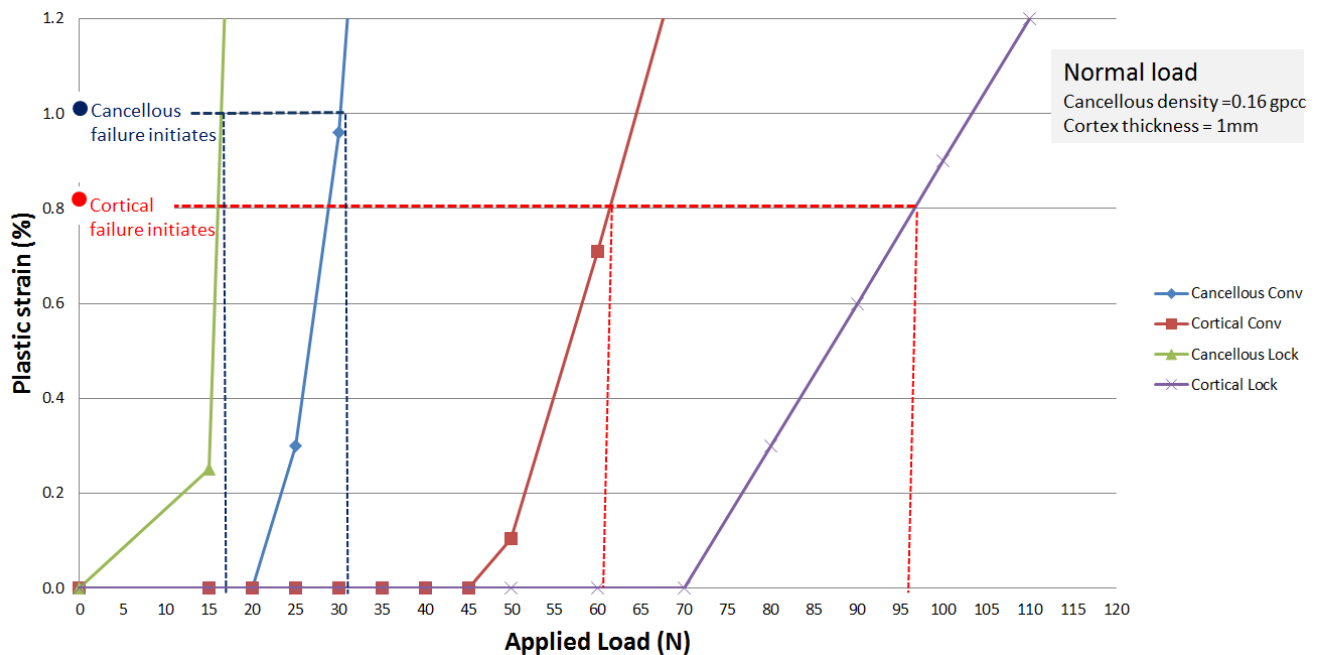


Figure 4.35: Plastic strain for the failure initiation under normal load (Cancellous density = 0.16 gpcc, cortex thickness=1mm)

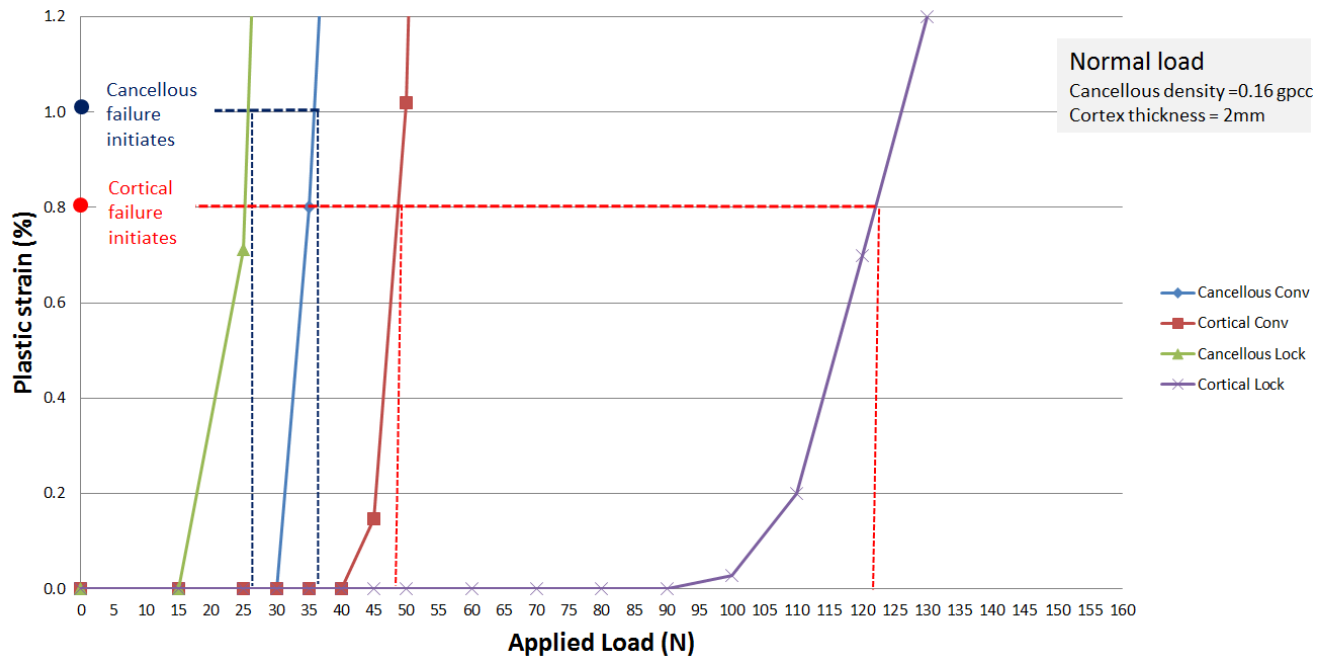
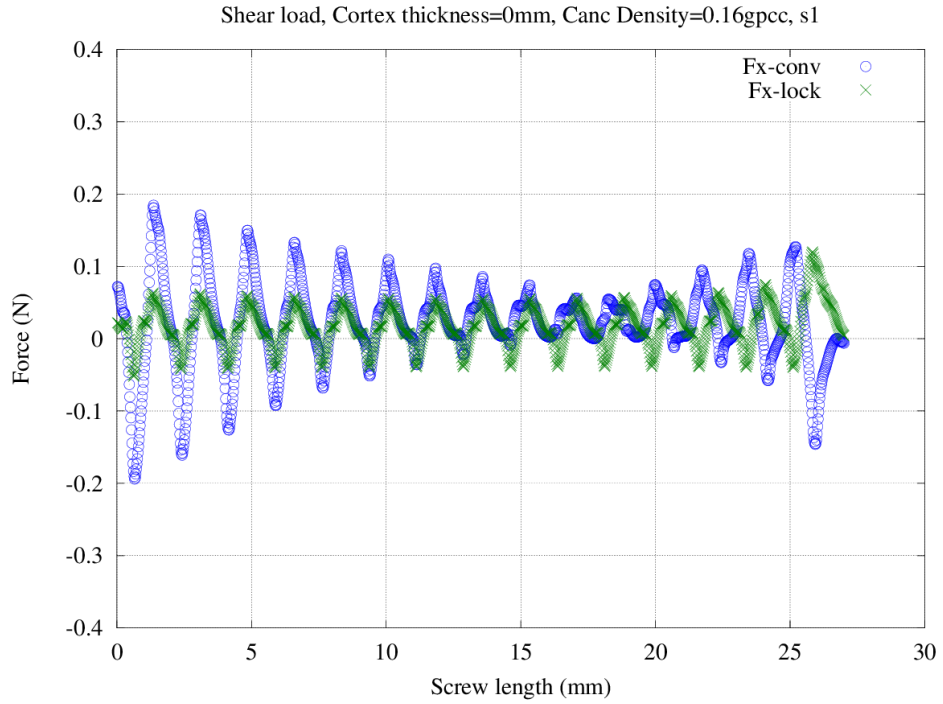


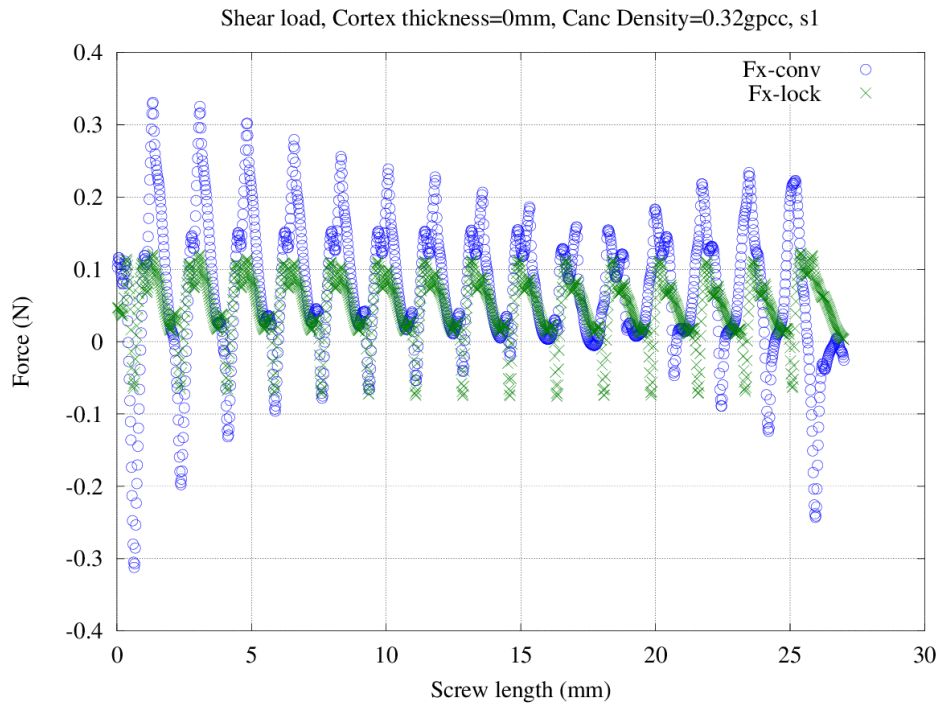
Figure 4.36: Plastic strain for the failure initiation under normal load (Cancellous density = 0.16 gpcc, cortex thickness=2mm)

4.2.3 Shear load

The shear load was applied at the plate end (Fig. 4.20). In order to evaluate the load transfer mechanism, the shear force component (F_x) and bending moment (M_z) were plotted along the screw length. It was observed that the locked screw experienced a more uniform force moment distribution along the screw length for the constructs with 0mm, 1mm and 2mm cortex thicknesses (Fig. 4.37 to Fig. 4.41). Conversely, the conventional screw experienced a non-uniform load distribution i.e. the greater force towards the screw extremes. The uniform force distribution with locked screws leads to the lower and more uniform bone strain (Fig. 4.42 to Fig. 4.44) and hence lower plastic dissipation (Fig. 4.46). In the contrary, the conventional screw resulted greater and more non-uniform bone damage. Thus, a locked screw construct offered a greater strength compared to the conventional screw construct under shear load. In addition, the uniformity of force distribution and load transfer mechanism were affected by the cortex thickness. The percentage of load transfer through the cortical bone increased with the cortex thickness (Fig. 4.38 vs Fig. 4.39). (*please see appendix sections D.2, E.2 and F.2 for the remaining force distribution, strain and plastic energy plots with shear load*)



(a) Cancellous density = 0.16gpcc



(b) Cancellous density = 0.32gpcc

Figure 4.37: Shear force (F_x) distribution over the threads (cortex thickness = 0mm) (*The locked screw caused a relatively more uniform force distribution along the screw length*)

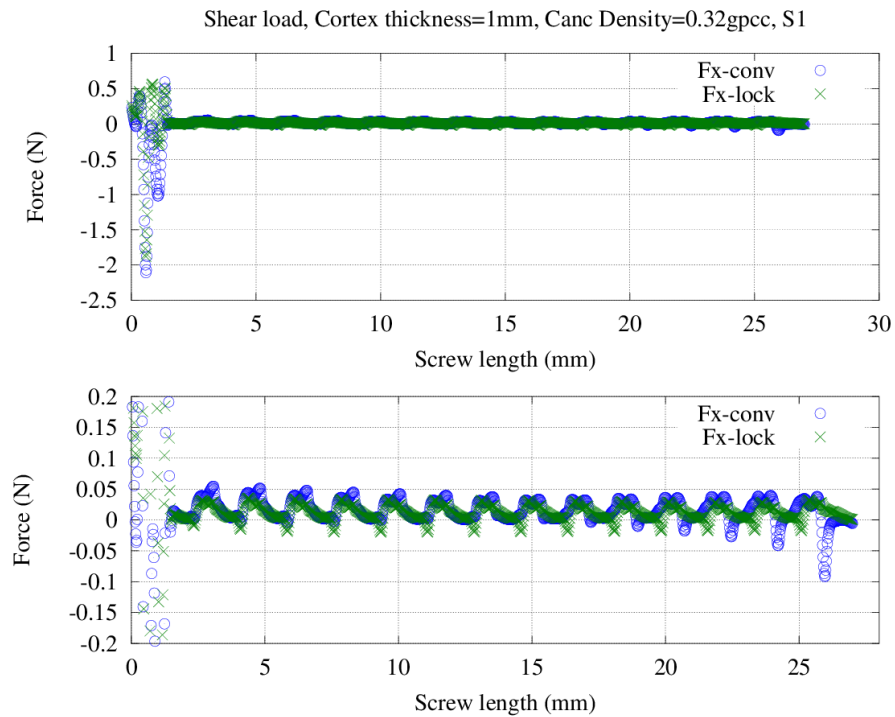
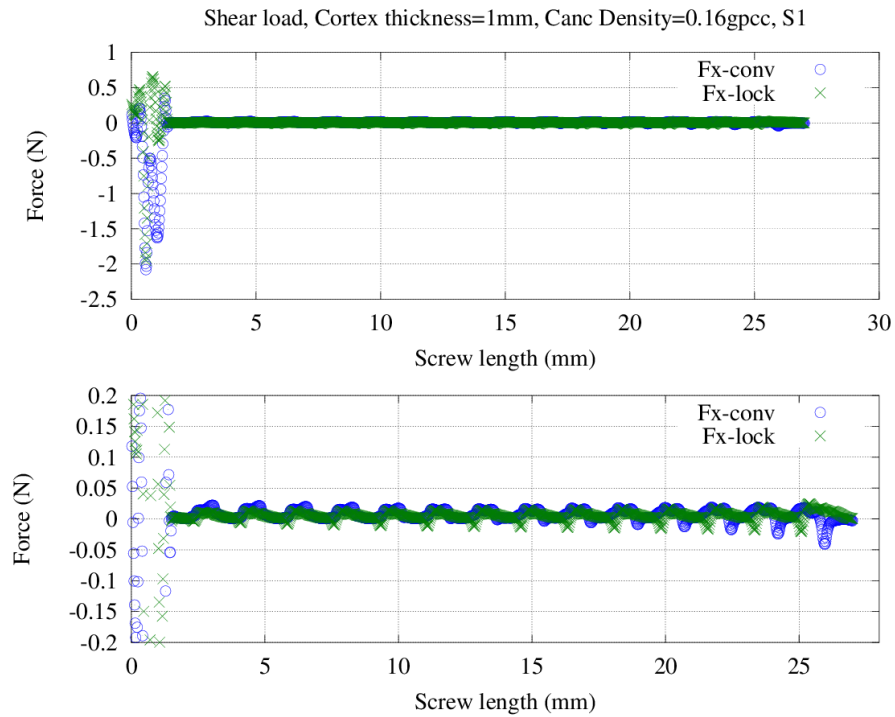


Figure 4.38: Shear force (Fx) distribution over the threads (cortex thickness = 1mm) (*The locked screw caused a relatively more uniform force distribution along the screw length*)

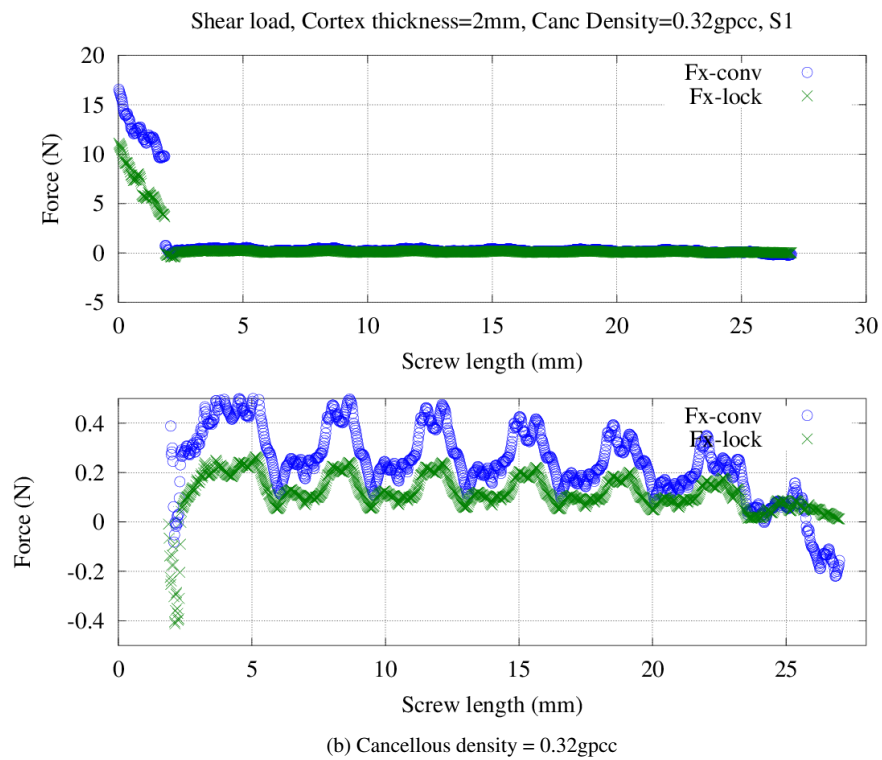
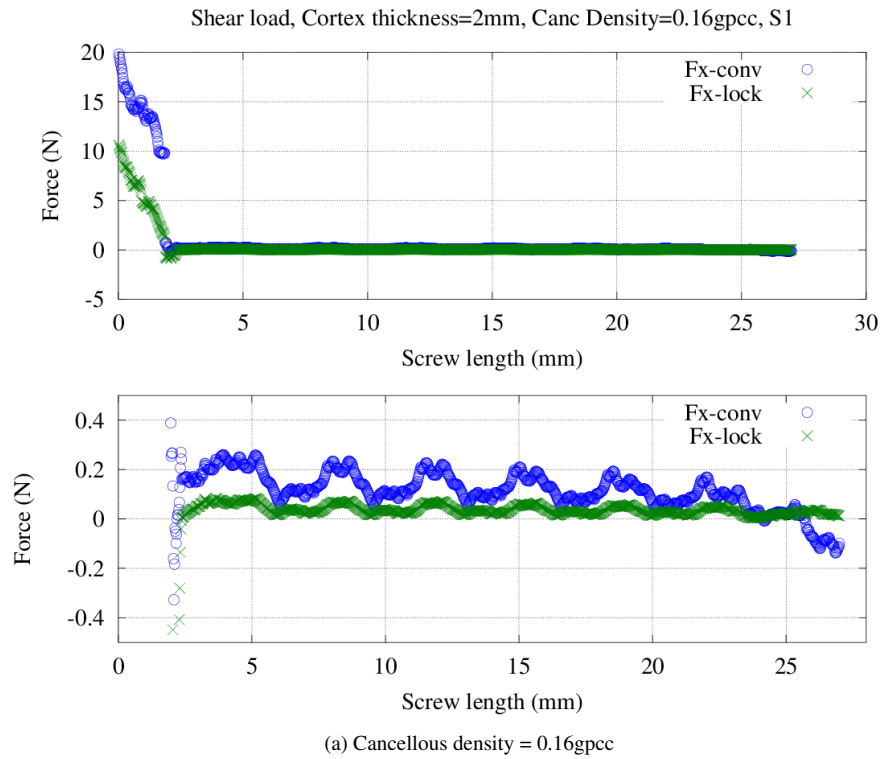
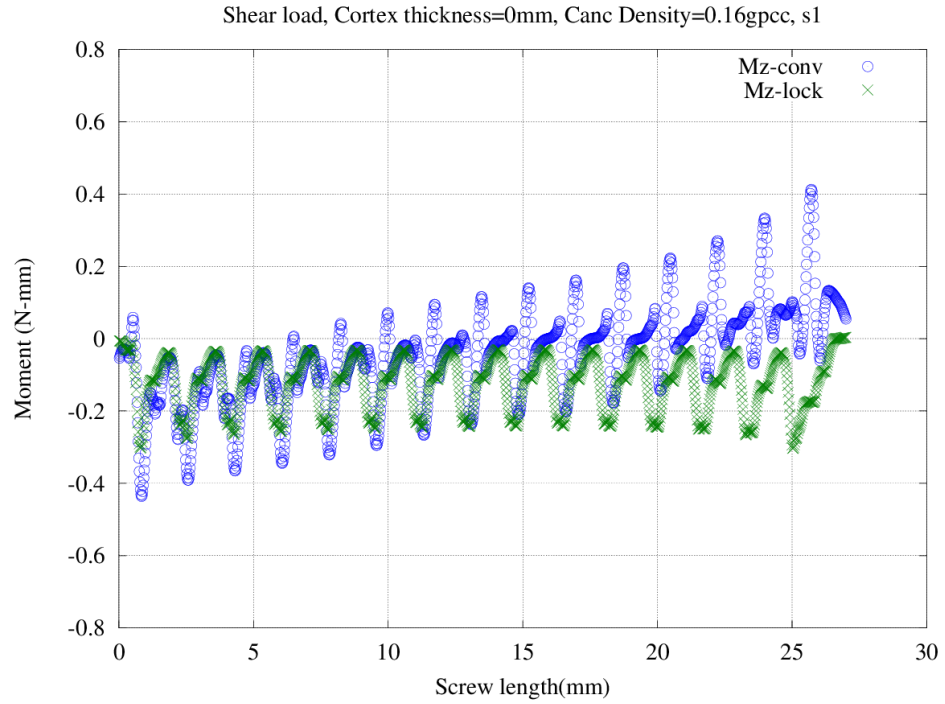
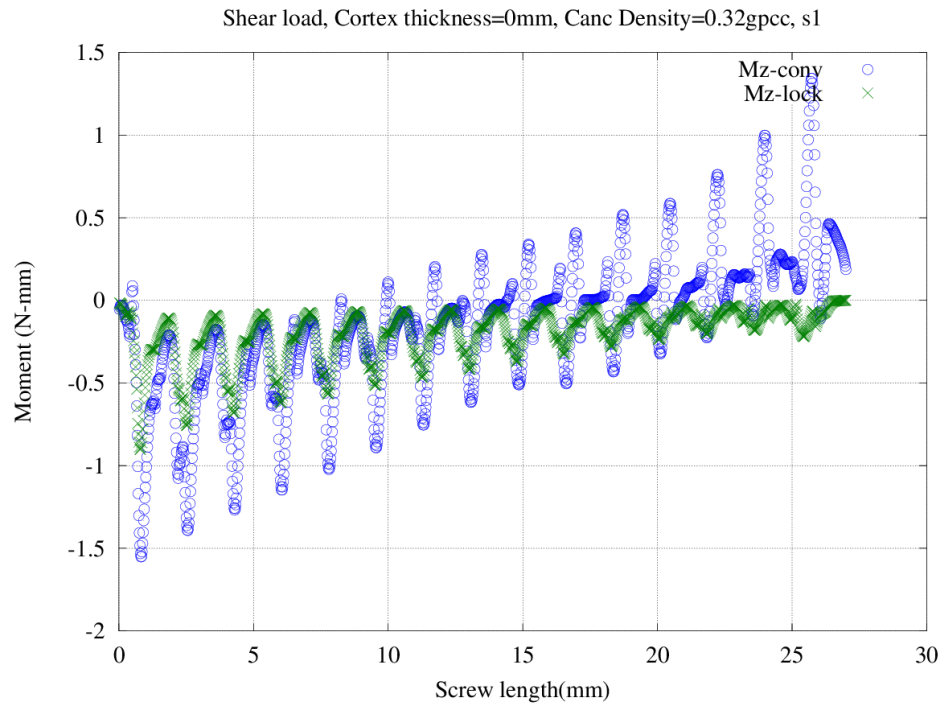


Figure 4.39: Shear force (F_x) distribution over the threads (cortex thickness = 2mm) (*The locked screw caused a relatively more uniform force distribution along the screw length*)



(a) Cancellous density = 0.16gpcc



(b) Cancellous density = 0.32gpcc

Figure 4.40: Moment (M_z) distribution over the threads (cortex thickness = 0mm) (*The locked screw caused a relatively more uniform moment distribution along the screw length*)

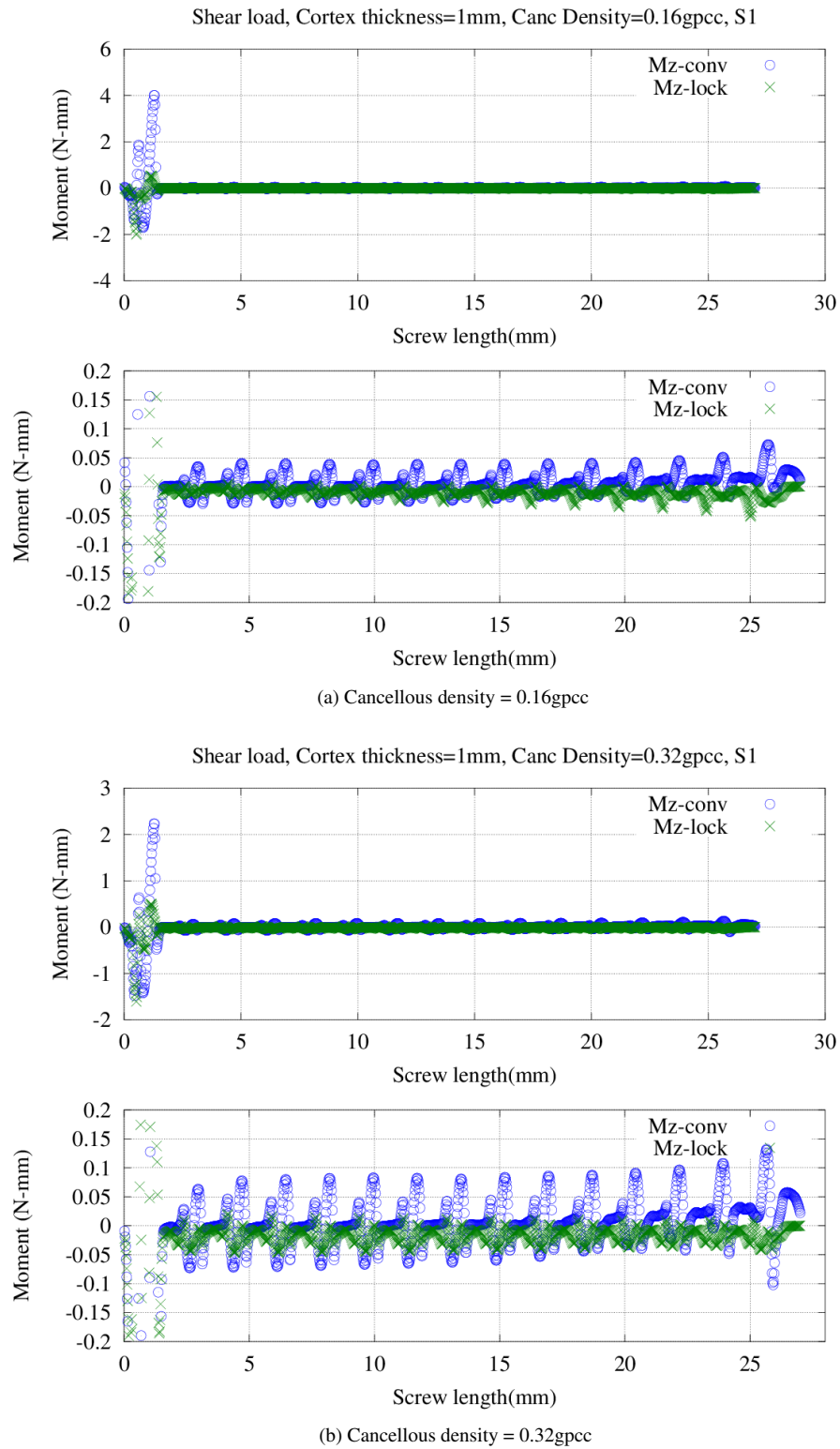
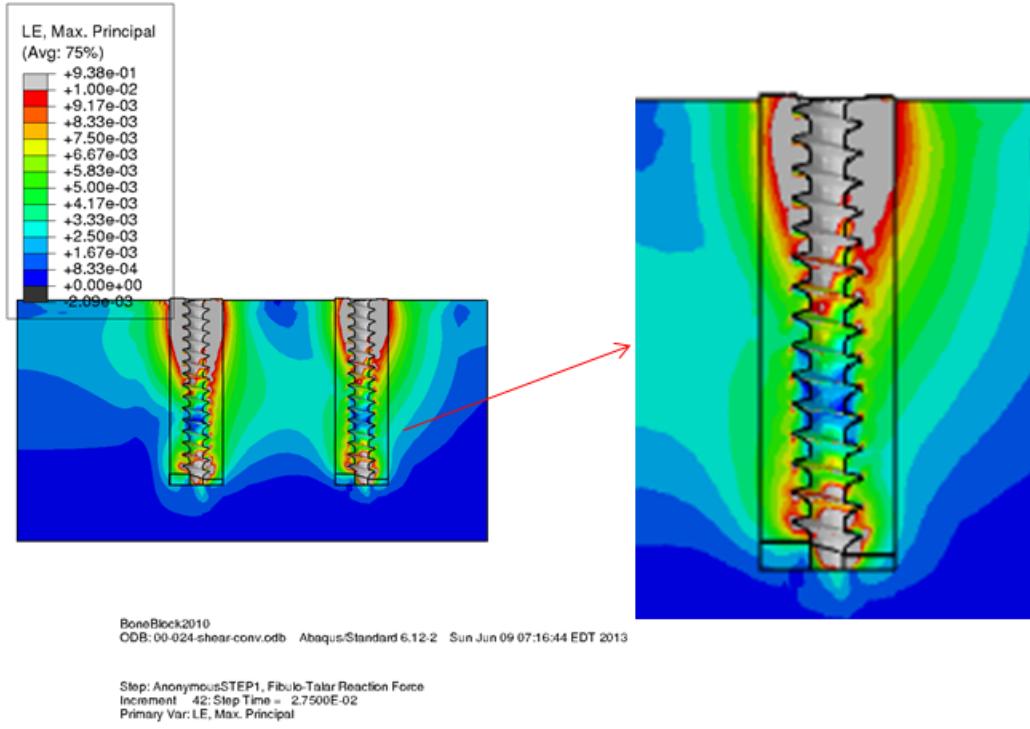
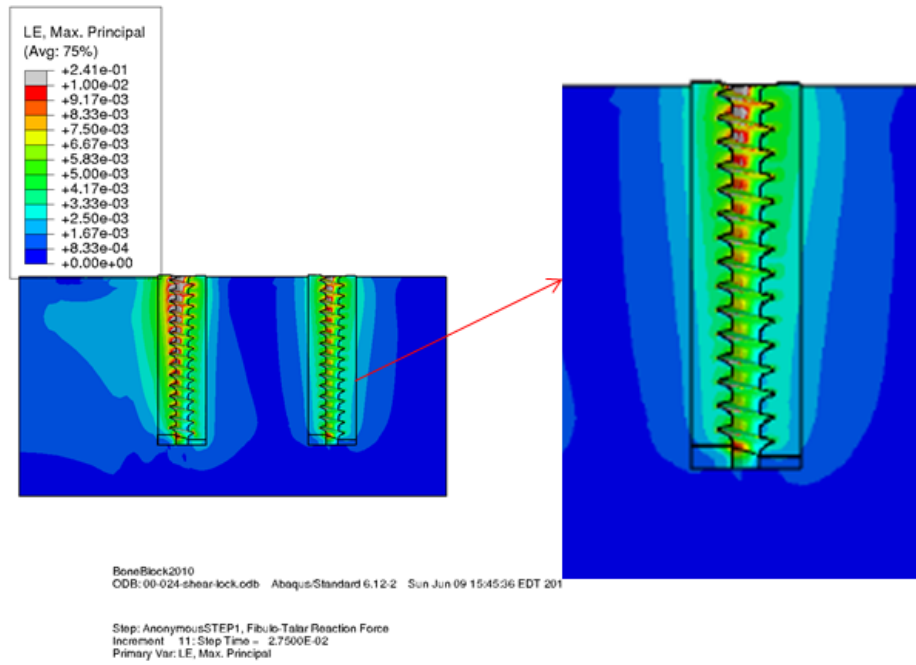


Figure 4.41: Moment (Mz) distribution over the threads (cortex thickness = 1mm) (*The locked screw caused a relatively more uniform moment distribution along the screw length*)

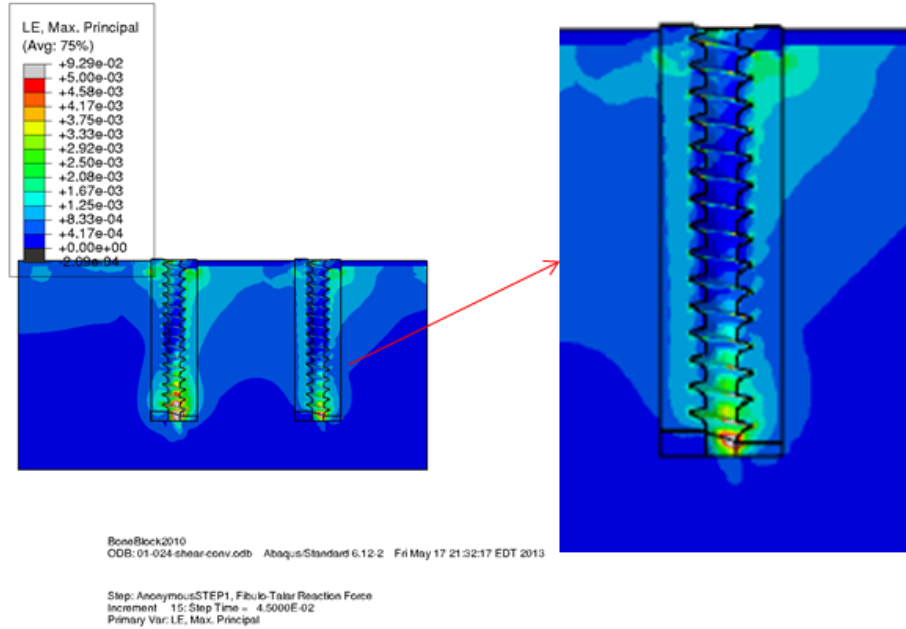


(a) Conventional screw construct

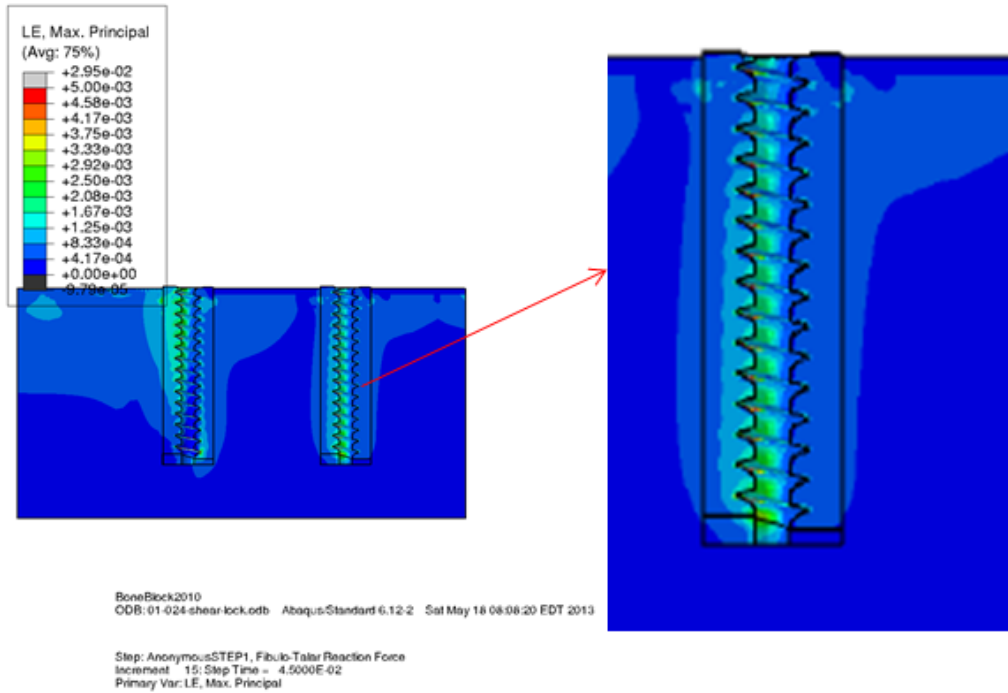


(b) Locking screw construct

Figure 4.42: Total strain under shear load (Bone density = 0.24 g cm⁻³, Cortex thickness=0mm) (The locked screw caused more uniform strain at screw-bone interface compared to the conventional screw)

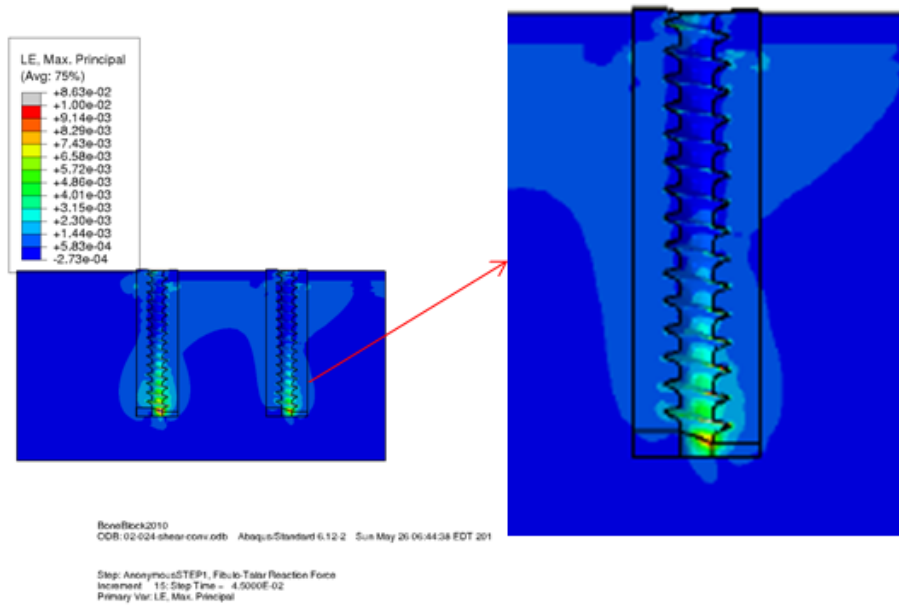


(a) Conventional screw construct

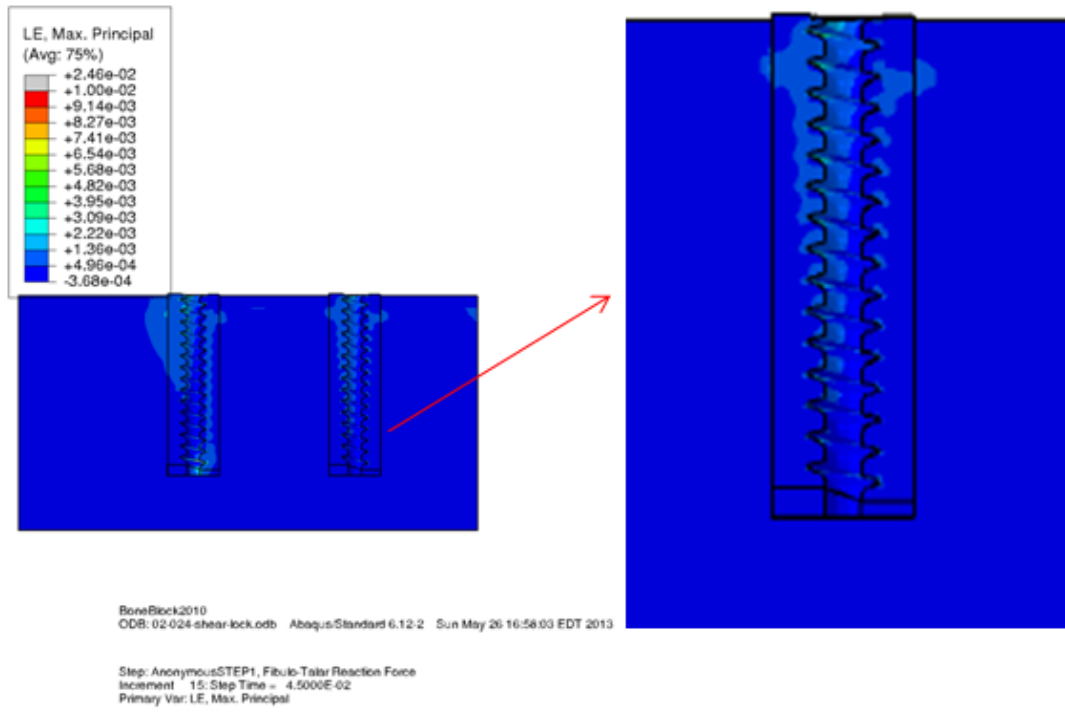


(b) Locking screw construct

Figure 4.43: Total strain under shear load (Bone density = 0.24 g cm^{-3} , Cortex thickness=1mm) (The locked screw caused more uniform strain at screw-bone interface compared to the conventional screw)

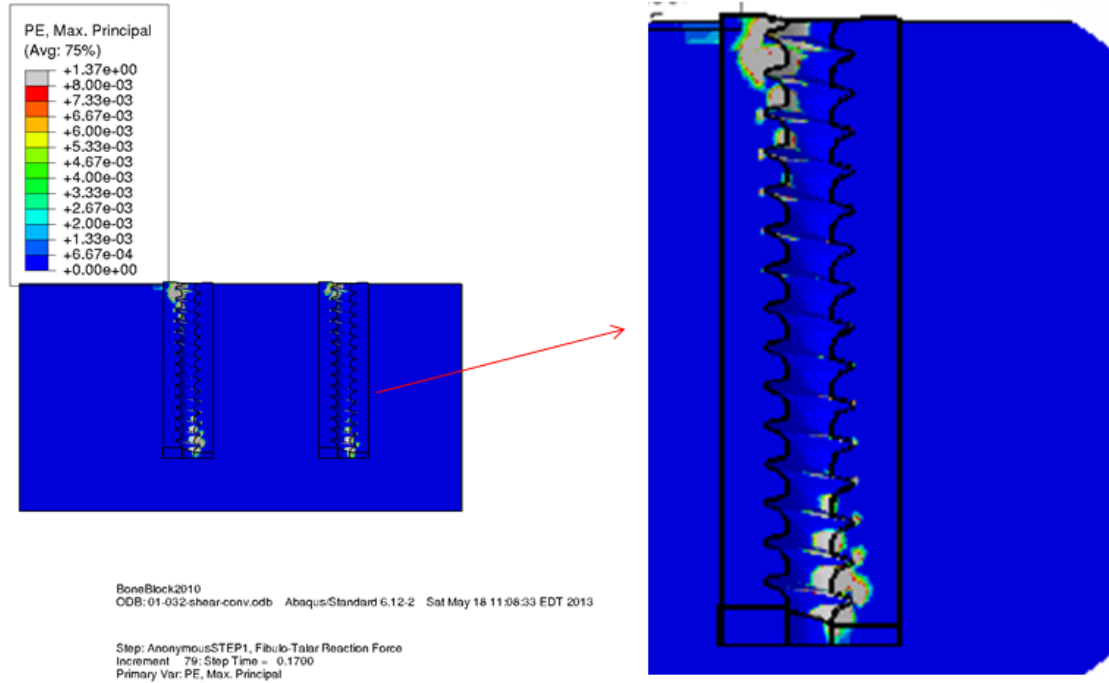


(a) Conventional screw construct

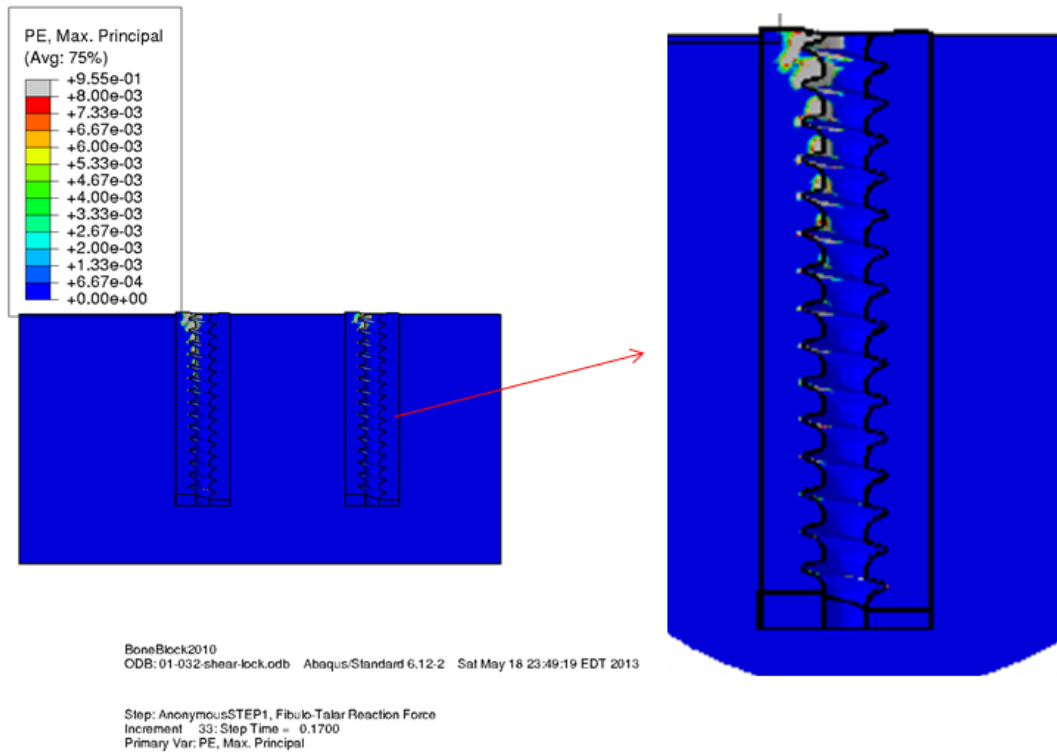


(b) Locking screw construct

Figure 4.44: Total strain under shear load (Bone density = 0.32 g cm^{-3} , Cortex thickness=2mm) (The locked screw caused more uniform strain at screw-bone interface compared to the conventional screw)



(a) Conventional screw construct



(b) Locking screw construct

Figure 4.45: Plastic strain under shear load (Bone density = 0.32 g cm^{-3} , Cortex thickness=1mm)

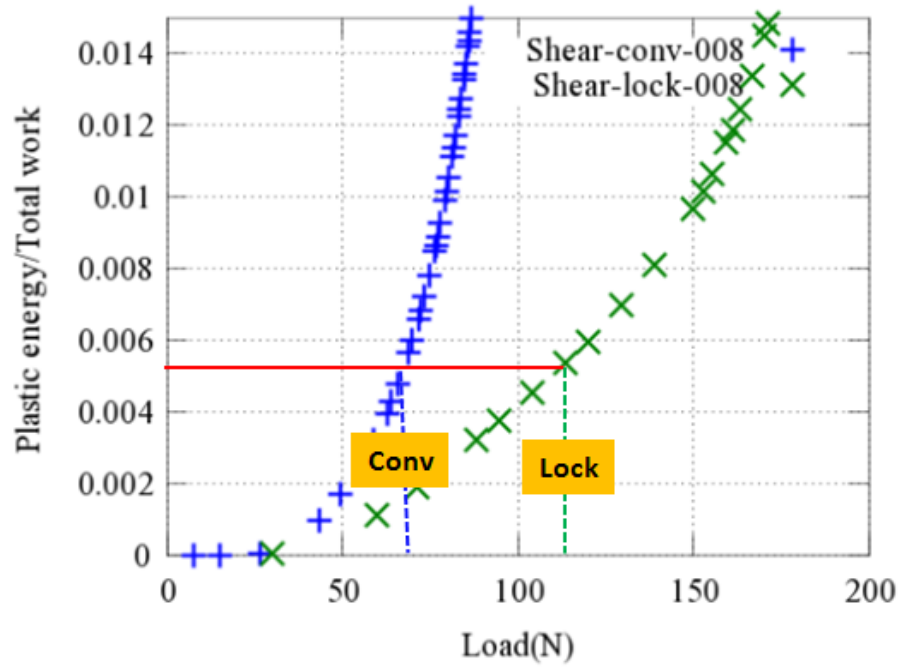


Figure 4.46: Plastic energy dissipation comparison under shear load (*The locked screw construct sustained the greater shear load compared to the conventional screw construct at assumed 0.5% plastic energy dissipation*)

The plastic failure initiation plot (Fig. 4.47) shows the shear load transfer sequence through the cortical and cancellous portion of the bone. For the conventional screw construct the failure initiated at the cancellous portion of the bone followed by a cortical failure (250 N vs 410 N). Conversely, with the locked screws the cortical bone failure initiated first followed by the cancellous bone failure at relatively greater load (350 N vs 470 N). Therefore, with the conventional screws an initial load bearing is done through the cancellous bone followed by the cortical bone. However, locked screws transferred initial load to the cortex followed by the cancellous bone. Thus, the initial load bearing through the cortex makes the locked screw a stronger construct compared to the conventional screw construct, where the initial strength relied on cancellous bone. Moreover, this failure sequence within the cortical and cancellous bone regions showed a similar trend for all analyzed cancellous bone densities and cortex thicknesses (Fig. 4.47 vs Fig. 4.48). Thus, irrespective of the bone quality (i.e. cancellous densities and cortex thicknesses) the locked screw construct offered the greater strength under applied shear load. (*please see appendix section G.2 for the remaining plastic strain plots with shear load*)

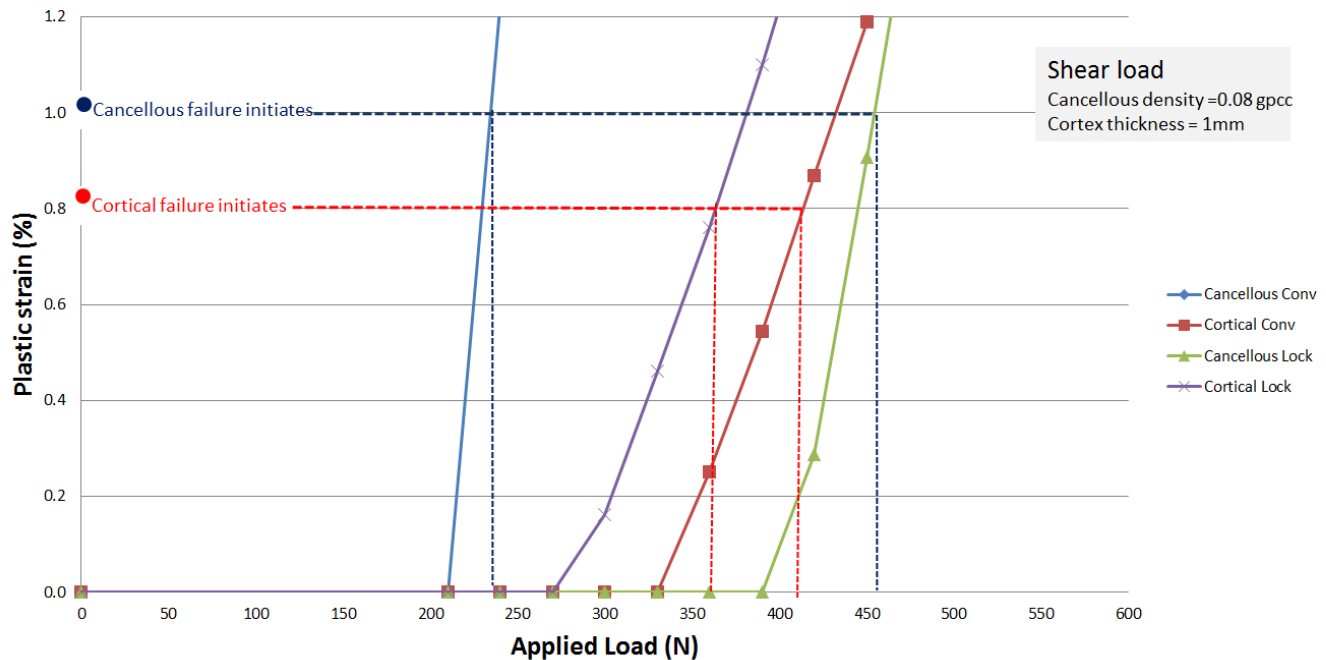


Figure 4.47: Plastic strain for the failure initiation under shear load (Cancellous density = 0.08 gpcc, cortex thickness=1mm)

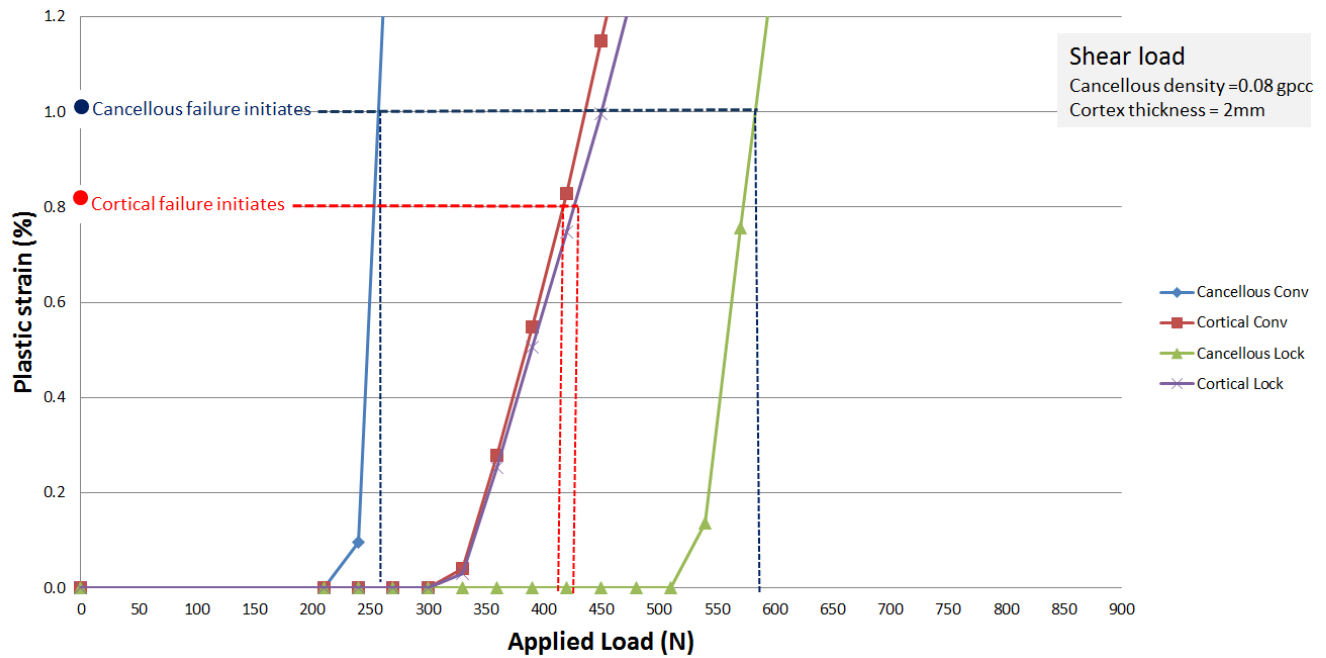


Figure 4.48: Plastic strain for the failure initiation under shear load (Cancellous density = 0.08 gpcc, cortex thickness=2mm)

4.2.4 Oblique load

The oblique pullout load was applied to the plate end at 45 °to the normal load direction (Fig. 4.20). The conventional screw experienced relatively more uniform force distribution along the screw length for the constructs with 0mm, 1mm and 2mm cortex thicknesses (Fig. 4.49 to Fig. 4.51). Conversely, the locked screw experienced a non-uniform load transfer i.e. a greater force towards the screw tail. The uniform force distribution with conventional screws leads to the lower bone strain (Fig. 4.52 to Fig. 4.54) and hence lower plastic dissipation (Fig. 4.56). Thus, a conventional screw construct offered the greater strength compared to the locked screw construct under oblique load. (*please see appendix sections D.3 and F.3 for the remaining force distribution, strain and plastic energy plots with oblique load*)

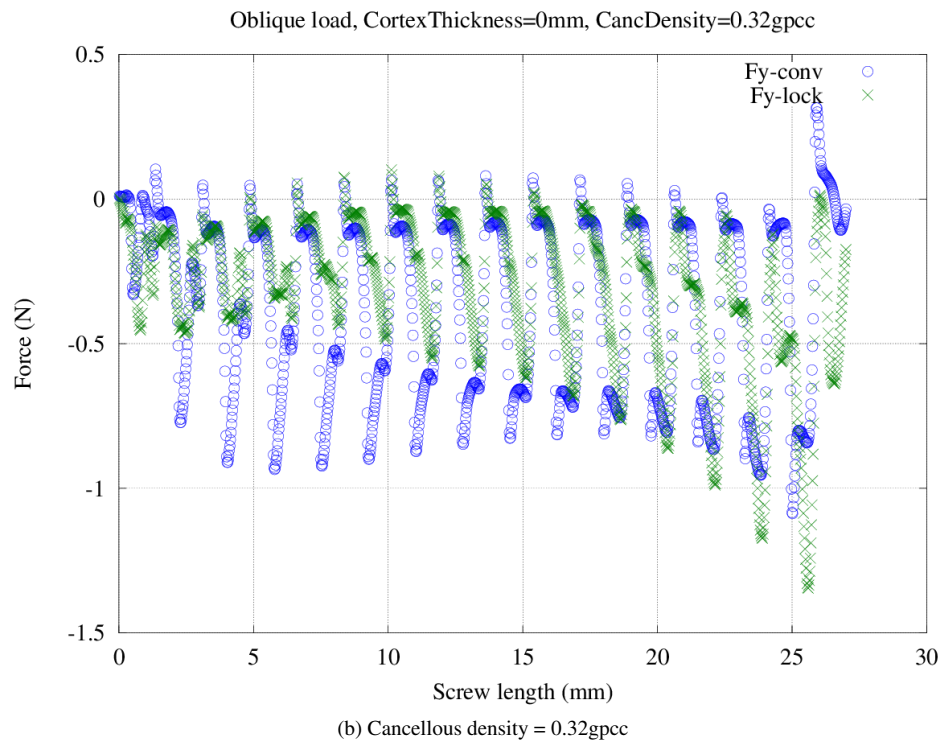
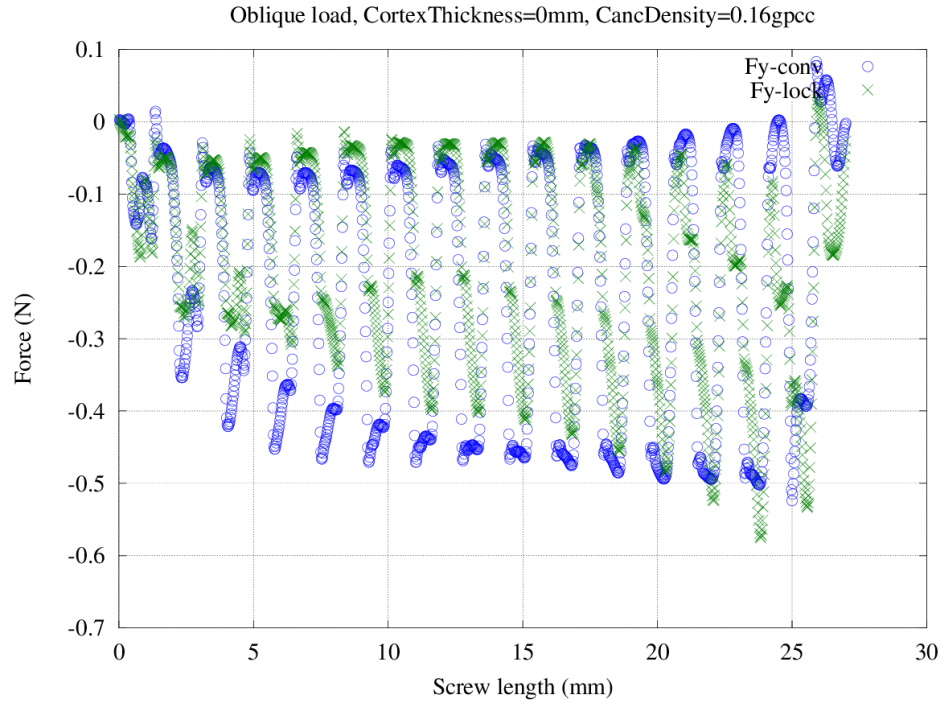


Figure 4.49: Force (F_y) distribution over the threads under oblique load (cortex thickness = 0mm) (*The conventional screw caused a relatively more uniform force distribution along the screw length*)

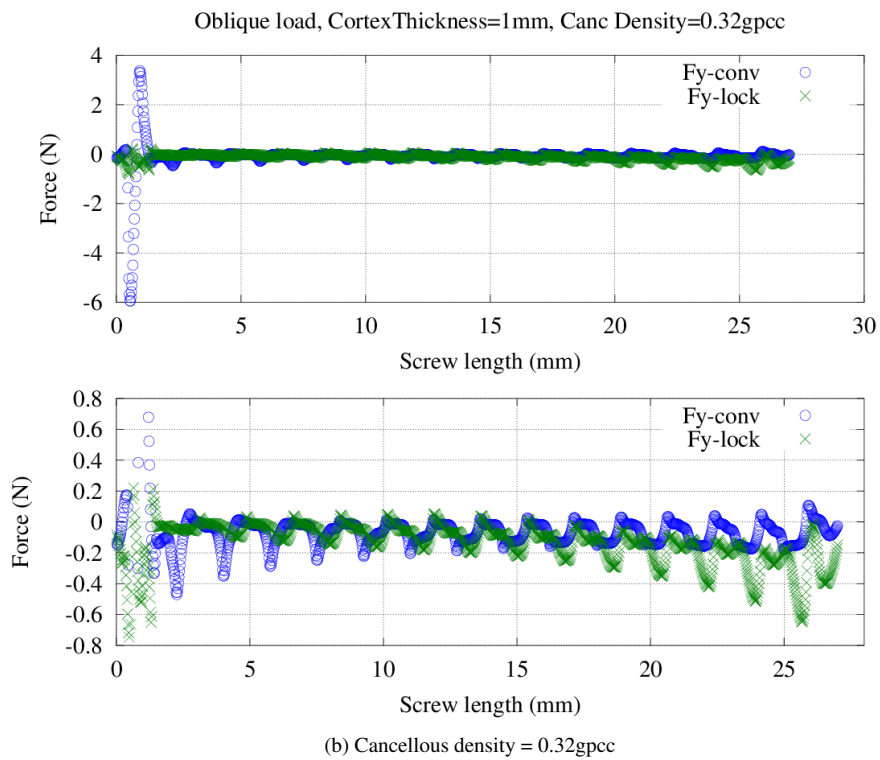
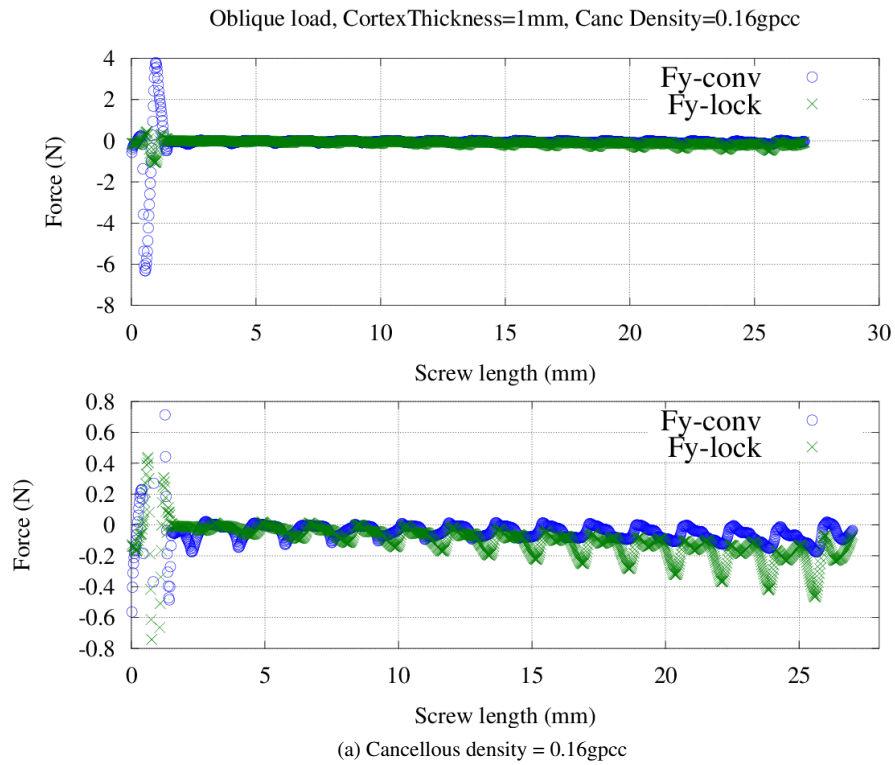
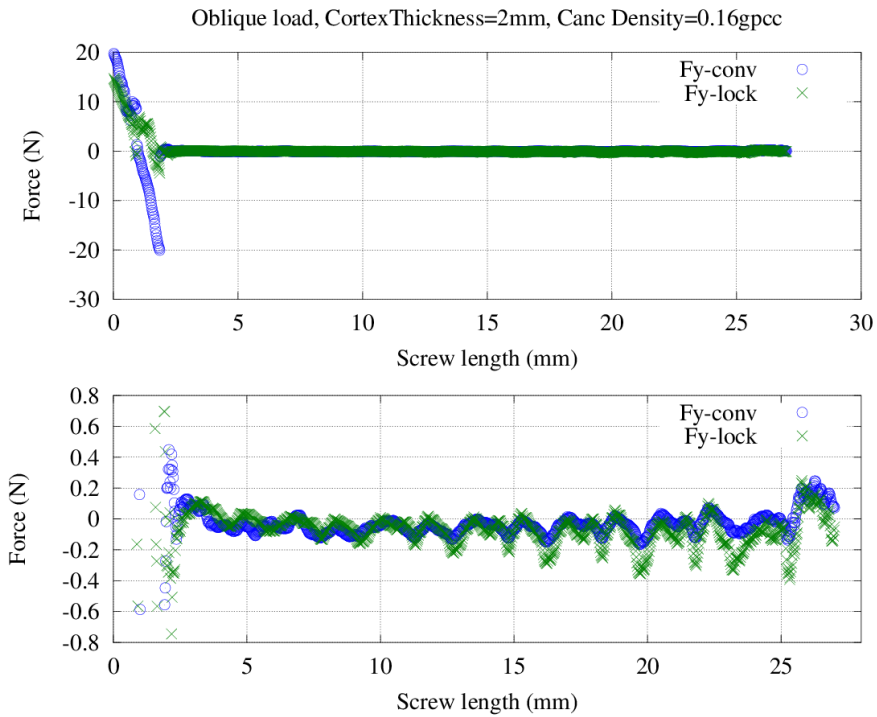
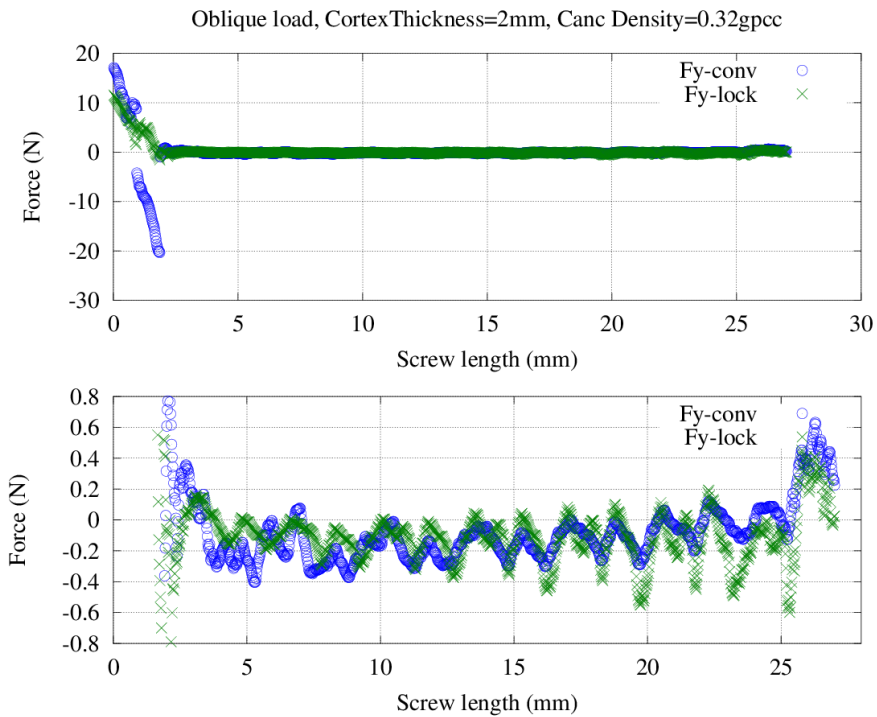


Figure 4.50: Force (F_y) distribution over the threads under oblique load (cortex thickness = 1mm) (The conventional screw caused a relatively more uniform force distribution along the screw length)

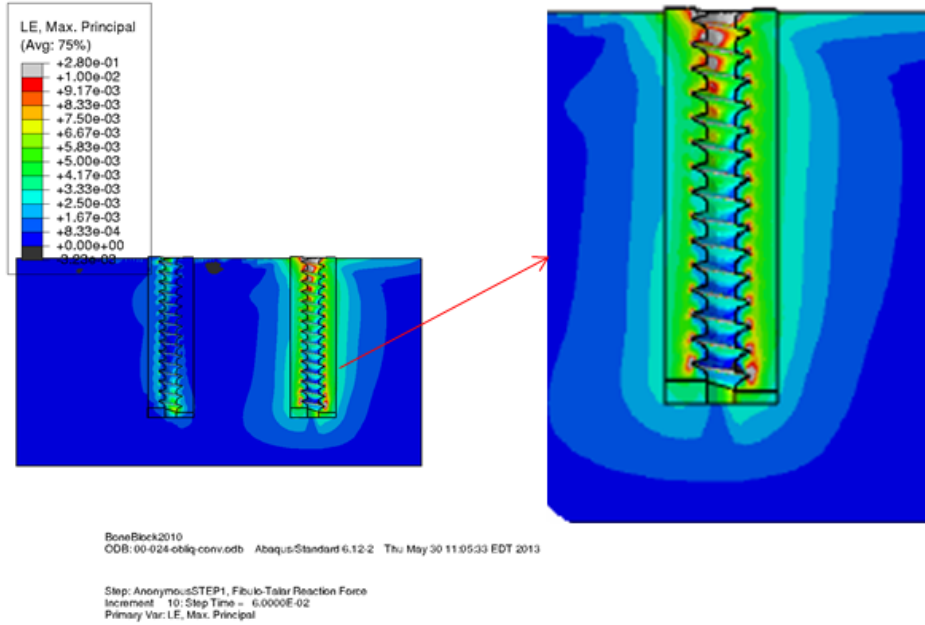


(a) Cancellous density = 0.16gpcc

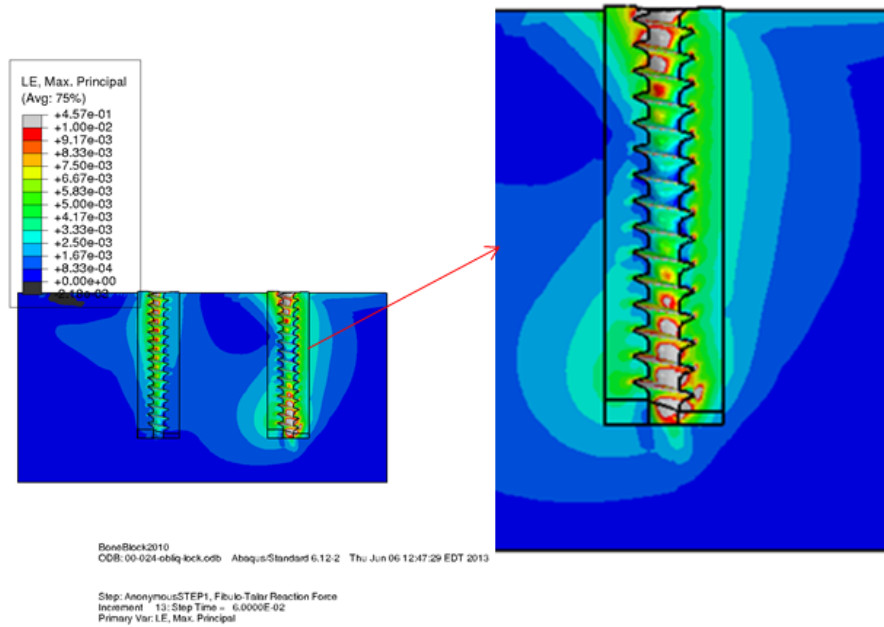


(b) Cancellous density = 0.32gpcc

Figure 4.51: Force (Fy) distribution over the threads under oblique load (cortex thickness = 2mm) (The conventional screw caused a relatively more uniform force distribution along the screw length)

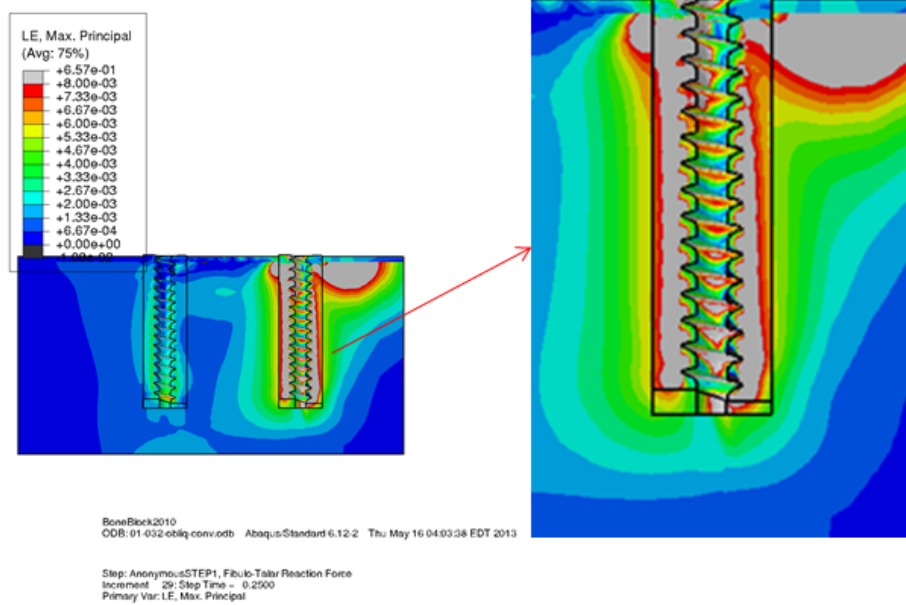


(a) Conventional screw construct

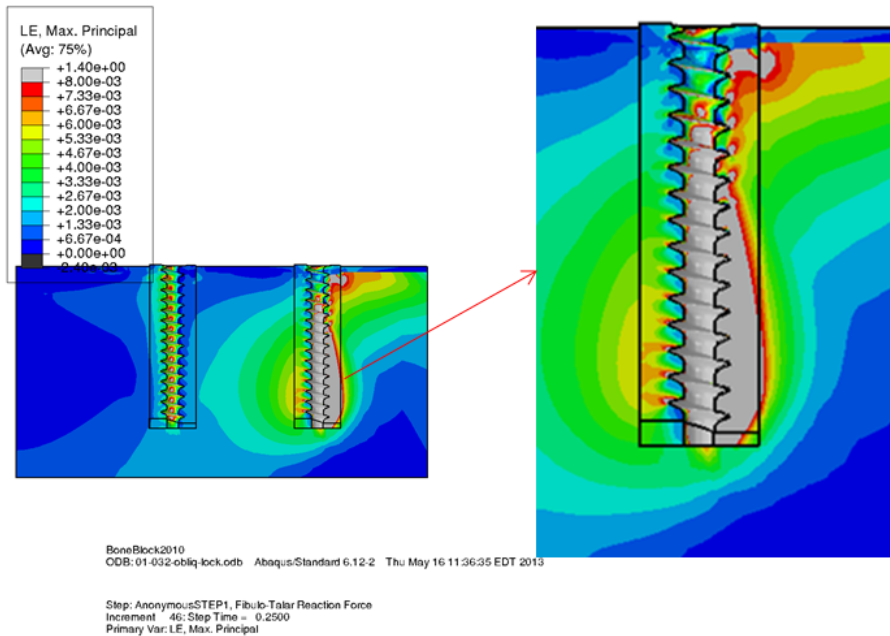


(b) Locking screw construct

Figure 4.52: Total strain under oblique load (Bone density = 0.24 g cm^{-3} , Cortex thickness=0mm) (The conventional screw caused more uniform strain at screw-bone interface compared to the locked screw)

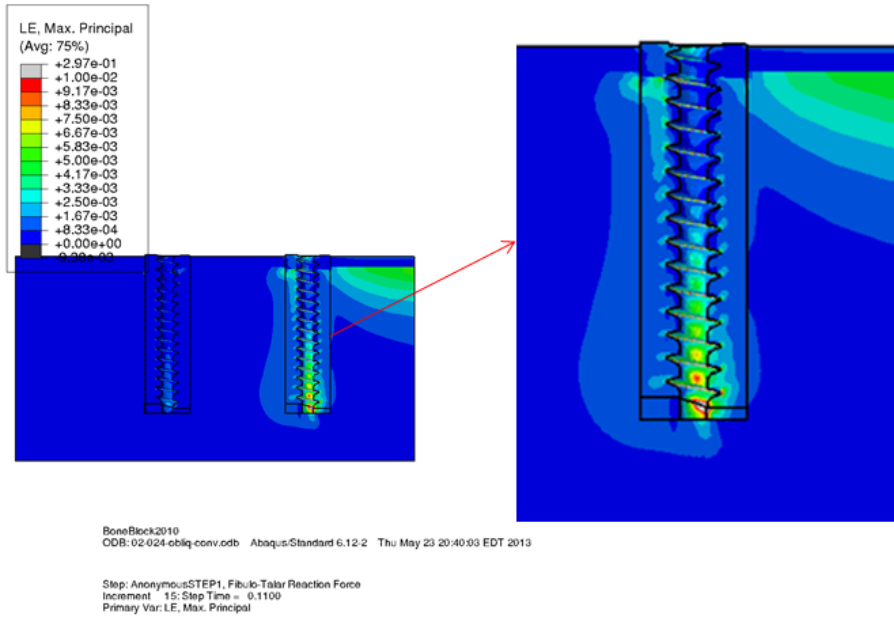


(a) Conventional screw construct

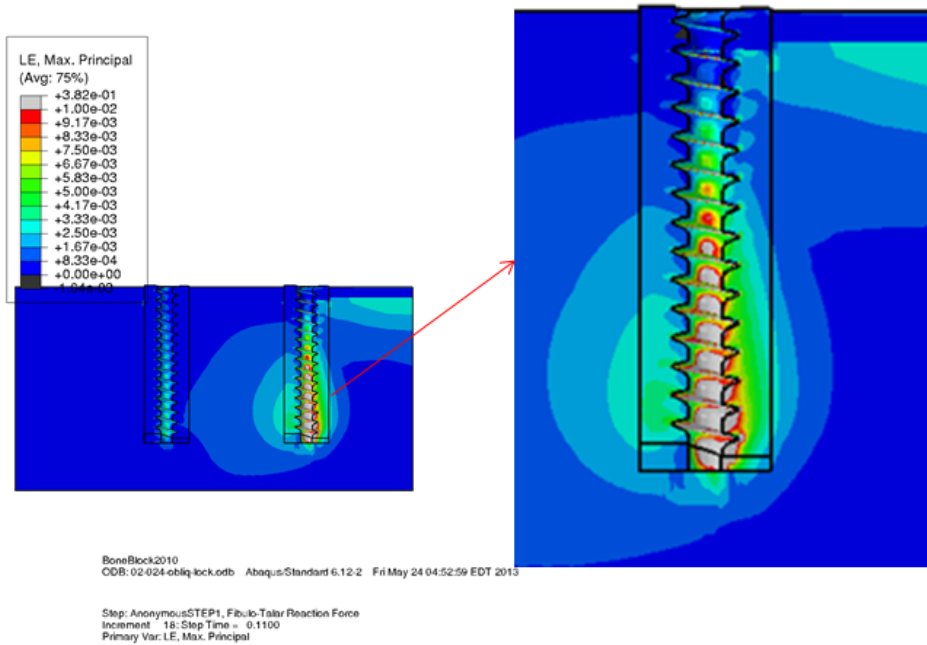


(b) Locking screw construct

Figure 4.53: Total strain under oblique load (Bone density = 0.32 g cm^{-3} , Cortex thickness=1mm) (The conventional screw caused more uniform strain at screw-bone interface compared to the locked screw)

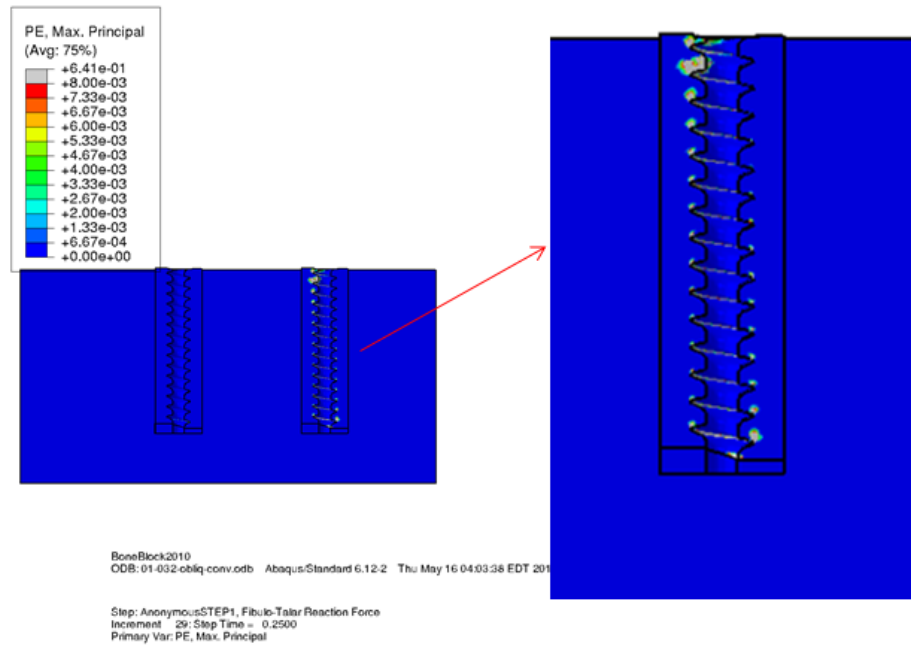


(a) Conventional screw construct

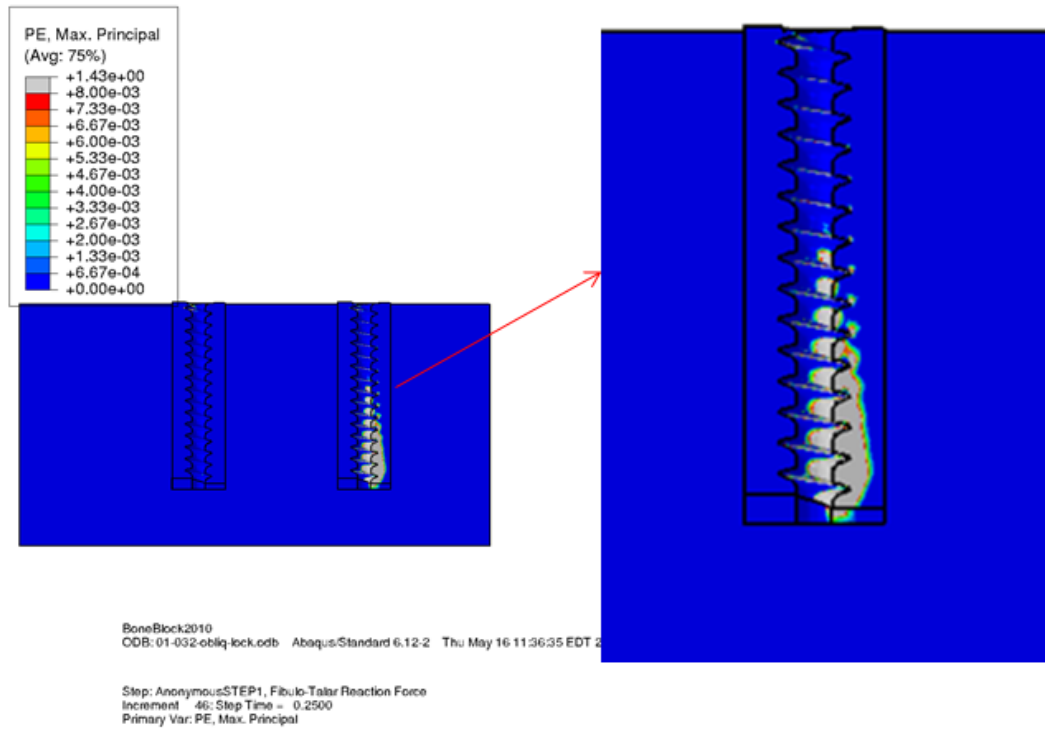


(b) Locking screw construct

Figure 4.54: Total strain under oblique load (Bone density = 0.24 g cm^{-3} , Cortex thickness=2mm) (The conventional screw caused more uniform strain at screw-bone interface compared to the locked screw)



(a) Conventional screw construct



(b) Locking screw construct

Figure 4.55: Plastic strain under oblique load (Bone density = 0.32 g cm^{-3} , Cortex thickness=1mm) (The conventional screw caused less bone plastic strain due to the uniform force distribution at the screw-bone interface)

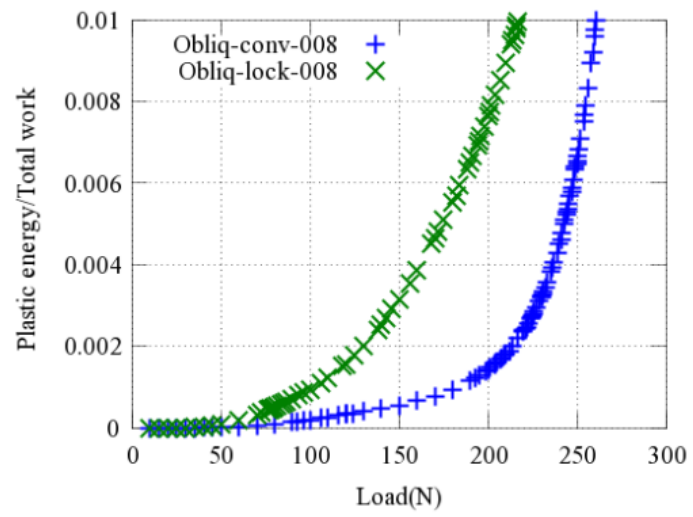


Figure 4.56: Plastic energy dissipation comparison under oblique load

The plastic failure initiation plots (Fig. 4.57) show that for both the construct types (locked and conventional) the cancellous portion of the bone started failing first followed by the cortical bone failure at relatively greater loads. However, the locked screw construct experienced cancellous bone failure initiation at comparatively lower loads which makes the conventional construct relatively stronger.

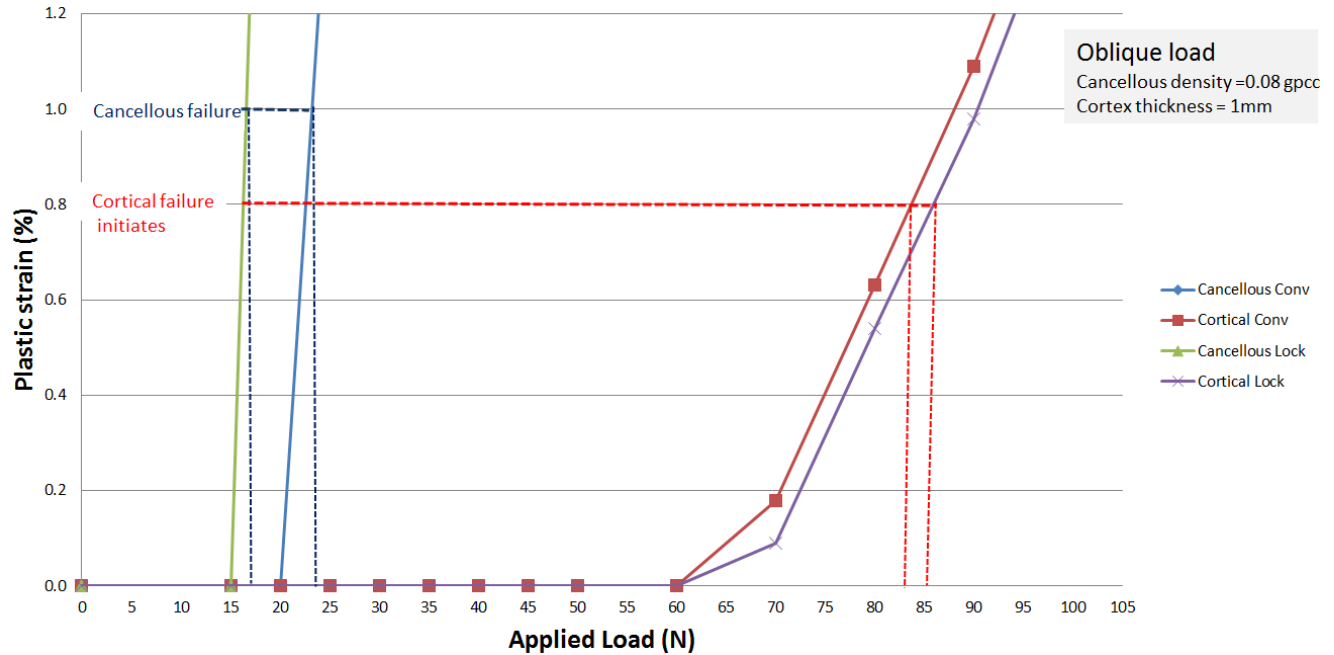


Figure 4.57: Plastic strain for the failure initiation under oblique load (Cancellous density = 0.08 gpcc, cortex thickness=1mm)

4.2.5 Conclusions

In summary, the finite element analysis outcomes showed that the uniformity of force distribution at the bone-screw interface and the bone plastic strain distribution determined the construct strength behavior. The locking screw construct provided the greater strength under shear load and the conventional screw construct offered greater strength under the normal and oblique pullout loads for the analyzed cortex thicknesses, cancellous bone densities and screw diameter. Furthermore, the load transfer mechanism (the force distribution) at screw-bone interface was affected by the cortical bone thickness.

Chapter 5

Surgeon perception and its influence on fracture fixation quality

In addition to pullout strength, the fracture fixation stability of conventional (non-locking) plate is related to the ability of a construct to resist the motion between the plate and bone [21, 10, 22]. Sufficient friction between the plate and bone is required to resist this motion is dictated by generating adequate compressive force at the plate-bone interface. This compression is directly proportional to the applied torque [21]. Moreover, the stripped bone due to the screw over-tightening can significantly compromise the construct stiffness [48] and strength [49].

The axial compression generated between the bone and plate primarily depends on the bone quality (i.e. bone density). Hence, achieving stable fixation can be difficult in osteoporotic bone. In these situations, a surgeon's goal is to achieve torque that maximizes plate-bone compression without compromising the structural stability of the fixation.

5.1 Effect of applied torque (pre-tension) on construct strength

The screw tightening (torque) effect on the conventional screw construct strength was evaluated using finite element model with different pre-tension levels applied to the screws. The force distributions at screw-bone interface were compared for 0N, 500N and 1000N pre-tensions. The analysis outcome shows that the pre-tension increases the bone stress which decreases the stress margins available to carry additional load (Figs. 5.1 and 5.2). Hence, the construct strength also relies on the surgeon's perception to apply an optimum torque. Therefore, the next section includes an experimental investigation performed to evaluate the surgeons' ability to perceive bone stripping.

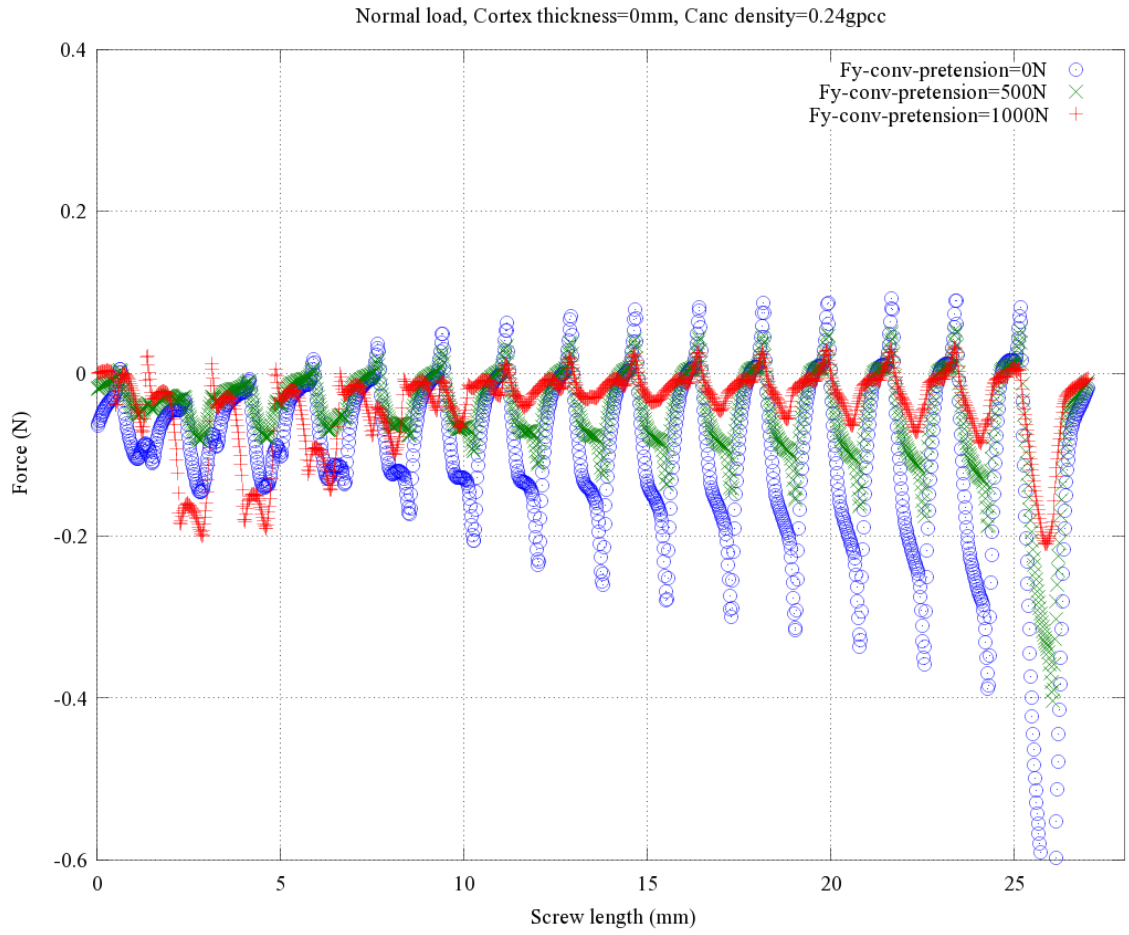


Figure 5.1: Effect of pre-tension on force at screw-bone interface (Cancellous density = 0.24 gpc, cortex thickness=0mm)

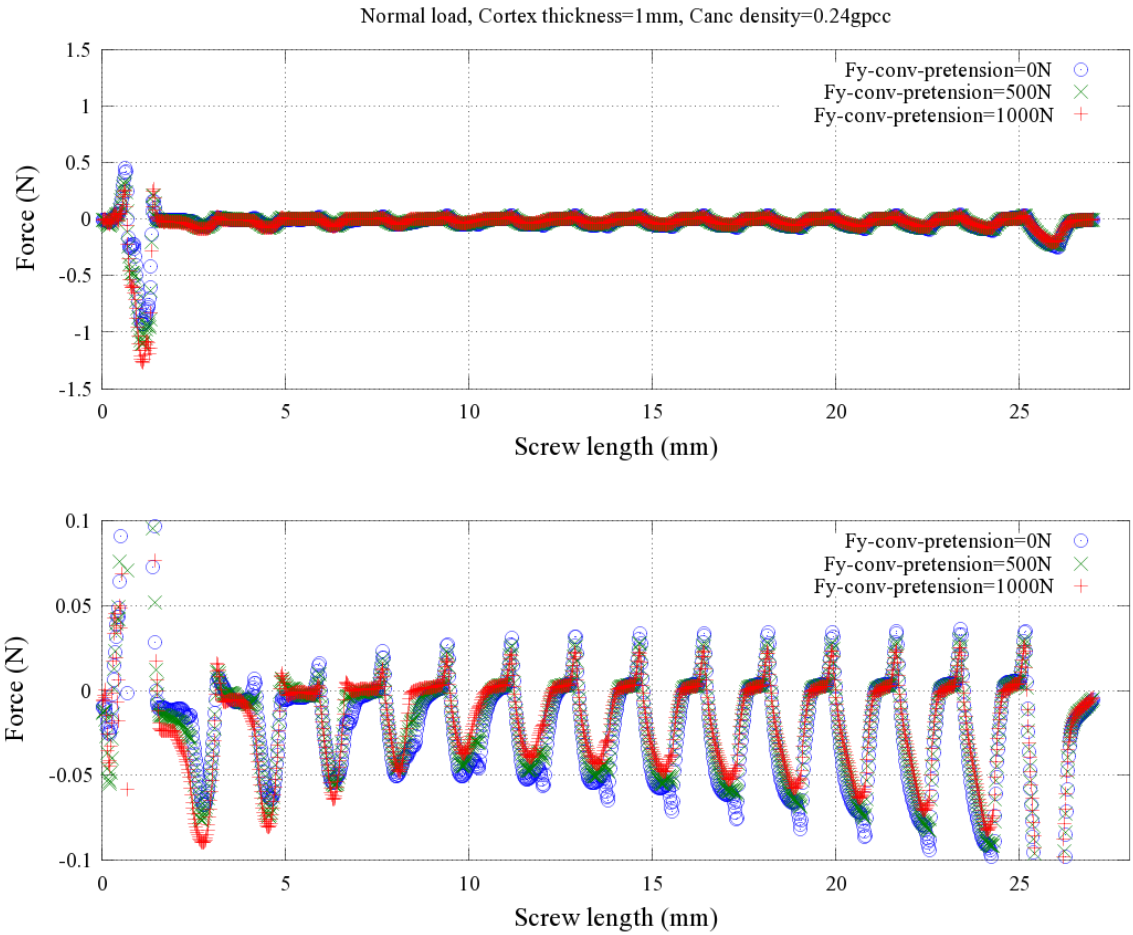


Figure 5.2: Effect of pre-tension on force at screw-bone interface (Cancellous density = 0.24 gpcc, cortex thickness=1mm)

5.2 Evaluation of surgeon ability to perceive optimum torque in synthetic cancellous bones

Ten orthopaedic (five residents and five attending surgeons) of varying experience who have completed the AO basic course and are skilled with common fracture fixation practices were voluntarily recruited. Prior to test, the plates were loosely mounted on the bone blocks (40 mm by 40 mm by 130 mm) with screws initiated into each of eight pre-drilled holes (2.5 mm). The pre-drilled holes were at least five screw diameters from the nearest edge and all testing parameters were set according to the ASTM F 543-07 Standard Specification and Test Methods for Metallic Medical Bone Screws. The constructs were secured to the reaction torque load cell with the pre-drilled hole positioned to ensure accurate torque measurements (Fig. 5.3).

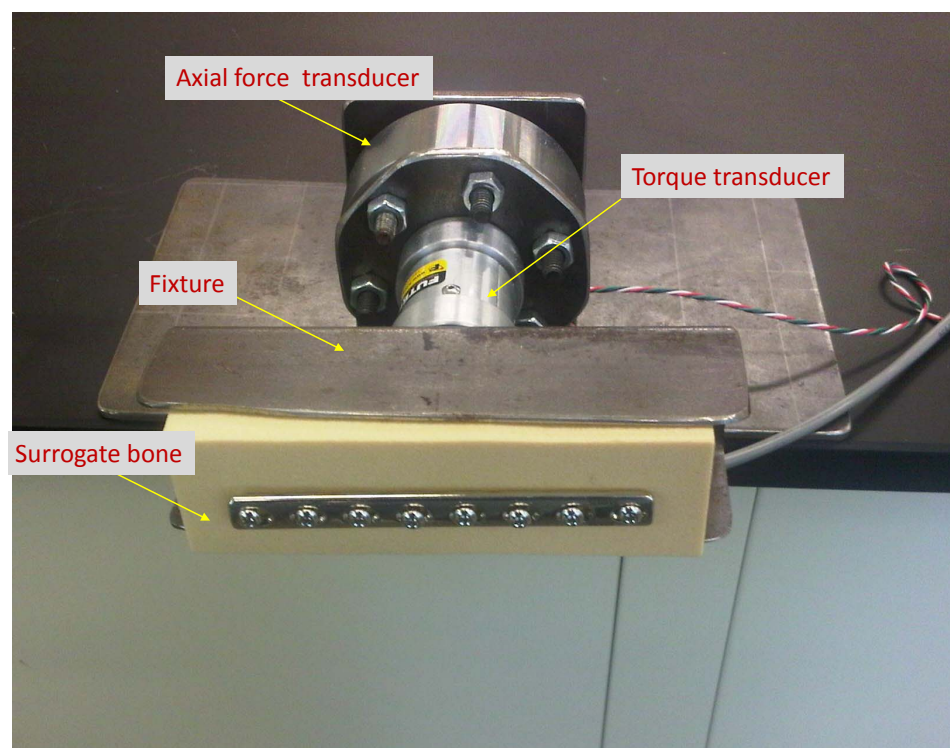


Figure 5.3: Surgeon evaluation test setup

Each surgeon inserted the cancellous bone screw using standard technique that simulates intraoperative fracture fixation to achieve maximum construct stability. Each surgeon placed eight screws into each of three different surrogate bone densities (0.08 g cm^{-3} , 0.16 g cm^{-3} , and 0.32 g cm^{-3}). The screw was aligned with the axis of the transducer prior to each screw insertion. After insertion of each screw, they were then be asked to a) rate the screw purchase on a scale of 1 to 10, b) report what percentage of maximum torque was achieved, and c) identify whether or not the bone was stripped during insertion. At the end of each screw insertion by surgeon, while surgeon was answering the mentioned three questions in data sheet, the investigator finished rest of the turns to strip the bone. For each screw, the largest torque achieved by both the surgeon (TS) and the investigator (TI) were

compared, the greater being the maximum torque (T_M). These values were determined within the appropriate time intervals depicted in (Figs. 5.4 and 5.5). If T_I was greater than T_S , the screw was deemed to have not stripped by the surgeon. If T_S was greater than T_I , the surgeon had advanced the screw past T_M and it was deemed to be stripped. This process was followed for each screw insertion in order to check the perceptions about bone stripping. All the data was acquired using Labview express and portable wireless data acquisition system and was post-processed using MATLAB. Statistical calculations were made using R, a statistical software package (<http://www.r-project.org/>).

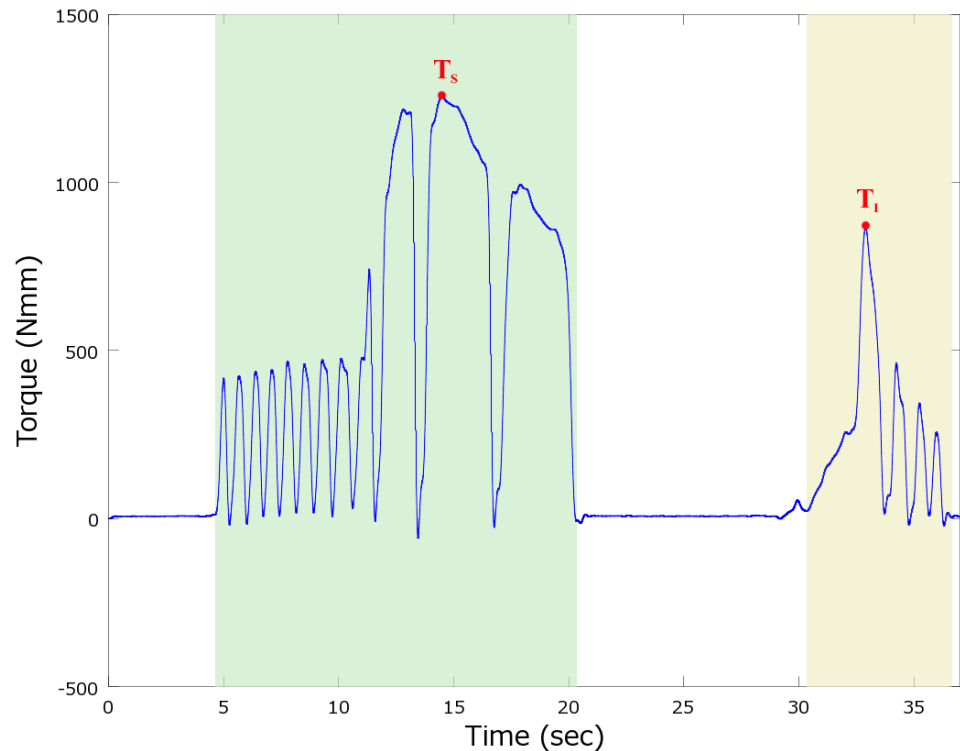


Figure 5.4: Bone stripped by surgeon ($T_S < T_I$)

Observations from post processed data

The data was post processed to investigate the surgeons' proficiency in optimizing peak torque, the effect of axial force on max torque, the influence of years of surgical practice, as well how often the screws were stripped for each bone density. Plots for surgeon's max torque for each screw insertion (total of 240 screw insertions for 10 surgeons each with three surrogate bone densities) and investigators max torque with corresponding axial forces were examined (for example Fig. 5.6). The standard deviation and mean max torque plots for each densities are shown in (Fig. 5.9 to Fig. 5.11).

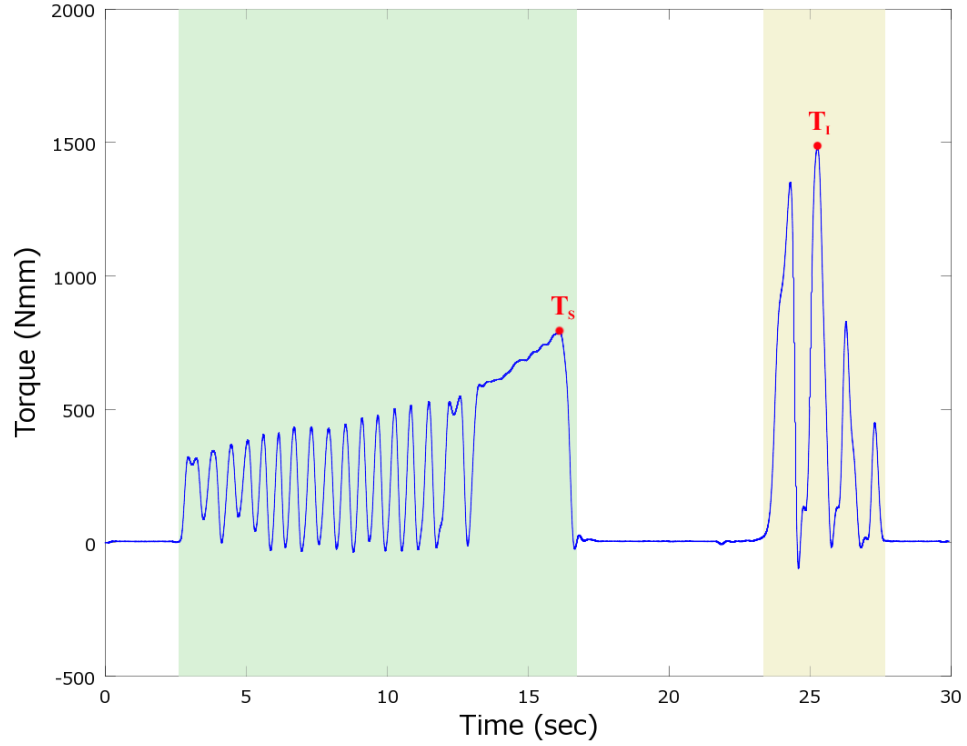


Figure 5.5: Bone not stripped by surgeon ($T_s > T_l$)

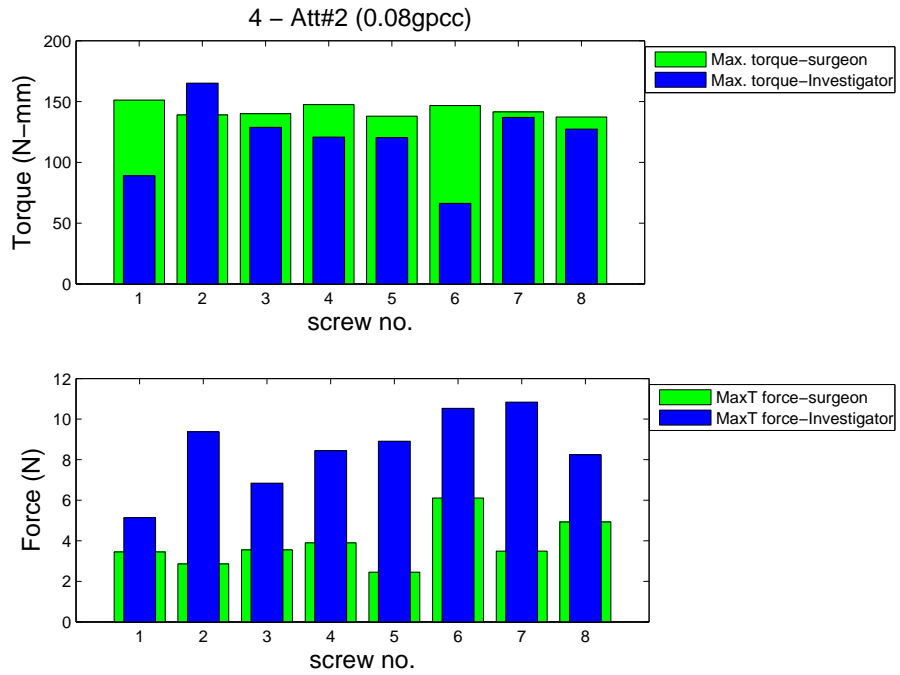


Figure 5.6: Effects of applied axial force and bone density ($0.08\text{g}/\text{cm}^{-3}$)

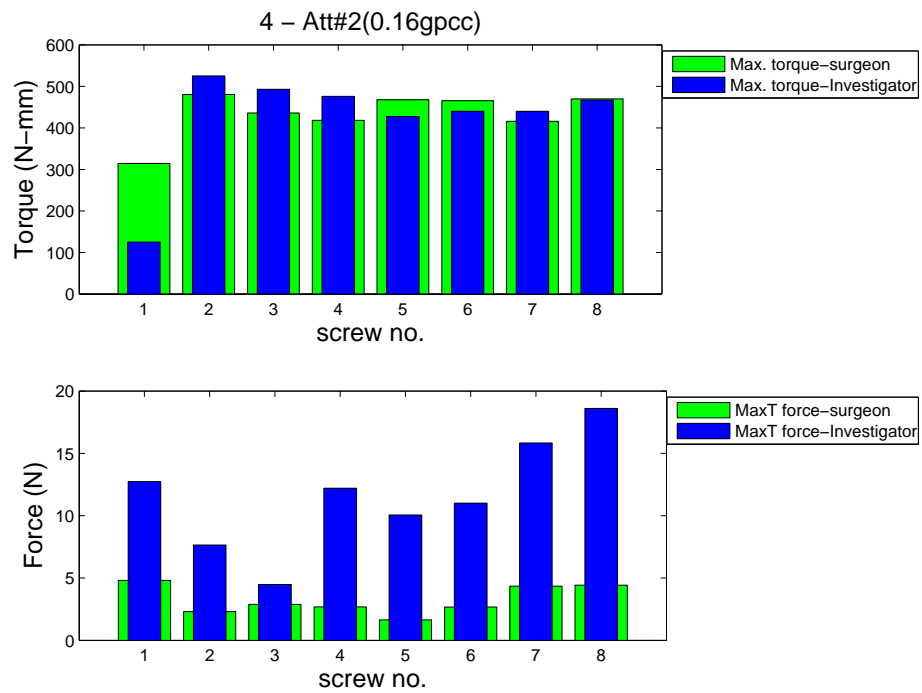


Figure 5.7: Effects of applied axial force and bone density ($0.16\text{g}/\text{cm}^{-3}$)

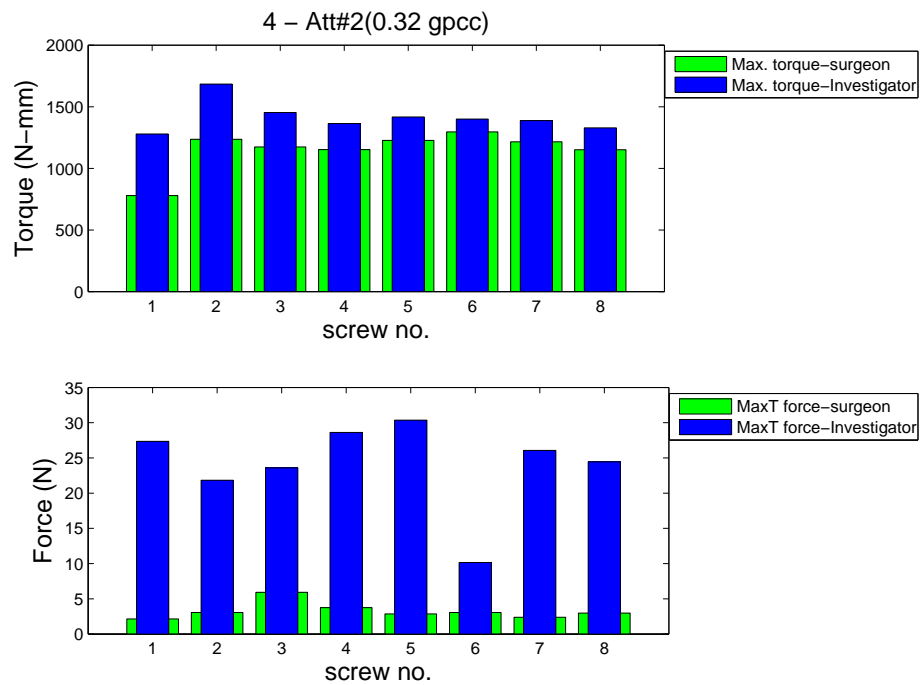


Figure 5.8: Effects of applied axial force and bone density ($0.32\text{g}/\text{cm}^{-3}$)

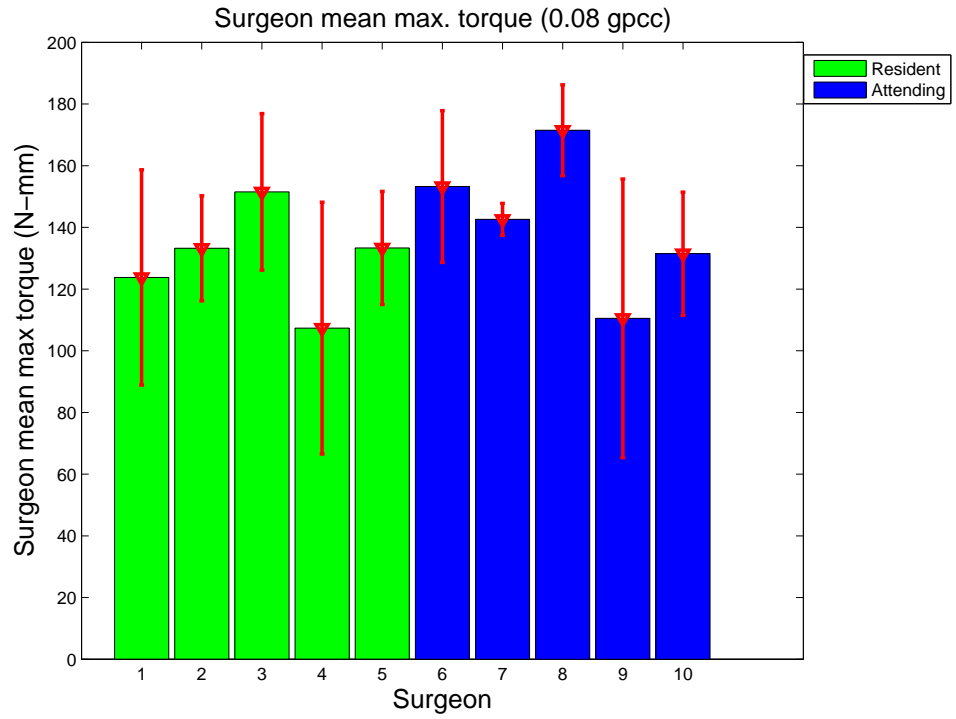


Figure 5.9: Max torque and standard deviation (0.08g/cm⁻³)

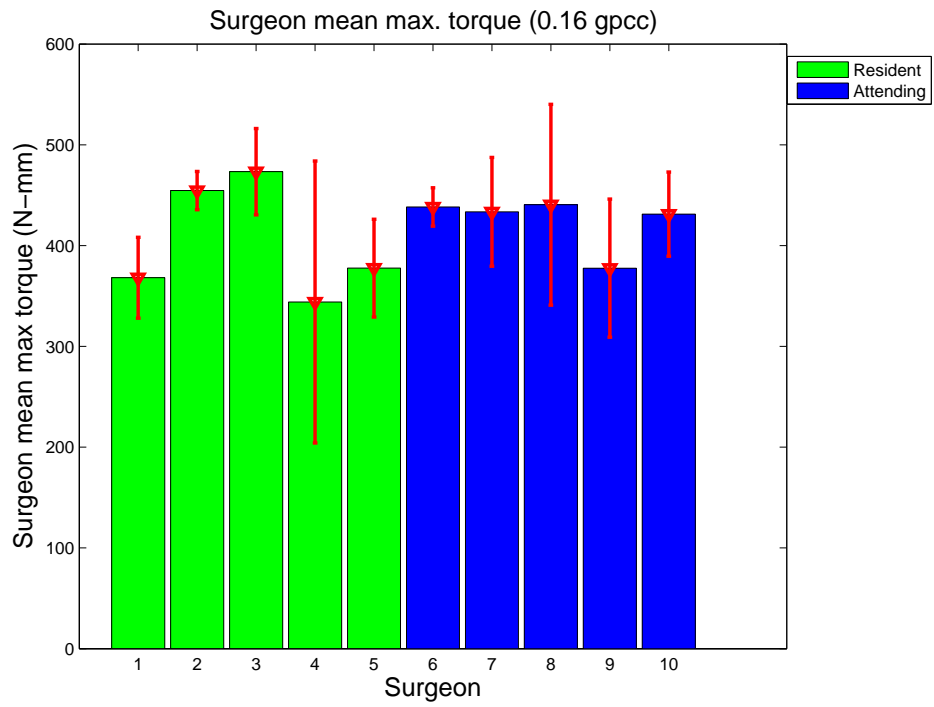


Figure 5.10: Max torque and standard deviation (0.16g/cm⁻³)

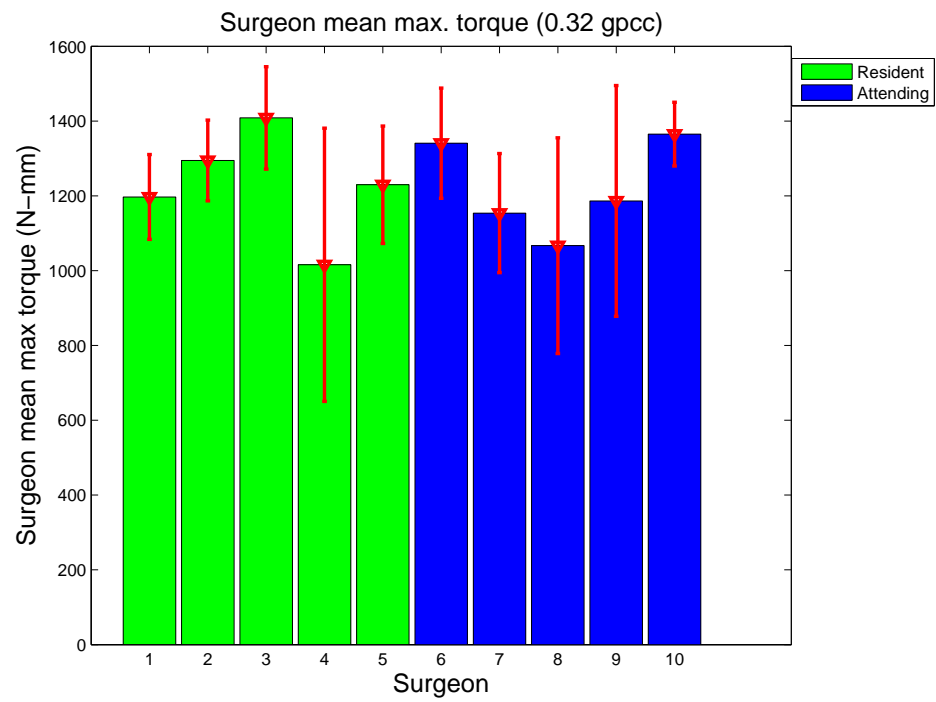


Figure 5.11: Max torque and standard deviation ($0.32\text{g}/\text{cm}^{-3}$)

Screw stripping

Surgeons stripped 109 of 240 (45%) screws. Significant relationships were not found between the incidence of screw stripping and density ($p = 0.1862$) (Tab. 5.1), nor between screw stripping and surgical rank (attending vs. resident, $p = 0.4366$) (Tab. 5.2). However, there was a statistically significant correlation between individual surgeons and the incidence of stripping ($p = 0.0001$), demonstrating that some surgeons frequently over-tightened screws and other surgeons did so much less often (Tab. 5.3). Moreover, screw stripping was also found to be related to order of insertion ($p = 0.0218$), they did not strip the first very often but get worse after that (Tab. 5.4). In addition, no significant relationship was found between axial force and stripping at the measured load levels ($p = 0.3174$). However, surgeons had tendency to apply more axial force for higher bone density (i.e. with good quality bones).

Table 5.1: Relationship of stripping with density

Density	Stripped	Not Stripped
low (0.08 g cm^{-3})	33	47
medium (0.16 g cm^{-3})	43	37
high (0.32 g cm^{-3})	33	47

Table 5.2: Relationship of stripping with rank of surgeon

Rank	Stripped	Not Stripped
Resident	58	62
Attending	51	69

Table 5.3: Importance of individual surgeon to stripping

Order	Stripped	Not Stripped
Surgeon 1	9	15
Surgeon 2	20	4
Surgeon 3	17	7
Surgeon 4	11	13
Surgeon 5	8	16
Surgeon 6	10	14
Surgeon 7	10	14
Surgeon 8	4	20
Surgeon 9	5	19
Surgeon 10	15	9

Table 5.4: Importance of screw sequence

Order	Stripped	Not Stripped
1	5	25
2	11	19
3	13	17
4	15	15
5	16	14
6	19	11
7	15	15
8	15	15

Percentage of Tmax achieved

Surgeons achieved a mean of 81.2% of maximum torque (standard deviation 16.0) with the 131 screws that were not stripped. In addition, there seems to be consistency in the data to support that the measurements are correct. For the different densities, the means and standard deviation are consistent and close to what was measured with the load frame (Tab. 5.5).

Table 5.5: Mean max. torque +/- standard deviation

Density	Surgeon (N-mm)	Load frame (N-mm)
low (0.08 g cm^{-3})	154 ± 20.97	167 ± 13
medium (0.16 g cm^{-3})	454.3 ± 46.30	484 ± 70
high (0.32 g cm^{-3})	1386 ± 121.38	1480 ± 48

Surgeon Recognition of stripping

Surgeons were poor at identifying when they had stripped a screw. They correctly identified only 10 of 109 stripped screws. Seven of 131 screws were incorrectly reported to be stripped and 6 of these were reported by the same surgeon.

In summary, this study finds that surgeons stripped 45.4% of screws placed into synthetic cancellous bone and were generally unable to recognize it. The higher bone stripping rate and poor surgeon's perception about optimal screw insertion torque can lead to the poor fracture fixation. A significant drop in screw pullout strength due to the screw tightening beyond yield torque can significantly reduce the fracture fixation strength.

Chapter 6

Summary

This dissertation investigated the stiffness and strength of the non-locking (conventional) and locking (fixed angle) type screw-plate constructs and some of the factors that contribute to them, such as screw-plate interface, screw design, bone density, cortical bone thickness and load orientation. Additionally, the surgeon's ability to prevent and perceive stripping of the bone while driving screws was evaluated. Finite element analyses and experiments were performed for these investigations.

The type of construct was found to have a minimal effect on the stiffness of the construct, whereas the plate geometry had a larger influence. There was a negligible difference in construct stiffness between conventional and fixed angle screw constructs for a five screw neutralization plate when the plate geometry was identical. Thus, locked screw heads did not offer superiority in the biomechanical stiffness of the plate. This result is significant to clinical practice as the stiffness is used to judge stability and quality of fixation. A locked fibular neutralization plate allowed more displacement of the distal fibula than was allowed by the lateral periarticular distal fibular plate with locked screws. Thus, the stiffness of the construct was found to be dependent on plate geometry (thickness) and/or the number of screws used to hold the fracture.

The finite element analysis outcomes showed that the uniformity of force distribution at the bone-screw interface and the bone plastic strain distribution determined the construct strength behavior. A uniform force distribution at screw-bone interface demonstrates an efficient load bearing through the bone. This uniform load bearing by the bone leads to the lesser bone damage (plastic strain). The locking screw construct provided the greater strength under shear load and the conventional screw construct offered greater strength under the normal and oblique loads for the analyzed cortex thicknesses, cancellous bone densities and screw diameters. Moreover, the load carried through the cancellous bone increased with density as expected. The uniformity of force distribution and load transfer mechanism were affected by the cortex thickness. Furthermore, the percentage fraction of load transfer through the cortical bone increased with the cortex thickness.

A similar trend was observed from the experiments performed to investigate the construct strength. The con-

ventional screw construct had the greater strength against normal and oblique loads. The locked screw constructs were stronger against shear loads. The strength of all the constructs were increased with bone density. Hence, with a similar fixation device, fracture fixation performance is expected to be better with younger patients than with older patients because bone mass density decreases at older age. Video observation of the experiments demonstrated that under oblique (combined normal and shear) load, the conventional screw-plate constructs failed by pullout and the locking screw-plate constructs failed by a combination of initial pullout followed by cut out. Moreover, under pure shear load, the locked screw construct performed better than the conventional screw construct due to the greater material resistance against pure cut-out. Also the screw design has a major effect on the pullout strength.

In non-locking plates, construct stability relies on the friction between the plate and bone. This friction is controlled by the compressive force produced through applied screw torque. The finite element analysis demonstrated that an over-tightened (higher pre-tension) screw deteriorates the load carrying ability of the bone. In addition, the surgeons' perception was poor to prevent and perceive bone stripping. Furthermore, the maximum torque achieved before stripping is surgeon dependent and surgeons stripped bone more frequently than they perceived.

This research will help enhance engineers' and surgeons' knowledge of the mechanics of fracture fixation. While much attention has been paid to developing expensive locking plate technology, it may not be appropriate to claim superiority of the locked plating over the conventional plates for all the fracture fixation scenarios. This research demonstrates that the conventional screw with greater thread diameter may provide an equivalent or better performance for the fracture fixation experiencing pullout loads. Therefore, the research outcomes will also provide a reference for the appropriate device selection (locking or conventional) as per the physiological fracture location. In addition, the surgeon perception is found to be an important factor that may compromise the fixation stability. Thus, there is a scope of the future work to quantify factors affecting surgeons' perception, optimal torque and bone stripping.

Chapter 7

Future research

It was observed that incident of stripping is related to individual surgeon. The reason for higher stripping rate can be the absence of an indicator (or feedback system) which can stop surgeons from over-tightening the conventional screw. Thus, ongoing research about the screw tightening device with live feedback of screw insertion torque curve may help reduce stripping rate. Surgeons will be able to visualize the process of torque application on the screen and stop driving screw further before maximum torque is achieved. Furthermore, surgeons' perception about bone stripping was evaluated with the assumption of an extremely osteoporotic bone (cortical bone absent). Therefore, future investigations can be performed on specimen with cortical bone.

The bone stripping can be avoided by using the locked screw. However, use of locked screw can eliminate some of the advantages of the conventional screw, such as loss of tactile feel when inserting a screw in the bone, and loss of ability to use the plate as a reduction tool. The conventional plate may offer a more stable construct by increasing pullout resistance with an additional anti-pullout nut (Fig. 7.1) at the screw tail.

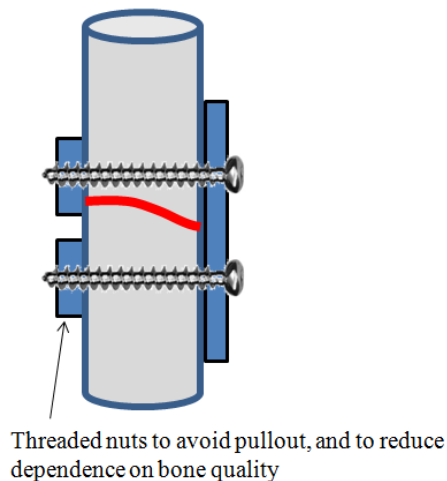


Figure 7.1: A combination of conventional plate with anti-pullout nut

Moreover, the addition of threaded nut may alleviate the construct's dependence on bone quality for screw purchase/holding. The plate construct may include at least two bi-cortical screws with nut on the either side of the fracture location (as shown in Fig. 7.1) along with the rest of the uni-cortical screws. Two bi-cortical screws may reduce the magnitude of the pullout forces transferred to other screws due to increased pullout resistance. Therefore, the proposed construct may help create stable fixation in poor quality osteoporotic bone.

In current research the construct strength was evaluated on the bone blocks with assumed flat (non-curved) bone-plate contact surface. Moreover, the symmetric loadings such as bending and shear loads were applied. Thus, the research can be continued with the cylindrical specimen under non-symmetric loading such as torsion load.

The continuum solid assumption for cancellous bone in the current research limits the investigation to be interpreted at the macroscopic level, rather than at the scale of individual trabeculae. Thus, there is a scope of future research to model the cancellous bone with micro-structural details in order to study more realistic failure at screw-bone interface. Also, isotropic material properties were assumed for the bone to evaluate the construct strength. Future investigation can be performed with directionally dependent bone properties. Furthermore, future experiments can be performed with greater than two screws and with identical screw geometries for locked and conventional constructs.

This dissertation evaluated the strength of the construct under static load to simulate the construct failure under static loads. Future research can consider cyclic loading to evaluate the failure under fatigue loads.

References

- [1] Browner, B., 2003. Skeletal trauma: basic science, management, and reconstruction, Vol. 1. WB Saunders Co.
- [2] Muller, M., Allgower, M., and Willenegger, H., 1965. "Technique of internal fixation of fractures".
- [3] Johnell, O., and Kanis, J., 2006. "An estimate of the worldwide prevalence and disability associated with osteoporotic fractures". Osteoporosis International, **17**(12), pp. 1726–1733.
- [4] Nelson, F., Lucie, K., Michael, J., Barkha, G., Clifford, Y., David, S., et al., 2009. "Complication rates following open reduction and internal fixation of ankle fractures". The Journal of Bone and Joint Surgery (American), **91**(5), pp. 1042–1049.
- [5] Ge, X., Zhang, J., Lu, W., and Qiu, S., 2009. "Selection of the internal fixation for various types of intertrochanteric fracture in aged patients and prevention for complication". Zhongguo gu shang= China journal of orthopaedics and traumatology, **22**(5), p. 385.
- [6] Henderson, C., Bottlang, M., Marsh, J., Fitzpatrick, D., and Madey, S., 2008. "Does locked plating of periprosthetic supracondylar femur fractures promote bone healing by callus formation? two cases with opposite outcomes". The Iowa Orthopaedic Journal, **28**, p. 73.
- [7] Lujan, T., Henderson, C., Madey, S., Fitzpatrick, D., Marsh, J., and Bottlang, M., 2010. "Locked plating of distal femur fractures leads to inconsistent and asymmetric callus formation". Journal of orthopaedic trauma, **24**(3), p. 156.
- [8] Davidescu, A., and Sticlaru, C., 2007. "Studies by finite element method of some devices for treatment of intertrochanteric fractures". pp. 112–117.
- [9] Taljanovic, M., Jones, M., Ruth, J., Benjamin, J., Sheppard, J., and Hunter, T., 2003. "Fracture fixation1". Radiographics, **23**(6), p. 1569.
- [10] Egol, K., Kubiak, E., Fulkerson, E., Kummer, F., and Koval, K., 2004. "Biomechanics of locked plates and screws". Journal of orthopaedic trauma, **18**(8), p. 488.

- [11] Stiffler, K., 2004. "Internal fracture fixation". Clinical Techniques in Small Animal Practice, **19**(3), pp. 105–113.
- [12] Szypryt, P., and Forward, D., 2009. "The use and abuse of locking plates". Orthopaedics and Trauma, **23**(4), pp. 281–290.
- [13] Strauss, E., Schwarzkopf, R., Kummer, F., and Egol, K., 2008. "The current status of locked plating: the good, the bad, and the ugly". Journal of orthopaedic trauma, **22**(7), p. 479.
- [14] Chao, E., Kasman, R., and An, K., 1982. "Rigidity and stress analyses of external fracture fixation devices—a theoretical approach". Journal of Biomechanics, **15**(12), pp. 971–983.
- [15] McKibbin, B., 1978. "The biology of fracture healing in long bones". Journal of Bone and Joint Surgery-British Volume, **60**(2), p. 150.
- [16] Gilron, I., Bailey, J. M., Tu, D., Holden, R. R., Weaver, D. F., and Houlden, R. L., 2005. "Morphine, gabapentin, or their combination for neuropathic pain". New England Journal of Medicine, **352**(13), pp. 1324–1334.
- [17] Shapiro, F., 1988. "Cortical bone repair. the relationship of the lacunar-canalicular system and intercellular gap junctions to the repair process". The Journal of Bone and Joint Surgery, **70**(7), p. 1067.
- [18] Rahn, B., 2002. "Bone healing: histological and physiological concepts". Bone in clinical orthopaedics. Stuttgart: Thieme, pp. 287–325.
- [19] Perren, S., 2002. "Evolution of the internal fixation of long bone fractures: the scientific basis of biological internal fixation: choosing a new balance between stability and biology". Journal of Bone and Joint Surgery-British Volume, **84**(8), p. 1093.
- [20] Mann, F., and Payne, J., 1989. "Bone healing." p. 312.
- [21] Ricci, W., Tornetta, P., Petteys, T., Gerlach, D., Cartner, J., Walker, Z., and Russell, T. A., 2010. "A comparison of screw insertion torque and pullout strength". J Orthop Trauma, **24**, pp. 374–378.
- [22] Cordey, J., Borgeaud, M., and Perren, S., 2000. "Force transfer between the plate and the bone: relative importance of the bending stiffness of the screws and the friction between plate and bone". Injury, **31**, pp. 21–28.
- [23] Sikes, J. W., Smith, B. R., Mukherjee, D. P., and Coward, K. A., 1998. "Comparison of fixation strengths of locking head and conventional screws, in fracture and reconstruction models". Journal of oral and maxillofacial surgery, **56**(4), Apr, pp. 468–473.

- [24] Spivak, J. M., Chen, D., and Kummer, F. J., 1999. "The effect of locking fixation screws on the stability of anterior cervical plating". Spine, **24**(4), Feb, pp. 334–338.
- [25] Kregor, P. J., Stannard, J., Zlowodzki, M., Cole, P. A., and Alonso, J., 2001. "Distal femoral fracture fixation utilizing the Less Invasive Stabilization System (L.I.S.S.): the technique and early results". Injury, **32 Suppl 3**, Dec, pp. SC32–SC47.
- [26] Schtz, M., Mller, M., Krettek, C., Hntzsch, D., Regazzoni, P., Ganz, R., and Haas, N., 2001. "Minimally invasive fracture stabilization of distal femoral fractures with the liss: a prospective multicenter study. results of a clinical study with special emphasis on difficult cases". Injury, **32 Suppl 3**, Dec, pp. SC48–SC54.
- [27] Haidukewych, G. J., and Ricci, W., 2008. "Locked plating in orthopaedic trauma: a clinical update". J Am Acad Orthop Surg, **16**(6), Jun, pp. 347–355.
- [28] Gardner, M., Helfet, D., and Lorich, D., 2004. "Has locked plating completely replaced conventional plating?". Am J Orthop, **33**, pp. 440–446.
- [29] Minihane, K. P., Lee, C., Ahn, C., Zhang, L.-Q., and Merk, B. R., 2006. "Comparison of lateral locking plate and antiglide plate for fixation of distal fibular fractures in osteoporotic bone: a biomechanical study". J Orthop Trauma, **20**(8), Sep, pp. 562–566.
- [30] Kim, T., Ayturk, U. M., Haskell, A., Miclau, T., and Puttlitz, C. M., 2007. "Fixation of osteoporotic distal fibula fractures: A biomechanical comparison of locking versus conventional plates". The Journal of foot and ankle surgery, **46**(1), pp. 2–6.
- [31] Trease, C., McIff, T., and Toby, E., 2005. "Locking versus nonlocking t-plates for dorsal and volar fixation of dorsally comminuted distal radius fractures: a biomechanical study". The Journal of hand surgery, **30**(4), pp. 756–763.
- [32] Illert, T., Rammelt, S., Drewes, T., Grass, R., and Zwipp, H., 2011. "Stability of locking and non-locking plates in an osteoporotic calcaneal fracture model". Foot & ankle international/American Orthopaedic Foot and Ankle Society [and] Swiss Foot and Ankle Society, **32**(3), p. 307.
- [33] Ferguson, S., Wyss, U., and Pichora, D., 1996. "Finite element stress analysis of a hybrid fracture fixation plate". Medical engineering & physics, **18**(3), pp. 241–250.
- [34] Fouad, H., 2010. "Effects of the bone-plate material and the presence of a gap between the fractured bone and plate on the predicted stresses at the fractured bone". Medical engineering & physics, **32**(7), pp. 783–789.
- [35] Joslin, C., Eastaugh-Waring, S., Hardy, J., and Cunningham, J., 2003. "Weight bearing after tibial fracture as a guide to healing". p. 5.

- [36] Moorcroft, C., Thomas, P., and Ogrodnik, P., 2008. "Reliability of fracture stiffness as a measurement of clinical union and visco-elastic properties of callus". p. 465.
- [37] Shah, K., Nicol, A., and Hamblen, D., 1995. "Fracture stiffness measurement in tibial shaft fractures: a non-invasive method". Clinical Biomechanics, **10**(8), pp. 395–400.
- [38] Wehner, T., Claes, L., Niemeyer, F., Nolte, D., and Simon, U., 2010. "Influence of the fixation stability on the healing time—a numerical study of a patient-specific fracture healing process". Clinical Biomechanics, **25**(6), pp. 606–612.
- [39] Augat, P., Margevicius, K., Simon, J., Wolf, S., Suger, G., and Claes, L., 1998. "Local tissue properties in bone healing: influence of size and stability of the osteotomy gap". Journal of orthopaedic research, **16**(4), pp. 475–481.
- [40] Kaspar, K., Schell, H., Seebeck, P., Thompson, M., Schutz, M., Haas, N., and Duda, G., 2005. "Angle stable locking reduces interfragmentary movements and promotes healing after unreamed nailing. study of a displaced osteotomy model in sheep tibiae". The Journal of Bone and Joint Surgery, **87**(9), p. 2028.
- [41] Schell, H., Epari, D., Kassi, J., Bragulla, H., Bail, H., and Duda, G., 2005. "The course of bone healing is influenced by the initial shear fixation stability". Journal of orthopaedic research, **23**(5), pp. 1022–1028.
- [42] Asnis, S., Ernberg, J., Bostrom, M., Wright, T., Harrington, R., Tencer, A., and Peterson, M., 1996. "Cancellous bone screw thread design and holding power". Journal of orthopaedic trauma, **10**(7), p. 462.
- [43] Chapman, J., Harrington, R., Lee, K., Anderson, P., Tencer, A., and Kowalski, D., 1996. "Factors affecting the pullout strength of cancellous bone screws". Journal of biomechanical engineering, **118**, p. 391.
- [44] Brown, G., McCarthy, T., Bourgeault, C., and Callahan, D., 2000. "Mechanical performance of standard and cannulated 4.0-mm cancellous bone screws". Journal of Orthopaedic Research, **18**(2), pp. 307–312.
- [45] Zdero, R., and Schemitsch, E., 2009. "The effect of screw pullout rate on screw purchase in synthetic cancellous bone". Journal of biomechanical engineering, **131**, p. 024501.
- [46] Singh, V., Kumar, I., and Bhagol, A., 2011. "Comparative evaluation of 2.0-mm locking plate system vs 2.0-mm nonlocking plate system for mandibular fracture: a prospective randomized study". International journal of oral and maxillofacial surgery, **40**(4), pp. 372–377.
- [47] Hou, S.-M., Hsu, C.-C., Wang, J.-L., Chao, C.-K., and Lin, J., 2004. "Mechanical tests and finite element models for bone holding power of tibial locking screws". Clinical Biomechanics, **19**(7), pp. 738–745.
- [48] Cleek, T., Reynolds, K., and Hearn, T., 2007. "Effect of screw torque level on cortical bone pullout strength". Journal of orthopaedic trauma, **21**(2), p. 117.

- [49] Collinge, C., Hartigan, B., and Lautenschlager, E., 2006. "Effects of surgical errors on small fragment screw fixation". Journal of orthopaedic trauma, **20**(6), p. 410.
- [50] Drobetz, H., and Kutscha-Lissberg, E., 2003. "Osteosynthesis of distal radial fractures with a volar locking screw plate system". Int Orthop, **27**(1), pp. 1–6.
- [51] Sommer, C., Gautier, E., Müller, M., Helfet, D. L., and Wagner, M., 2003. "First clinical results of the locking compression plate (lcp)". Injury, **34**, Nov., pp. 43–54.
- [52] Stoffel, K., Wysocki, D., Baddour, E., Nicholls, R., and Yates, P., 2009. "Comparison of two intraoperative assessment methods for injuries to the ankle syndesmosis. a cadaveric study". J Bone Joint Surg, **91**(11), Nov, pp. 2646–2652. American volume.
- [53] Zehnder, S., Bledsoe, J. G., and Puryear, A., 2009. "The effects of screw orientation in severely osteoporotic bone: A comparison with locked plating". Clinical Biomechanics, **24**, pp. 589–591.
- [54] Simulia, Inc, 2009. Abaqus User Manual v6.8. Electronic Version.
- [55] Nigg, B., Herzog, W., and Herzog, W., 1999. Biomechanics of the musculo-skeletal system. Wiley.
- [56] Yamada, H., and Evans, F., 1970. Strength of biological materials. Williams & Wilkins.
- [57] Nordin, M., and Frankel, V., 2001. Basic biomechanics of the musculoskeletal system. Lippincott Williams & Wilkins.
- [58] Bartel, D., Davy, D., and Keaveny, T., 2006. Orthopaedic biomechanics: mechanics and design in musculoskeletal systems. Pearson/Prentice Hall.
- [59] Smith, W. R., Ziran, B. H., Anglen, J. O., and Stahel, P. F., 2007. "Locking plates: Tips and tricks". J Bone Joint Surg, **89**(10), pp. 2298–2307. American volume.
- [60] Lambert, K. L., 1971. "Study: The weight-bearing function of the fibula: A strain gauge". J Bone Joint Surg, **53**, pp. 507–513. American volume.
- [61] Jagodzinski, M., and Krettek, C., 2007. "Effect of mechanical stability on fracture healing – an update". Injury, **38**(1, Supplement 1), pp. S3–S10. Scientific basis of fracture healing: an update.
- [62] Harwood, P. J., Newman, J. B., and Michael, A. L., 2010. "An update on fracture healing and non-union". Orthopaedics and Trauma, **24**(1), pp. 9–23.
- [63] Claes, L. E., Heigele, C. A., Neidlinger-Wilke, C., Kaspar, D., Seidl, W., Margevicius, K. J., and Augat, P., 1998. "Effects of mechanical factors on the fracture healing process.". Clin Orthop Relat Res(355 Suppl), Oct, pp. S132–S147.

- [64] Brown, T. D., 2004. "Finite element modeling in musculoskeletal biomechanics". Journal of Applied Biomechanics, **20**(4), pp. 336–366.
- [65] Gautier, E., and Sommer, C., 2003. "Guidelines for the clinical application of the lcp.". Injury, **34**, p. B63.
- [66] Schaffer, J., and Manoli, A., 1987. "The antiglide plate for distal fibular fixation. a biomechanical comparison with fixation with a lateral plate". J Bone Joint Surg, **69**(4), pp. 596–604. American volume.
- [67] Hente, R., Fichtmeier, B., Schlegel, U., Ernstberger, A., and Perren, S. M., 2004. "The influence of cyclic compression and distraction on the healing of experimental tibial fractures". Journal of orthopaedic research, **22**(4), Jul, pp. 709–715.
- [68] Hente, R., Lechner, J., Fuechtmeier, B., Schlegel, U., and Perren, S., 2001. "Der einfluss einer zeitlich limitierten kontrollierten bewegung auf die frakturheilung". Hefte Unfallchirurg, **283**, pp. 23–24.
- [69] Patel, P., Shepherd, D., and Hukins, D., 2010. "The effect of screw insertion angle and thread type on the pullout strength of bone screws in normal and osteoporotic cancellous bone models". Medical Engineering & Physics, **32**, pp. 822–828.
- [70] ASTM F543-07: standard specification and test methods for metallic medical bone screws.
- [71] Li, B., and Aspden, R., 1997. "Composition and mechanical properties of cancellous bone from the femoral head of patients with osteoporosis or osteoarthritis". Journal of Bone and Mineral Research, **12**, pp. 641–651.
- [72] Kennedy, J., and Carter, D., 1985. "Long bone torsion: effects of heterogeneity, anisotropy and geometric irregularity". J Biomech Eng, **107**, pp. 183–188.
- [73] Rovinsky, D., Haskell, A., Liu, Q., Paiement, G., and Robinovitch, S., 2000. "Evaluation of a new method of small fragment fixation in a medial malleolus fracture model". J Orthop Trauma, **14**(6), pp. 420–425.
- [74] Edwards, T., Tevelen, G., English, H., and Crawford, R., 2005. "Stripping torque as a predictor of successful internal fracture fixation". ANZ J Surg, **75**(12), pp. 1096–1099.
- [75] Wen-Chi, T., Po-Quang, C., Tung-Wu, L., Shing-Sheng, W., Kao-Shang, S., and Shang-Chih, L., 2009. "Comparison and prediction of pullout strength of conical and cylindrical pedicle screws within synthetic bone". BMC Musculoskeletal Disorders, **10**.
- [76] Chatzistergosa, P., Magnissalis, E., and Kourkoulisa, S., 2010. "A parametric study of cylindrical pedicle screw design implications on the pullout performance using an experimentally validated finite-element model". Medical Engineering & Physics, **32**, pp. 145–154.
- [77] Thomas, C., and Taber, C., 1997. Taber's cyclopedic medical dictionary.

Appendices

Appendix A

Glossary of orthopaedic terms

References [58, 77]

Osteosynthesis: A surgical procedure that stabilizes and joins the ends of fractured (broken) bones by mechanical devices such as metal plates, pins, rods, wires or screws.

Splinting: A technique to secure the part of the body that is injured to decrease further damage or injury.

Callus: A new growth of osseous matter at the end of fractured bone, serving to unite them.

Nonunion: A fracture that fails to heal in a reasonable amount of time is called a nonunion.

Malunion: A fracture that does not heal in a normal alignment is called a malunion.

Delayed union: A fracture that takes longer to heal than expected is a delayed union.

Cortical bone: Cortical bone, synonymous with compact bone forms the cortex or outer shell of bones.

Cancellous bone: Cancellous bone, synonymous with trabecular bone or spongy bone forms inner portion of bone. It is highly vascular and contains red bone marrow.

Interosseous membrane: A broad and thin plane of fibrous tissue that separates many of the bones of the body.

Proximal aspect: Nearest to the top of the body. Usually only used in conjunction with the bones of appendicular skeleton. Thus, we talk of the proximal femur, which is at the hip joint.

Distal aspect: The opposite to the proximal – nearest to the bottom of the body. The distal femur, for example, is at knee joint.

Inferior: Beneath or lower.

Superior: opposite of inferior.

Lateral: The part closest to the outside of the body or farthest from the body's midline. So the lateral aspect of the femur is on the outside of your (left or right) thigh.

Medial: Opposite of lateral – the part closest to the midline of the body.

Anterior: Before or in front.

Posterior: Behind or in back.

Dorsal: Near or on the back.

Ventral: Near or on the anterior

Flexion: A folding movement in which the anterior angle between two bones is decreased. It generally means that you are moving bone closer to the body with respect to its anatomical position.

Extension: The opposite of flexion - an increase in anterior angle between two bones.

Abduction: Movement away from middle line of the body. Usually in frontal plane.

Adduction: Movement toward the middle line of the body. Usually in frontal plane.

Appendix B

Comparison of displacement contours of the distal fibula

B.1 Displacement contours for comminuted fracture

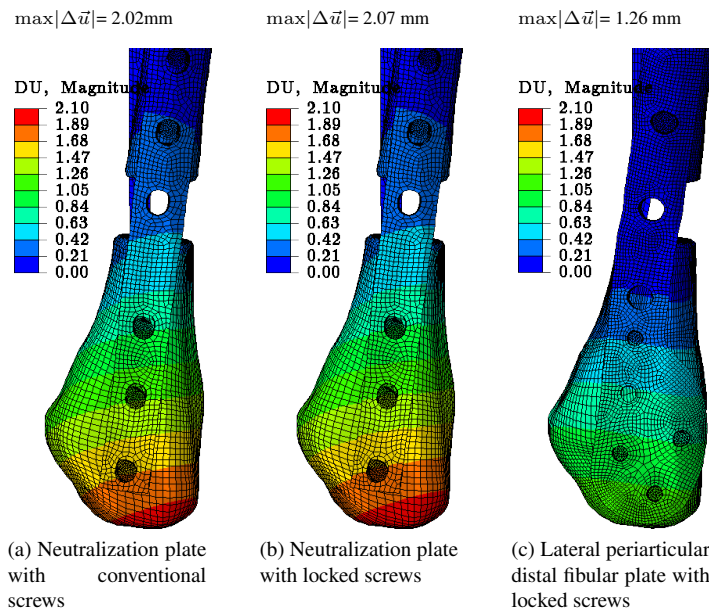


Figure B.1: Displacement ($|\Delta\vec{u}|$) due to fibulotalar reaction load with comminuted fracture

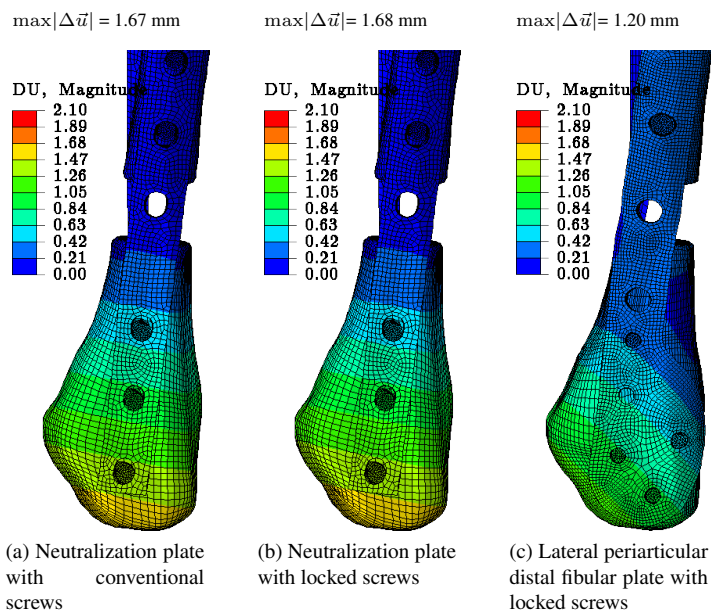


Figure B.2: Displacement ($|\Delta \vec{u}|$) due to cotton test load with comminuted fracture

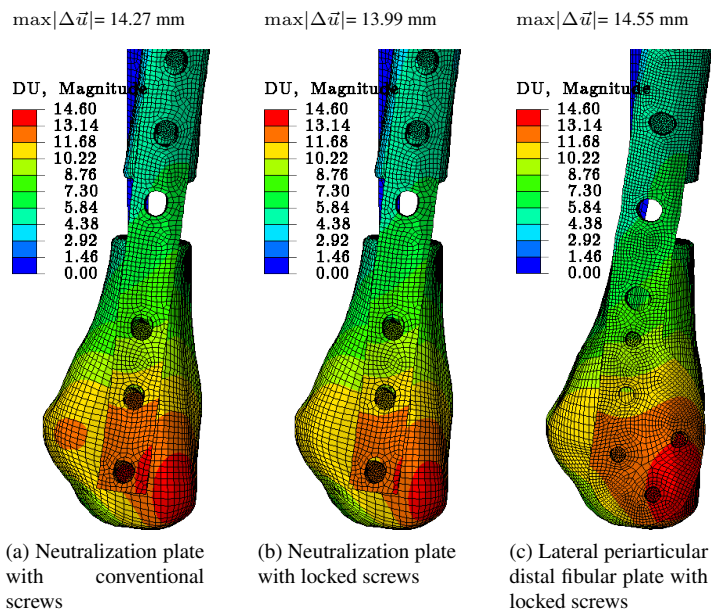


Figure B.3: Displacement ($|\Delta \vec{u}|$) due to external rotation moment with comminuted fracture

B.2 Displacement contours for danis-weber B fracture

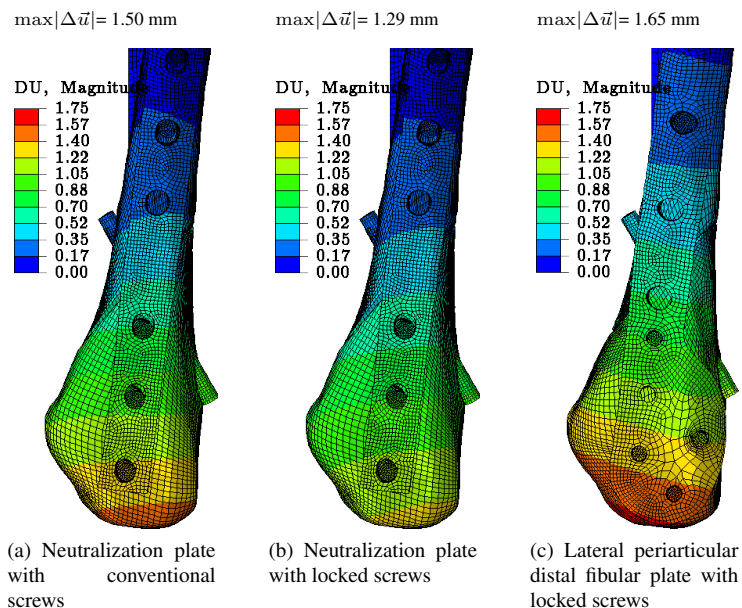


Figure B.4: Displacement ($|\Delta\vec{u}|$) due to fibulotalar reaction load with danis-weber B fracture

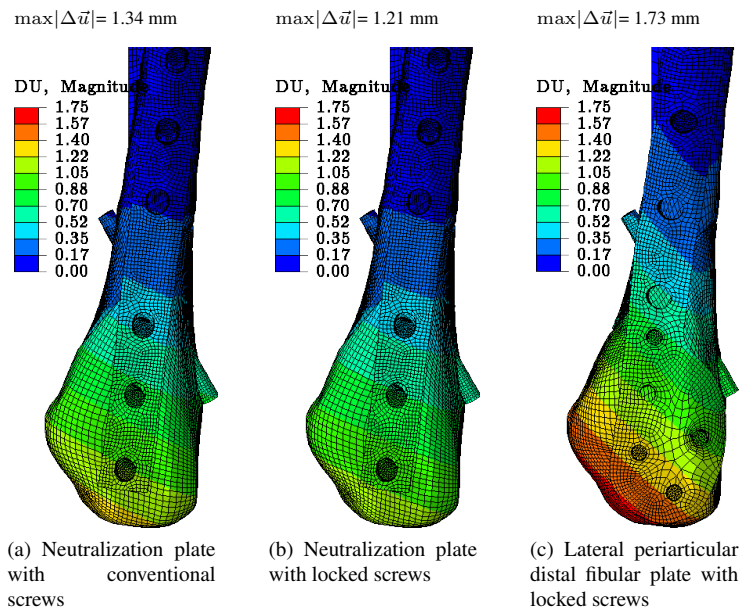


Figure B.5: Displacement ($|\Delta\vec{u}|$) due to cotton test load with danis-weber B fracture

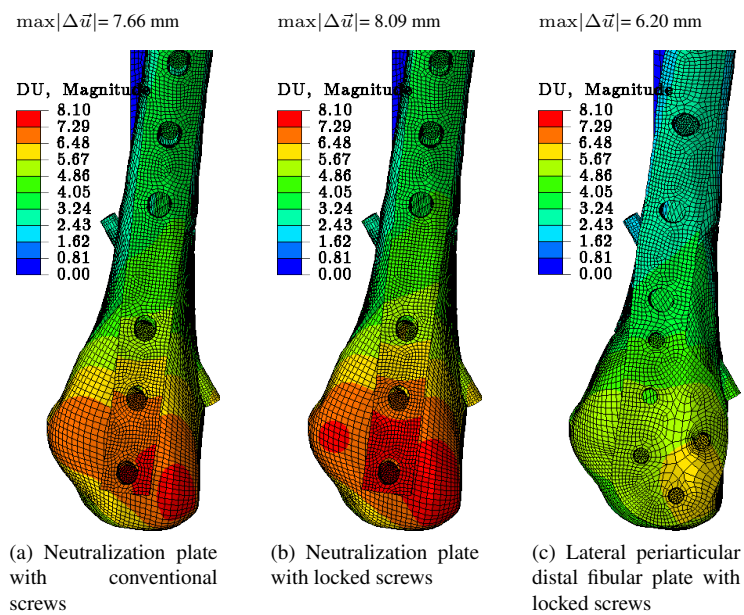
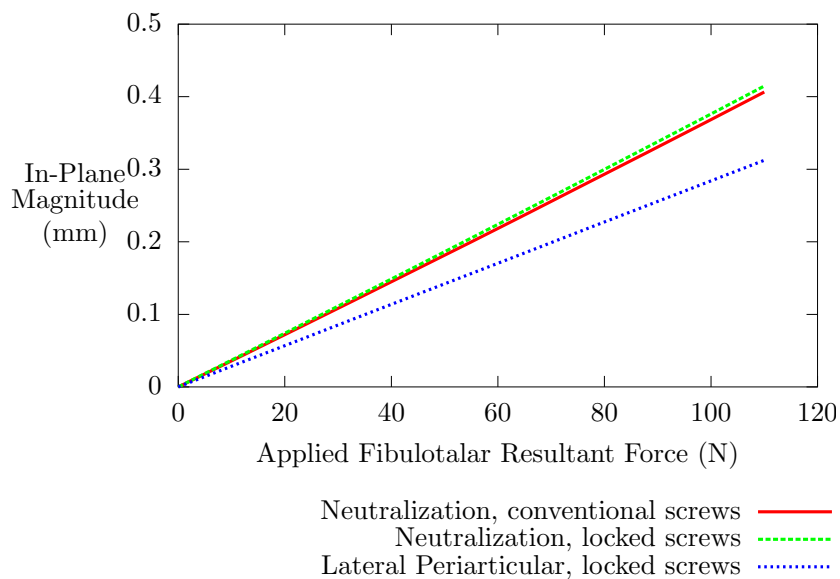


Figure B.6: Displacement ($|\Delta\vec{u}|$) due to external rotation moment with danis-weber B fracture

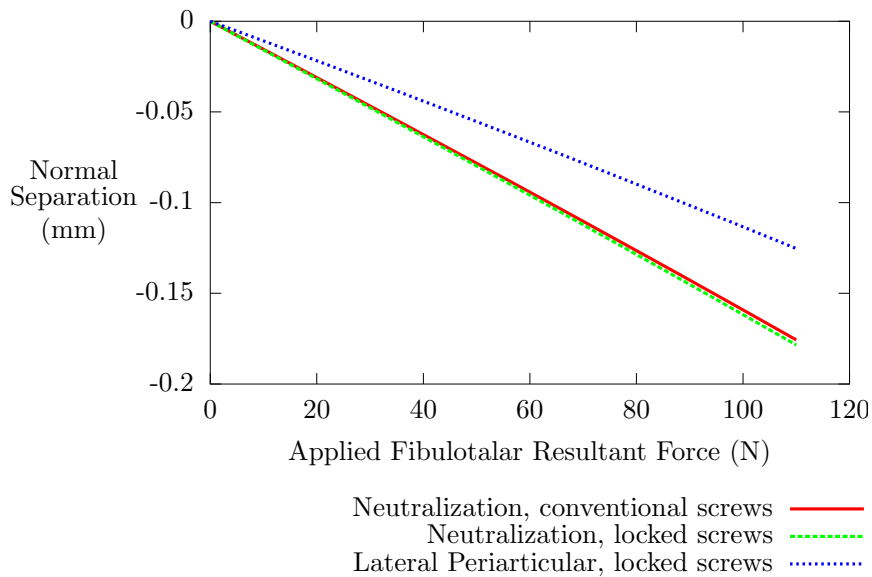
Appendix C

Comparison of construct stiffnesses about the fracture plane

C.1 Stiffness for comminuted fracture



(a) Magnitude of the in-plane translation vector



(b) Normal separation

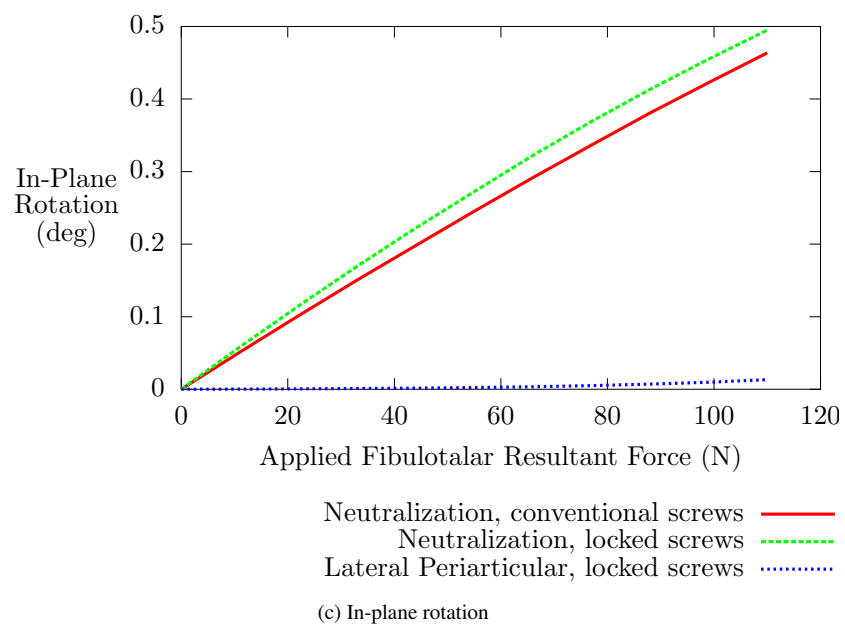
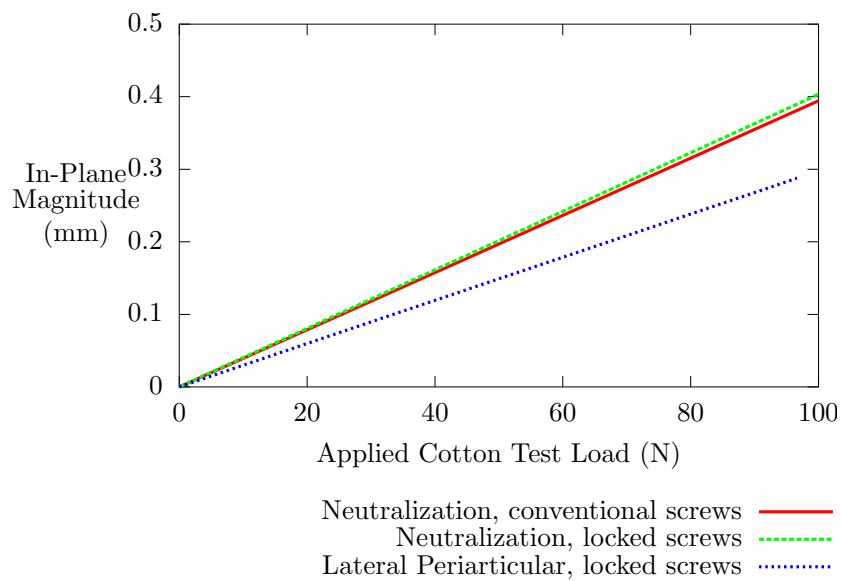
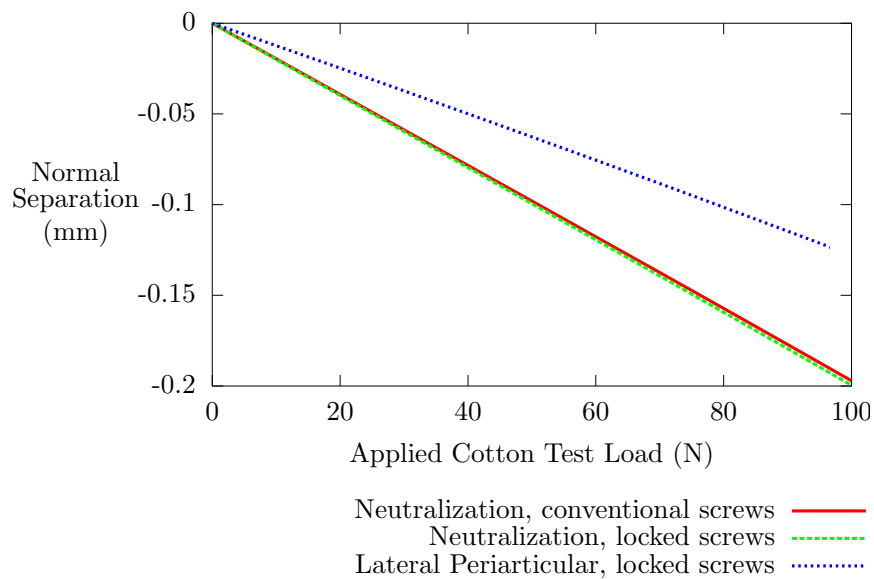


Figure C.0: Relative motion of the comminuted fracture surfaces due to the applied fibulotalar load



(a) Magnitude of the in-plane translation vector



(b) Normal separation

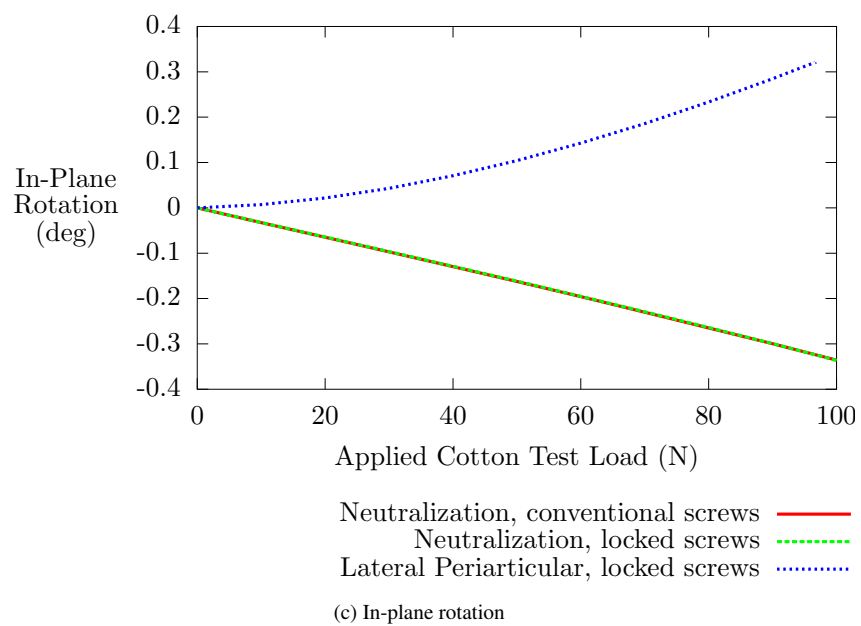
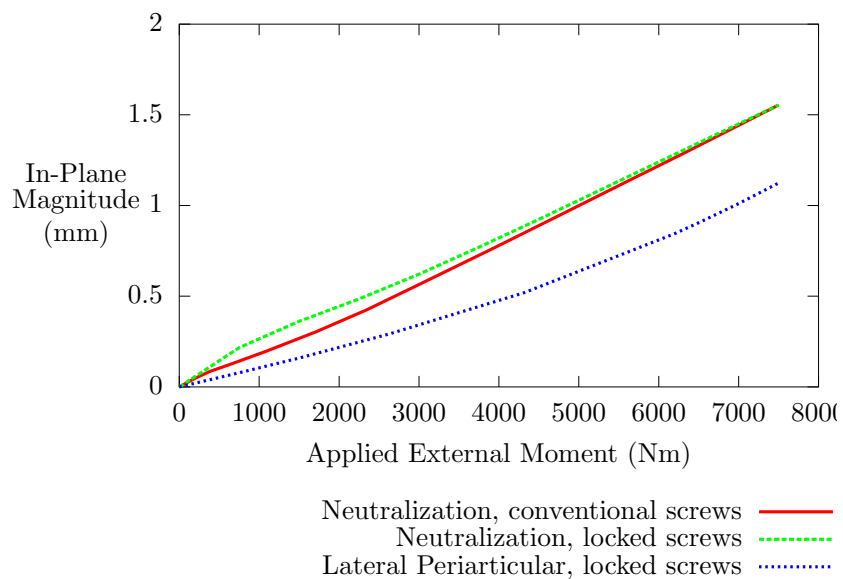
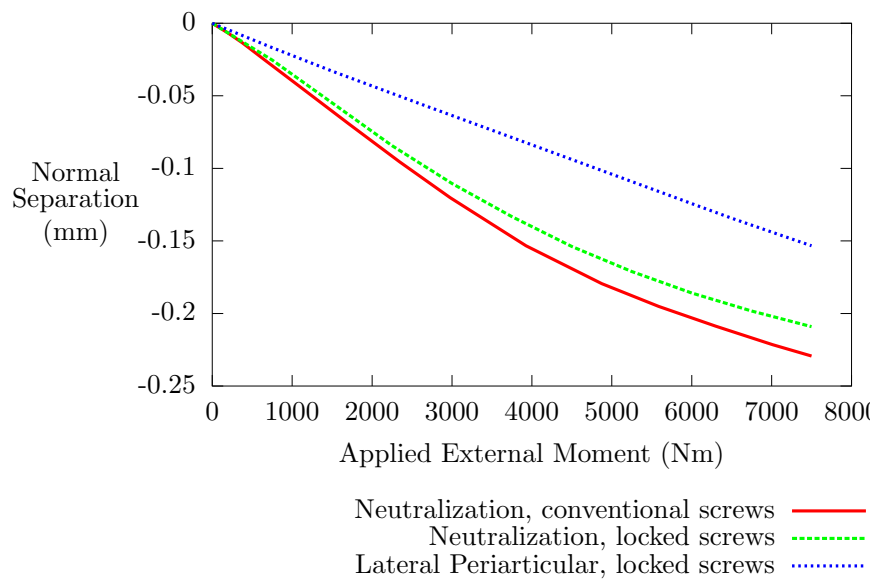


Figure C.0: Relative motion of the comminuted fracture surfaces due to the applied cotton test load



(a) Magnitude of the in-plane translation vector



(b) Normal separation

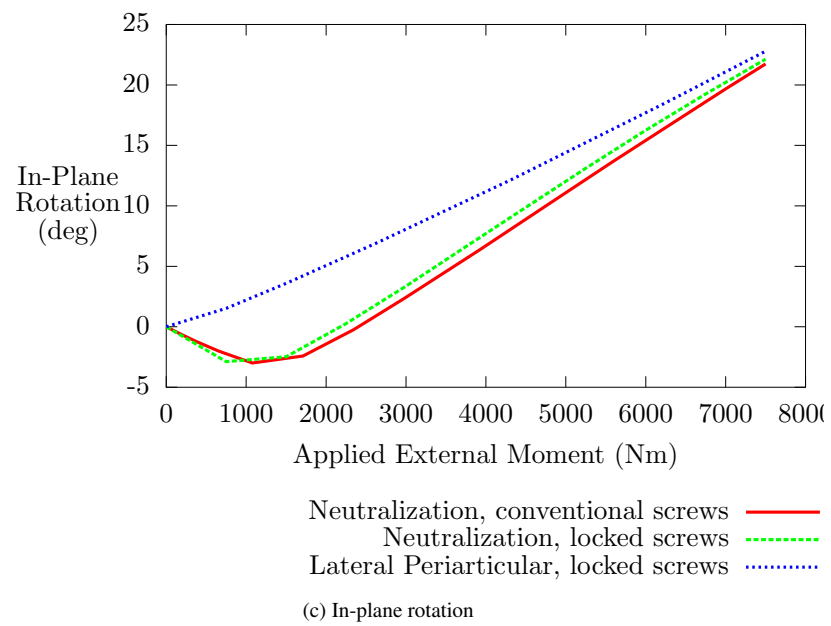
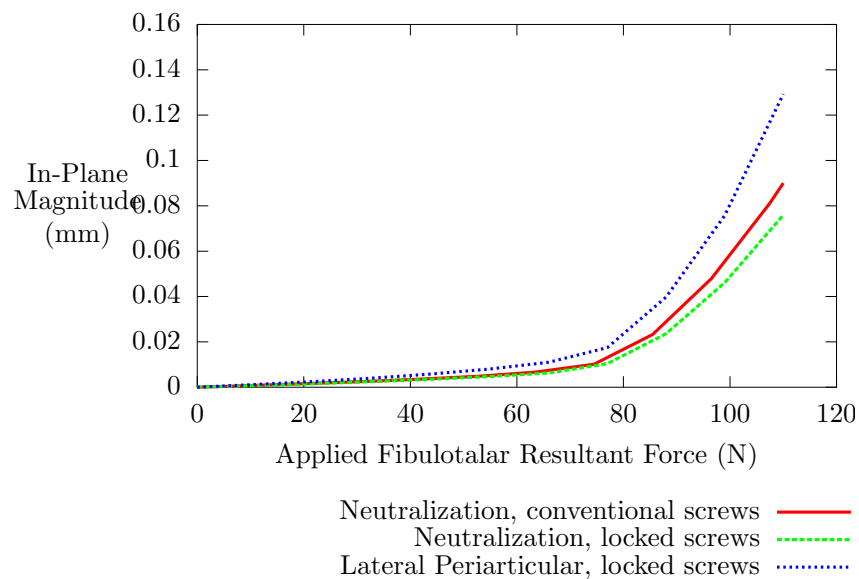
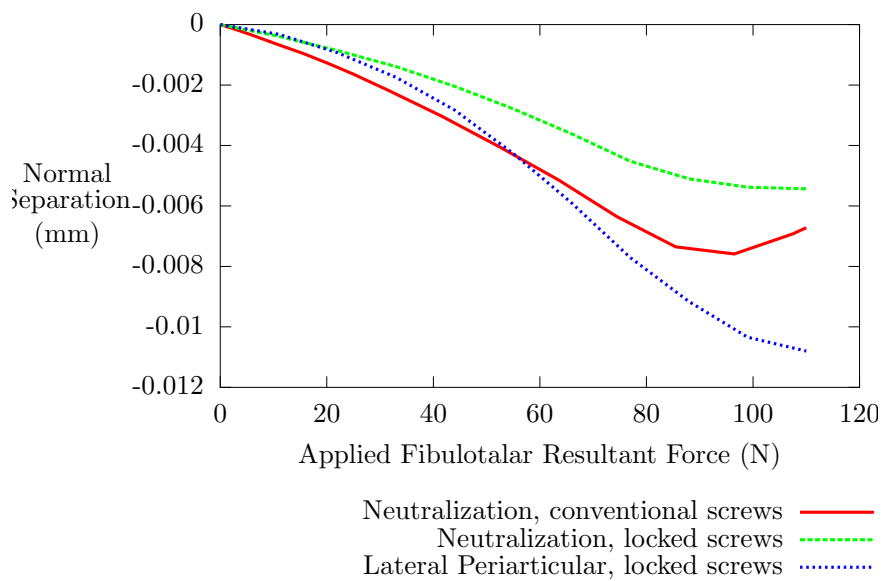


Figure C.0: Relative motion of the comminuted fracture surfaces due to the applied external moment

C.2 Stiffness for danis-weber B fracture



(a) Magnitude of the in-plane translation vector



(b) Normal separation

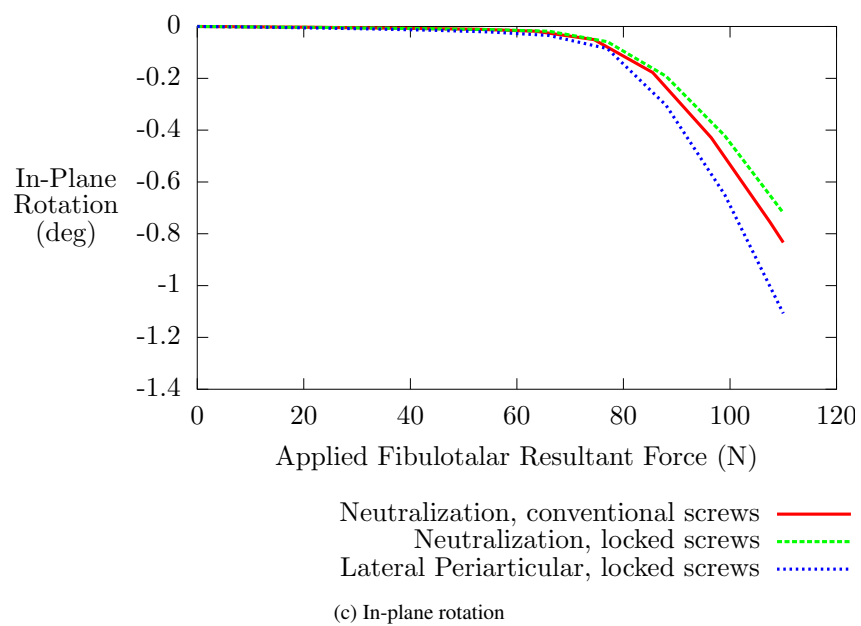
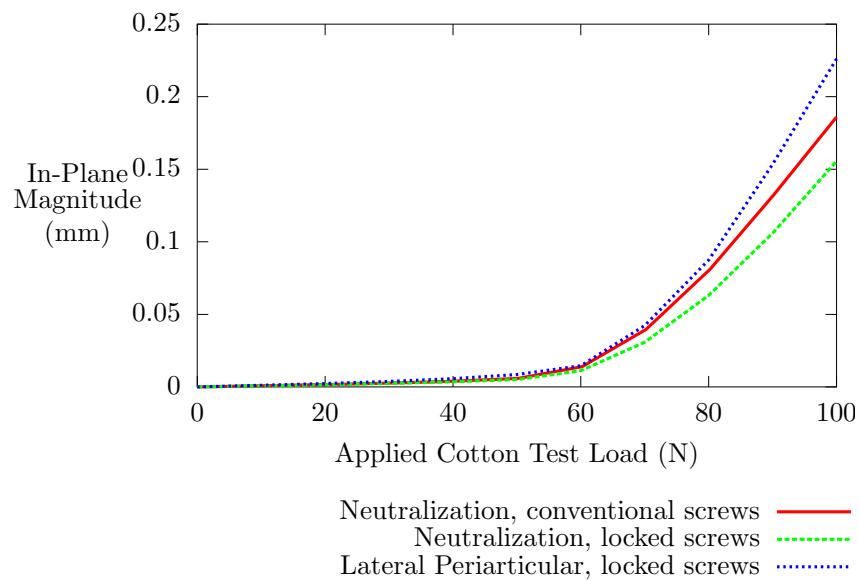
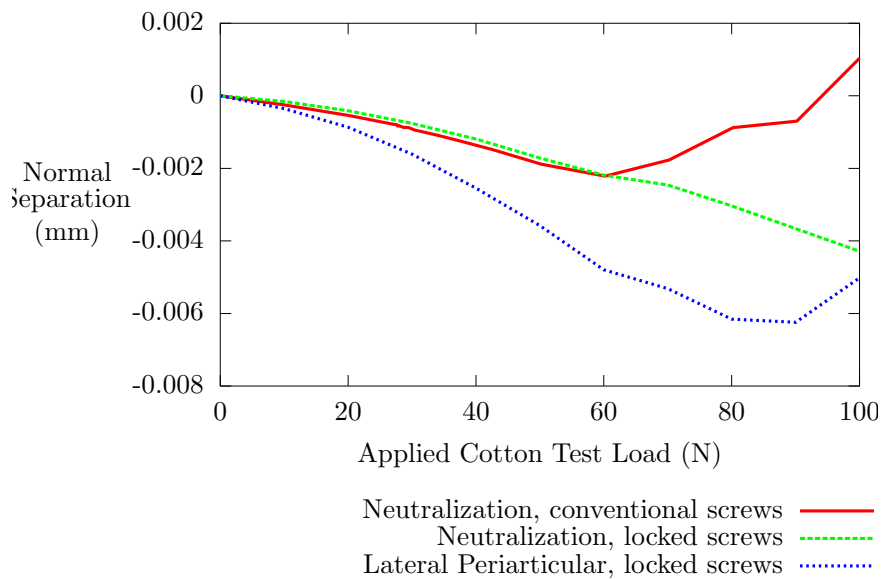


Figure C.0: Relative motion of the Danis-weber B fracture surfaces due to the applied fibulotalar load



(a) Magnitude of the in-plane translation vector



(b) Normal separation

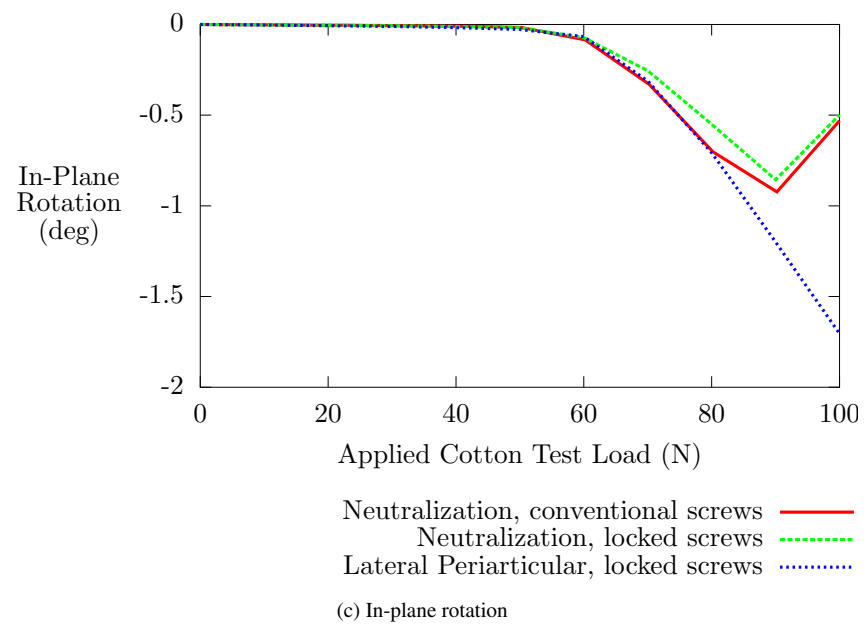
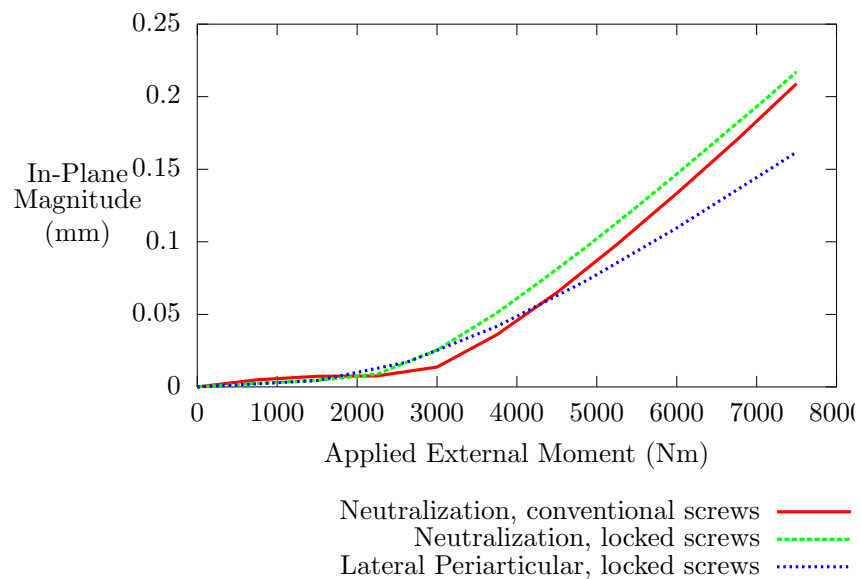
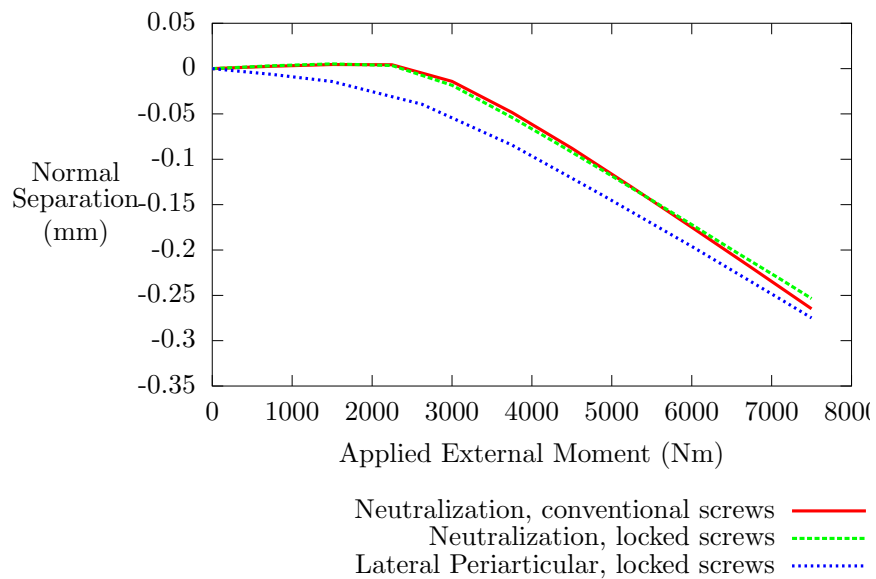


Figure C.0: Relative motion of the Danis-weber B fracture surfaces due to the applied cotton test load



(a) Magnitude of the in-plane translation vector



(b) Normal separation

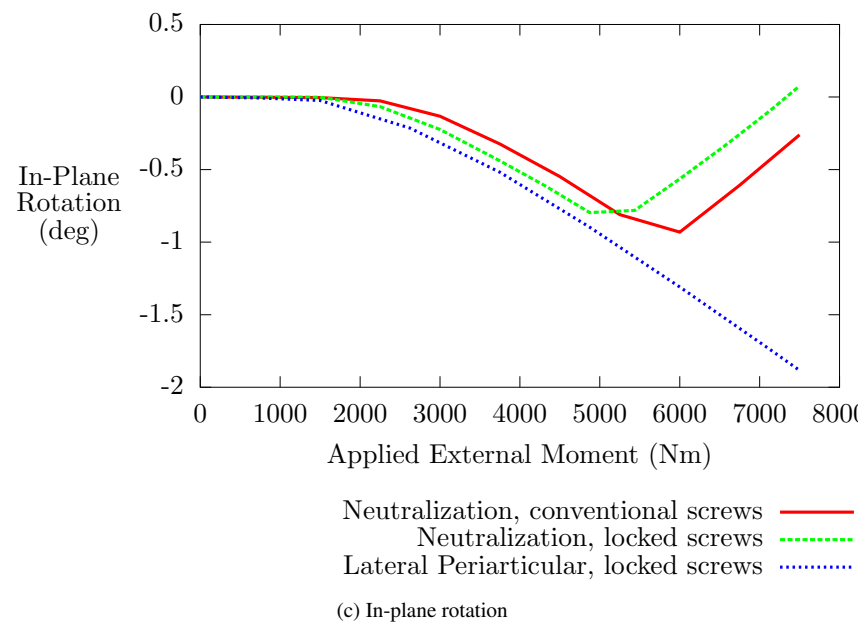


Figure C.0: Relative motion of the Danis-weber B fracture surfaces due to the applied external moment

Appendix D

Force distribution at screw bone interface

D.1 Normal load

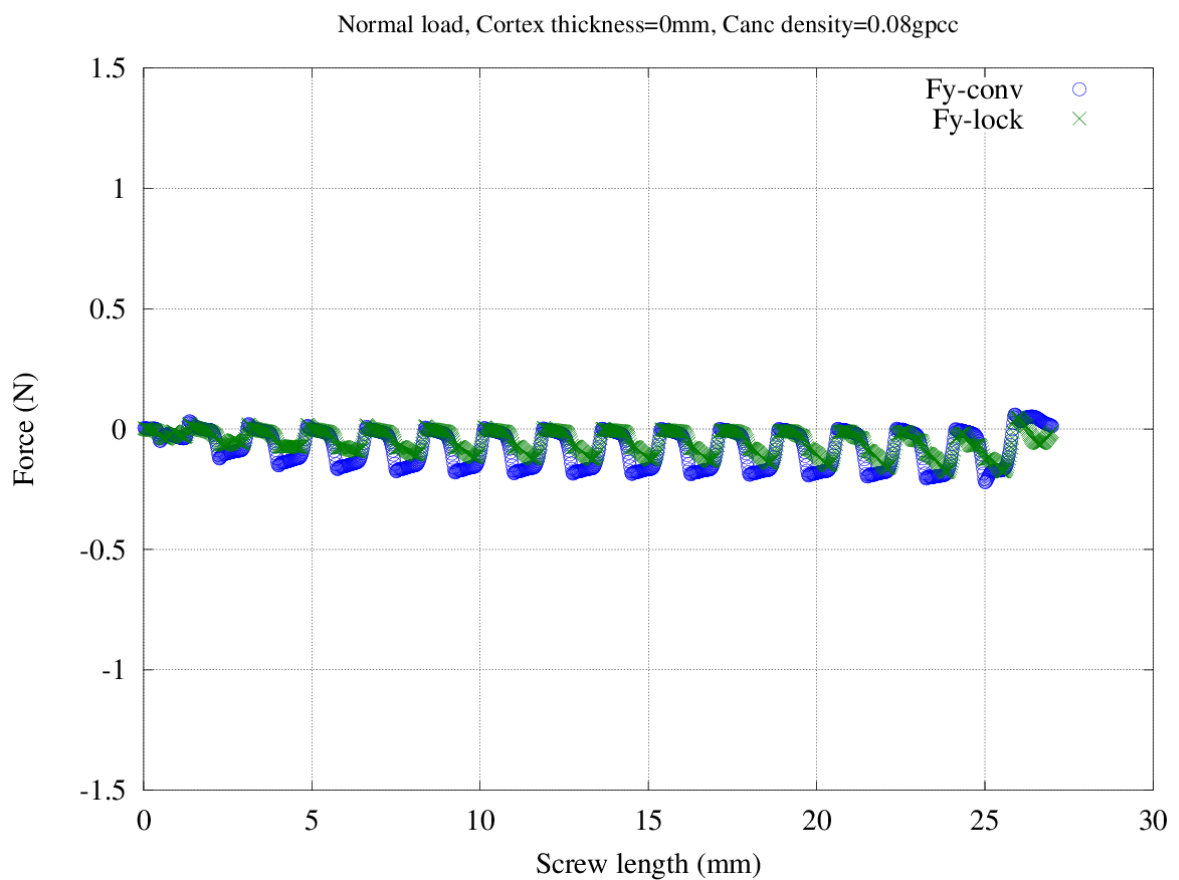


Figure D.1: Pullout force (F_y) distribution at screw bone interface under normal load (Cancellous density = 0.08gpcc, cortex thickness=0mm)

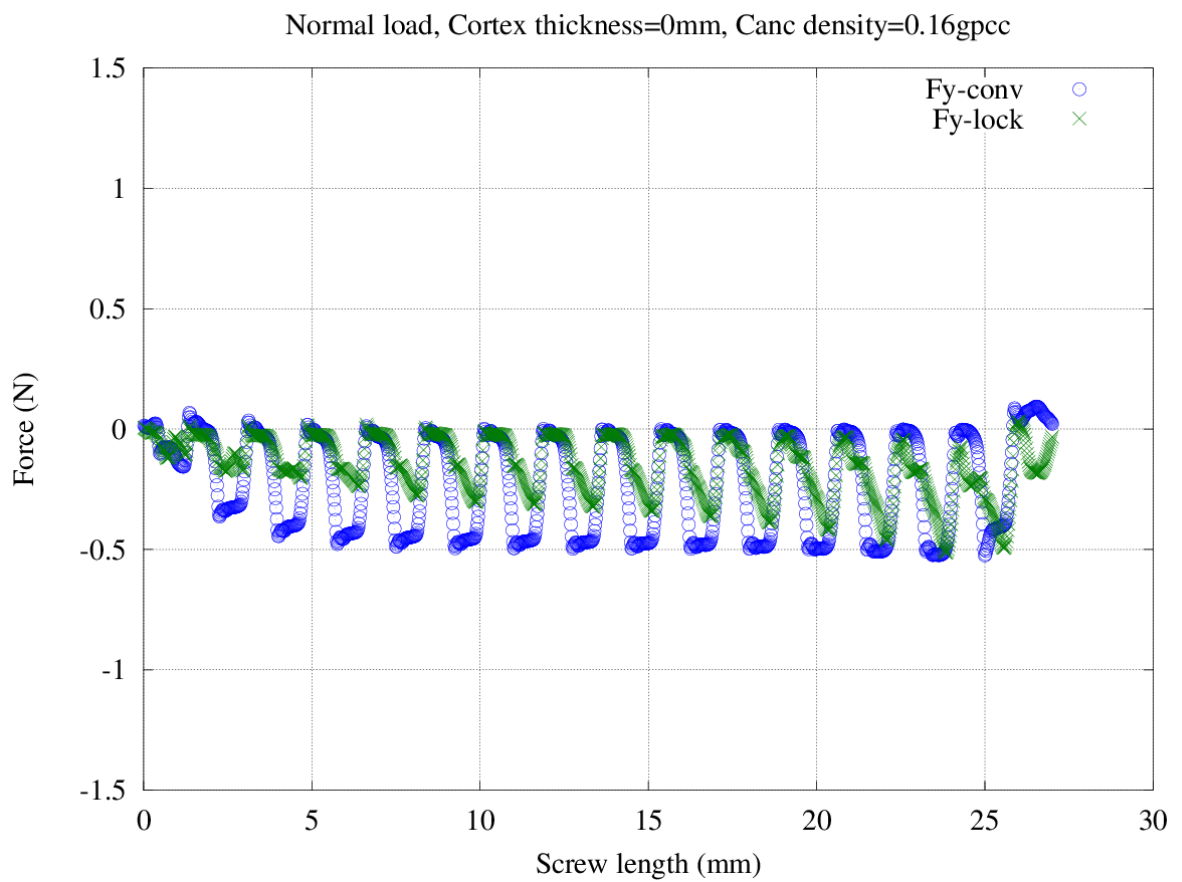


Figure D.2: Pullout force (F_y) distribution at screw bone interface under normal load (Cancellous density = 0.16gpcc, cortex thickness=0mm)

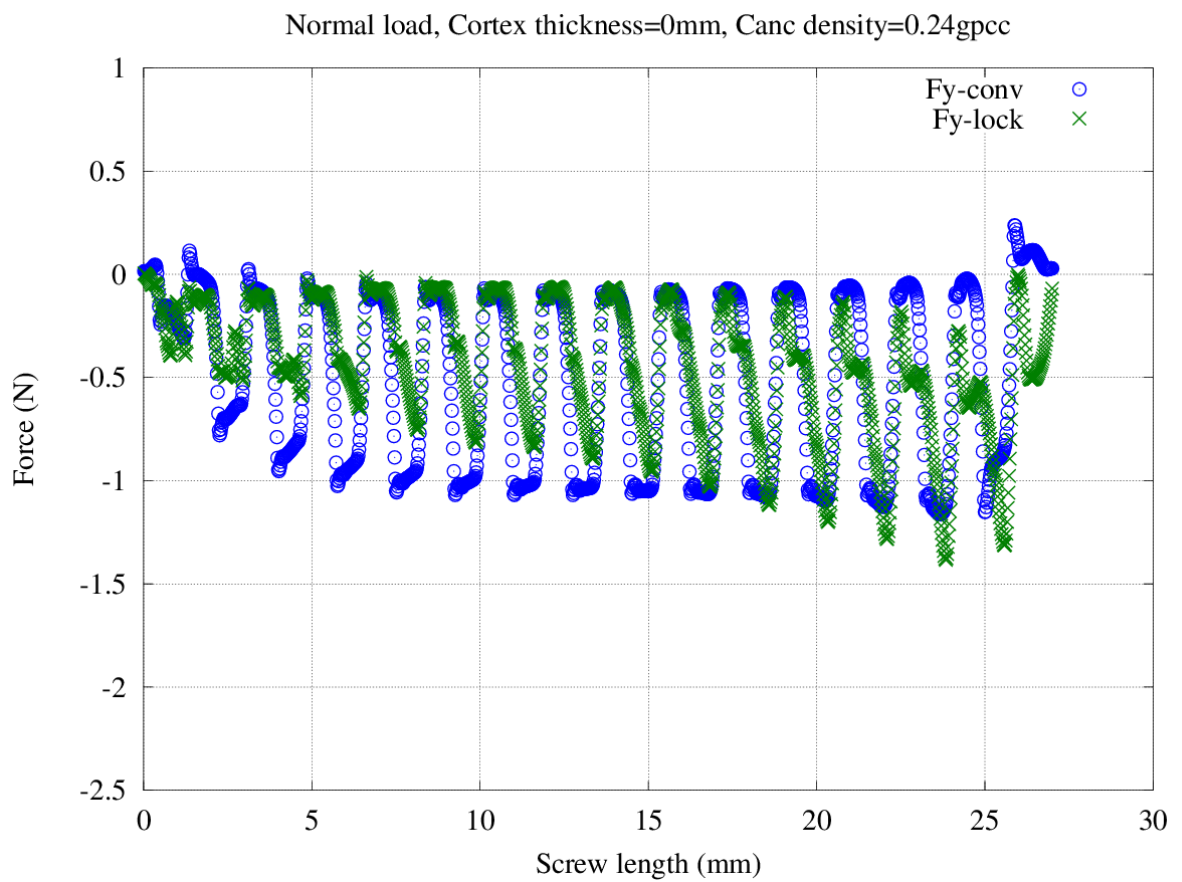


Figure D.3: Pullout force (F_y) distribution at screw bone interface under normal load (Cancellous density = 0.24gpcc, cortex thickness=0mm)

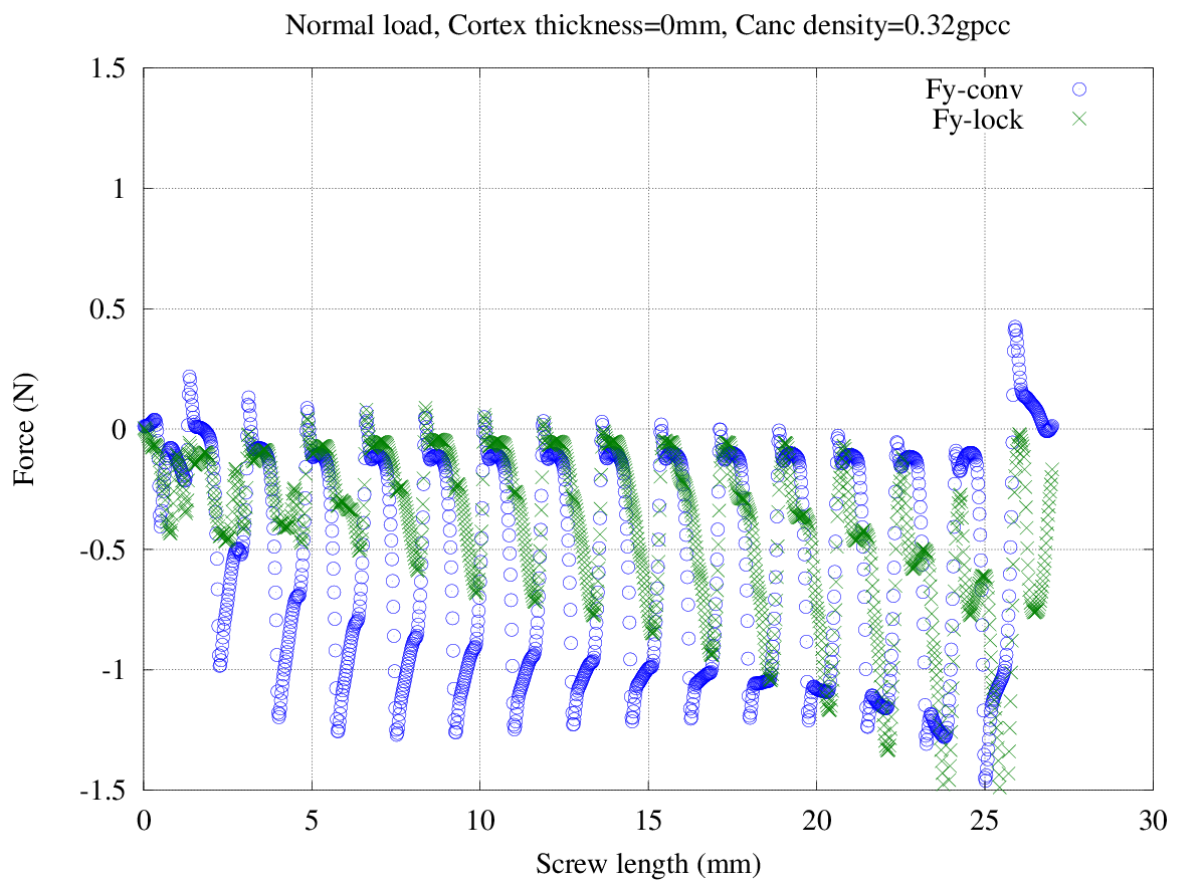


Figure D.4: Pullout force (F_y) distribution at screw bone interface under normal load (Cancellous density = 0.32gpcc, cortex thickness=0mm)

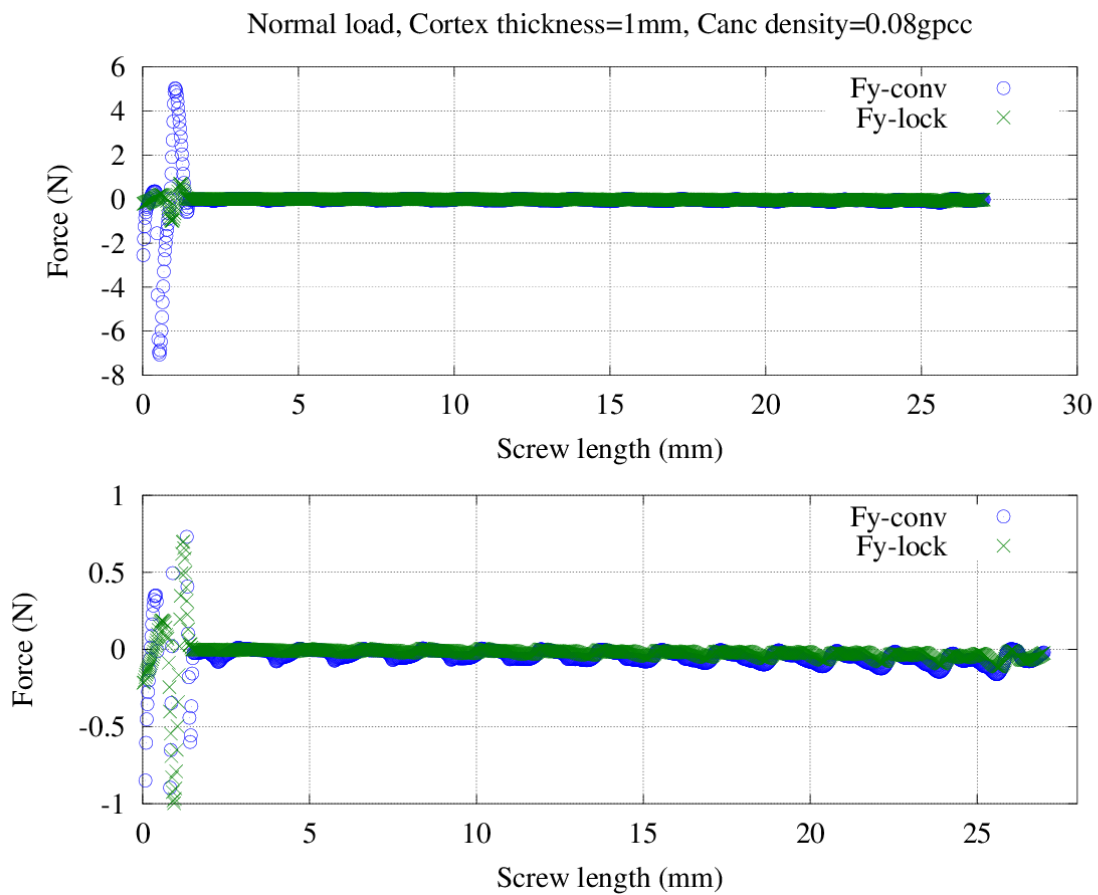


Figure D.5: Pullout force (F_y) distribution at screw bone interface under normal load (Cancellous density = 0.08gpcc, cortex thickness=1mm)

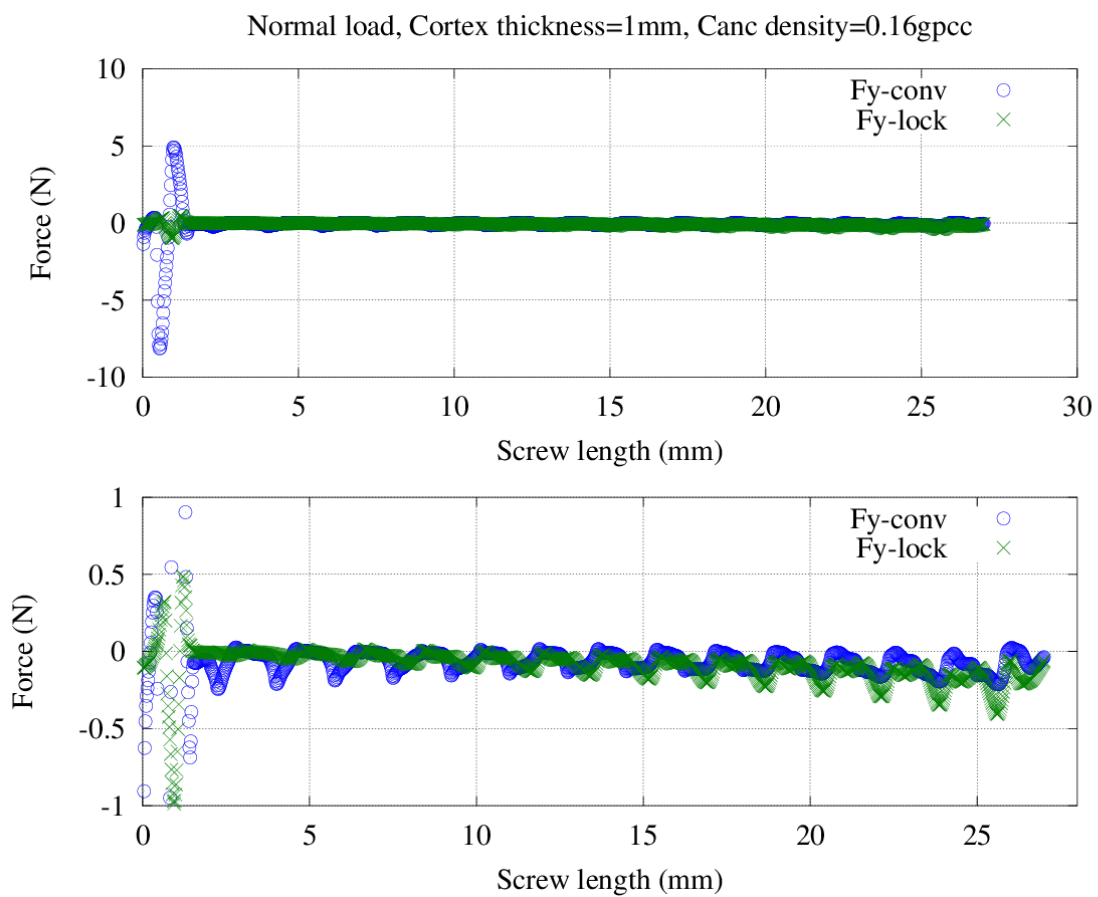


Figure D.6: Pullout force (F_y) distribution at screw bone interface under normal load (Cancellous density = 0.16gpcc, cortex thickness=1mm)

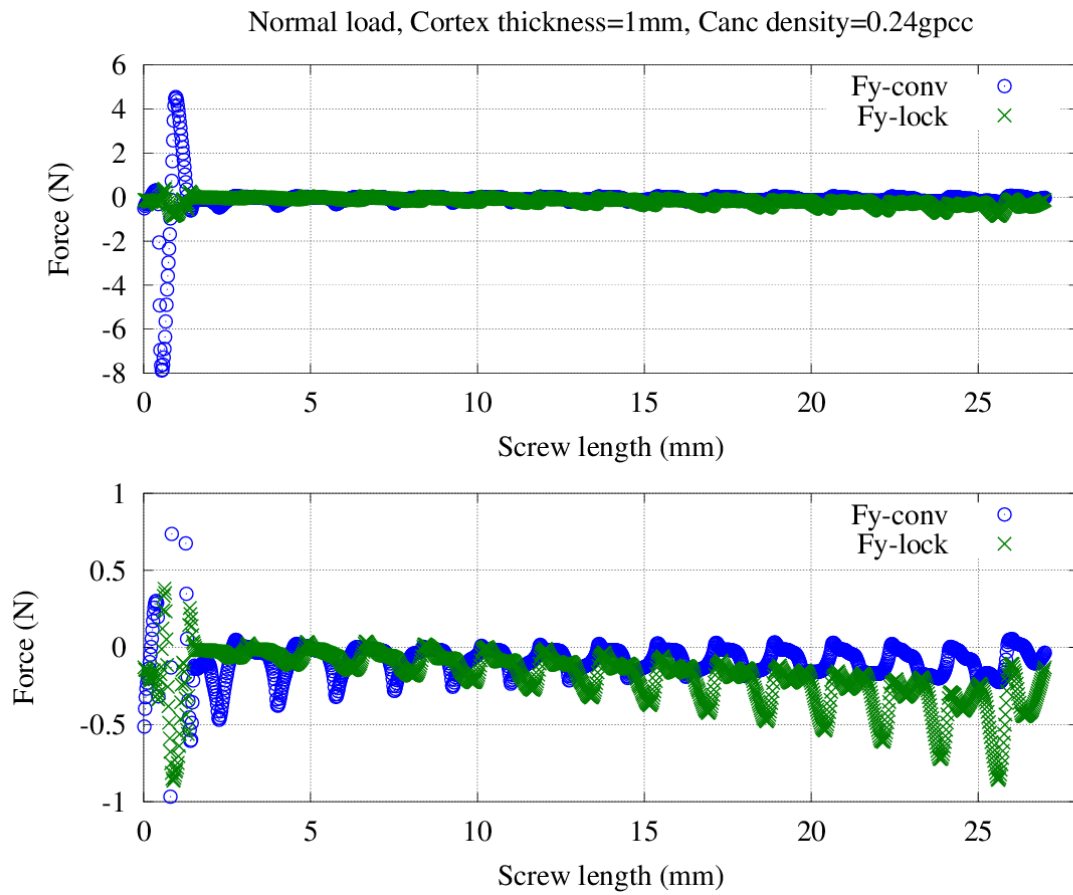


Figure D.7: Pullout force (F_y) distribution at screw bone interface under normal load (Cancellous density = 0.24gpcc, cortex thickness=1mm)

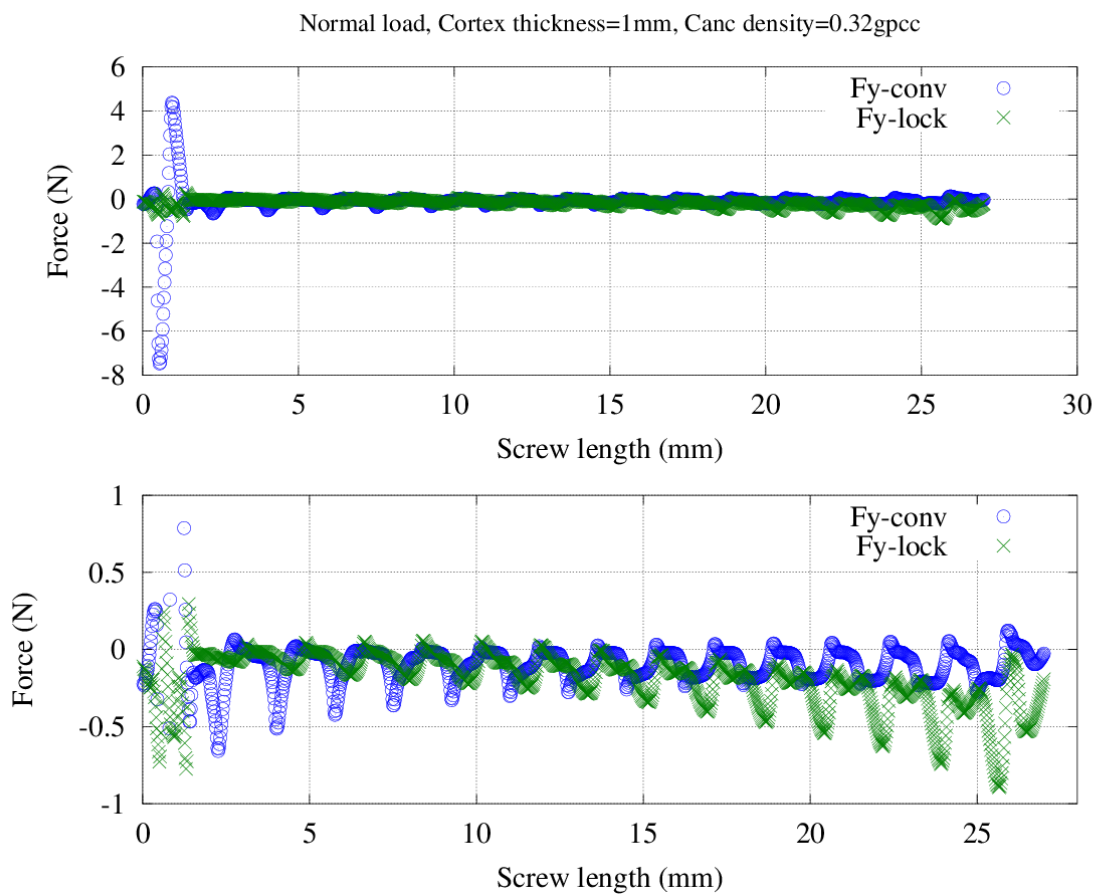


Figure D.8: Pullout force (F_y) distribution at screw bone interface under normal load (Cancellous density = 0.32gpc, cortex thickness=1mm)

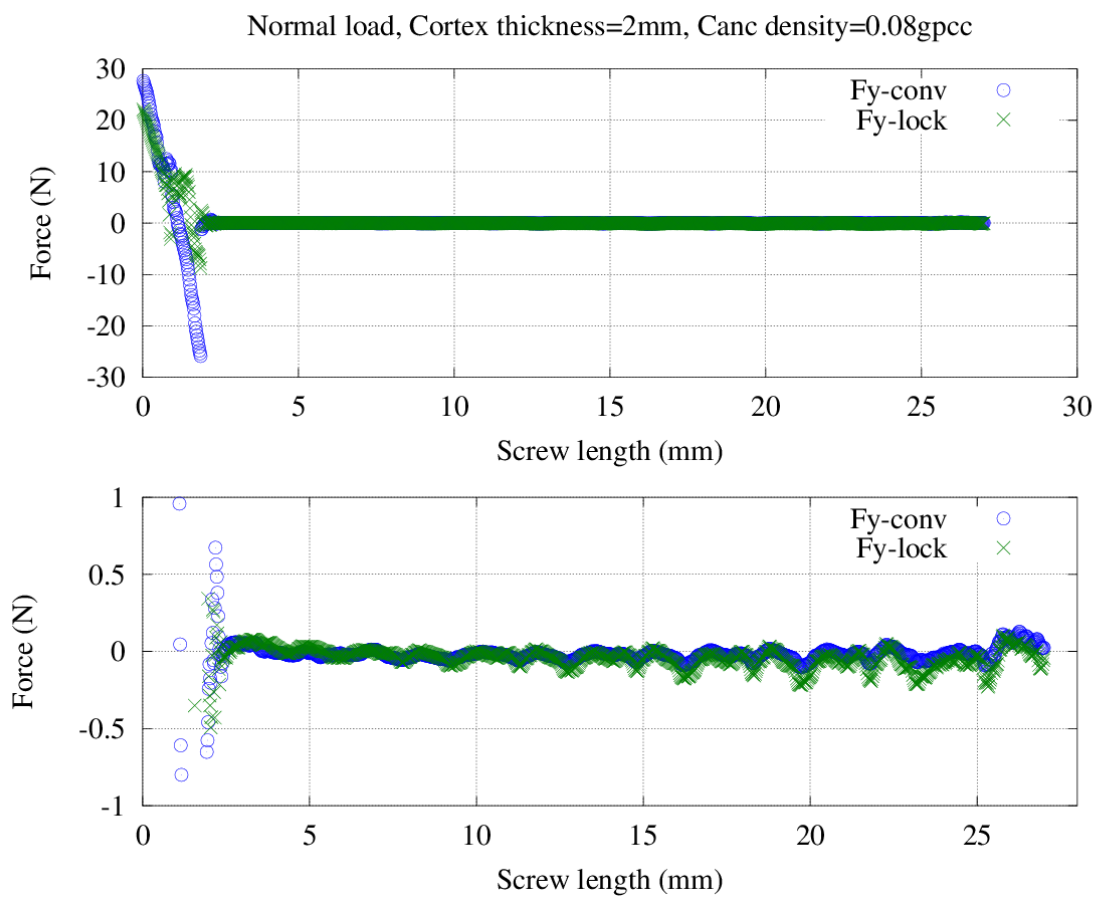


Figure D.9: Pullout force (F_y) distribution at screw bone interface under normal load (Cancellous density = 0.08gpcc, cortex thickness=2mm)

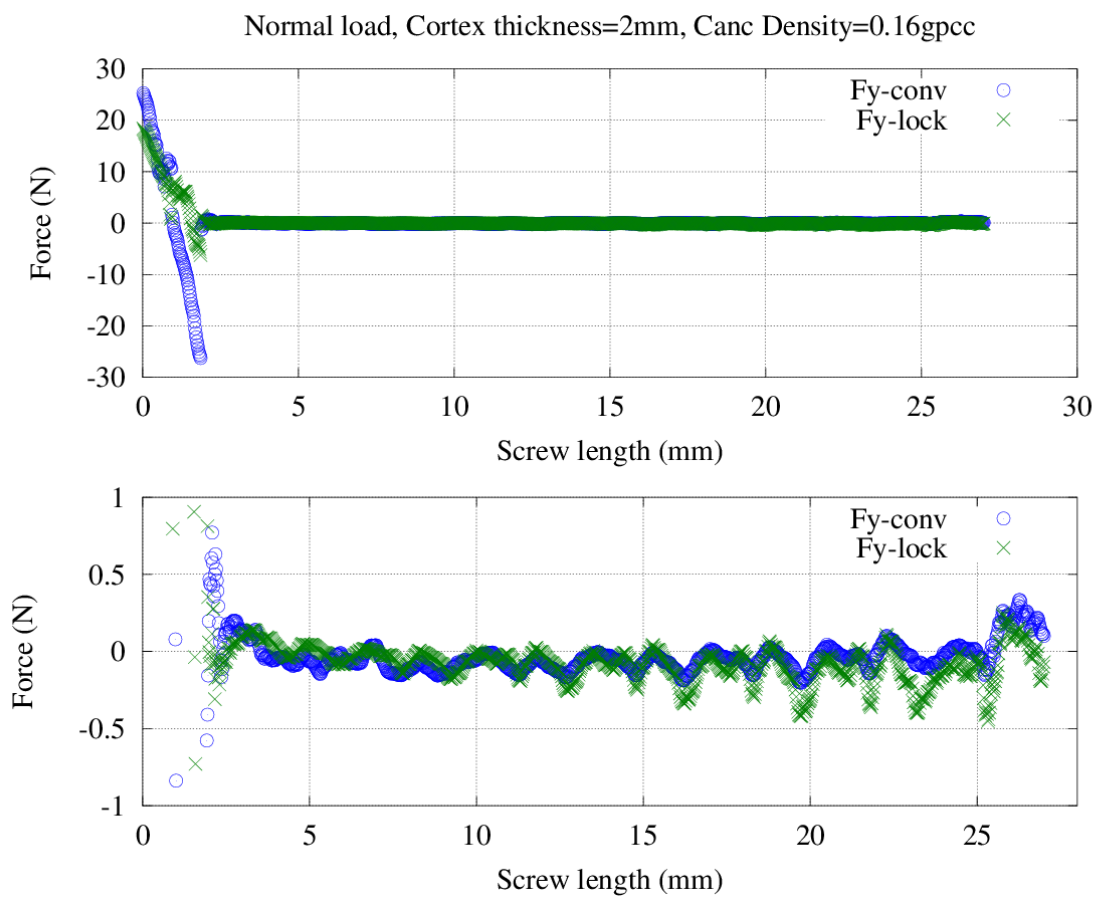


Figure D.10: Pullout force (F_y) distribution at screw bone interface under normal load (Cancellous density = 0.16gpcc, cortex thickness=2mm)

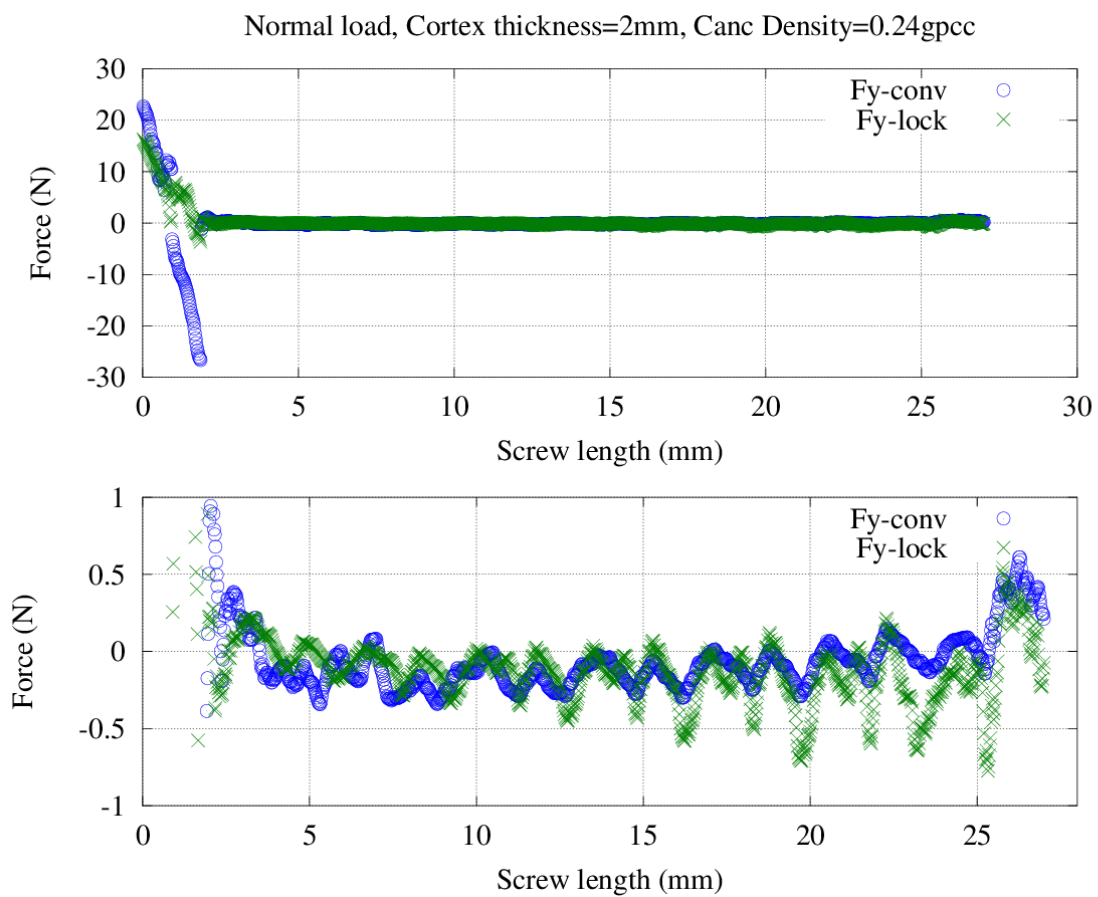


Figure D.11: Pullout force (F_y) distribution at screw bone interface under normal load (Cancellous density = 0.24gpcc, cortex thickness=2mm)

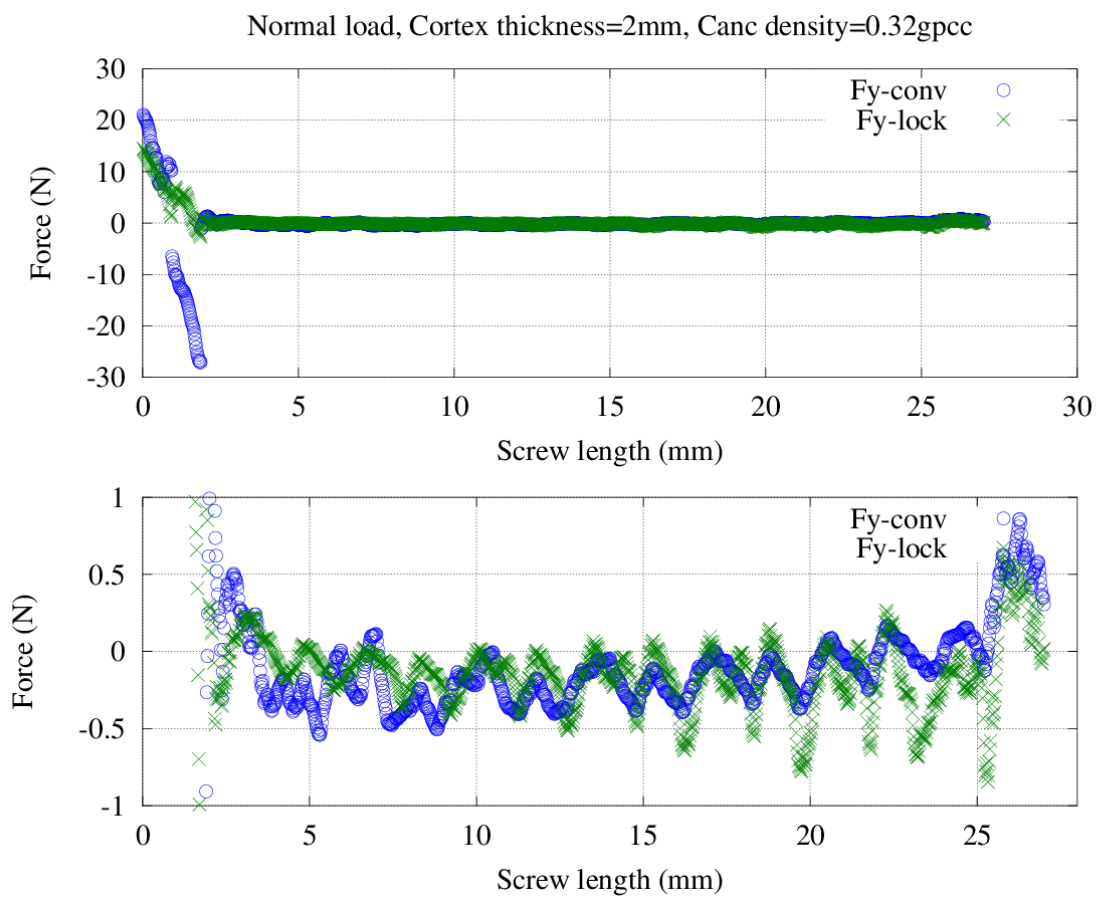


Figure D.12: Pullout force (F_y) distribution at screw bone interface under normal load (Cancellous density = 0.32gpcc, cortex thickness=2mm)

D.2 Shear load

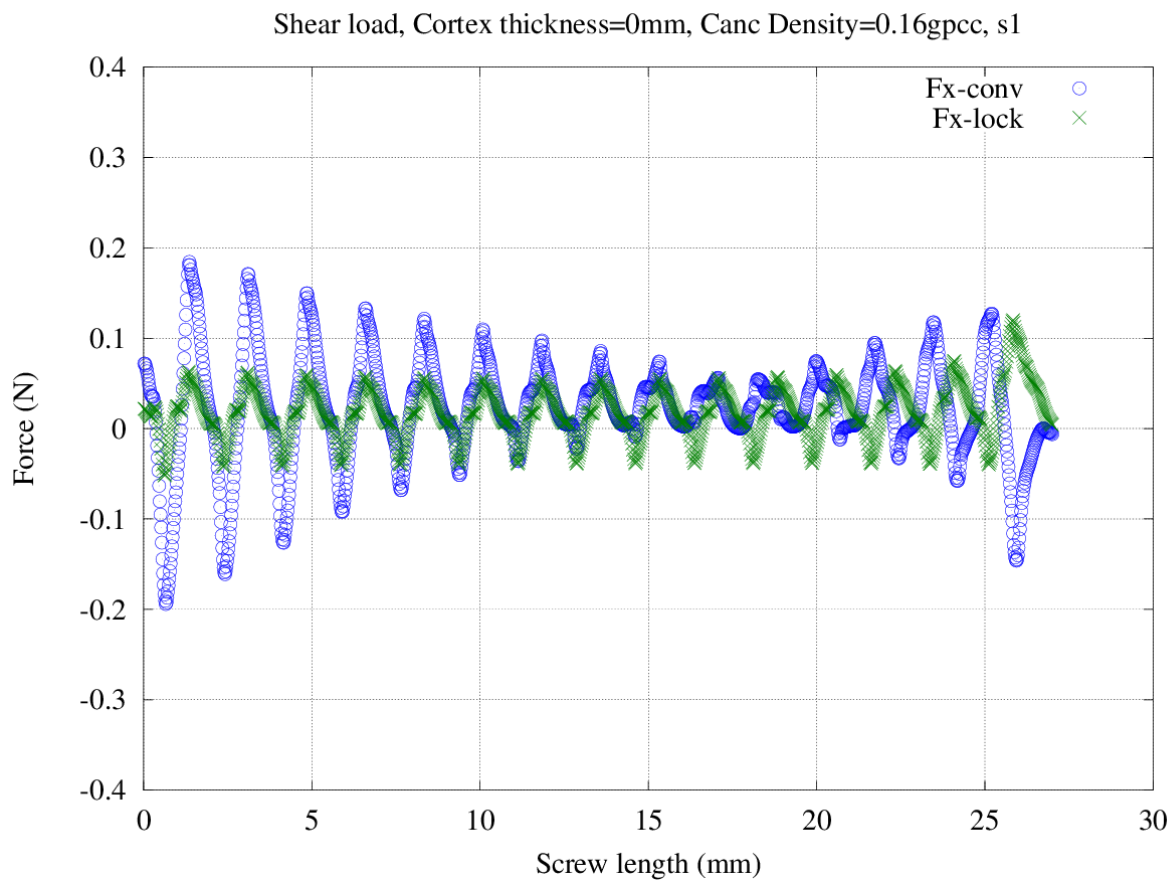


Figure D.13: Shear force (Fx) distribution at screw bone interface under shear load (Cancellous density = 0.16gpcc, cortex thickness=0mm)

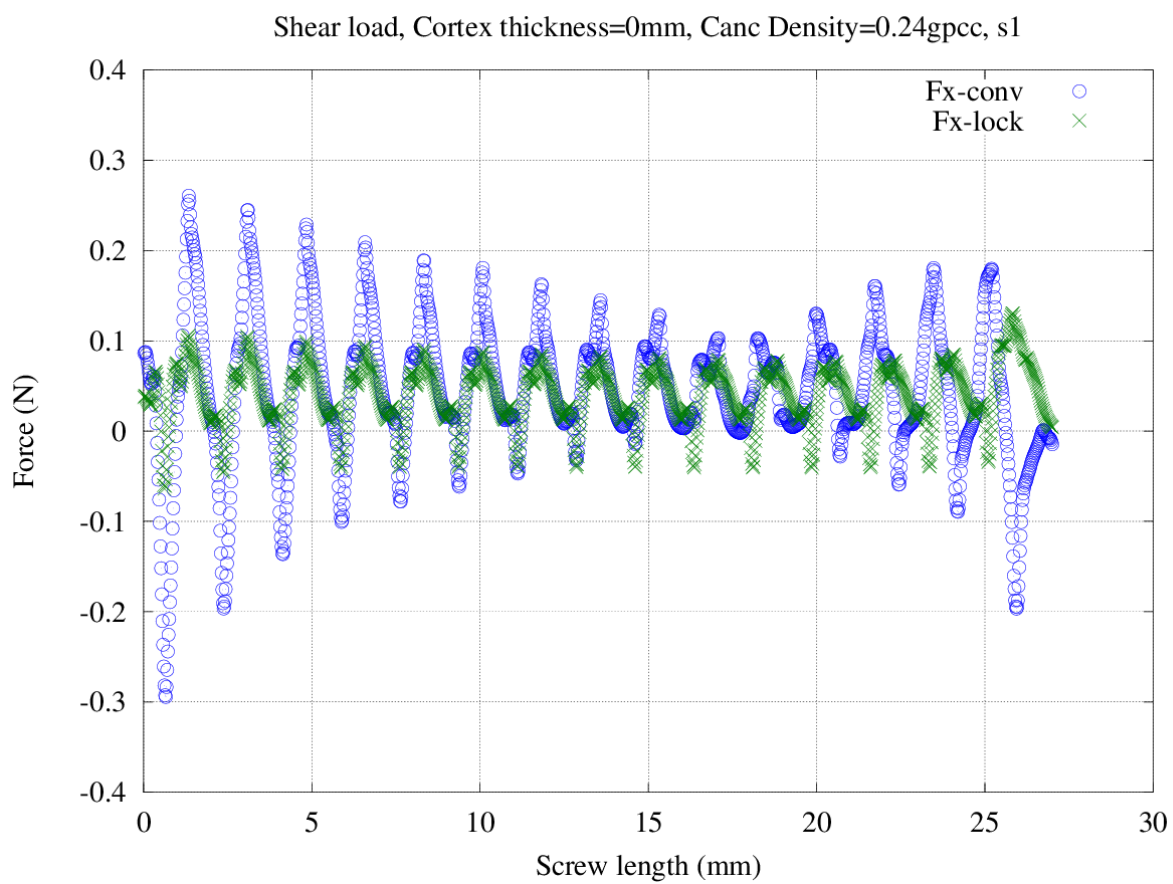


Figure D.14: Shear force (Fx) distribution at screw bone interface under shear load (Cancellous density = 0.24gpcc, cortex thickness=0mm)

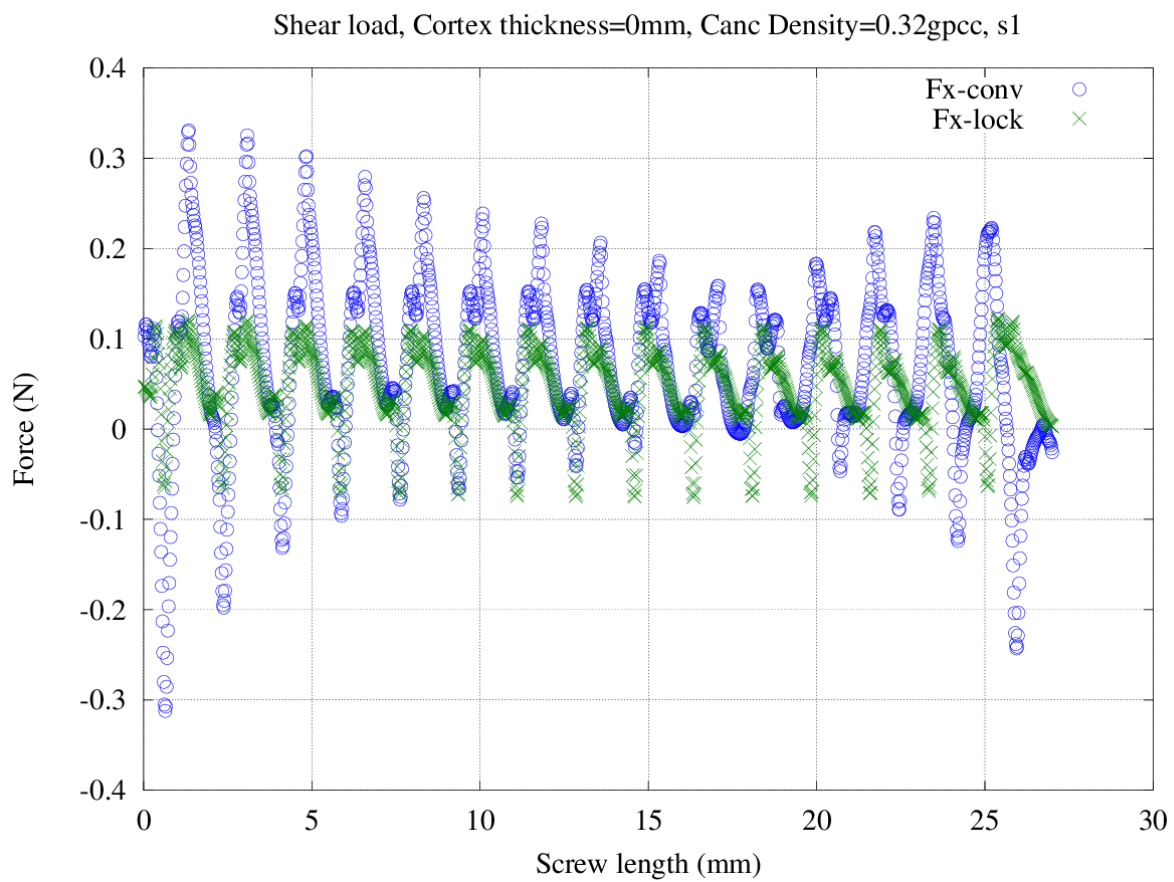


Figure D.15: Shear force (F_x) distribution at screw bone interface under shear load (Cancellous density = 0.32gpcc, cortex thickness=0mm)

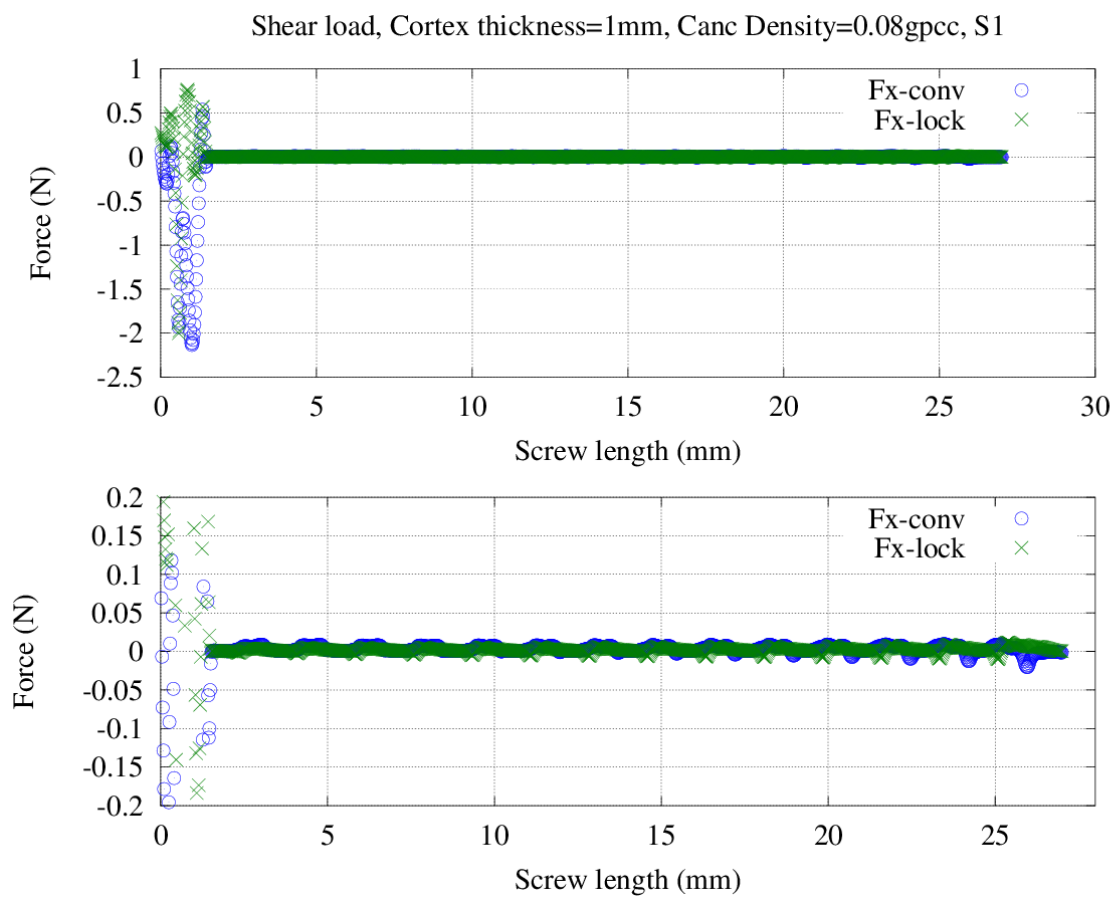


Figure D.16: Shear force (F_x) distribution at screw bone interface under shear load (Cancellous density = 0.08gpcc, cortex thickness=1mm)

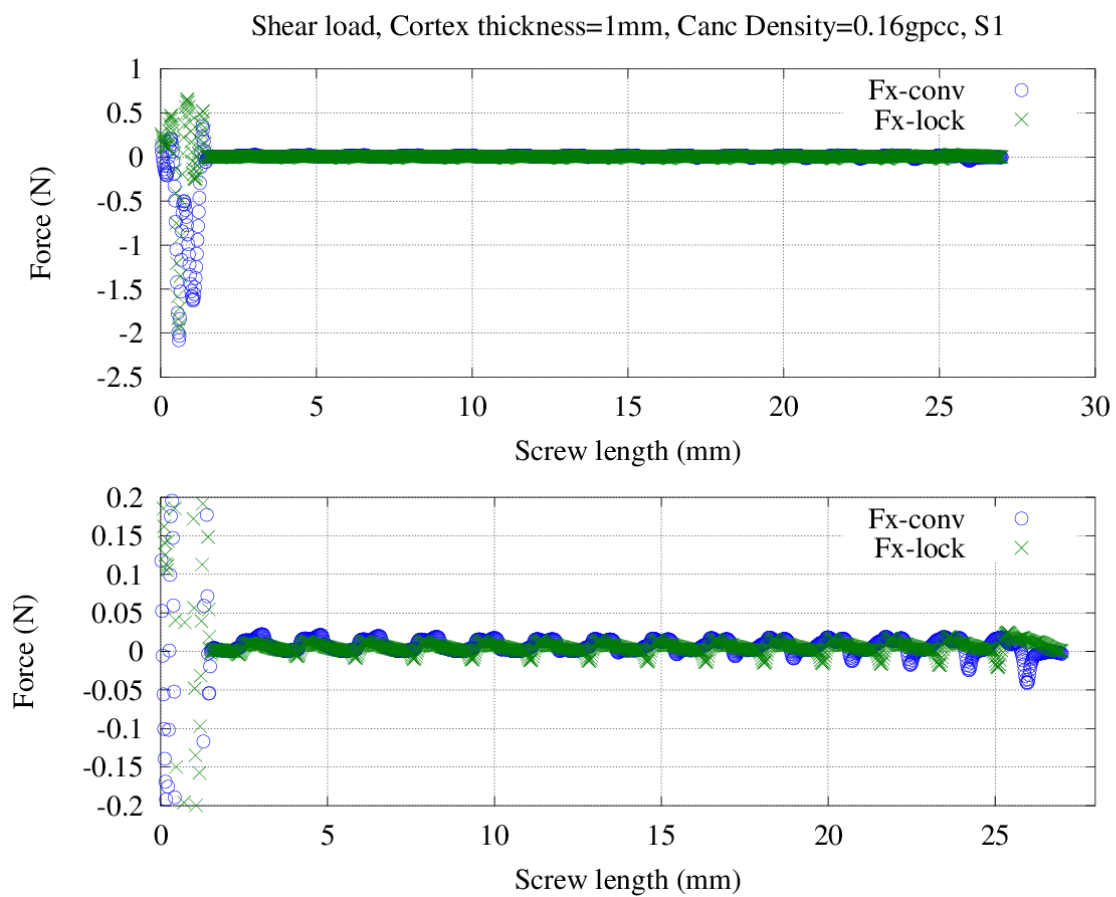


Figure D.17: Shear force (F_x) distribution at screw bone interface under shear load (Cancellous density = 0.16gpcc, cortex thickness=1mm)

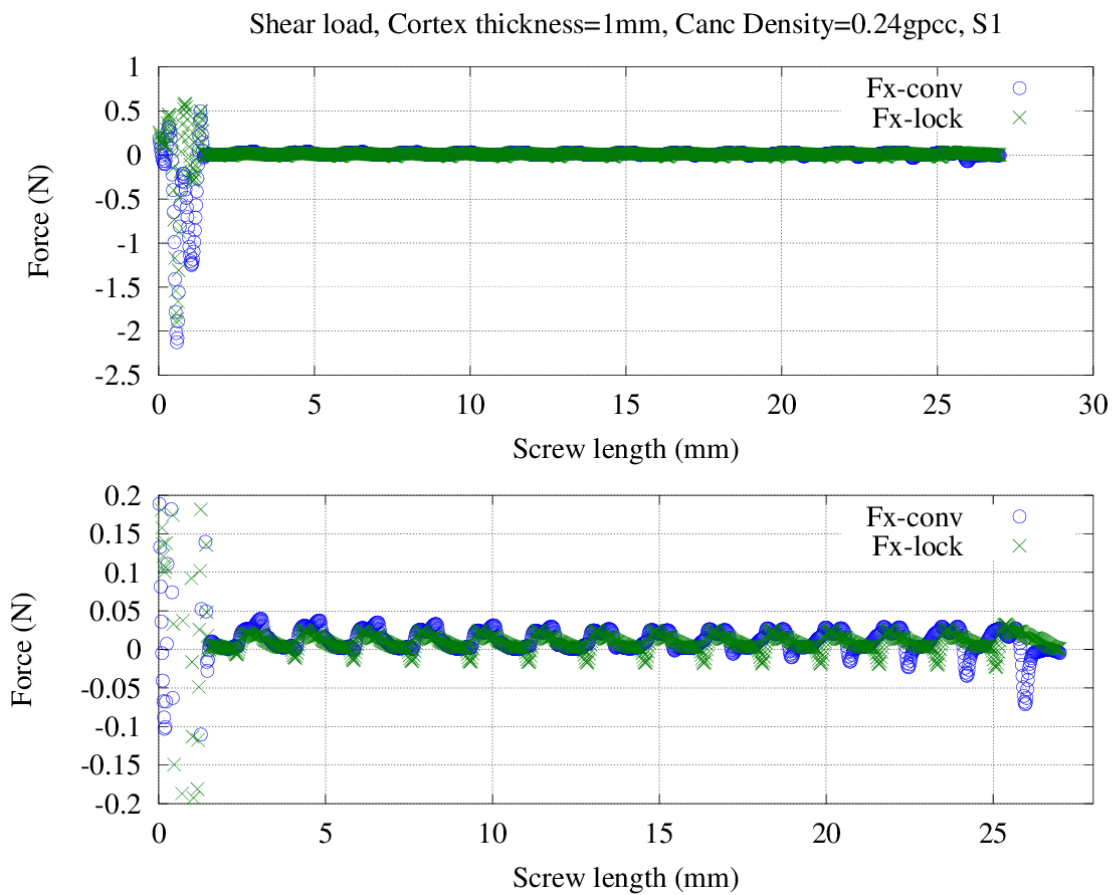


Figure D.18: Shear force (F_x) distribution at screw bone interface under shear load (Cancellous density = 0.24gpcc, cortex thickness=1mm)

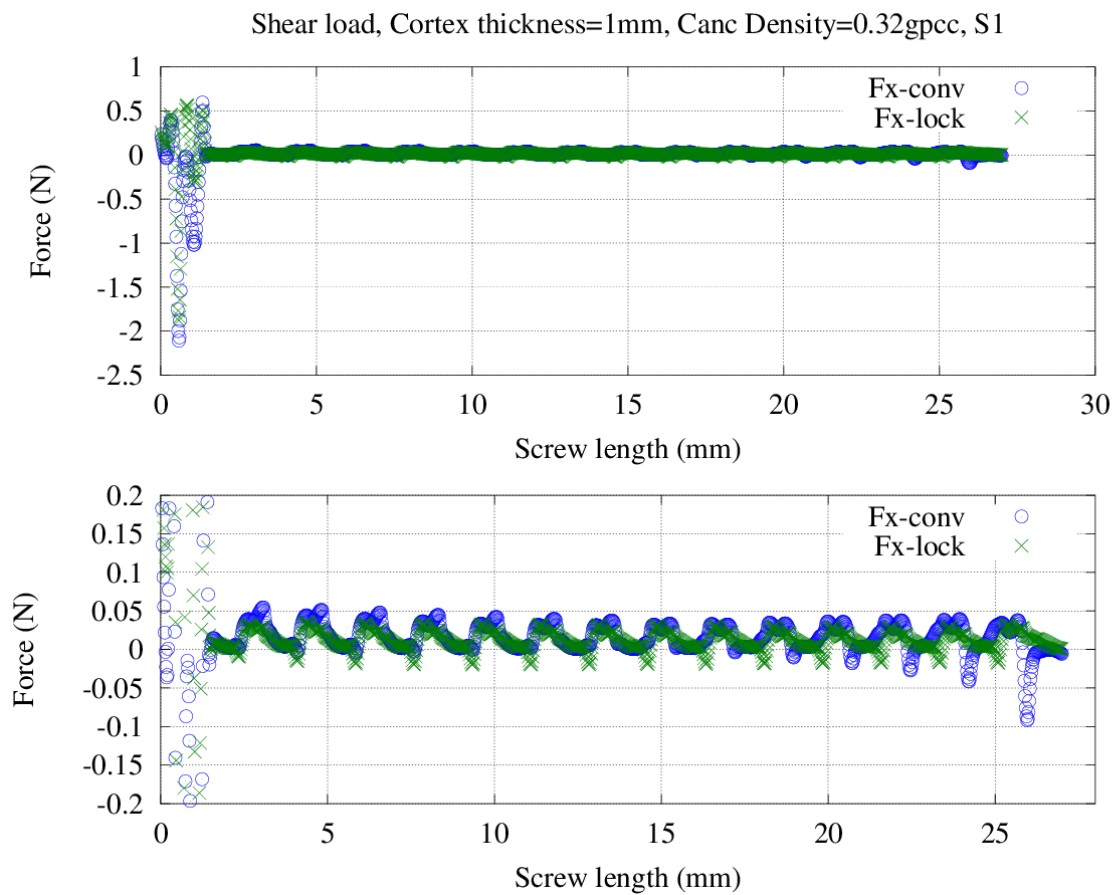


Figure D.19: Shear force (F_x) distribution at screw bone interface under shear load (Cancellous density = 0.32gpcc, cortex thickness=1mm)

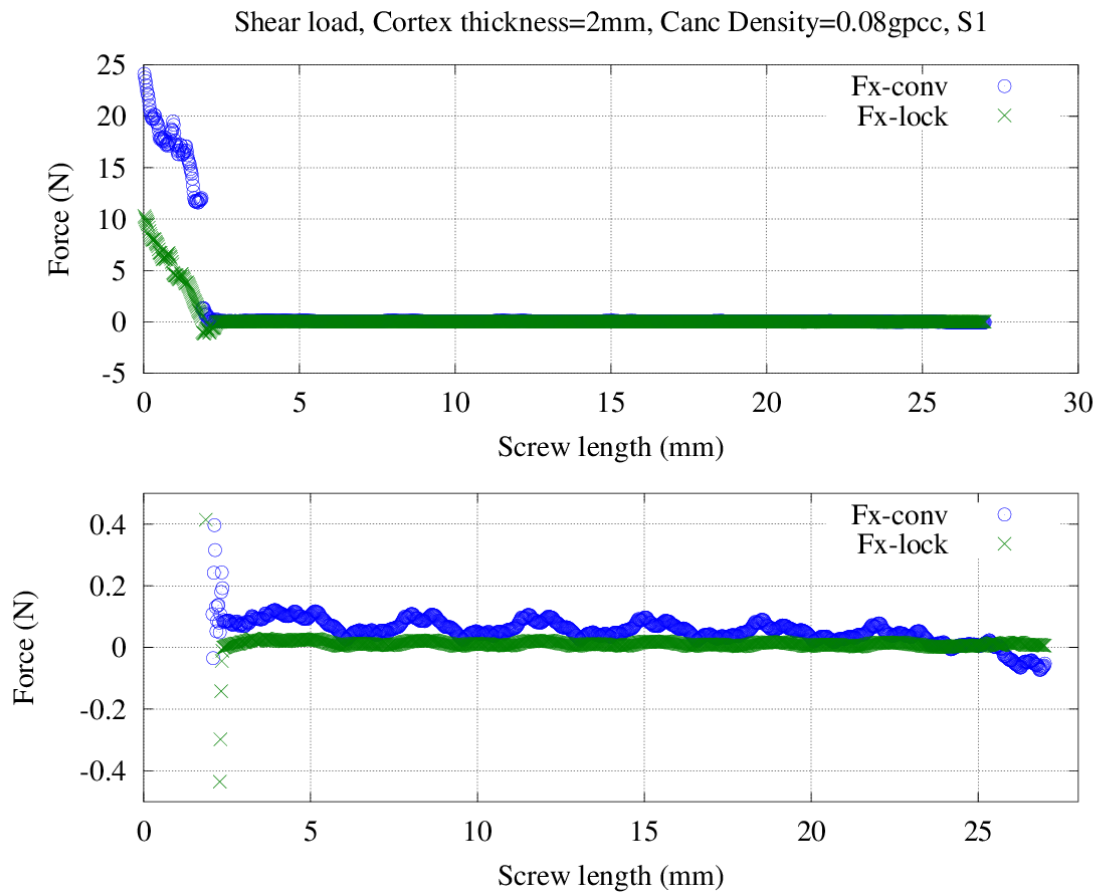


Figure D.20: Shear force (F_x) distribution at screw bone interface under shear load (Cancellous density = 0.08gpcc, cortex thickness=2mm)

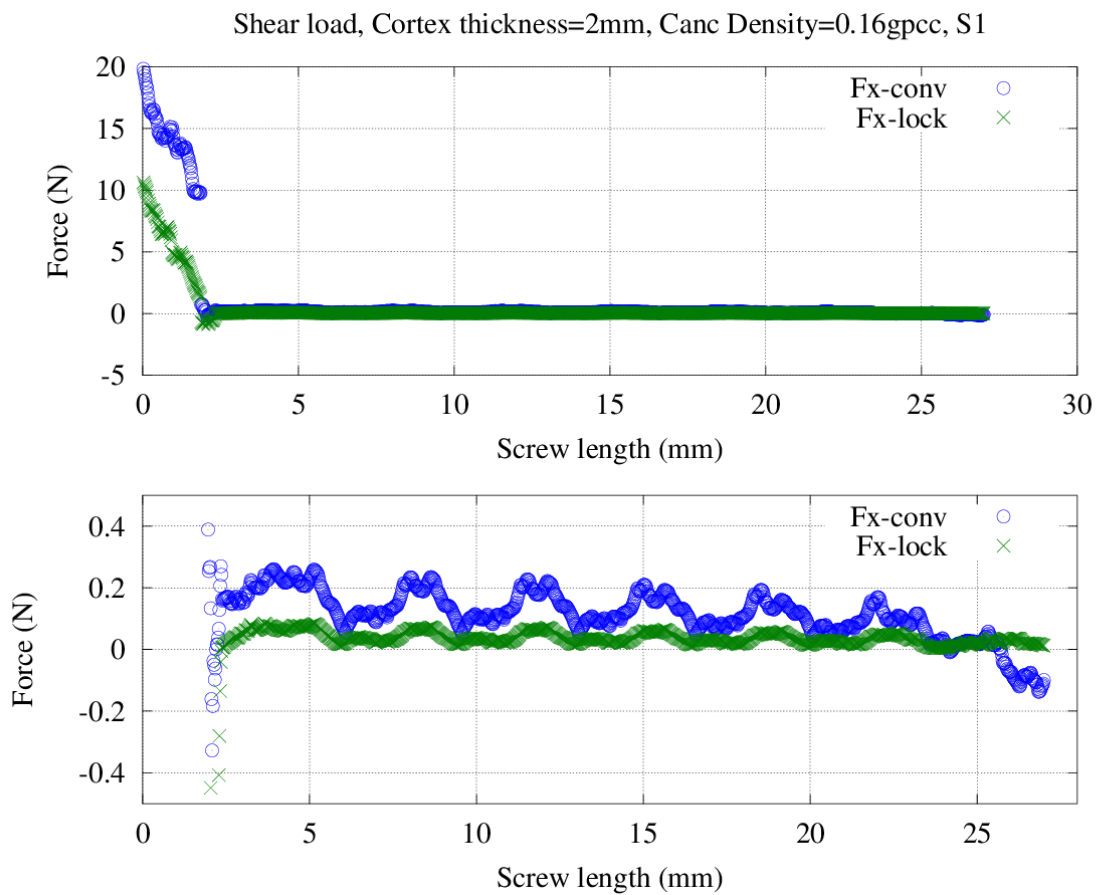


Figure D.21: Shear force (F_x) distribution at screw bone interface under shear load (Cancellous density = 0.16gpcc, cortex thickness=2mm)

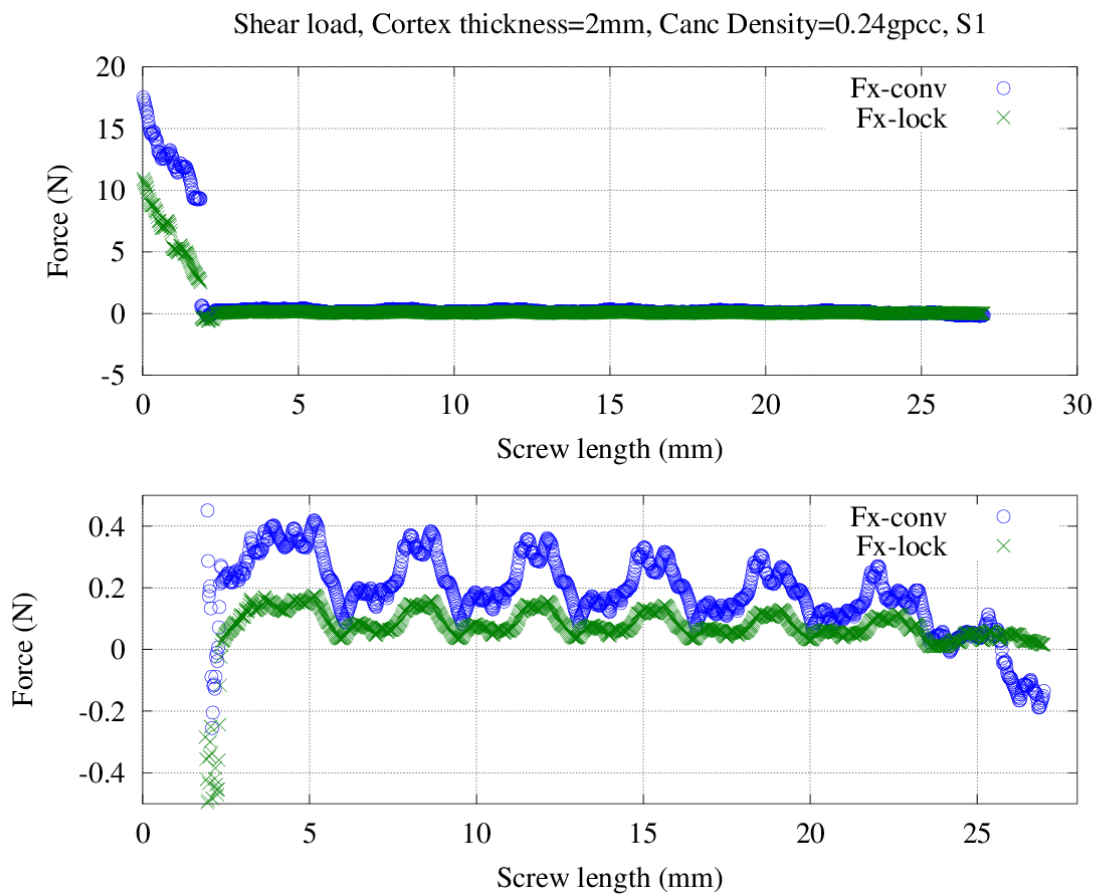


Figure D.22: Shear force (F_x) distribution at screw bone interface under shear load (Cancellous density = 0.24gpcc, cortex thickness=2mm)

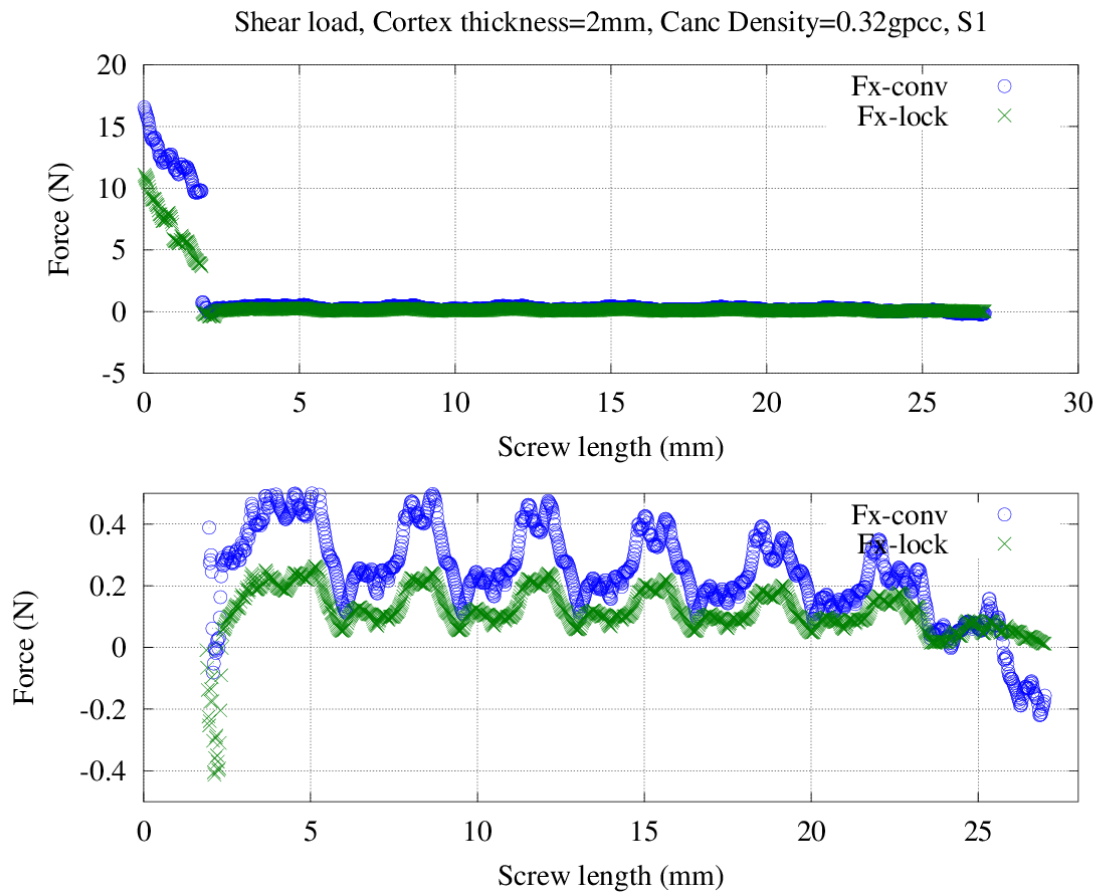


Figure D.23: Shear force (F_x) distribution at screw bone interface under shear load (Cancellous density = 0.32gpcc, cortex thickness=2mm)

D.3 Oblique load

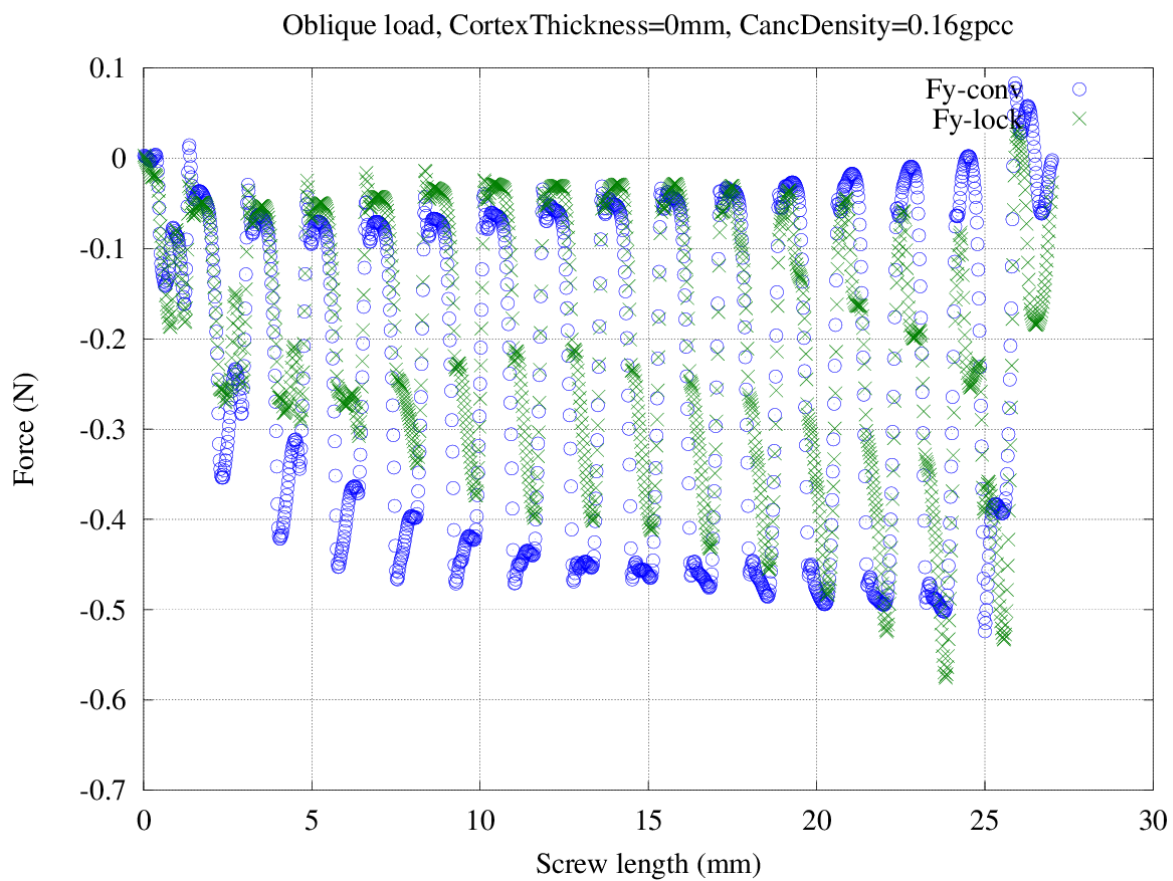


Figure D.24: Pullout force (F_y) distribution at screw bone interface under oblique load (Cancellous density = 0.16gpcc, cortex thickness=0mm)

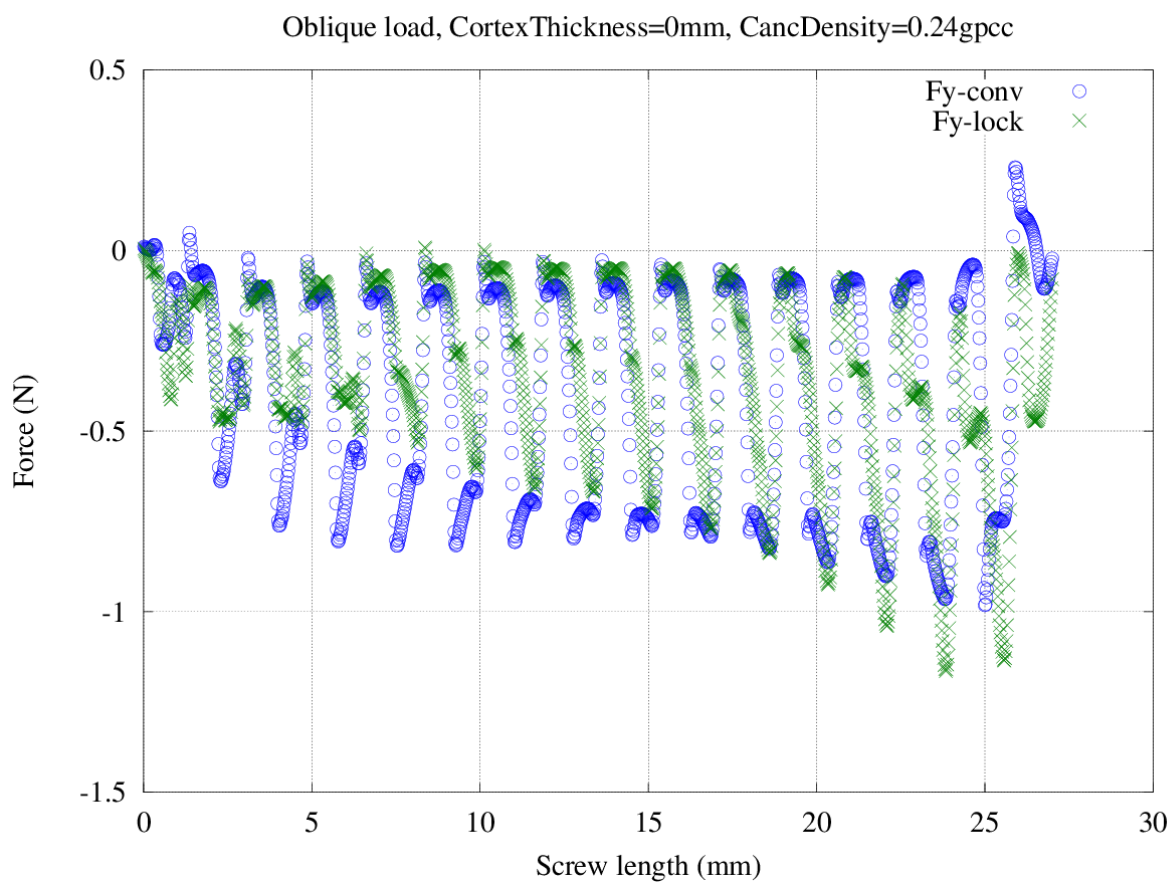


Figure D.25: Pullout force (F_y) distribution at screw bone interface under oblique load (Cancellous density = 0.24gpcc, cortex thickness=0mm)

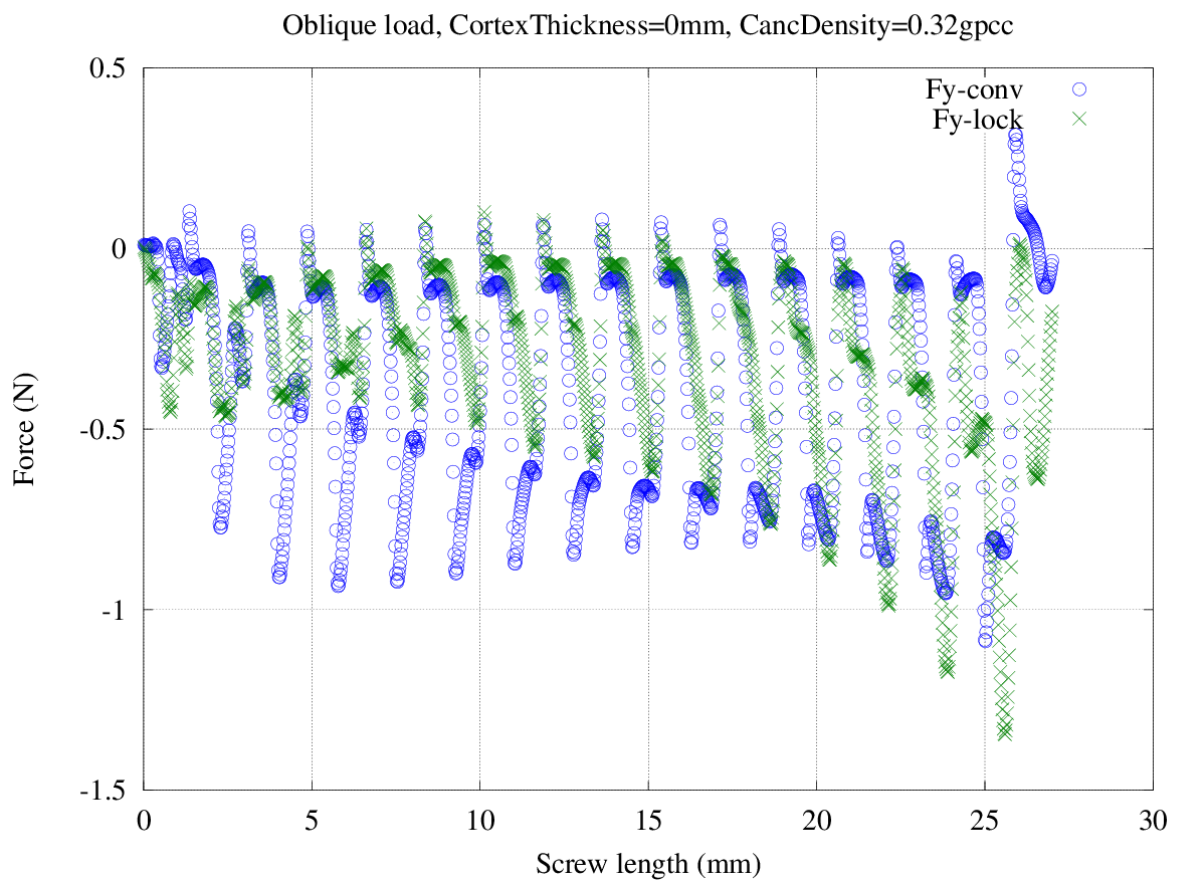


Figure D.26: Pullout force (F_y) distribution at screw bone interface under oblique load (Cancellous density = 0.32gpcc, cortex thickness=0mm)

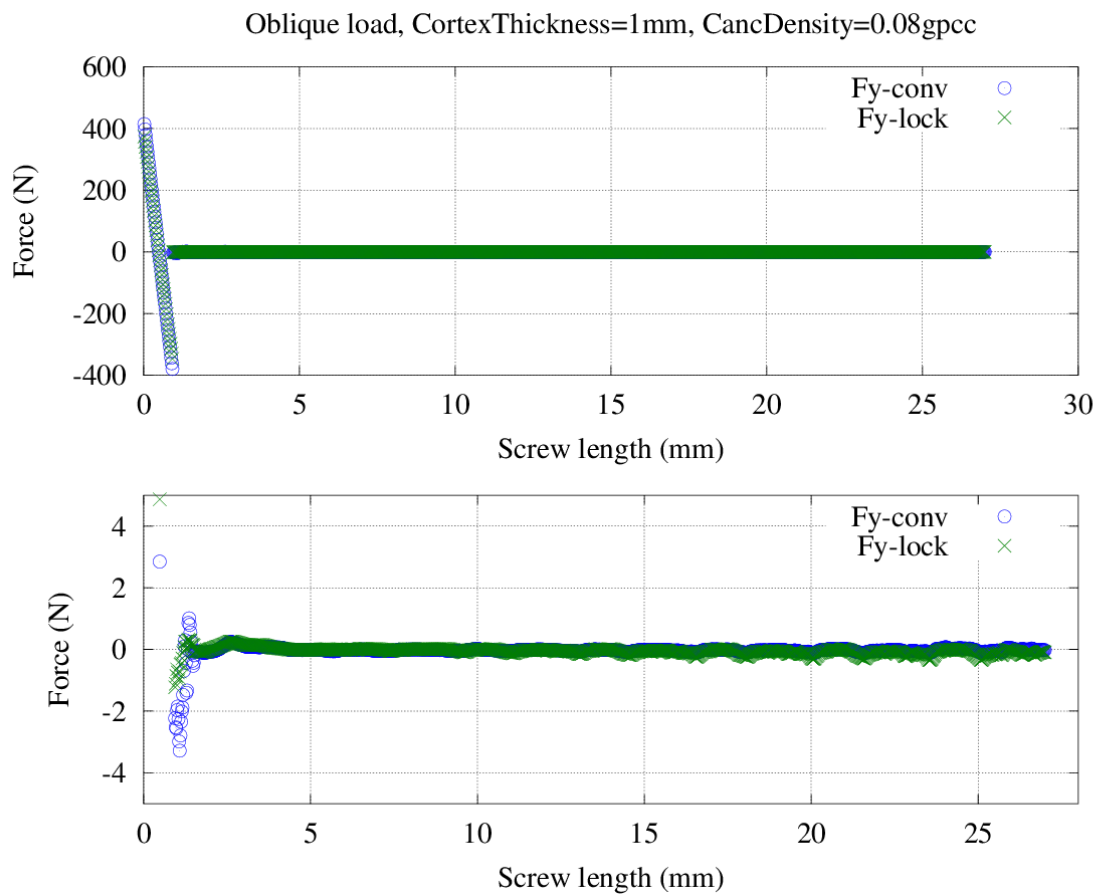


Figure D.27: Pullout force (F_y) distribution at screw bone interface under oblique load (Cancellous density = 0.08gpcc, cortex thickness=1mm)

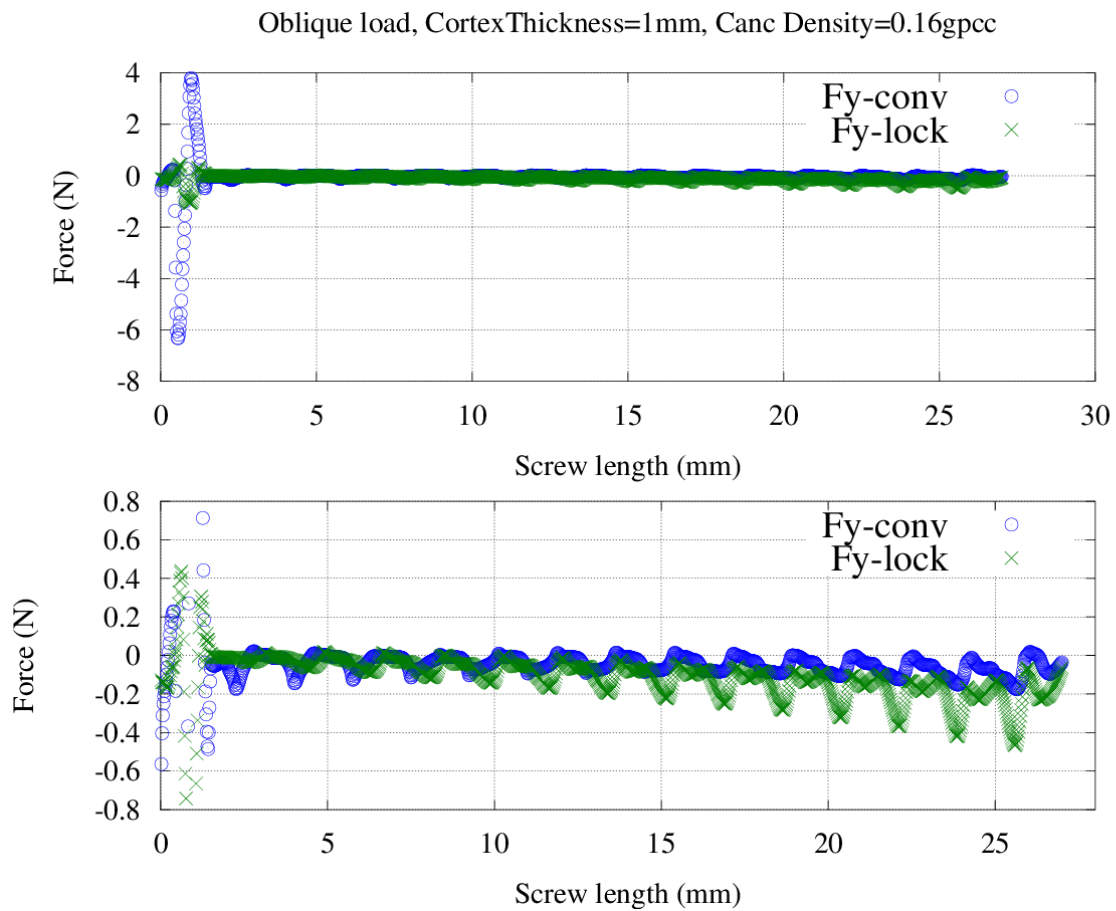


Figure D.28: Pullout force (F_y) distribution at screw bone interface under oblique load (Cancellous density = 0.16gpcc, cortex thickness=1mm)

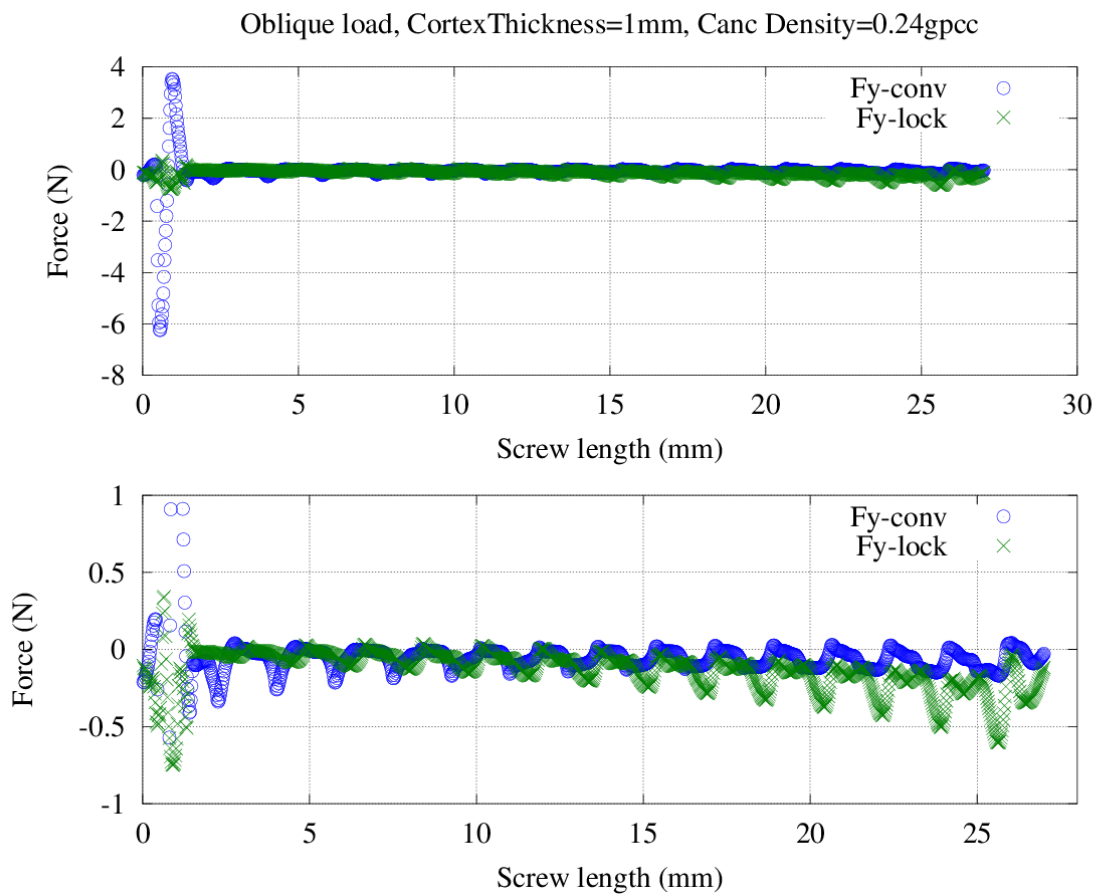


Figure D.29: Pullout force (F_y) distribution at screw bone interface under oblique load (Cancellous density = 0.24gpcc, cortex thickness=1mm)

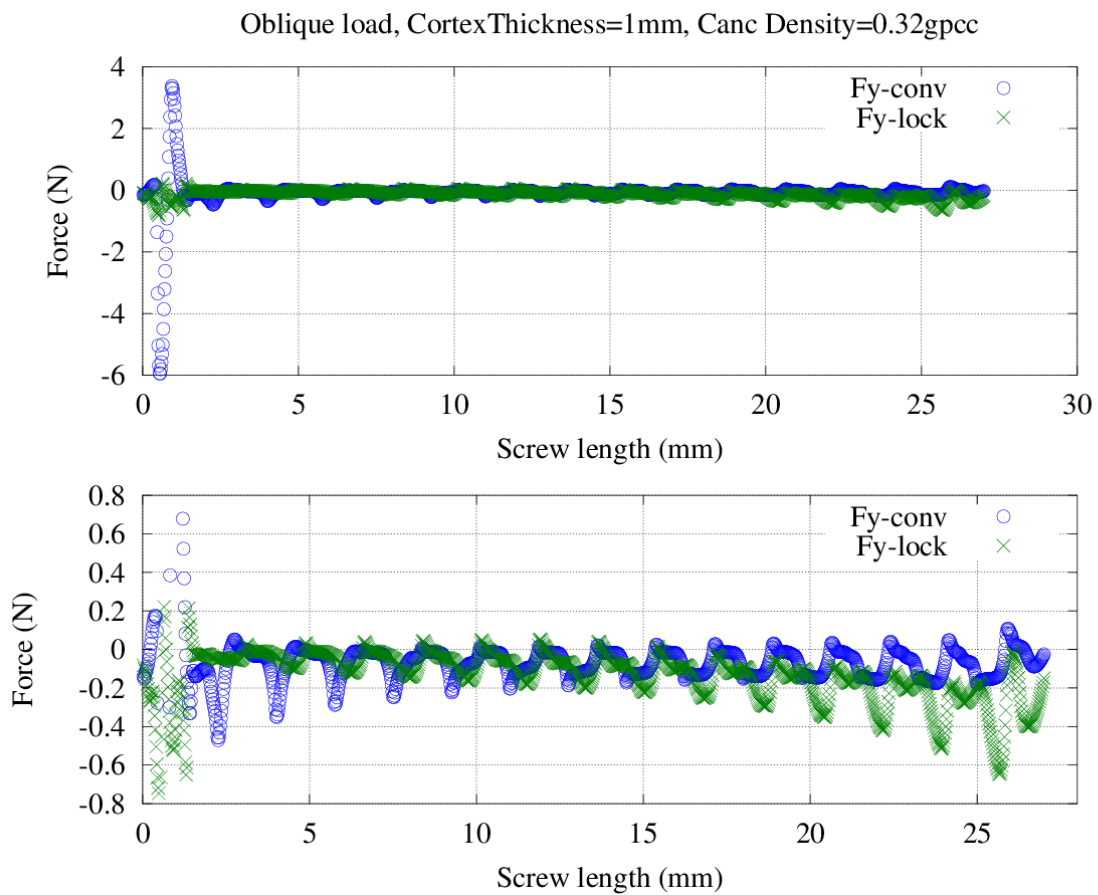


Figure D.30: Pullout force (F_y) distribution at screw bone interface under oblique load (Cancellous density = 0.32gpcc, cortex thickness=1mm)

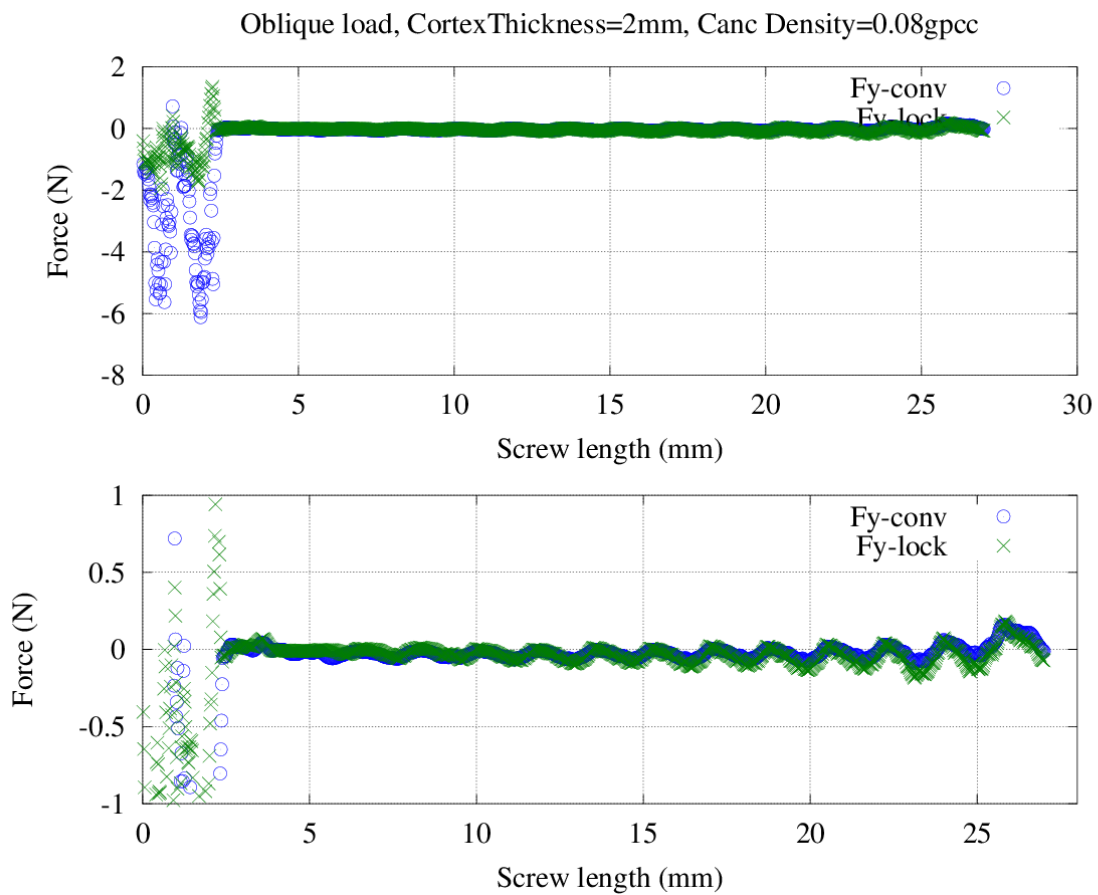


Figure D.31: Pullout force (F_y) distribution at screw bone interface under oblique load (Cancellous density = 0.08gpc, cortex thickness=2mm)

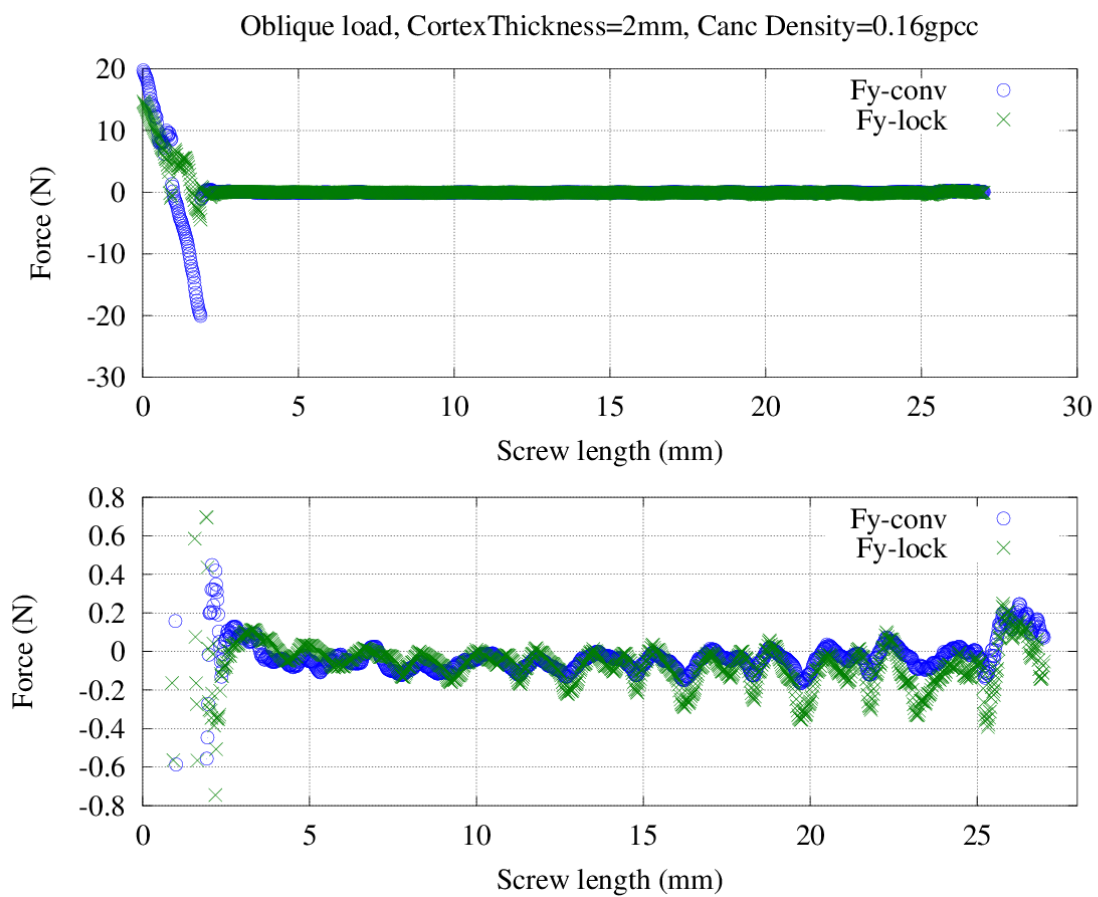


Figure D.32: Pullout force (F_y) distribution at screw bone interface under oblique load (Cancellous density = 0.16gpcc, cortex thickness=2mm)

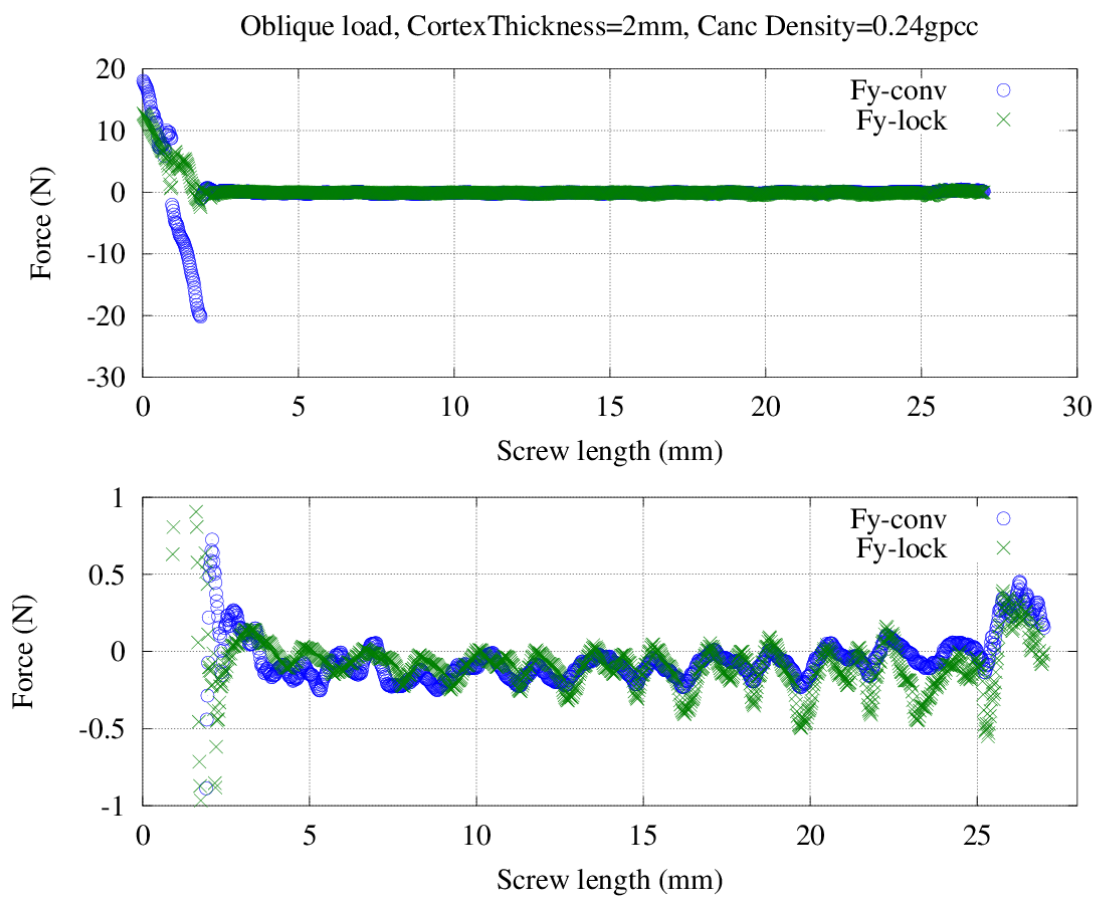


Figure D.33: Pullout force (F_y) distribution at screw bone interface under oblique load (Cancellous density = 0.24gpcc, cortex thickness=2mm)

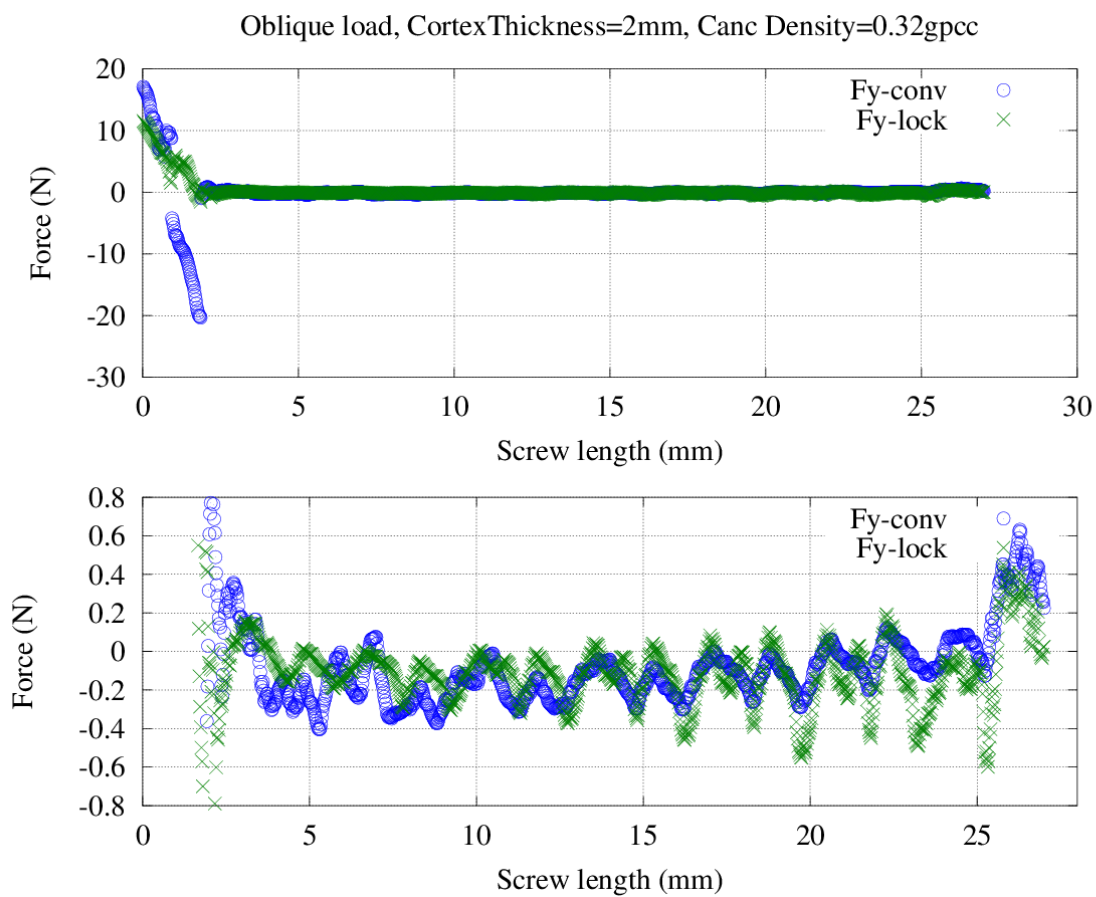
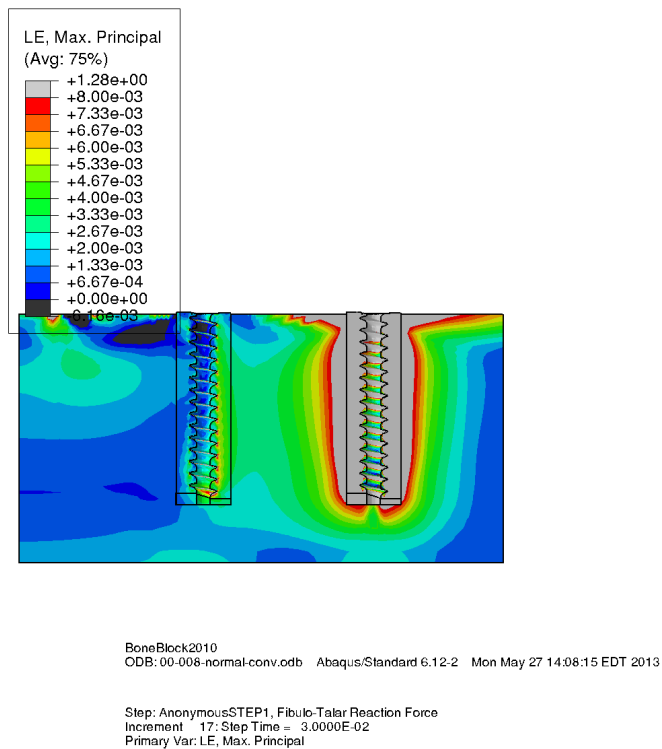


Figure D.34: Pullout force (F_y) distribution at screw bone interface under oblique load (Cancellous density = 0.32gpcc, cortex thickness=2mm)

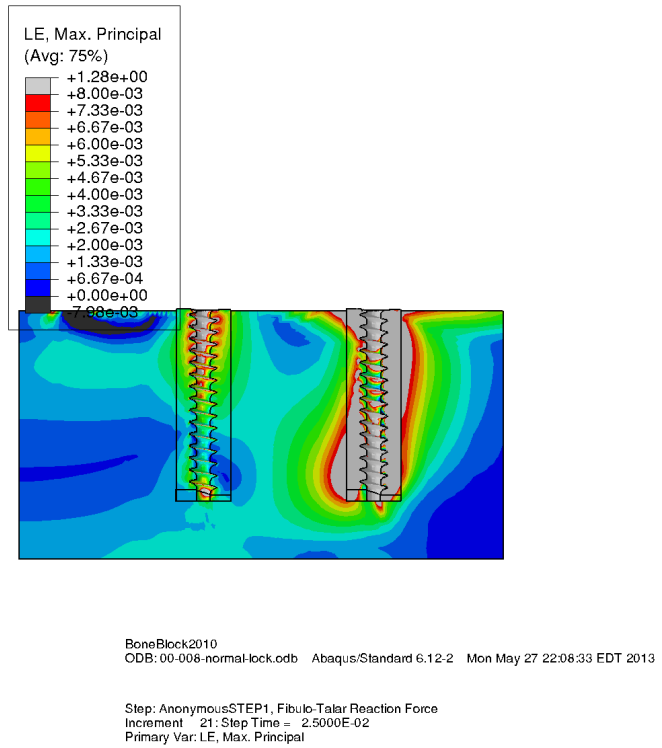
Appendix E

Total strain comparison plots

E.1 Normal load

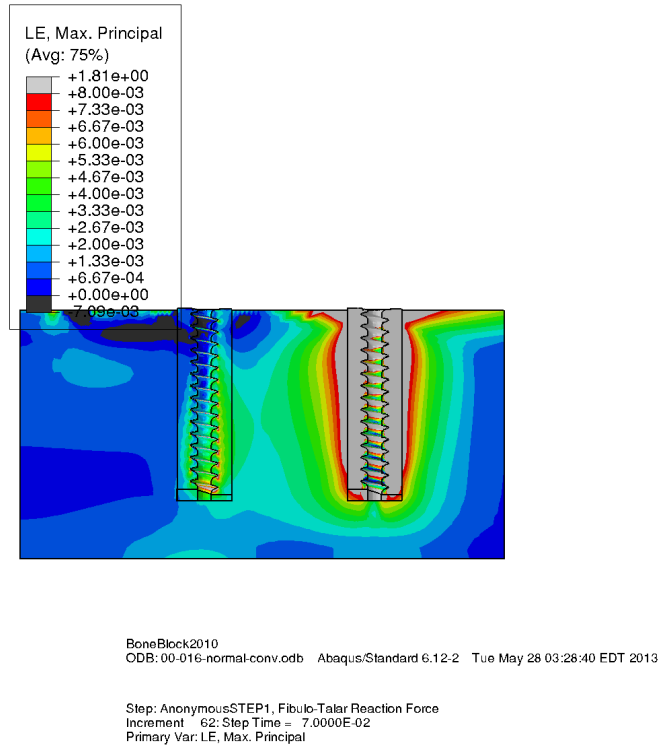


(a) Conventional screw construct

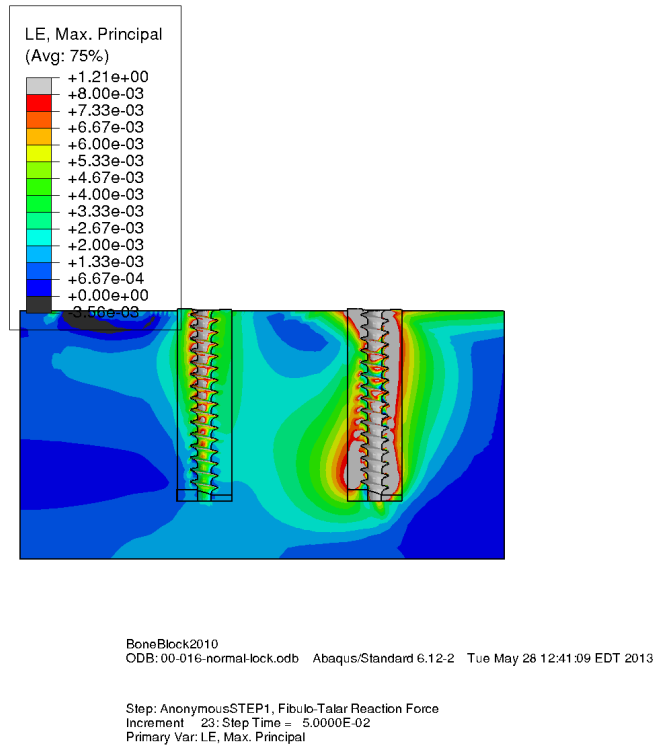


(b) Locking screw construct

Figure E.1: Total strain under normal load (Bone density = 0.08 g cm^{-3} , Cortex thickness=0mm)

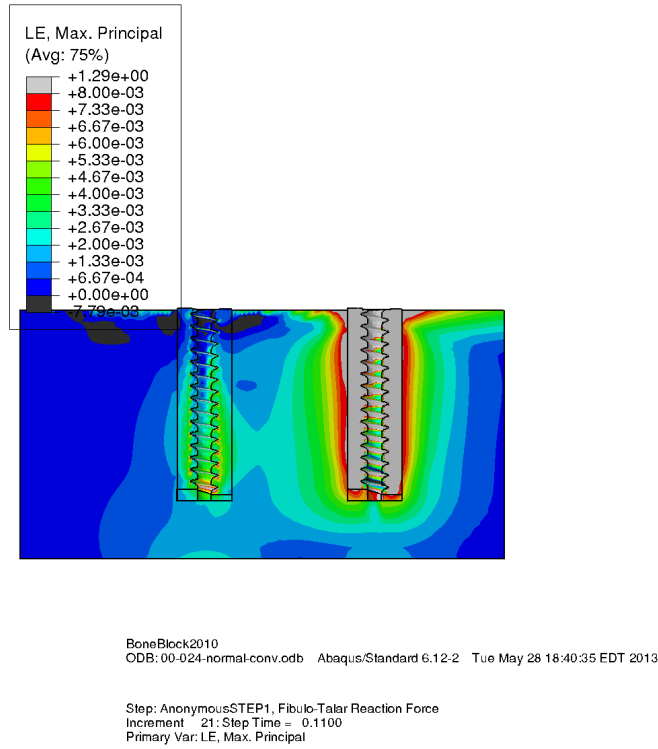


(a) Conventional screw construct

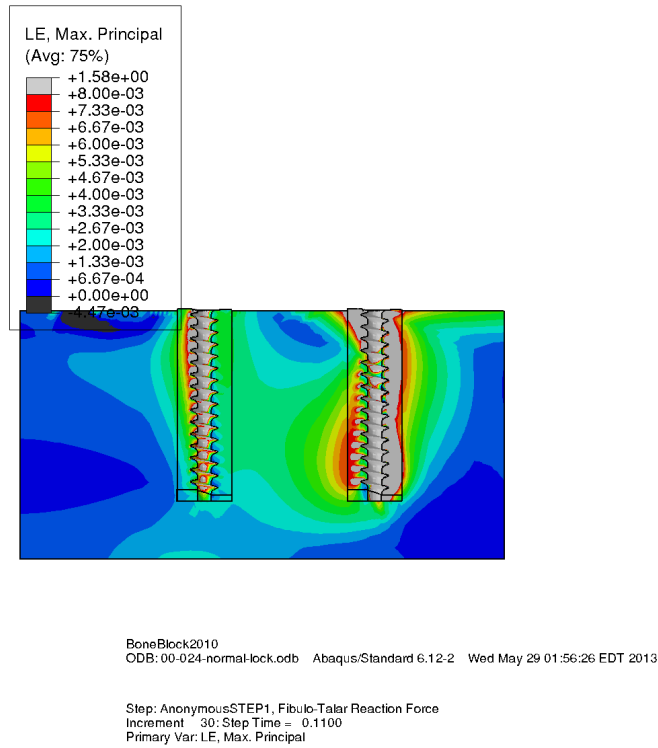


(b) Locking screw construct

Figure E.2: Total strain under normal load (Bone density = 0.16 g cm^{-3} , Cortex thickness=0mm)

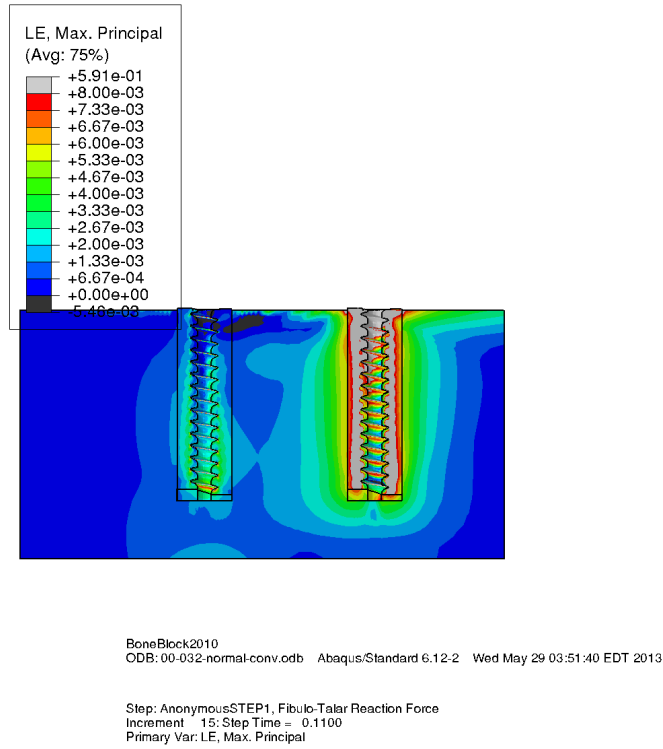


(a) Conventional screw construct

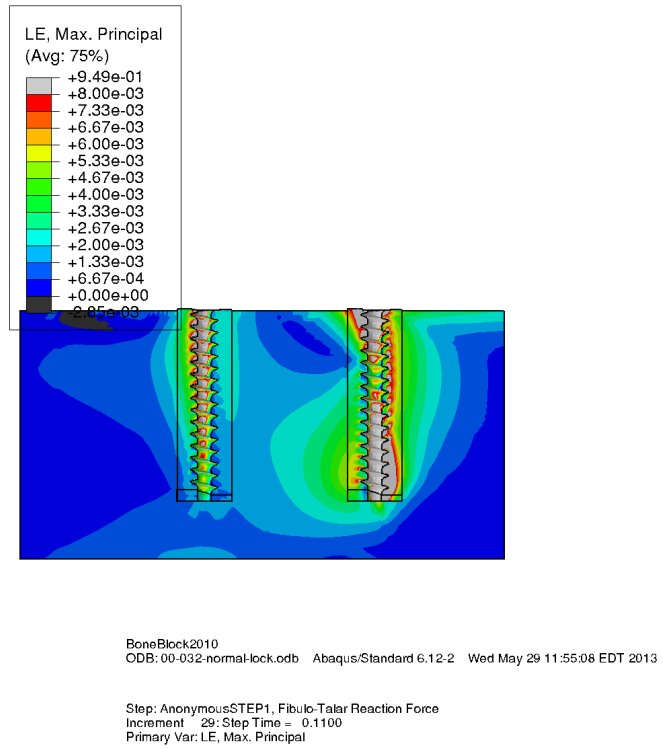


(b) Locking screw construct

Figure E.3: Total strain under normal load (Bone density = 0.16 g cm⁻³, Cortex thickness=0mm)

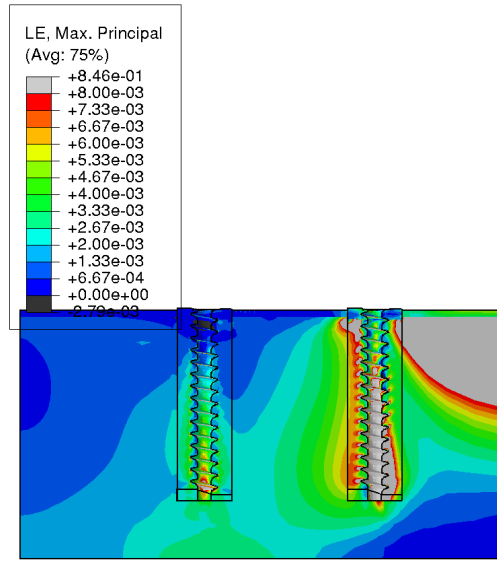


(a) Conventional screw construct



(b) Locking screw construct

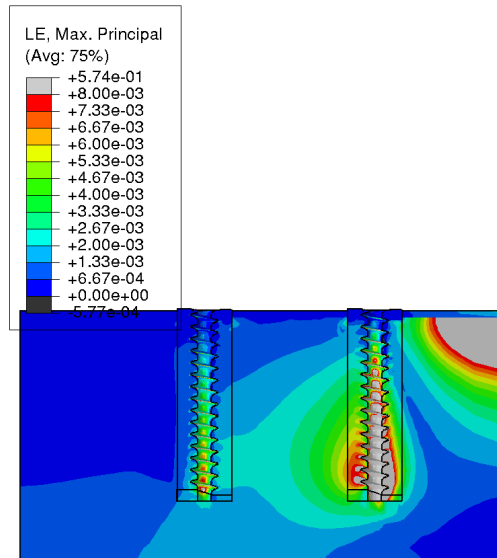
Figure E.4: Total strain under normal load (Bone density = 0.16 g cm⁻³, Cortex thickness=0mm)



BoneBlock2010
ODB: 01-008-normal-conv.odb Abaqus/Standard 6.12-2 Tue May 07 10:46:08 EDT 2013

Step: AnonymousSTEP1, Fibulo-Talar Reaction Force
Increment 21: Step Time = 0.1100
Primary Var: LE, Max. Principal

(a) Conventional screw construct

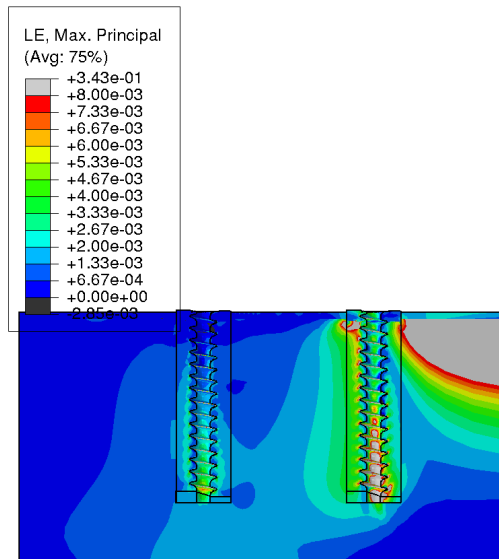


BoneBlock2010
ODB: 01-008-normal-lock.odb Abaqus/Standard 6.12-2 Tue May 07 16:16:40 EDT 2013

Step: AnonymousSTEP1, Fibulo-Talar Reaction Force
Increment 21: Step Time = 5.0000E-02
Primary Var: LE, Max. Principal

(b) Locking screw construct

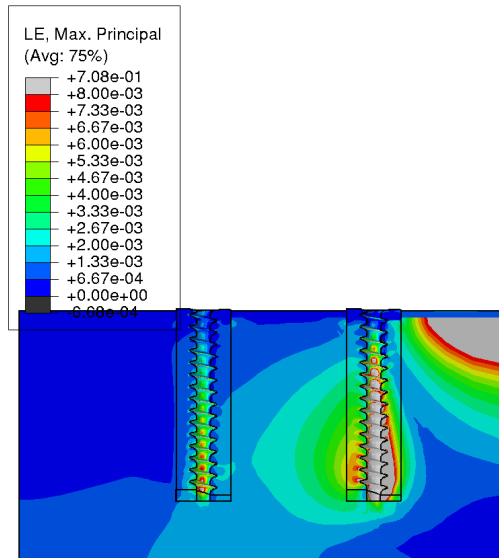
Figure E.5: Total strain under normal load (Bone density = 0.08 g cm^{-3} , Cortex thickness=1mm)



BoneBlock2010
ODB: 01-016-normal-conv.odb Abaqus/Standard 6.12-2 Tue May 07 21:50:56 EDT 2013

Step: AnonymousSTEP1, Fibulo-Talar Reaction Force
Increment 15; Step Time = 0.1100
Primary Var: LE, Max. Principal

(a) Conventional screw construct

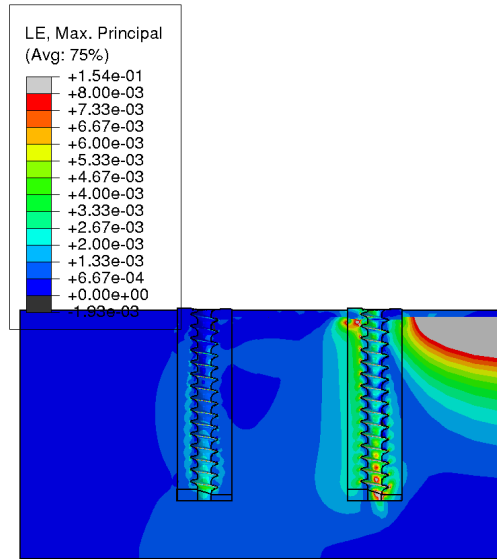


BoneBlock2010
ODB: 01-016-normal-lock.odb Abaqus/Standard 6.12-2 Wed May 08 02:51:38 EDT 2013

Step: AnonymousSTEP1, Fibulo-Talar Reaction Force
Increment 24; Step Time = 8.0000E-02
Primary Var: LE, Max. Principal

(b) Locking screw construct

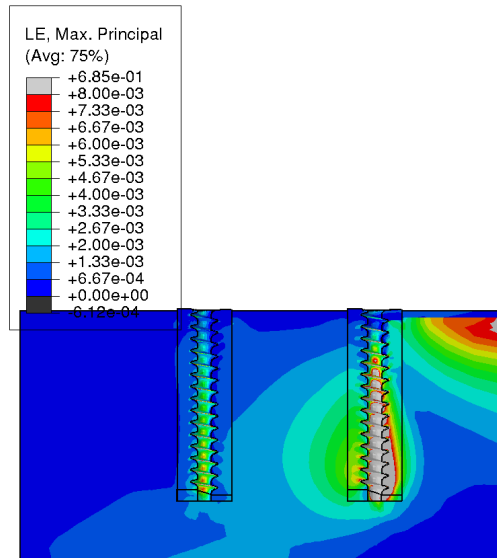
Figure E.6: Total strain under normal load (Bone density = 0.16 g cm⁻³, Cortex thickness=1mm)



BoneBlock2010
ODB: 01-024-normal-conv.odb Abaqus/Standard 6.12-2 Fri May 10 15:24:46 EDT 2013

Step: AnonymousSTEP1, Fibulo-Talar Reaction Force
Increment 15; Step Time = 0.1100
Primary Var: LE, Max. Principal

(a) Conventional screw construct

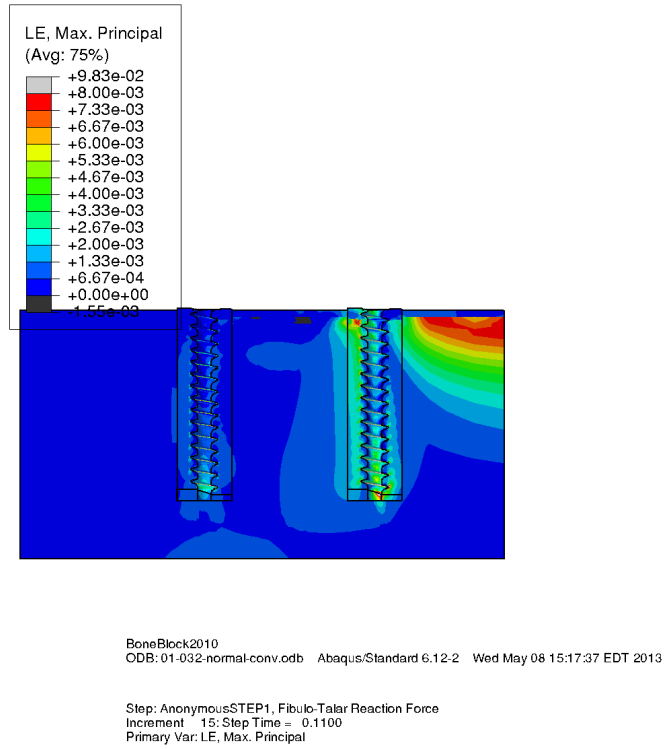


BoneBlock2010
ODB: 01-024-normal-lock.odb Abaqus/Standard 6.12-2 Wed May 08 15:16:42 EDT 2013

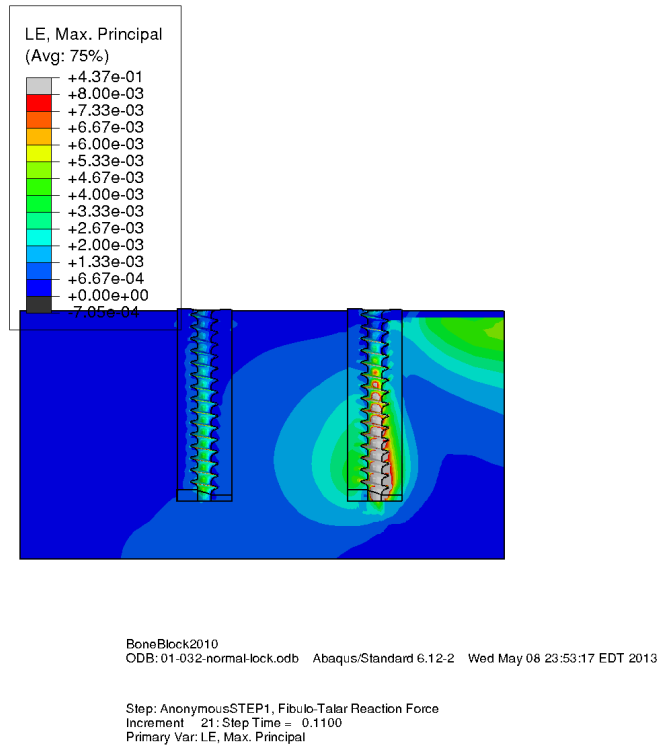
Step: AnonymousSTEP1, Fibulo-Talar Reaction Force
Increment 29; Step Time = 0.1100
Primary Var: LE, Max. Principal

(b) Locking screw construct

Figure E.7: Total strain under normal load (Bone density = 0.16 g cm^{-3} , Cortex thickness=1mm)

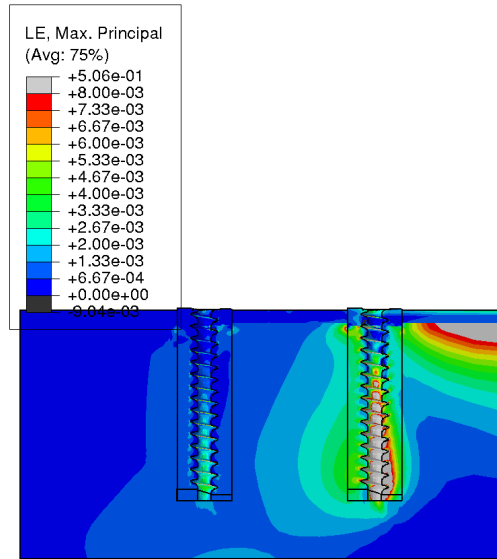


(a) Conventional screw construct



(b) Locking screw construct

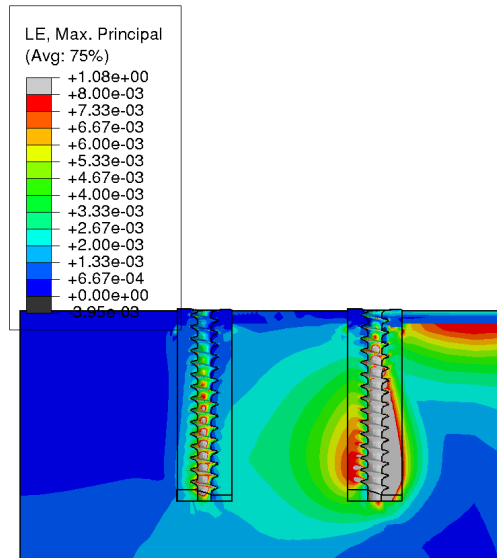
Figure E.8: Total strain under normal load (Bone density = 0.16 g cm^{-3} , Cortex thickness=1mm)



BoneBlock2010
ODB: 02-008-normal-conv.odb Abaqus/Standard 6.12-2 Thu May 09 02:35:47 EDT 2013

Step: AnonymousSTEP1, Fibulo-Talar Reaction Force
Increment 30; Step Time = 0.1100
Primary Var: LE, Max. Principal

(a) Conventional screw construct

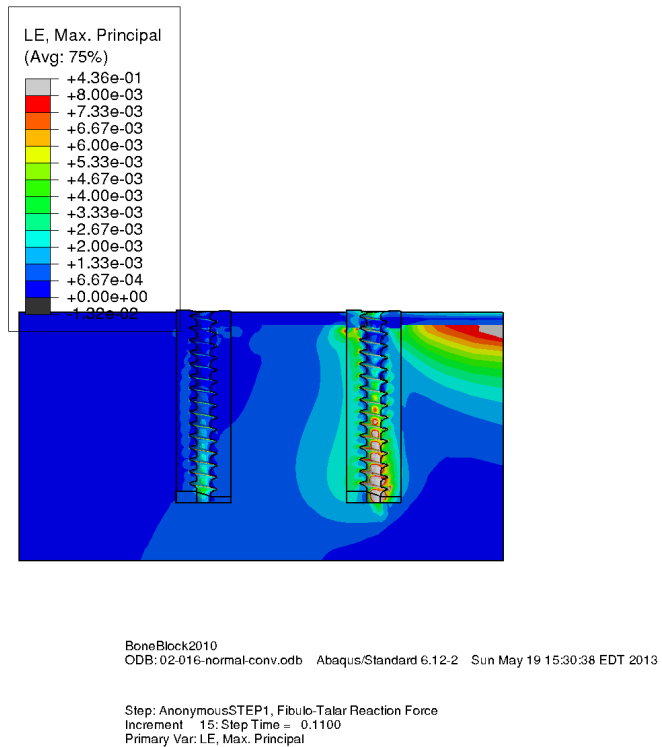


BoneBlock2010
ODB: 02-008-normal-lock.odb Abaqus/Standard 6.12-2 Sun May 19 10:12:01 EDT 2013

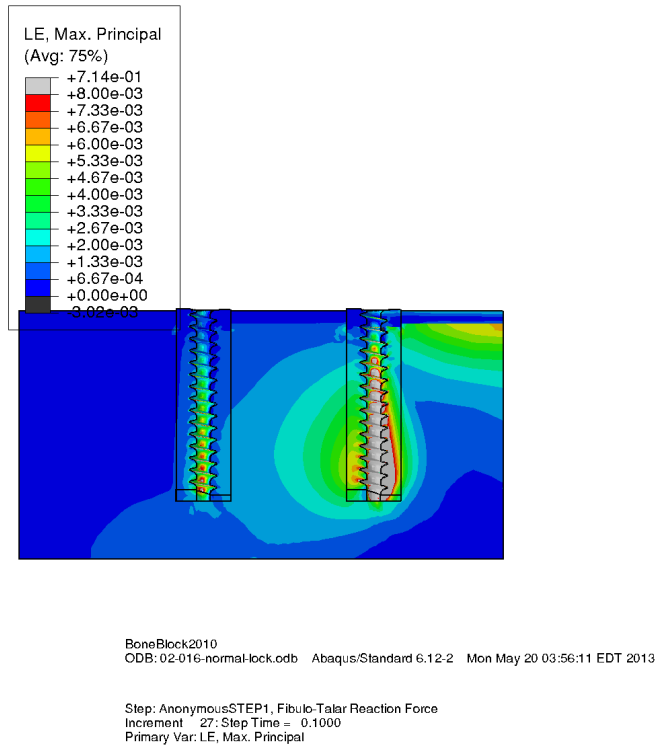
Step: AnonymousSTEP1, Fibulo-Talar Reaction Force
Increment 32; Step Time = 0.1100
Primary Var: LE, Max. Principal

(b) Locking screw construct

Figure E.9: Total strain under normal load (Bone density = 0.08 g cm⁻³, Cortex thickness=2mm)

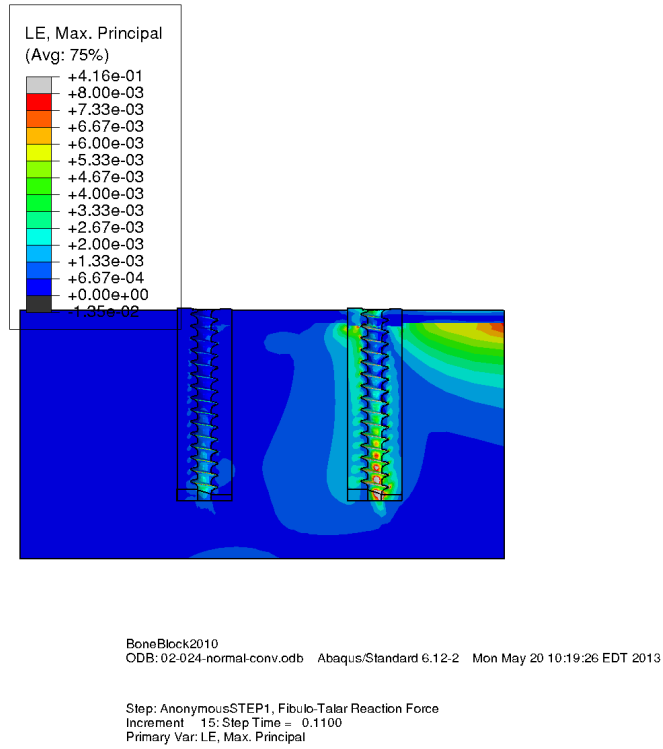


(a) Conventional screw construct

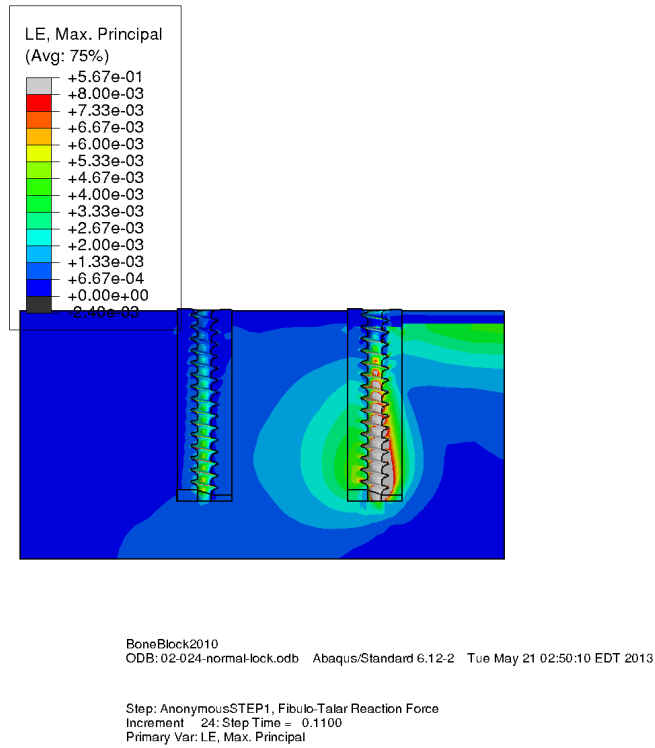


(b) Locking screw construct

Figure E.10: Total strain under normal load (Bone density = 0.16 g cm^{-3} , Cortex thickness=2mm)

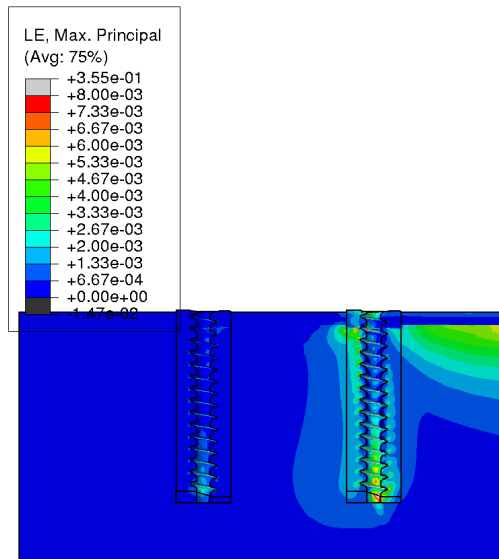


(a) Conventional screw construct



(b) Locking screw construct

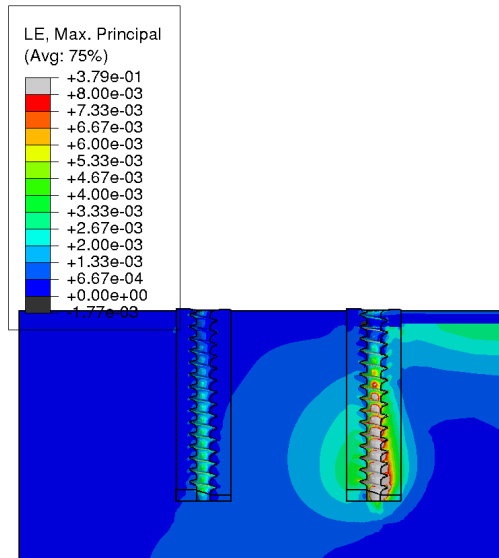
Figure E.11: Total strain under normal load (Bone density = 0.16 g cm^{-3} , Cortex thickness=2mm)



BoneBlock2010
ODB: 02-032-normal-conv.odb Abaqus/Standard 6.12-2 Tue May 21 09:53:11 EDT 2013

Step: AnonymousSTEP1, Fibulo-Talar Reaction Force
Increment 15; Step Time = 0.1100
Primary Var: LE, Max. Principal

(a) Conventional screw construct



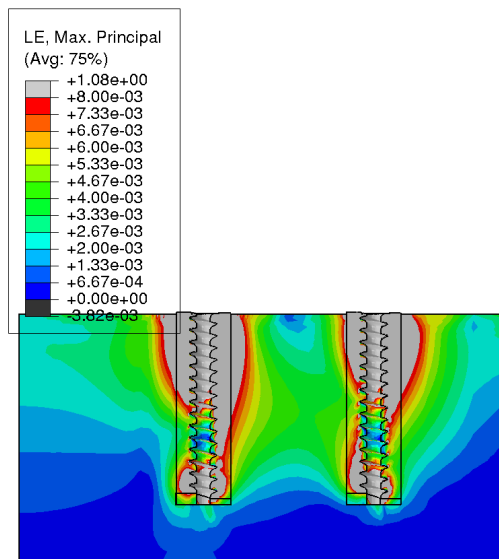
BoneBlock2010
ODB: 02-032-normal-lock.odb Abaqus/Standard 6.12-2 Wed May 22 02:21:09 EDT 2013

Step: AnonymousSTEP1, Fibulo-Talar Reaction Force
Increment 21; Step Time = 0.1100
Primary Var: LE, Max. Principal

(b) Locking screw construct

Figure E.12: Total strain under normal load (Bone density = 0.16 g cm^{-3} , Cortex thickness=2mm)

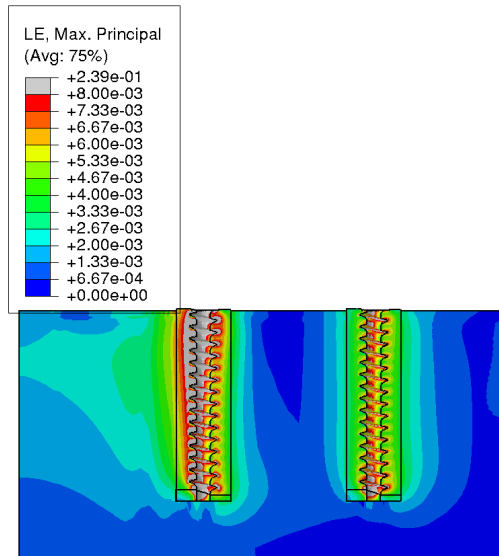
E.2 Shear load



BoneBlock2010
ODB: 00-016-shear-conv.odb Abaqus/Standard 6.12-2 Sat Jun 08 16:38:44 EDT 2013

Step: AnonymousSTEP1, Fibulo-Talar Reaction Force
Increment 48; Step Time = 1.7500E-02
Primary Var: LE, Max. Principal

(a) Conventional screw construct

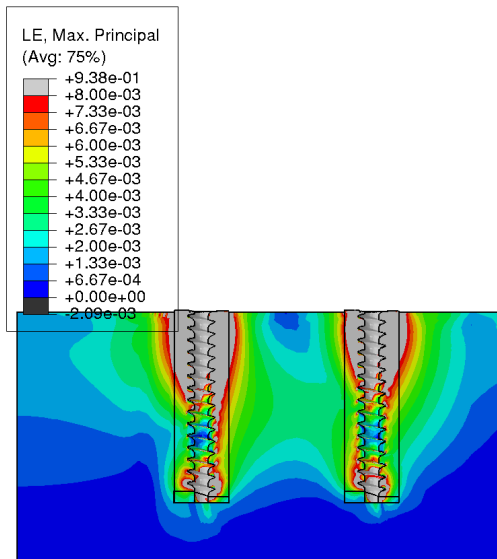


BoneBlock2010
ODB: 00-016-shear-lock.odb Abaqus/Standard 6.12-2 Sun Jun 09 03:13:37 EDT 2013

Step: AnonymousSTEP1, Fibulo-Talar Reaction Force
Increment 7; Step Time = 1.7500E-02
Primary Var: LE, Max. Principal

(b) Locking screw construct

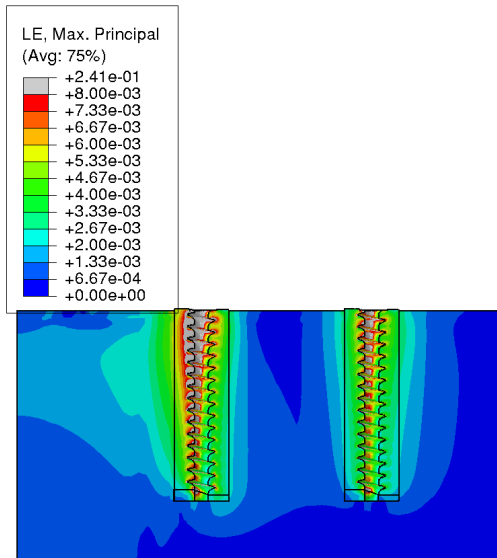
Figure E.13: Total strain under shear load (Bone density = 0.16 g cm⁻³, Cortex thickness=0mm)



BoneBlock2010
ODB: 00-024-shear-conv.odb Abaqus/Standard 6.12-2 Sun Jun 09 07:16:44 EDT 2013

Step: AnonymousSTEP1, Fibulo-Talar Reaction Force
Increment 42; Step Time = 2.7500E-02
Primary Var: LE, Max. Principal

(a) Conventional screw construct

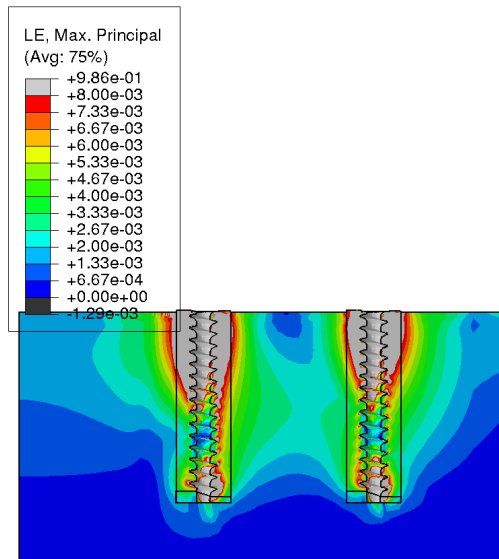


BoneBlock2010
ODB: 00-024-shear-lock.odb Abaqus/Standard 6.12-2 Sun Jun 09 15:45:36 EDT 2013

Step: AnonymousSTEP1, Fibulo-Talar Reaction Force
Increment 11; Step Time = 2.7500E-02
Primary Var: LE, Max. Principal

(b) Locking screw construct

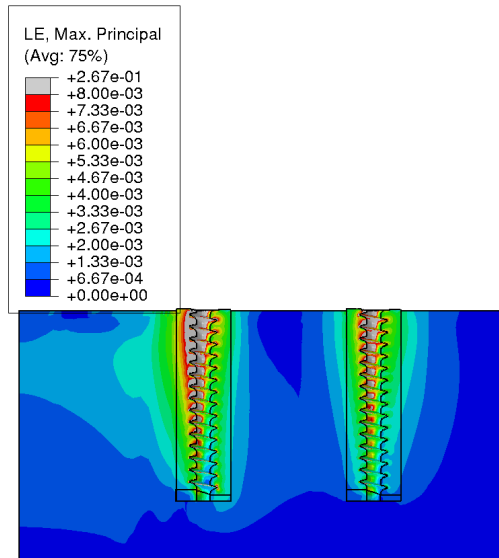
Figure E.14: Total strain under shear load (Bone density = 0.16 g cm⁻³, Cortex thickness=0mm)



BoneBlock2010
ODB: 00-032-shear-conv.odb Abaqus/Standard 6.12-2 Sun Jun 09 15:46:03 EDT 2013

Step: AnonymousSTEP1, Fibulo-Talar Reaction Force
Increment 20; Step Time = 3.7500E-02
Primary Var: LE, Max. Principal

(a) Conventional screw construct

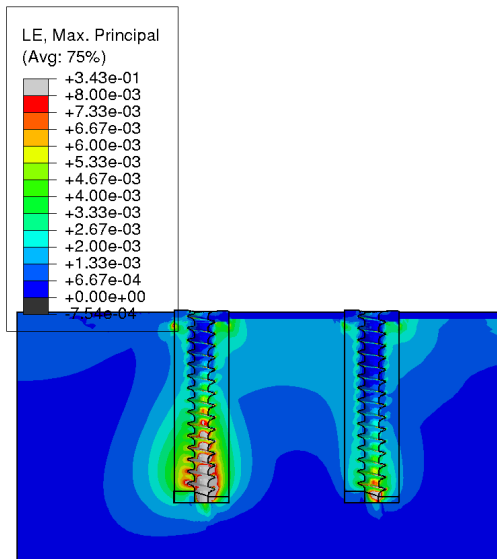


BoneBlock2010
ODB: 00-032-shear-lock.odb Abaqus/Standard 6.12-2 Sun Jun 09 21:16:30 EDT 2013

Step: AnonymousSTEP1, Fibulo-Talar Reaction Force
Increment 15; Step Time = 3.7500E-02
Primary Var: LE, Max. Principal

(b) Locking screw construct

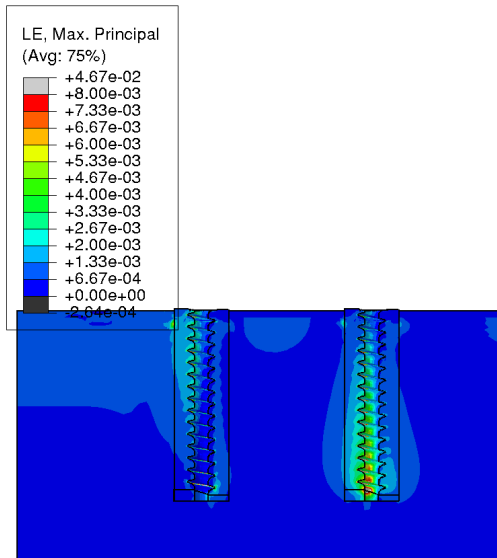
Figure E.15: Total strain under shear load (Bone density = 0.16 g cm⁻³, Cortex thickness=0mm)



BoneBlock2010
ODB: 01-008-shear-conv.odb Abaqus/Standard 6.12-2 Thu May 16 13:58:24 EDT 2013

Step: AnonymousSTEP1, Fibulo-Talar Reaction Force
Increment 18; Step Time = 4.5000E-02
Primary Var: LE, Max. Principal

(a) Conventional screw construct

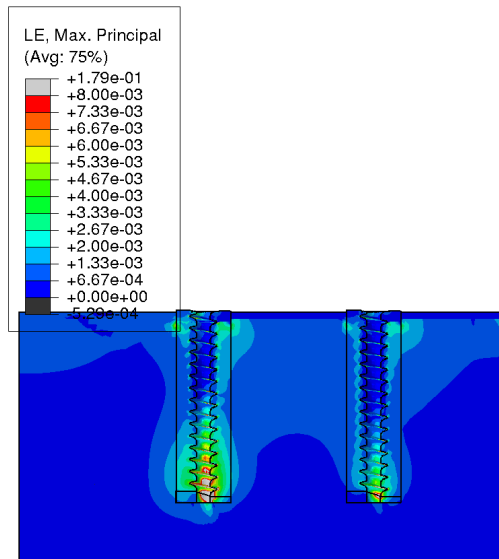


BoneBlock2010
ODB: 01-008-shear-lock.odb Abaqus/Standard 6.12-2 Fri May 17 05:28:09 EDT 2013

Step: AnonymousSTEP1, Fibulo-Talar Reaction Force
Increment 18; Step Time = 4.5000E-02
Primary Var: LE, Max. Principal

(b) Locking screw construct

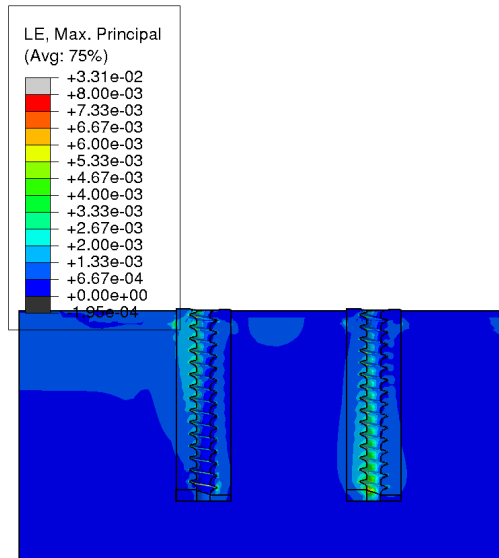
Figure E.16: Total strain under shear load (Bone density = 0.08 g cm⁻³, Cortex thickness=1mm)



BoneBlock2010
ODB: 01-016-shear-conv.odb Abaqus/Standard 6.12-2 Fri May 17 08:00:32 EDT 2013

Step: AnonymousSTEP1, Fibulo-Talar Reaction Force
Increment 15; Step Time = 4.5000E-02
Primary Var: LE, Max. Principal

(a) Conventional screw construct

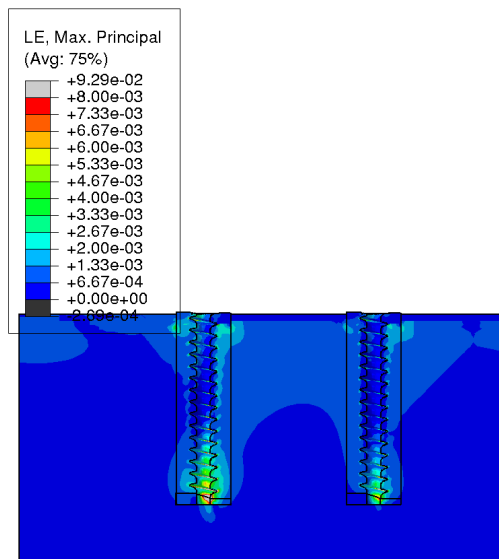


BoneBlock2010
ODB: 01-016-shear-lock.odb Abaqus/Standard 6.12-2 Fri May 17 14:54:14 EDT 2013

Step: AnonymousSTEP1, Fibulo-Talar Reaction Force
Increment 15; Step Time = 4.5000E-02
Primary Var: LE, Max. Principal

(b) Locking screw construct

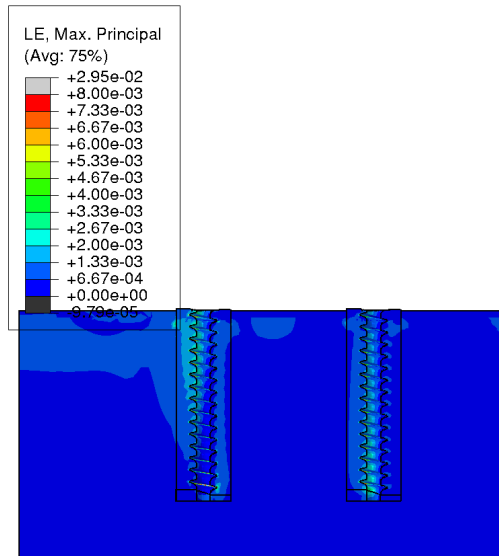
Figure E.17: Total strain under shear load (Bone density = 0.16 g cm⁻³, Cortex thickness=1mm)



BoneBlock2010
ODB: 01-024-shear-conv.odb Abaqus/Standard 6.12-2 Fri May 17 21:32:17 EDT 2013

Step: AnonymousSTEP1, Fibulo-Talar Reaction Force
Increment 15; Step Time = 4.5000E-02
Primary Var: LE, Max. Principal

(a) Conventional screw construct

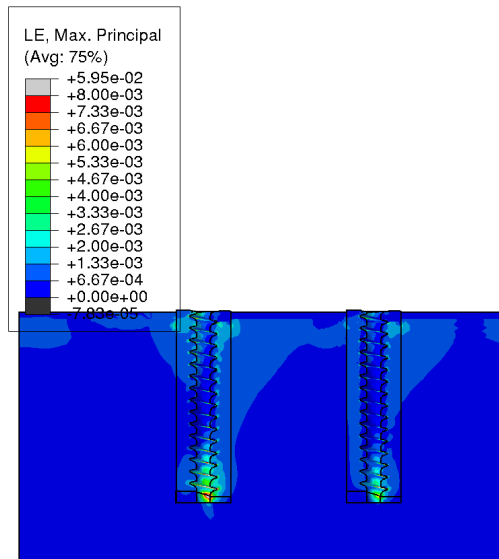


BoneBlock2010
ODB: 01-024-shear-lock.odb Abaqus/Standard 6.12-2 Sat May 18 08:08:20 EDT 2013

Step: AnonymousSTEP1, Fibulo-Talar Reaction Force
Increment 15; Step Time = 4.5000E-02
Primary Var: LE, Max. Principal

(b) Locking screw construct

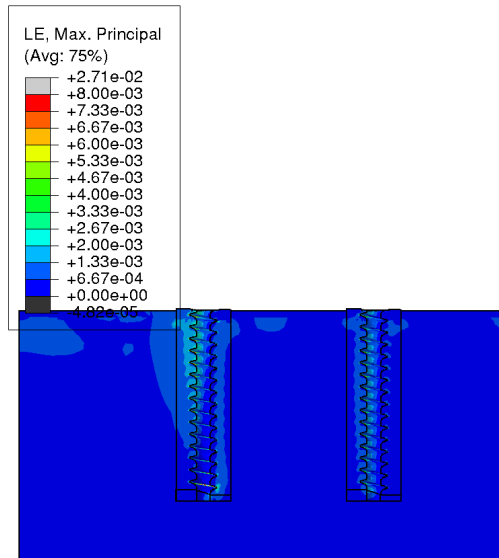
Figure E.18: Total strain under shear load (Bone density = 0.16 g cm^{-3} , Cortex thickness=1mm)



BoneBlock2010
ODB: 01-032-shear-conv.odb Abaqus/Standard 6.12-2 Sat May 18 11:08:33 EDT 2013

Step: AnonymousSTEP1, Fibulo-Talar Reaction Force
Increment 15; Step Time = 4.5000E-02
Primary Var: LE, Max. Principal

(a) Conventional screw construct

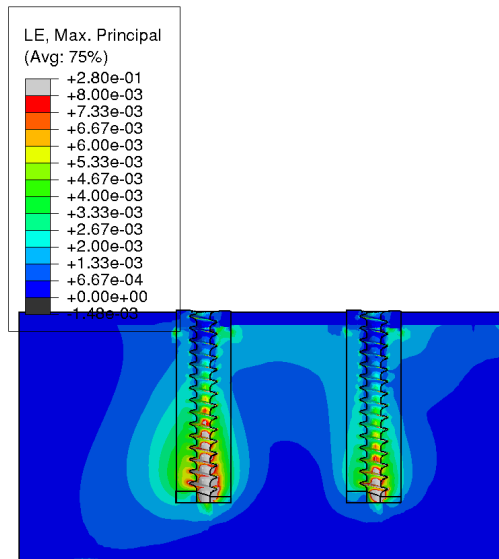


BoneBlock2010
ODB: 01-032-shear-lock.odb Abaqus/Standard 6.12-2 Sat May 18 23:49:19 EDT 2013

Step: AnonymousSTEP1, Fibulo-Talar Reaction Force
Increment 15; Step Time = 4.5000E-02
Primary Var: LE, Max. Principal

(b) Locking screw construct

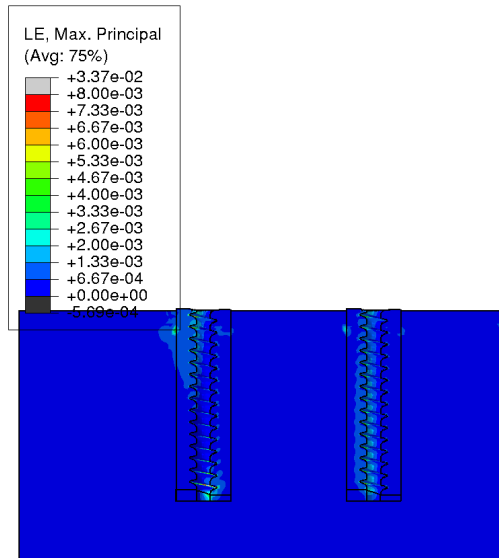
Figure E.19: Total strain under shear load (Bone density = 0.16 g cm⁻³, Cortex thickness=1mm)



BoneBlock2010
ODB: 02-008-shear-conv.odb Abaqus/Standard 6.12-2 Sat May 25 14:04:21 EDT 2013

Step: AnonymousSTEP1, Fibulo-Talar Reaction Force
Increment 15; Step Time = 4.5000E-02
Primary Var: LE, Max. Principal

(a) Conventional screw construct

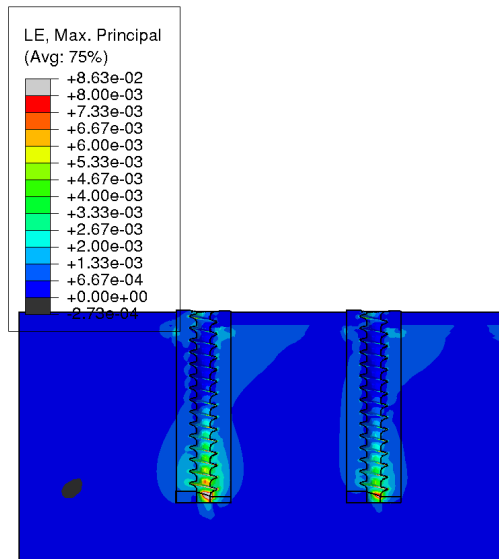


BoneBlock2010
ODB: 02-008-shear-lock.odb Abaqus/Standard 6.12-2 Sun May 26 02:45:28 EDT 2013

Step: AnonymousSTEP1, Fibulo-Talar Reaction Force
Increment 15; Step Time = 4.5000E-02
Primary Var: LE, Max. Principal

(b) Locking screw construct

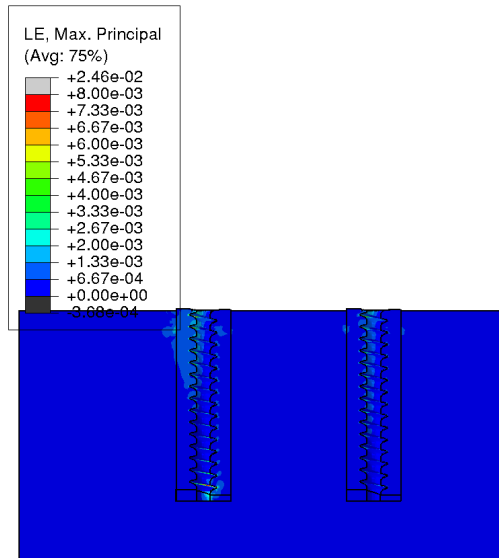
Figure E.20: Total strain under shear load (Bone density = 0.08 g cm⁻³, Cortex thickness=2mm)



BoneBlock2010
ODB: 02-024-shear-conv.odb Abaqus/Standard 6.12-2 Sun May 26 06:44:38 EDT 2013

Step: AnonymousSTEP1, Fibulo-Talar Reaction Force
Increment 15; Step Time = 4.5000E-02
Primary Var: LE, Max. Principal

(a) Conventional screw construct

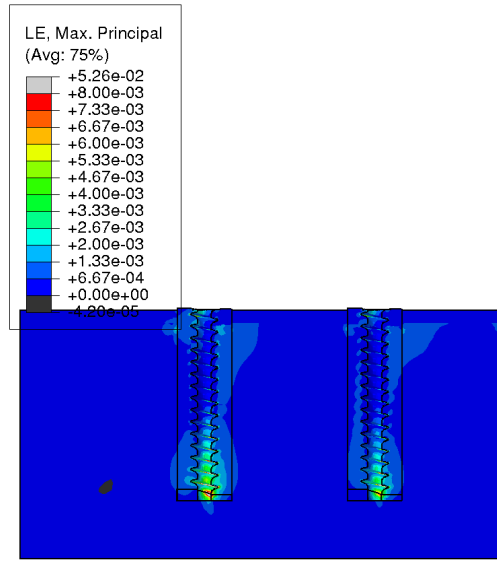


BoneBlock2010
ODB: 02-024-shear-lock.odb Abaqus/Standard 6.12-2 Sun May 26 16:58:03 EDT 2013

Step: AnonymousSTEP1, Fibulo-Talar Reaction Force
Increment 15; Step Time = 4.5000E-02
Primary Var: LE, Max. Principal

(b) Locking screw construct

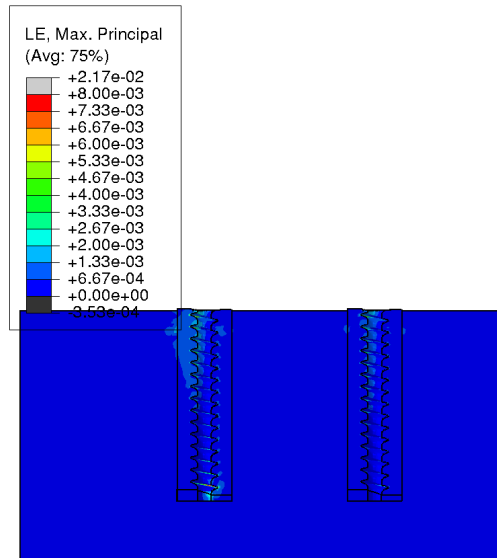
Figure E.21: Total strain under shear load (Bone density = 0.16 g cm⁻³, Cortex thickness=2mm)



BoneBlock2010
ODB: 02-032-shear-conv.odb Abaqus/Standard 6.12-2 Sun May 26 22:39:14 EDT 2013

Step: AnonymousSTEP1, Fibulo-Talar Reaction Force
Increment 15; Step Time = 4.5000E-02
Primary Var: LE, Max. Principal

(a) Conventional screw construct



BoneBlock2010
ODB: 02-032-shear-lock.odb Abaqus/Standard 6.12-2 Mon May 27 13:26:06 EDT 2013

Step: AnonymousSTEP1, Fibulo-Talar Reaction Force
Increment 15; Step Time = 4.5000E-02
Primary Var: LE, Max. Principal

(b) Locking screw construct

Figure E.22: Total strain under shear load (Bone density = 0.16 g cm^{-3} , Cortex thickness=2mm)

Appendix F

Plastic energy to total work ratio plots

F.1 Normal load

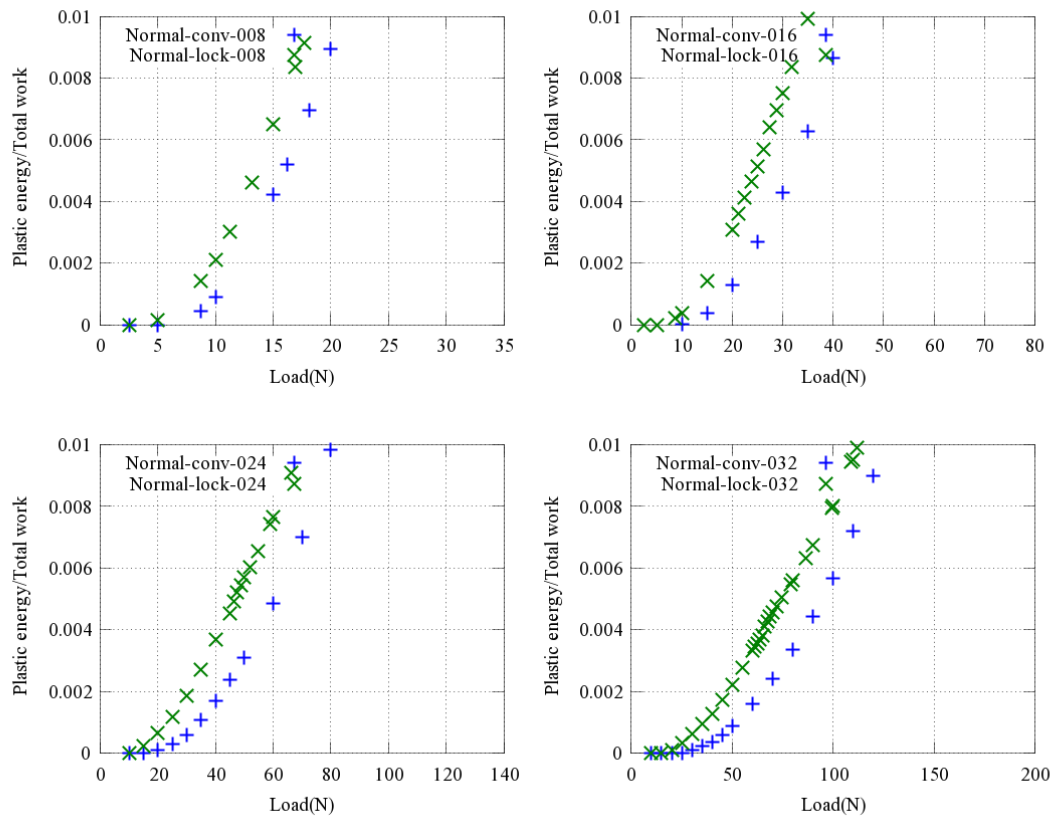


Figure F.1: Plastic energy dissipation comparison under normal load (cortex thickness=0mm)

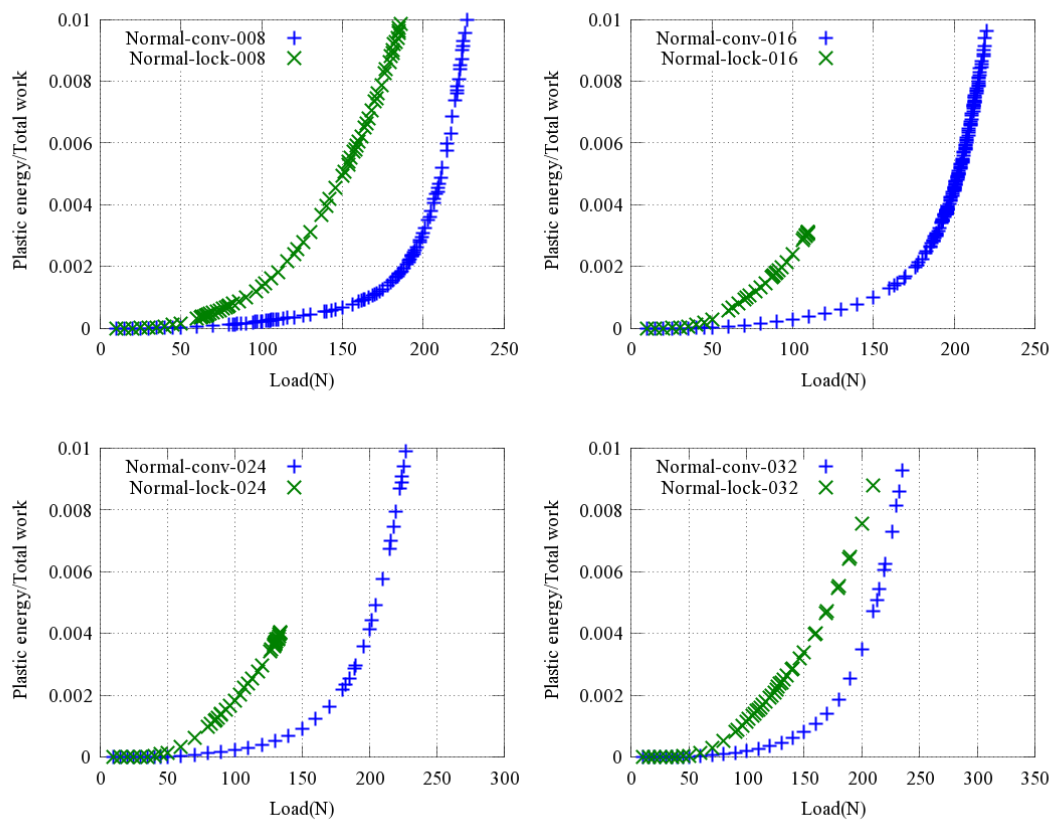


Figure F.2: Plastic energy dissipation comparison under normal load (cortex thickness=2mm)

F.2 Shear load

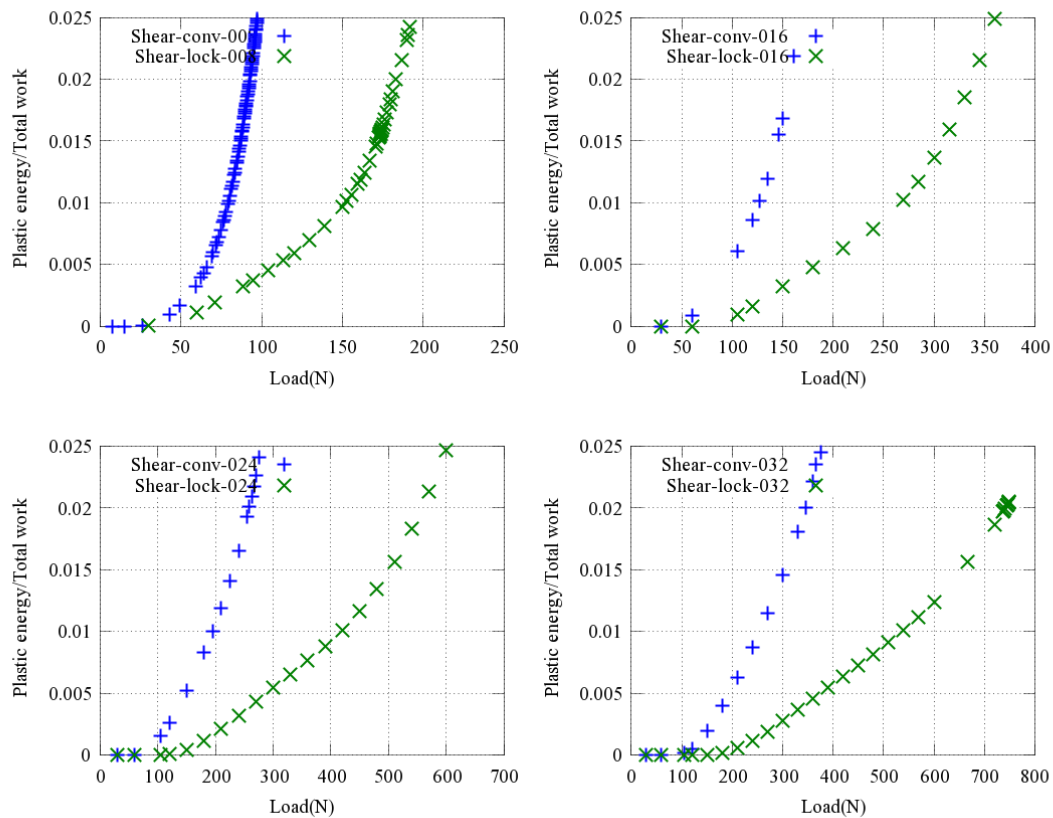


Figure F.3: Plastic energy dissipation comparison under shear load (cortex thickness=0mm)

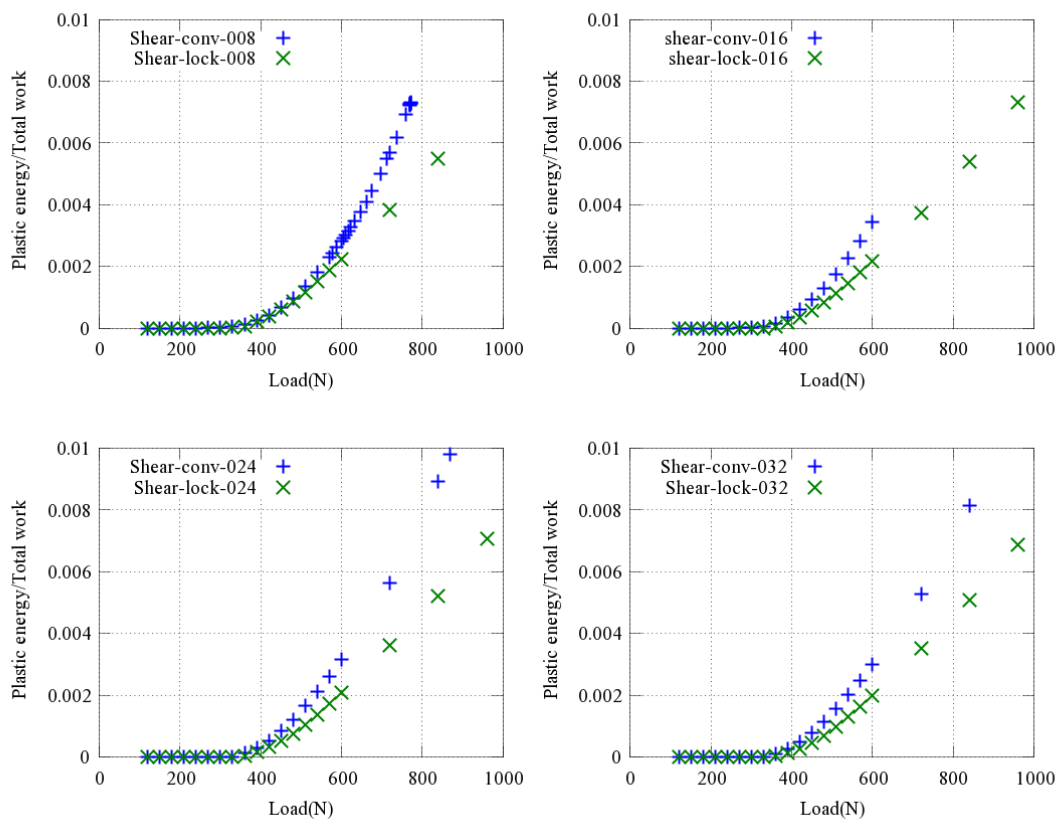


Figure F.4: Plastic energy dissipation comparison under shear load (cortex thickness=2mm)

F.3 Oblique load

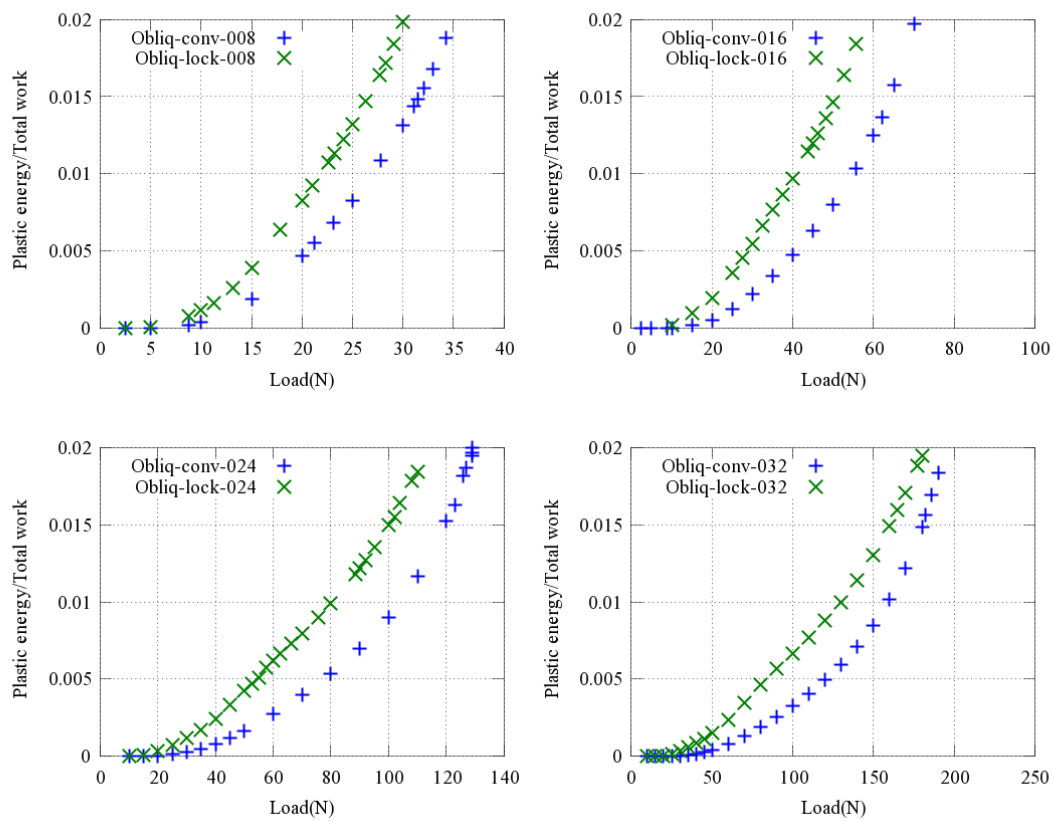


Figure F.5: Plastic energy dissipation comparison under obliq load (cortex thickness=0mm)

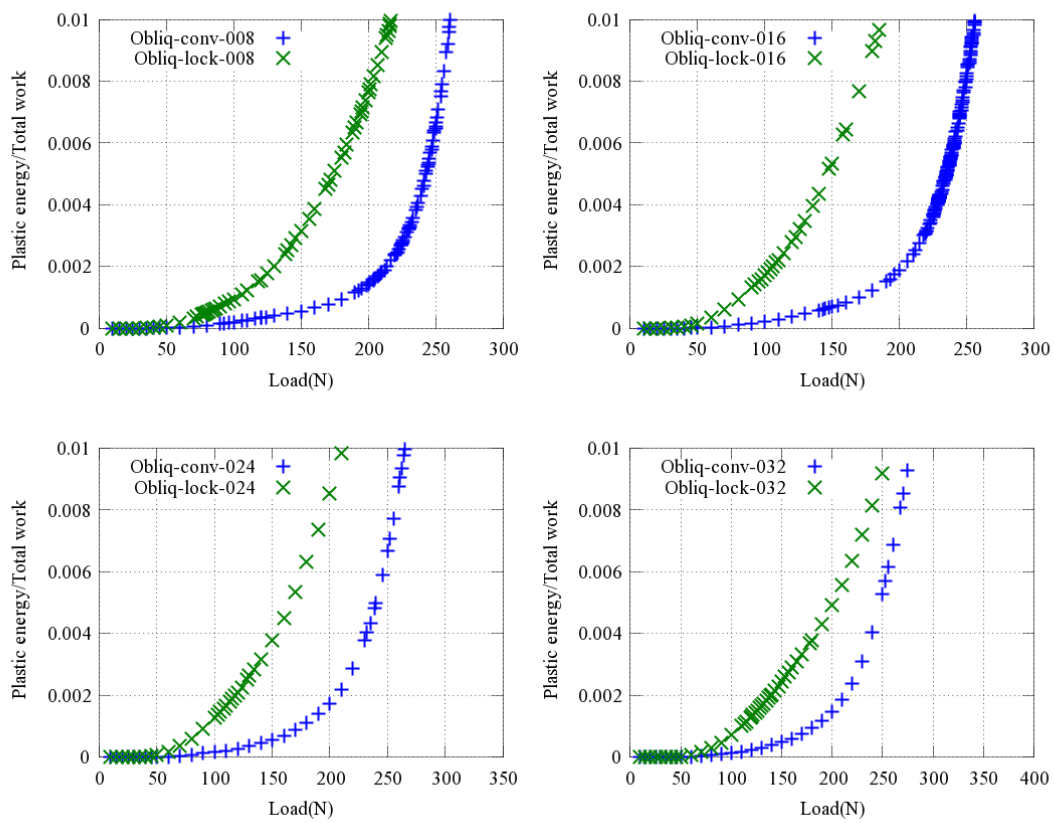


Figure F.6: Plastic energy dissipation comparison under obliq load (cortex thickness=2mm)

Appendix G

Plastic strain at the failure initiation

G.1 Normal load

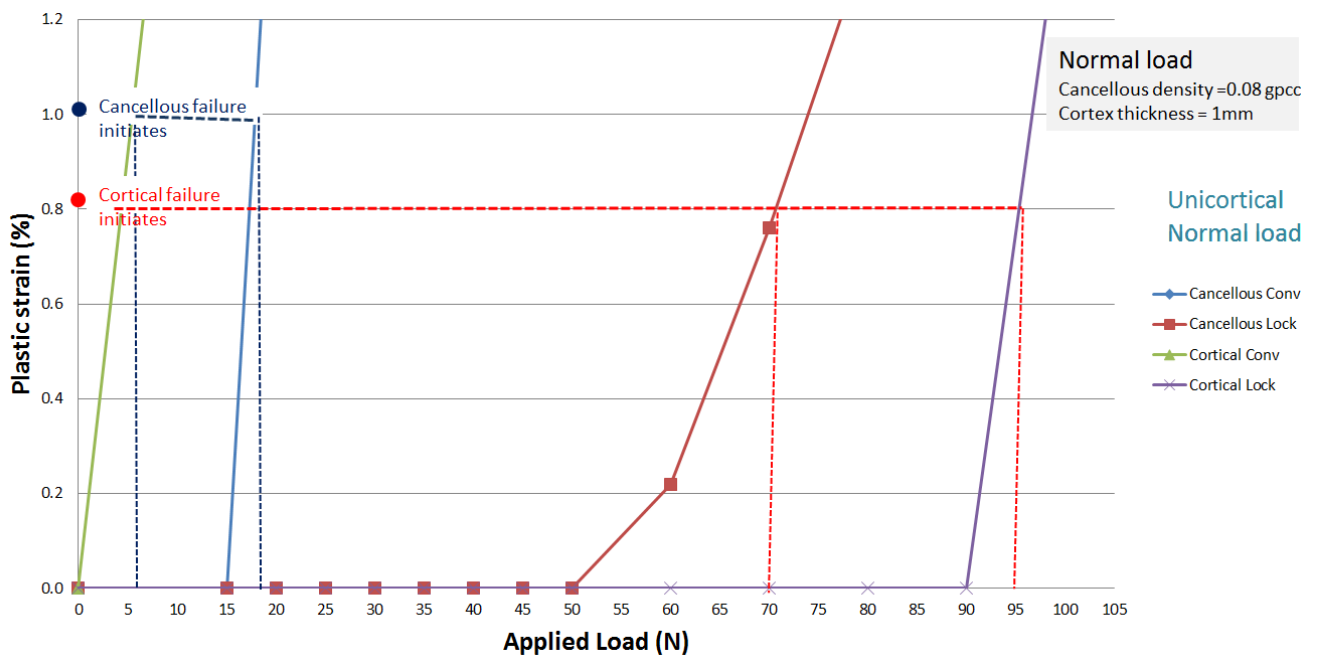


Figure G.1: Plastic strain for the failure initiation (Cancellous density = 0.08 gpcc, cortex thickness=1mm)

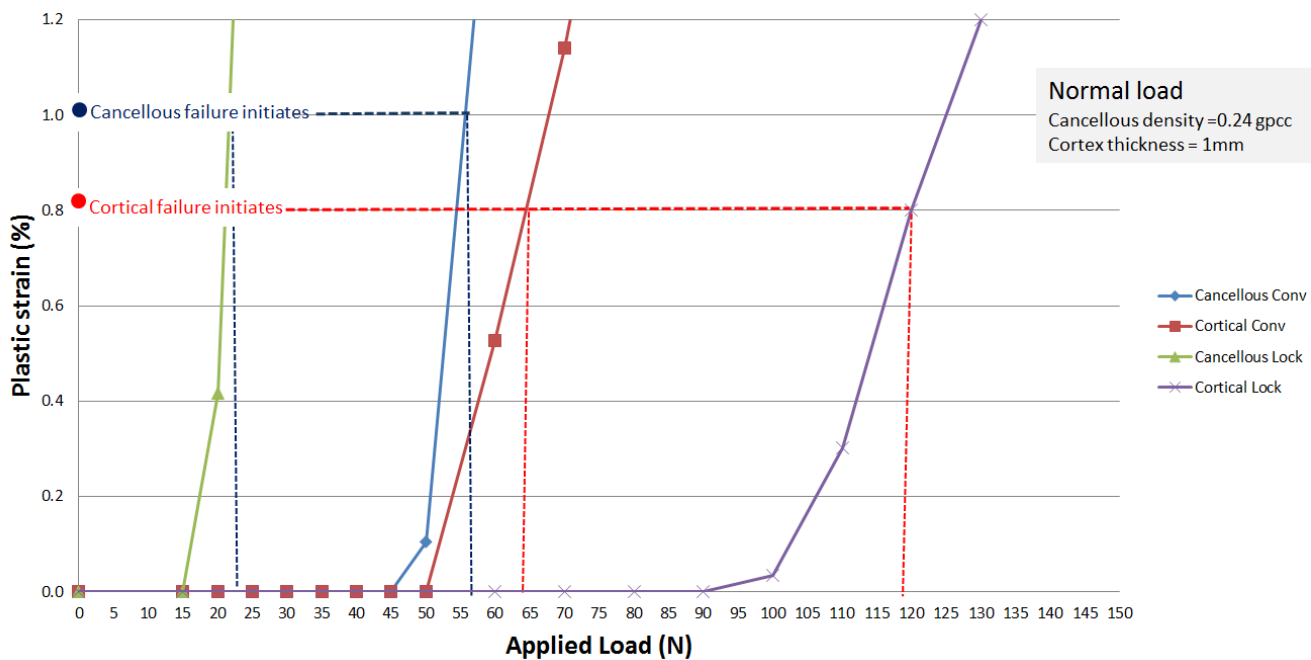


Figure G.2: Plastic strain for the failure initiation (Cancellous density = 0.24 gpcc, cortex thickness=1mm)

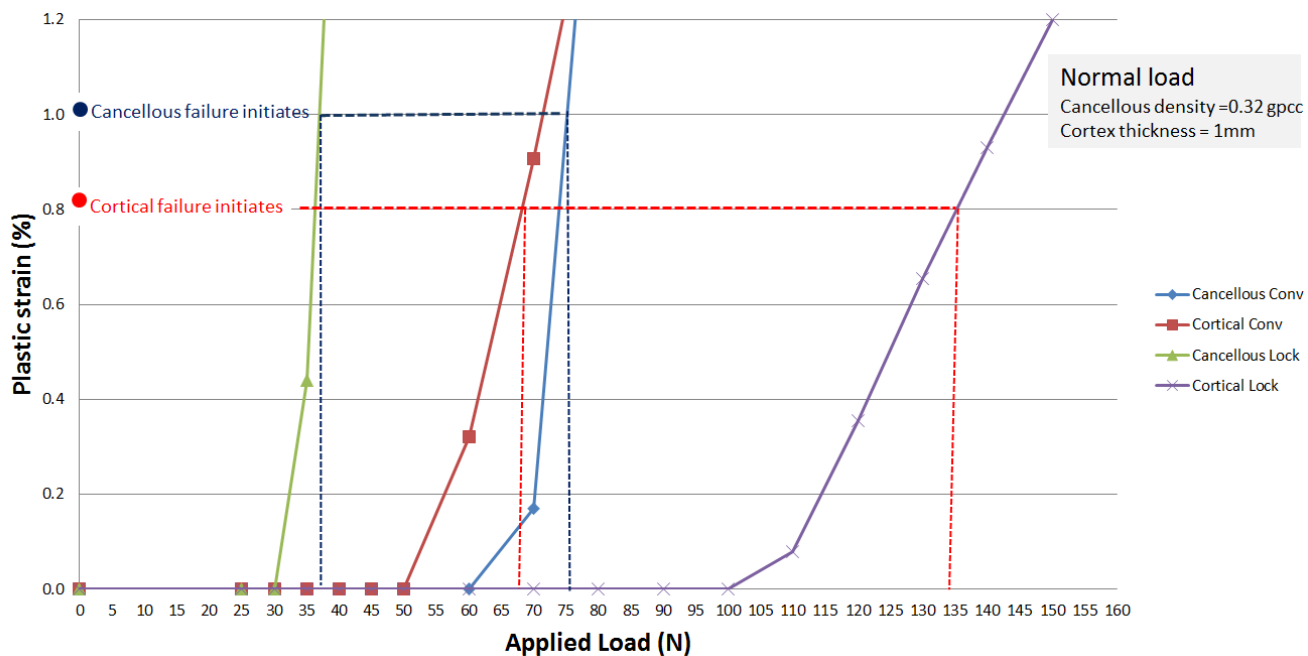


Figure G.3: Plastic strain for the failure initiation (Cancellous density = 0.32 gpcc, cortex thickness=1mm)

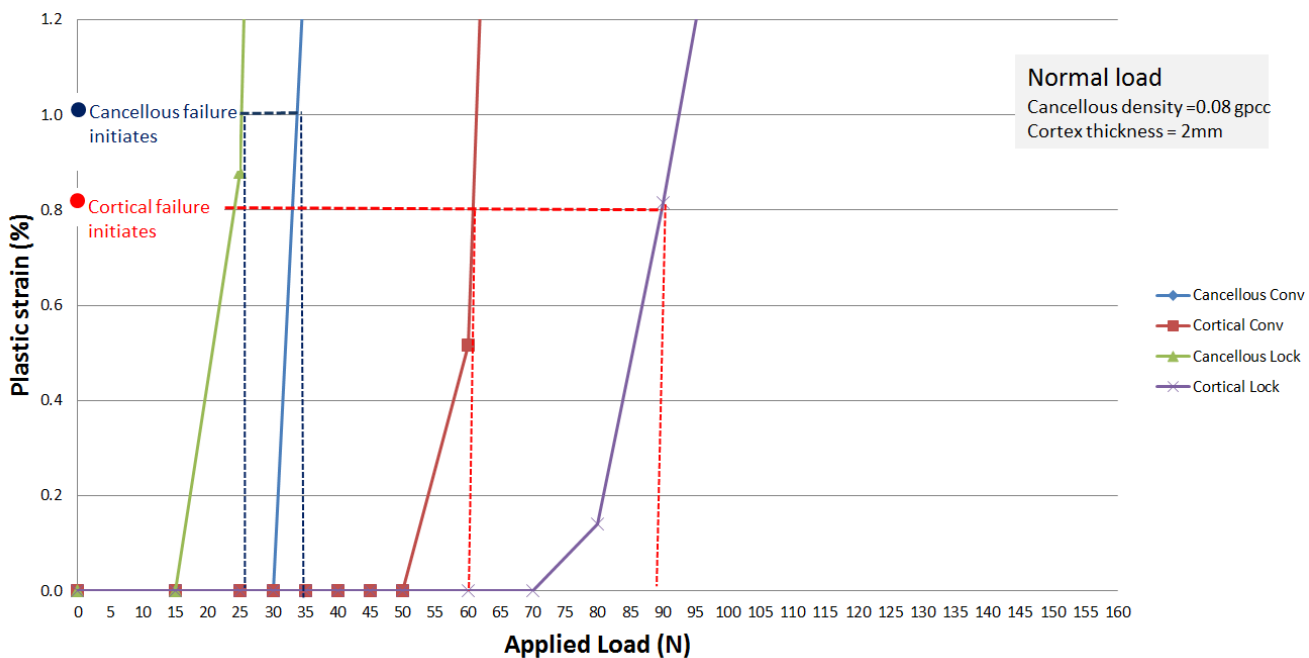


Figure G.4: Plastic strain for the failure initiation (Cancellous density = 0.08 gpcc, cortex thickness=2mm)

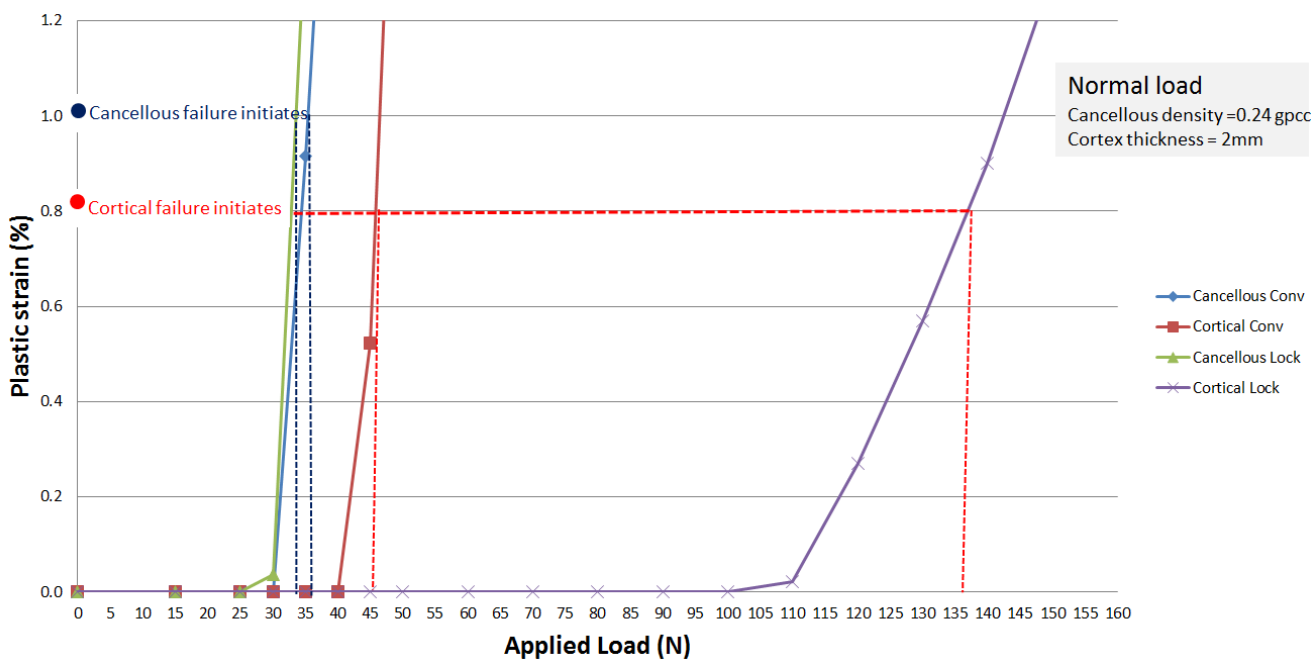


Figure G.5: Plastic strain for the failure initiation (Cancellous density = 0.24 gpcc, cortex thickness=2mm)

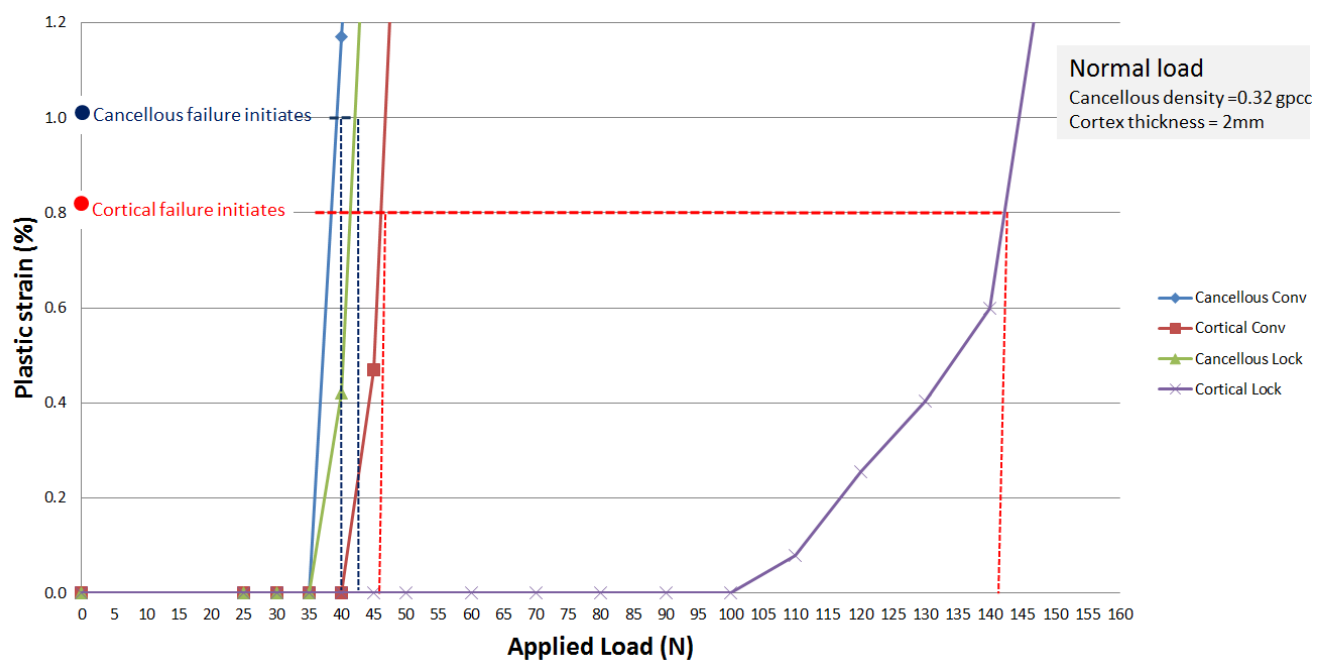


Figure G.6: Plastic strain for the failure initiation (Cancellous density = 0.32 gpcc, cortex thickness=2mm)

G.2 Shear load

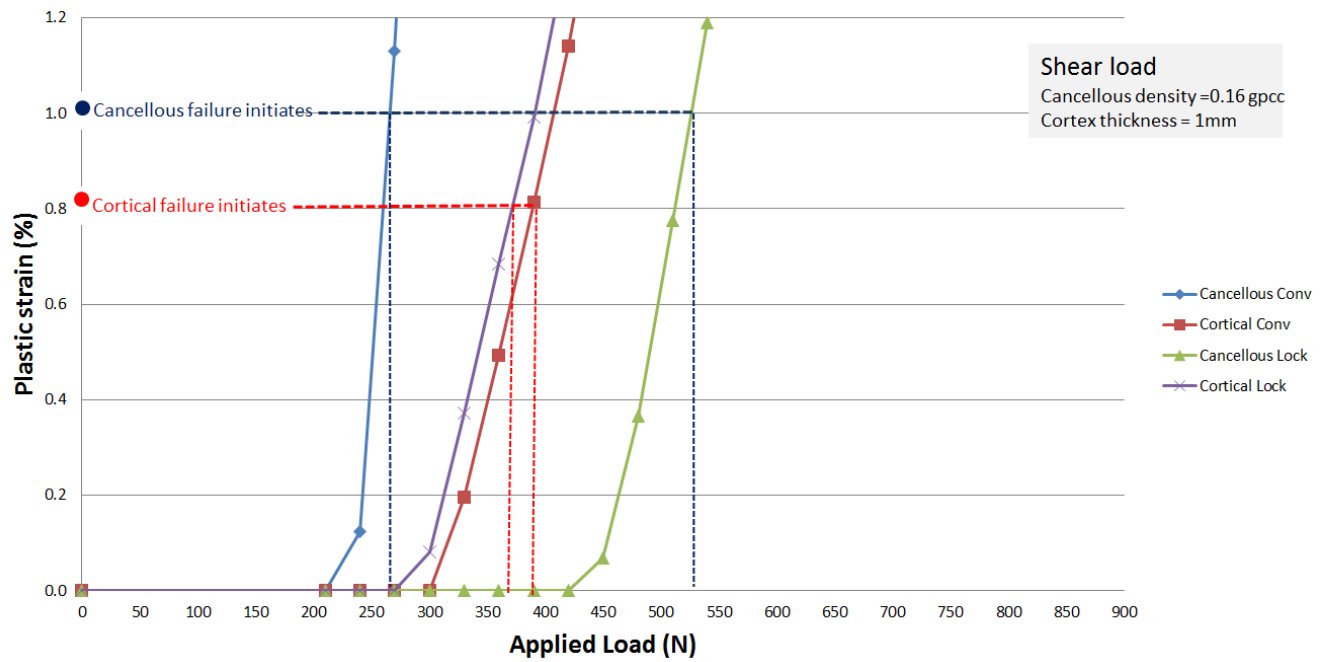


Figure G.7: Plastic strain for the failure initiation (Cancellous density = 0.16 gpcc, cortex thickness=1mm)

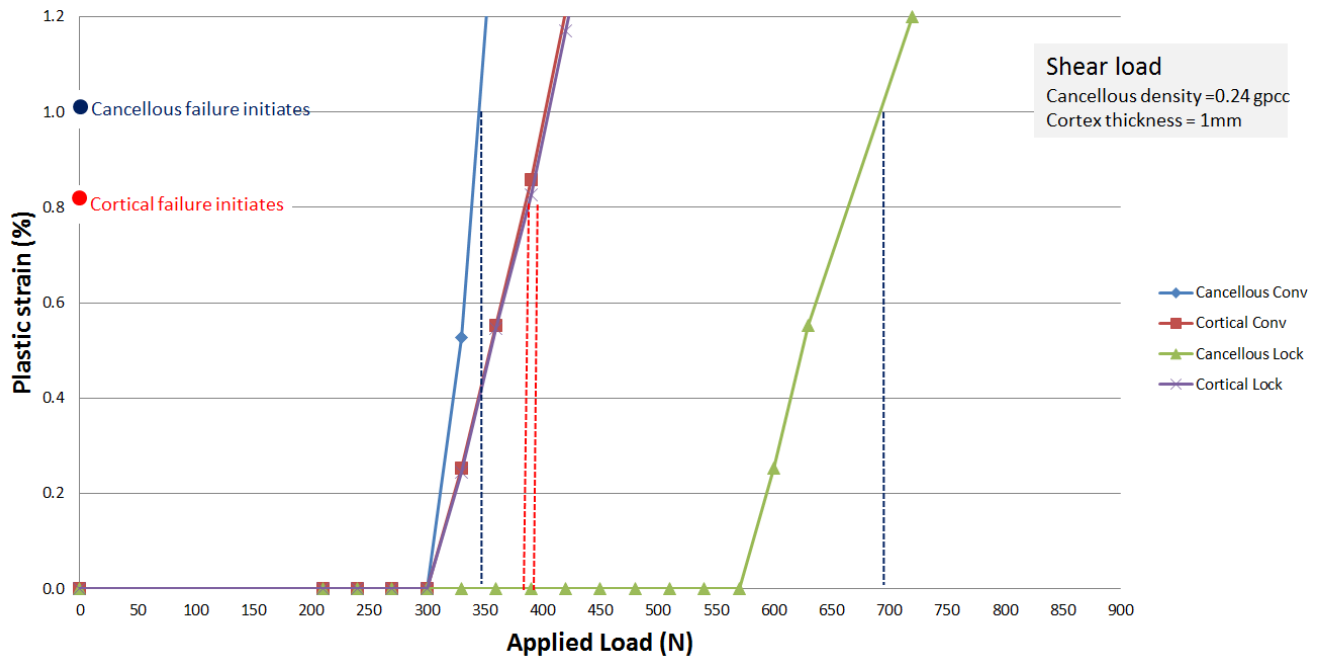


Figure G.8: Plastic strain for the failure initiation (Cancellous density = 0.24 gpcc, cortex thickness=1mm)

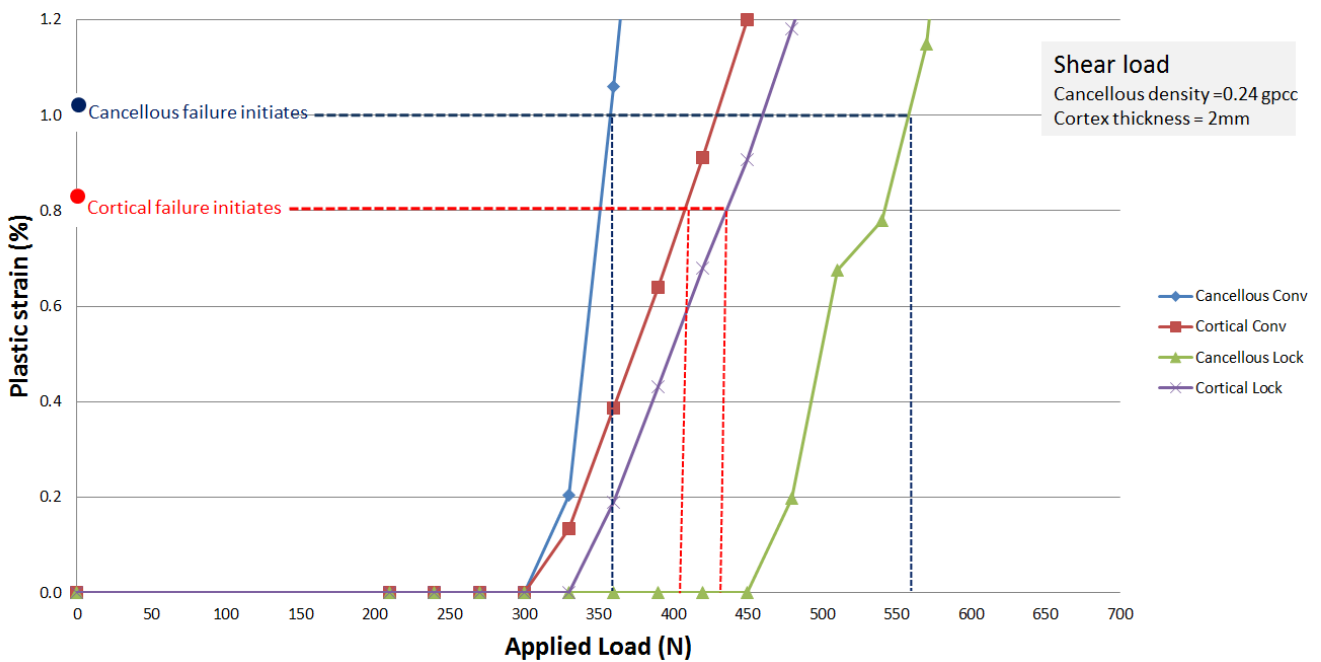


Figure G.9: Plastic strain for the failure initiation (Cancellous density = 0.24 gpcc, cortex thickness=2mm)

Appendix H

HSIRB approval forms

WESTERN MICHIGAN UNIVERSITY



Human Subjects Institutional Review Board

Date: January 21, 2011

To: Peter Gustafson, Principal Investigator
Bipin Patel, Student Investigator

From: Amy Naugle, Ph.D., Chair

A handwritten signature in black ink, appearing to read "Amy Naugle", written over the printed name "Amy Naugle, Ph.D., Chair".

Re: HSIRB Project Number: 11-01-05

This letter will serve as confirmation that your research project titled "Ability of Surgeons to Optimize Screw Fixation Torque in Osteoporotic Bone" has been **approved** under the **expedited** category of review by the Human Subjects Institutional Review Board. The conditions and duration of this approval are specified in the Policies of Western Michigan University. You may now begin to implement the research as described in the application.

Please note that you may **only** conduct this research exactly in the form it was approved. You must seek specific board approval for any changes in this project. You must also seek reapproval if the project extends beyond the termination date noted below. In addition if there are any unanticipated adverse reactions or unanticipated events associated with the conduct of this research, you should immediately suspend the project and contact the Chair of the HSIRB for consultation.

The Board wishes you success in the pursuit of your research goals.

Approval Termination: January 21, 2012

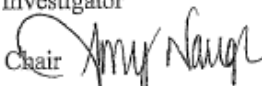
WESTERN MICHIGAN UNIVERSITY



Human Subjects Institutional Review Board

Date: June 18, 2013

To: Peter Gustafson, Principal Investigator
Bipin Patel, Student Investigator

From: Amy Naugle, Ph.D., Chair 

Re: HSIRB Project Number 13-06-05

This letter will serve as confirmation that your research project titled "Effects of Real Time Feedback on Surgeon Performance during Screw Placement" has been **approved** under the **expedited** category of review by the Human Subjects Institutional Review Board. The conditions and duration of this approval are specified in the Policies of Western Michigan University. You may now begin to implement the research as described in the application.

Please note: This research may **only** be conducted exactly in the form it was approved. You must seek specific board approval for any changes in this project (e.g., ***you must request a post approval change to enroll subjects beyond the number stated in your application under "Number of subjects you want to complete the study."*** Failure to obtain approval for changes will result in a protocol deviation. In addition, if there are any unanticipated adverse reactions or unanticipated events associated with the conduct of this research, you should immediately suspend the project and contact the Chair of the HSIRB for consultation.

Reapproval of the project is required if it extends beyond the termination date stated below.

The Board wishes you success in the pursuit of your research goals.

Approval Termination: June 18, 2014